TRANSACTIONS

Series A

Journal of ENGINEERING FOR POWER

April 1959

Divisions: POWER • GAS TURBINE POWER • NUCLEAR ENGINEERING • FUELS OIL AND GAS POWER • **Research Committees:** FURNACE PERFORMANCE FACTORS CORROSION AND DEPOSITS FROM COMBUSTION GASES • BOILER FEEDWATER STUDIES • HIGH TEMPERATURE STEAM GENERATION • CONDENSER TUBES PROPERTIES OF STEAM • **Committees on:** AIR POLLUTION CONTROLS • SOLAR ENERGY APPLICATION • **And:** POWER TEST CODES COMMITTEES

THE AMERICAN SOCIETY OF MECHANICAL ENGINEERS

TRANSACTIONS
OF THE ASME
Series A

EDITORIAL DEPARTMENT

OFFICERS OF THE ASME

PUBLICATIONS COMMITTEE

REGIONAL ADVISORY BOARD

Journal of
ENGINEERING FOR POWER
VOLUME 81 • SERIES A • NUMBER 2
April 1959

CONTENTS

111 **The Control System of a 225,000-Kw Double-Automatic Extraction Steam Turbine and Related Reducing Stations**
M. A. Eggenberger and P. G. Ipsen

123 **Design of 321-Mw Cross-Compound Steam Turbine—River Rouge Unit No. 3**
C. D. Wilson

133 **Five Years' Experience on the Consolidated Edison System With Protection of Turbine Generators and Boilers by Automatic Tripping**
W. C. Beattie, H. A. Bauman, J. M. Driscoll, P. T. Onderdonk, and R. L. Webb

142 **A Simplified Regenerator Theory**
W. F. Schalkwijk

151 **Development of a Smooth Running, Double-Spool, Gas-Turbine Rotor System**
J. R. Schnittger

161 **M-252 Alloy for Heavy-Duty Gas-Turbine Buckets**
G. R. Fusner and D. L. Newhouse

177 **The Calibration of Thermocouples by Freezing-Point Baths and Empirical Equations**
R. P. Benedict

189 **Theoretical Stresses Near a Circular Opening in a Flat Plate, Reinforced With a Cylindrical Outlet**
E. O. Waters

201 **Effect of Steam-Turbine Reheat on Speed-Governor Performance**
Charles Concordia

208 **Load Capacity Tests on Tapered-Land and Pivoted-Shoe Thrust Bearings for Large Steam-Turbine Application**
R. E. Brandon and H. C. Bahr

TRANSACTIONS OF THE ASME
Series B

Journal of
ENGINEERING FOR INDUSTRY
Volume 81 • Series B • Number 1

CONTENTS FOR FEBRUARY, 1959

1 Dynamic Loading of Spur Gear Teeth, by A. Y. Attia. (58—SA-32)
10 Analytical Design of an Ackermann Steering Linkage, by W. A. Wolfe. (58—SA-31)
15 Structural Error Analysis in Plane Kinematic Synthesis, by Ferdinand Freudenstein. (58—SA-12)
23 The Design of Linkages to Generate Functions of Two Variables, by C. W. Allen. (58—SA-57)
30 Helical Springs of Hollow Circular Cross Section, by C. W. Bert. (58—SA-18)
37 Design of Helical Springs for Minimum Weight, Volume, and Length, by R. T. Hinkle and I. E. Morse, Jr. (58—SA-9)
43 Stress and Strain in Spinning Paraboloid Dishes, by M. J. Cohen. (58—SA-8)
51 Torispherical Shells—A Caution to Designers, by G. D. Galletly. (58—PET-3)
67 Drilling by Vibration, by R. Simon. (58—PET-21)
77 Vibrations of Vertical Pressure Vessels, by C. E. Freese. (58—PET-13)
92 Technical Briefs—Revisions to Published Chart: Metals for High-Pressure Hydrogenation Plants, by G. A. Nelson.

TRANSACTIONS OF THE ASME
Series C

Journal of
HEAT TRANSFER
Vol. 81 • Series C • No. 1

CONTENTS FOR FEBRUARY, 1959

1 Wave Theory of Heat Transfer in Film Boiling, by Yan Po Chang. (58—SA-19)
13 A Boundary-Layer Treatment of Laminar-Film Condensation, by E. M. Sparrow and J. L. Gregg, (58—SA-2)
19 Transient Response of Heated Air in an Enclosure With Heat Losses, by W. A. Wolfe. (58—SA-3)
24 Natural-Convection Heat Transfer in Liquids Confined by Two Horizontal Plates and Heated From Below, by Samuel Globe and David Dropkin.
29 Transient Heat Transfer for Laminar Forced Convection in the Thermal Entrance Region of Flat Ducts, by R. Siegel and E. M. Sparrow. (58—HT-3)
37 Generalized Correlation of Boiling Heat Transfer, by S. Levy. (58—HT-8)
43 Heat Transfer to a Boiling Liquid—Mechanism and Correlations, by Kurt Engelberg-Forster and R. Greif. (58—HT-11)
54 Transient Heat Conduction in Elliptical Plates and Cylinders, by E. T. Kirkpatrick and W. F. Stokey. (58—HT-10)
61 Calculation of Transients in a Cross-Flow Heat Exchanger, by G. M. Dusinberre. (58—HT-5)
68 Free Convection, Forced Convection, and Acoustic Vibrations in a Constant Temperature Vertical Tube, by T. W. Jackson, W. B. Harrison, and W. C. Coteler. (58—HT-6)
75 Summary—Selected References on Gas Turbines, Regenerative Cycles, Rotary Regenerators, and Associated Heat-Exchange and Pressure-Drop Information, by W. E. Hammond.
79 Investigation of Heat Transfer, Flow, and Heat Exchangers as Related to Turbine Cooling, by H. H. Ellerbrock, Jr., and J. N. B. Livingood.
86 Progress and Development of Gas-Turbine Regenerators, by Sven Holm and R. L. Lyerly.
89 Heat Transfer and Friction for Fluids Flowing Over Surfaces at High Temperatures and High Velocities, by R. G. Deissler and A. L. Loeffler, Jr.
92 A New Technique for Measuring the Spectral Emissivity of Solids at High Temperatures, by P. E. Glaser and H. H. Blau, Jr. (58—AV-29)

TRANSACTIONS OF THE ASME
Series D

Journal of
BASIC ENGINEERING
Vol. 81 • Series D • No. 1

CONTENTS FOR MARCH, 1959

1 Ball Motion and Sliding Friction in Ball Bearings, by A. B. Jones. (58—AV-14)
13 A Variational Approach to Lubrication Problems and the Solution of the Finite Journal Bearing, by D. F. Hays. (58—SA-54)
24 On the Necessity of Unsteady Flow in Fluid Machines, by R. C. Dean, Jr.
29 Prediction of Choking Flow in Centrifugal Impellers, by Harold Lown and F. J. Wiesner, Jr. (58—SA-15)
37 Concerning Subharmonic Oscillations Which May Exist in Nonlinear Systems Having Odd Restoring Forces, by C. A. Ludeke and William Pong.
41 An Analytic Frequency-Response Solution for a Higher Order Servomechanism With a Nonlinear Control Element, by A. M. Hopkin and K. Ogata. (58—SA-35)
46 Antifriction Instrument-Bearing Torque Testing and the Resistance to Motion of Such Bearings, by A. B. Asch. (58—SA-34)
49 Analysis and Characteristics of the Three-Lobe Bearing, by O. Pinkus. (58—LUB-2)
56 An Investigation of Dry Adhesive Wear, by R. P. Steijn. (58—LUB-8)
67 Sliding Wear and Metal Transfer Under Unlubricated Conditions, by R. P. Steijn. (58—LUB-9)
79 On the Mechanism of Gear Lubrication, by V. N. Borsoff. (58—LUB-4)
94 The Influence of the Molecular Mean Free Path on the Performance of Hydrodynamic Gas Lubricated Bearings, by Albert Burgdorfer. (58—LUB-7)

TRANSACTIONS
Series E

Journal of
APPLIED MECHANICS
Volume 81 • Series E • Number 1

CONTENTS FOR MARCH, 1959

TECHNICAL PAPERS

3 Experimental Surface-Wave Method for Recording Force-Time Curves, J. N. Goodier, W. E. Jahsman, and E. A. Ripperger. (58—A-51)

8 Forced Torsional Vibration of Systems With Distributed Mass and Damping, K. E. Bisshopp. (58—A-8)

13 Frequencies of a Flexible Circular Plate and Light Elastic Half-Space, G. N. Bycroft. (58—A-37)

18 Analytical Design of Disk Cams by Independent Position Equations, F. H. Raven. (58—A-17)

25 Stress Distribution and Plastic Deformation in Rotating Cylinders, E. A. Davis and F. M. Connelly. (58—A-10)

31 Transient and Residual Stresses in Heat-Treated Cylinders, J. H. Weiner and J. V. Huddleston. (58—A-21)

40 The Nonlinear Bending of Thin Rods, T. P. Mitchell. (58—A-50)

44 Stresses and Deflections in Circular Plate Loaded Over a Segment, W. A. Bassali and M. Nassif. (58—A-27)

55 Transverse Flexure of a Thin Plate Containing Two Circular Holes, O. Tamate. (58—A-35)

61 Limit Analysis of Symmetrically Loaded Thin Shells of Revolution, D. C. Drucker and R. T. Shield. (58—A-26)

69 On Influence Coefficients and Nonlinearity for Thin Shells of Revolution, Eric Reissner. (58—A-33)

73 A Theorem of Maximum Strain Energy, E. H. Brown. (58—A-40)

77 Plastic Stress-Strain Relationships—Effect of Loading Path and History, S. S. Gill and J. Parker. (58—A-11)

88 A Stress-Strain Relation for Hexagonal Close-Packed Array of Spheres, J. Duffy. (58—A-53)

95 A Mathematical Model of the Stress-Strain Diagram and Hysteresis Loop, I. R. Whiteman. (58—A-68)

101 A Definition of Stable Inelastic Material, D. C. Drucker. (58—A-31)

107 Retarded Flow of Bingham Materials, Alfred Slibar and P. R. Paslay. (58—A-34)

114 An Experiment on Compressible-Flow Perturbations, T. A. D'Ews Thomson and R. E. Meyer. (58—A-52)

120 Transient Film Condensation, E. M. Sparrow and Robert Siegel. (58—A-13)

122 Effect of Turbulence on Slider-Bearing Lubrication, Y. T. Chou and Edward Saibel. (58—A-30)

127 Theory of Flight of the Sounding Rocket, V. C. Liu. (58—A-32)

DESIGN DATA AND METHODS

130 Stress-Concentration Factors for T-Heads, M. Hetényi.

BRIEF NOTES

133 Buoyancy Effects in Forced-Convection Flow, E. M. Sparrow and J. L. Gregg. 134 Thermally Induced Twists in Thin Plates, L. S. Han and K. L. Bergman. 136 Deflections and Vibrations of Clamped Sectorial Plates, M. Ben-Amoz. 137 Thermal Distributions Without Thermal Stresses, H. H. Hilton. 138 Thin-Walled Cylinders Under Torsion and Pressure, H. S. Suer and L. A. Harris. 140 Transient Heat Transfer for Flow in Ducts, Robert Siegel. 142 Upper and Lower Bounds for Stiffness of Plates, Eric Reissner. 143 Cross-Section Distortion and the Timoshenko Beam Equation, A. D. S. Barr. 144 Analysis of Paraboloidal Shells, Robert Schmidt. 145 Natural Frequencies of Two Nonlinear Systems, E. W. Gaylord. 146 Response of a Slab to Impact, J. N. Goodier and E. A. Ripperger. 147 Thermal Stresses in Long Cylindrical Shells, C. H. Tsao. 148 Dynamic Characteristics of Undamped Vibration Systems, M. E. Gurtin.

DISCUSSION

150 Discussion of previously published papers by A. J. Durelli and A. S. Kobayashi; J. W. Dally, A. J. Durelli, and W. F. Riley; R. Plunkett; J. W. Miles; T. H. Lin.

154 **BOOK REVIEWS**

M. A. EGGENBERGER

Design Engineer, Turbine Control Engineering, General Electric Company, Schnectady, N. Y. Mem. ASME

P. G. IPSEN

Supervisor, Turbine Control Engineering, General Electric Company, Schenectady, N. Y. Mem. ASME

The Control System of a 225,000-Kw Double-Automatic Extraction Steam Turbine and Related Reducing Stations

Three variables must be controlled on a double-automatic extraction turbine—speed (or power output), and the two process-header pressures—by controlling the flow of steam at different pressure levels. This has been done in a satisfactory manner on a large number of extraction turbines. However, the designs which had been developed for turbines of 50,000-kw capacity and smaller were not suitable for a turbine nearly five times as large, and a completely new control-system design had to be created.

Control Specification

THE SIGNIFICANT QUANTITIES and requirements which determine the control specification for the turbine are as follows:

1 Main steam conditions 2000 psig 1050 F
2 Main steam flow 2,800,000 lb/hr max
3 High-pressure process extraction—650 psig to 750 psig
4 Low-pressure process extraction—110 psig to 150 psig
5 Max h-p process-extraction flow—600,000 lb/hr at 750 psig
6 Max l-p process-extraction flow—1,000,000 lb/hr at 150 psig
7 Sum of h-p and l-p extraction flow limited to 1,150,000 lb/hr
8 Feedwater extraction from six points, four uncontrolled, and two from the controlled extraction points, to obtain a final feedwater temperature of about 510 F
9 Turbine to deliver any output from 100,000 kw to a maximum output of 225,000 kw with any process-extraction demand from zero to a total of 1,150,000 lb/hr
10 Control system to be capable of keeping turbine speed below trip speed of emergency governor set at 110 per cent on loss of 225,000 kw; initial acceleration rate of rotor, 15 per cent/sec
11 Control system to be "compensated" so that a change in the demand for one of the three quantities produces a minimum upset in the other two quantities
12 Control system to be designed for operation from a centralized control room

In order to insure continuity of steam supply to the two process headers, it was specified that two duplicate pressure-reducing stations be provided, either one of which could back up the turbine. Each of these reducing stations is to be capable of passing 500,000 lb/hr of 2000-psi 1050-F steam to the 750-psi header and 1,000,000 lb/hr of 2000-psi 1050-F steam to the 150-psi header under automatic or remote manual control. When the turbine trips out, the changeover to reducing-station control must be fully automatic and take place without significant variation in process-header pressures.

Selection of Arrangement

Two general arrangements were considered; these could be called the series-flow and parallel-flow arrangements, Figs. 1 and 2. In smaller size turbines, the series arrangement, Fig. 1 is more commonly used, but the unusually large flow requirements for this turbine Unit No. 1, Linden Generating Station, Public Service Electric and Gas Company, New Jersey, made the series arrangement unattractive for several reasons.

The series-flow design requires control valves and a partial-arc-admission stage at the 150-psi level for a flow of about 1,500,000 lb/hr. These valves would be very large and the admission stage

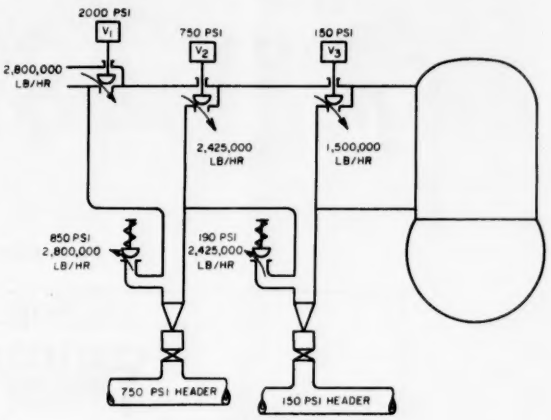

Fig. 1 Series-flow arrangement

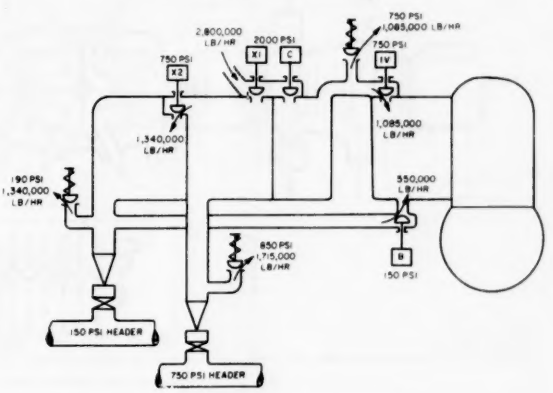

Fig. 2 Parallel-flow arrangement

Contributed by the Power Division and presented at the Semi-Annual Meeting, Detroit, Mich., June 15–19, 1958, of THE AMERICAN SOCIETY OF MECHANICAL ENGINEERS.

NOTE: Statements and opinions advanced in papers are to be understood as individual expressions of their authors and not those of the Society. Manuscript received at ASME Headquarters, March 27, 1958. Paper No. 58—SA-36.

would have to be double-flow to keep bucket-loading reasonable. The parallel-flow design, Fig. 2, requires control valves at the 150-psi level for only 550,000 lb/hr, and no partial arc-admission stage is involved. Also the required relief-valve capacity at 150 psi is reduced from 2,425,000 lb/hr to 1,340,000 lb/hr.

At the 750-psi level, the series-flow arrangement would require partial-arc-admission control of about 2,425,000 lb/hr as compared with 1,340,000 lb/hr for the parallel-flow design. It was necessary to control the remaining 1,085,000 lb/hr with intercept valves under overspeed conditions, but this is far easier than providing for full-time partial-arc-control of this steam.

The parallel-flow arrangement had the further advantage of being a natural one in view of the need for splitting the flow to keep bucket-loading to an acceptable level. The arrangement of turbine casings chosen is shown in Fig. 3. Fig. 4 shows the location of the various control valves and traces the path of the steam through the turbine.

The control valves for main steam are contained in two separate valve chests, one on each side of the double-flow turbine, just outside the foundation. The chest for the h-p extraction turbine contains six control valves, and the one for the h-p condensing turbine has seven valves, six of which are normal control valves and the seventh is a starting valve which feeds the first admission of each h-p section to insure proper flow distribution when starting. Each set of control valves is operated by a servomotor located in a base which supports the bearing housing between the l-p extraction turbine and the double-flow h-p turbine. The six 750-psi control valves are mounted in valve chests which are integral with the shell for the l-p extraction turbine. The servomotor for these valves is located in the same base with the two servomotors for the h-p valves. The two extraction-pressure regulators and the mechanical computer which positions all the valve servomotors are assembled on this base.

The energy stored in the cross-under from the h-p condensing turbine to the i-p condensing turbine represented an overspeed of $3^1/_2$ per cent. It was impossible to keep the turbine-generator speed below the emergency-governor trip setting on loss of maximum load with this large additional amount of entrained-steam energy. The only solution to this problem was to add intercept valves having a very fast closing time. These two valves are bolted to the top of the i-p turbine shell and are operated by servomotors located in a base which supports the bearing housing between the double flow h-p turbine and the i-p turbine.

The two bypass valves which admit 150-psi steam to the condensing turbine bolt to the crossover for the double-flow l-p turbine. The servomotors for these valves are located in the same base with the intercept-valve servomotors.

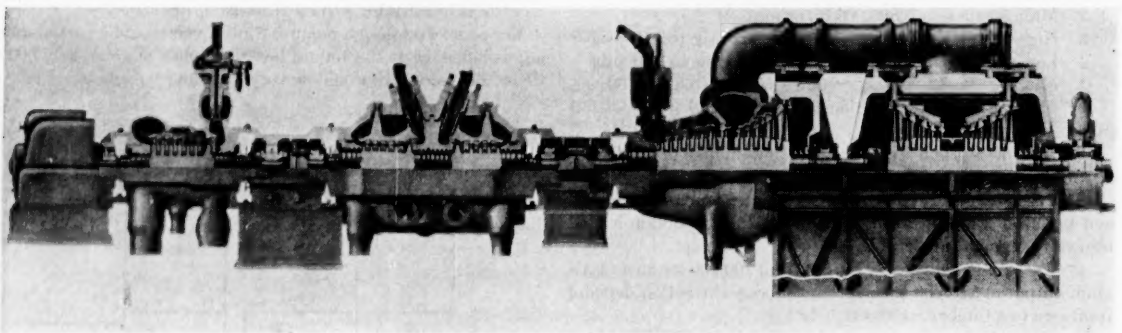

Fig. 3 Cross section of turbine

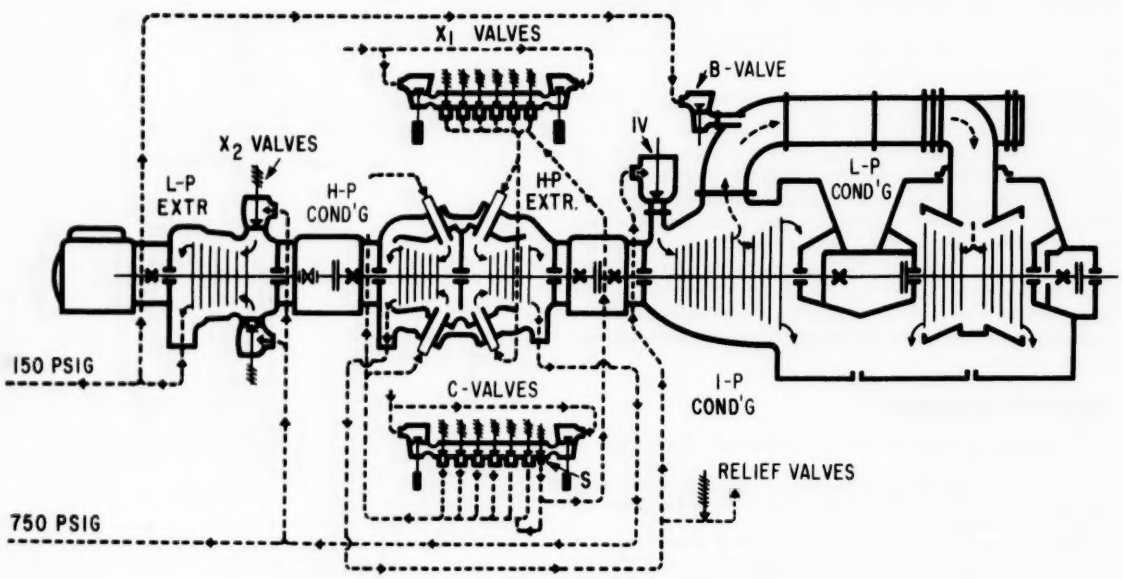

Fig. 4 Steam line diagram

THE TURBINE CONTROL SYSTEM

The Primary Functions of the Turbine Control

The turbine-control system is shown in much simplified form in Fig. 5. It consists of a multitude of control units which transmit their outputs either to a compound-lever system or directly to certain valves.

The main units of the control system grouped around the compound-lever system are:

1 The speed-load control unit
2 The h-p extraction-control unit
3 The l-p extraction-control unit

These three units satisfy the three controlled variables during normal operating conditions within a range in which no restrictive conditions on the turbine introduce limitations.

In order to make it possible to operate beyond this range at low loads and low extraction flows or at high load with small or no extraction, three more control units were necessary; they are:

4 The bypass-control unit
5 The condensing-section overheating protection
6 The extraction-section overheating protection

In order to protect the unit against overspeed and other incidents two more units are provided:

7 The pre-emergency control unit
8 The emergency-trip unit

The Function of the Compound-Lever System

The compound-lever system is the mechanical computer which takes the inputs of the various control units and combines them continuously in the proper manner to satisfy the output quantities or to limit them, if necessary, in order to maintain safe operating conditions. Certain points in this lever system have a very distinct significance which will be explained in the following, using the letter symbols of Fig. 5:

The point Z is controlled by the speed-control unit and its position is a measure of the load of the entire unit (except for a small uncompensated load produced by a flow through the bypass valve B).

The position of point Y represents extraction-section load and the point C is a measure of condensing-section load. The lever ratio of the load-compensating lever L is selected so that an increase in the position of Y produces a decrease in the lift of C to hold the load constant if the point Z is held fixed. (This action is referred to as load compensation.)

The point X is controlled by the l-p extraction-control unit and determines the position of the beam M on which the two angle levers for the control of the extraction turbine valves X_1 and X_2 are suspended. A rise of the position X will lift the points X_1 and X_2 simultaneously to increase the X_1 and X_2 valve flows by the same amount so that the l-p extraction flow will increase without affecting the h-p extraction flow.

If the point P_1 which is the output of the h-p extraction-control unit is lowered, the point X_1 will go up, thereby increasing the h-p extraction flow, but, since the h-p extraction pressure is held constant and the position of the X_2 valves stays fixed, the l-p extraction flow will not change.

The basic operation of the compound-lever system is shown in Fig. 6. For simplicity, the special operating conditions beyond the normal operating range have been disregarded and scales have been put at each point representing an operating quantity. These scales are calibrated in per cent of the maximum of each particular operating quantity.

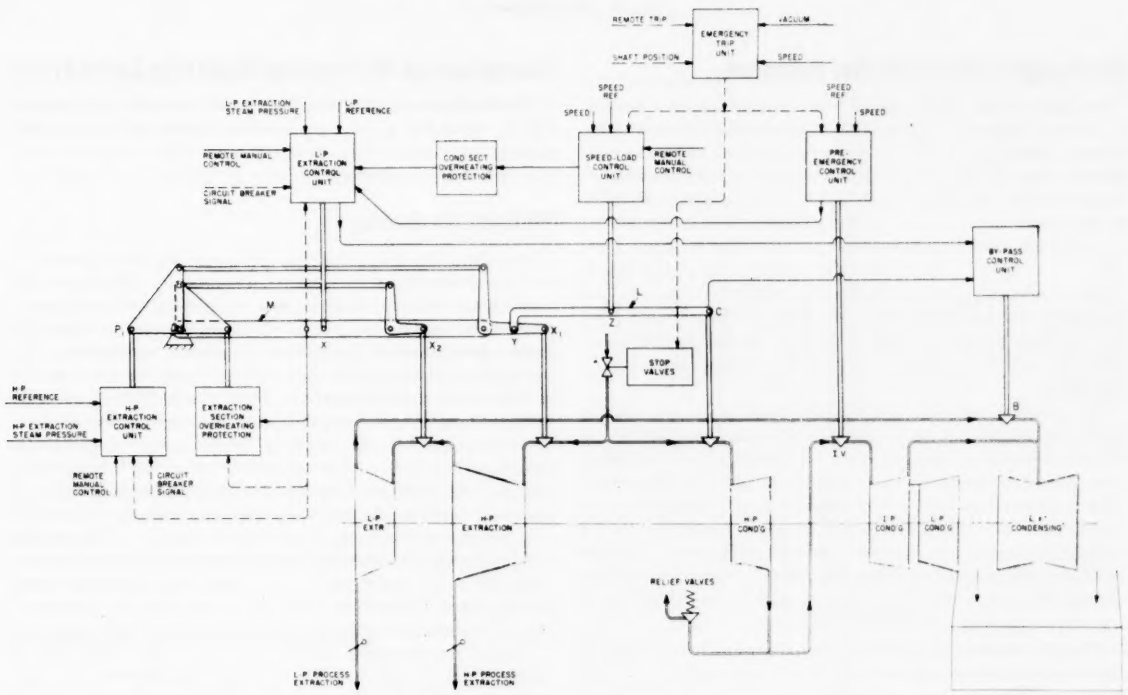

Fig. 5 Elementary block control diagram of turbine

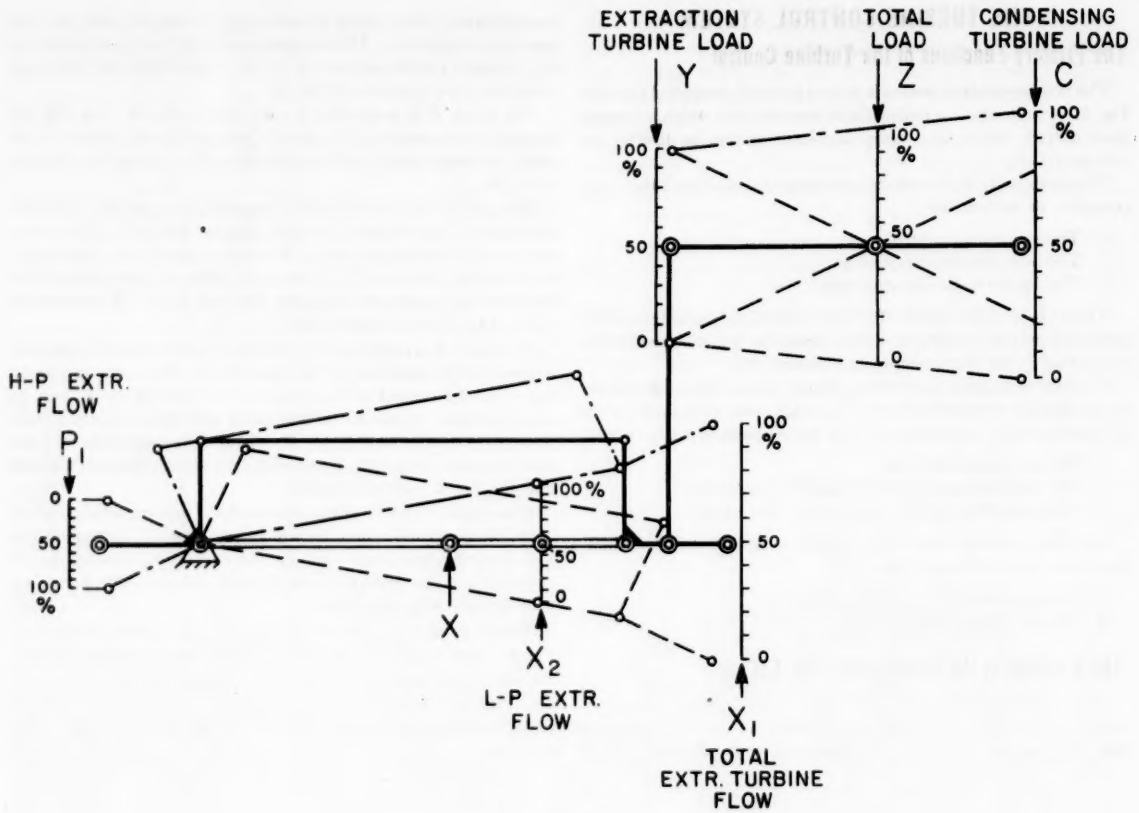

Fig. 6 Lever diagram

The Principle of the Overheating Protections

Because of the large size of the turbine steam passages, it became important to provide each turbine section with a certain minimum steam flow depending on the pressure level in the last stage of each section, in order to prevent overheating because of energy transformed into heat by rotation losses. In order to accomplish this, certain relaying systems had to be introduced which would prevent the steam flow in any section from going too low.

The condensing-section overheating protection monitors the position of the condensing valves and will take control away from the l-p extraction-control unit if the load demand should be insufficient to sustain a proper minimum flow through the condensing section.

The extraction-section overheating protection has a slightly more complicated task to accomplish. In order to permit the h-p extraction section to operate safely with the small no-load steam flow, it is necessary to lower the exhaust pressure of this section. This is achieved by the extraction-section overheating protection which will reopen the X_2 valves if the point X (output of the l-p extraction-control unit) is lowered beyond a certain level. By this method it was possible to reduce the necessary cooling steam flow through the h-p extraction section to slightly less than $^1/_4$ the amount required at rated extraction pressure.

The l-p extraction section is protected against overheating by the l-p extraction-control unit which will open the bypass valves if the l-p extraction demand should be insufficient to provide the necessary cooling steam flow.

Description of the Most Important Details of the Control System

The detailed control system is shown in block-diagram form in Fig. 7. As in Fig. 5, the h-p extraction turbine and the h-p condensing turbine have been switched in position in order to arrive at a clearer representation.

Provisions for Starting

In order to be able to start the unit a starting valve S operated by the servomotor for the C valves is provided. The S-valve admits steam to the No. 1 nozzle arcs of the condensing and the extraction sections across calibrated orifices in order to obtain the proper distribution of steam flows to prevent overheating. The necessary flow to the extraction section depends a great deal on the back pressure of this section. If the unit is started against the normal extraction pressure, the steam flow must be about 6 times as large as needed when starting straight condensing with the bypass valves open. An interlocking system which takes its input from the position of the l-p extraction gate valves will automatically position the orifice bypass valve and the bypass-control unit for either mode of starting the unit. The starting valve controls the steam flow to both sections of the turbine from standstill to full speed and to some small load after the unit is synchronized. Thereafter load can be increased by operation of the synchronizing device which will open the C valves only.

During this operation the X_1 valves are fully closed and the X_2 valves fully open. This position reproduces itself automatically if the two extraction-flow limits are tripped and the emergency-trip unit is reset. (Following loss of load this will also

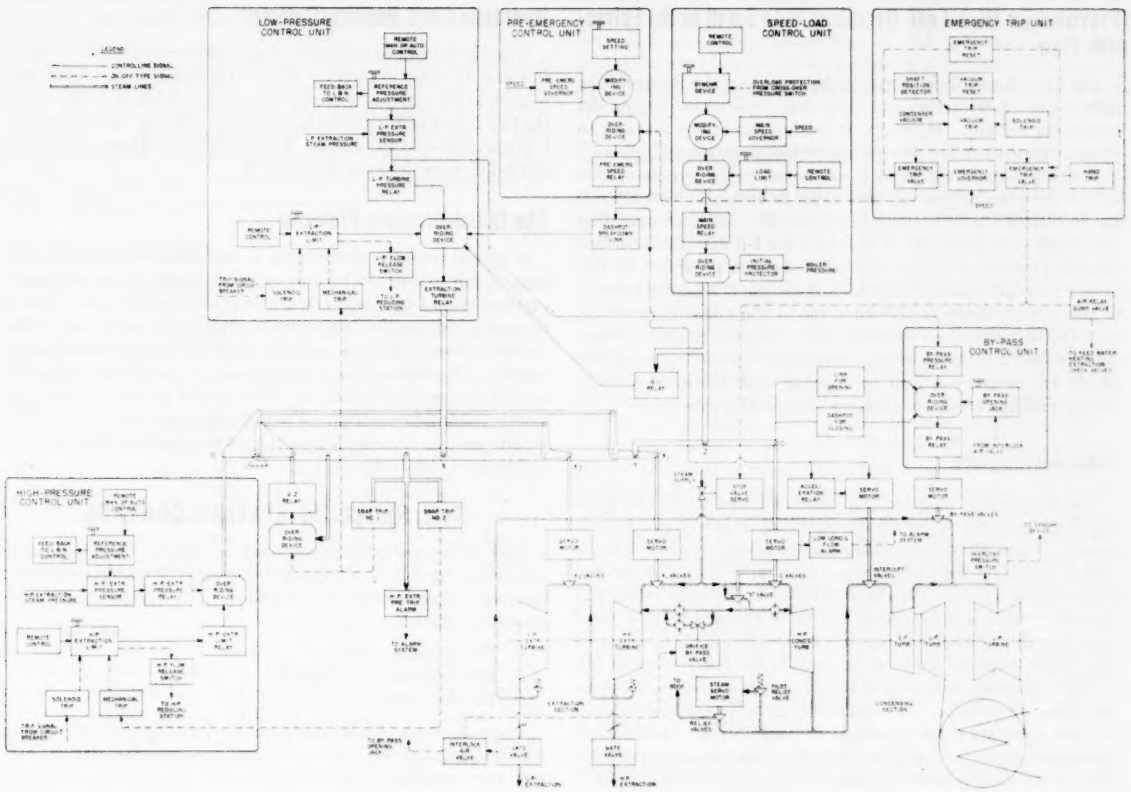

Fig. 7 Complete block control diagram

be the case because the snap trips No. 1 and No. 2 trip these extraction limits upon overspeed in excess of 5 per cent but they do not trip the emergency-trip unit.)

Provisions for Transfer of Extraction Flow

After the unit has been put on the line and is running at about $^1/_3$ load, the l-p extraction control can be put in operation, thereby transferring this flow from the reducing station to the turbine. This is done by opening the l-p extraction limit gradually with a slightly low setting of the pressure reference of the l-p extraction regulator. When the regulator takes over, the extraction limit can be screwed out of the way and the extraction flow increased by raising the setting of the reference of the l-p pressure regulator until the flow from the reducing station is zero.

Subsequently, the h-p extraction-control unit can be put in operation in a similar manner.

In case the turbine loses the load and, thereby, trips both extraction limits, a signal from each extraction limit will energize a flow release (to be discussed under the reducing-station control) at the respective control of the reducing station, and transfers the flow to the reducing station with only a minor pressure swing in either process-extraction line.

Provisions for Constant Pressure Control

Since both extraction-pressure regulators may be compelled to operate in parallel with either reducing station, it is necessary that they have a positive regulation (droop). Because of this feature, the extraction pressure would vary slightly with flow unless supplementary correction is made. Leeds and Northrup controllers are therefore provided which will reset the pressure reference on each regulator to obtain a constant steady-state pressure at the Public Service property line. Similar controllers and a fully automatic transfer system are used in connection with both reducing stations. These will be discussed under the description of the reducing station.

Acceleration-Responsive Intercept-Valve Control

Because of the large output of the unit with a relatively small rotor inertia this unit accelerates to 10 per cent overspeed in 0.68 sec, if full load is lost on the generator. Since the intercept valves are in control of the largest portion of this accelerating energy it was decided to use an acceleration-responsive control device to get these valves closed quickly upon accelerations in excess of 1 per cent/sec. The acceleration relay as used on this unit is described in Appendix 1.

Overpressure Protection of Cross-Under

The presence of the intercept valves after the cross-under of the condensing turbine made it necessary to provide a full complement of relief valves on this line. For this relatively small volume, normal pop valves could not be used because they would inherently chatter if called upon to relieve steam from this small storage vessel. In co-operation with Crosby Ashton, a set of pilot-operated relief valves was developed and tested and, on the occasion of several load-dump tests, these valves operated very satisfactorily.

Provision for High-Load Operation With Small or No Extraction Flow

The bypass system is primarily designed to make it possible to deliver less l-p extraction flow than that required for cooling the extraction section. However, it has an important function to obtain high load on low or zero-extraction operation.

For this purpose the point C can influence the bypass-control unit to open the bypass valves in order to obtain at least 225,000 kw no matter what the extraction flows are. For such operating conditions it is necessary to maintain the l-p extraction-turbine exhaust pressure at the normal process-steam pressure. If this pressure should become higher for any reason, it would be possible to admit more steam to the crossover of the condensing section than the l-p section can safely handle. In order to prevent such misoperation a pressure switch is provided on the crossover line which will reduce the load by running back the synchronizing device until the crossover pressure returns to a safe value.

Main Servomotors

The three sets of main control valves, labelled C, X_1, and X_2 in Fig. 2 are operated by servomotors of large capacity and fast response. These servomotors are a double-acting type which make high demands on the main pump during rapid closing or opening of the control valves. The distance between the main pump and the servomotor is appreciable and large changes in flow must occur rapidly to effect the necessary control action. These factors required that special provision be made in the design to avoid undesirable pressure transients in the oil system during rapid operation of the servomotor. The special-design servomotors developed for this application are described in Appendix 2. Oscillograph tests made when the unit was on factory test showed that there were no undesirable pressure transients in the hydraulic system.

Hydraulic Shaft-Position Detector

A newly developed hydraulic shaft-position detector is used on this unit in order to monitor the axial position of the shaft with respect to the stationary parts. If excessive wear of either one of the two thrust plates should take place, it will trip the emergency-trip unit and shut the turbine down instantly. This device is described in more detail in Appendix 3.

The Initial-Pressure Protector

A special pressure protector is incorporated in the speed-load control unit to close the turbine valves gradually in case the boiler pressure should drop below 90 per cent of rated pressure. This is necessary because the flow capacity of all valves connected to the boilers is about twice the capacity of all three boilers feeding the system. Considering the huge capacity of the process-extraction lines it is conceivable that all valves would go open at the same time by some misoperation. The initial-pressure protectors on the turbine and on the reducing station are designed to protect against incidents of this sort.

THE REDUCING STATION CONTROL

Each of the two reducing stations is equipped with an h-p and an l-p section capable of supplying steam into the respective process headers. Each section is controlled by a control unit which consists of the following elements:

1 The pressure regulator
2 The flow-limit mechanism
3 The flow-release mechanism

These elements plus the output of the initial-pressure protector, which is common to both sections of one reducing station, control the respective servomotors across an overriding device,

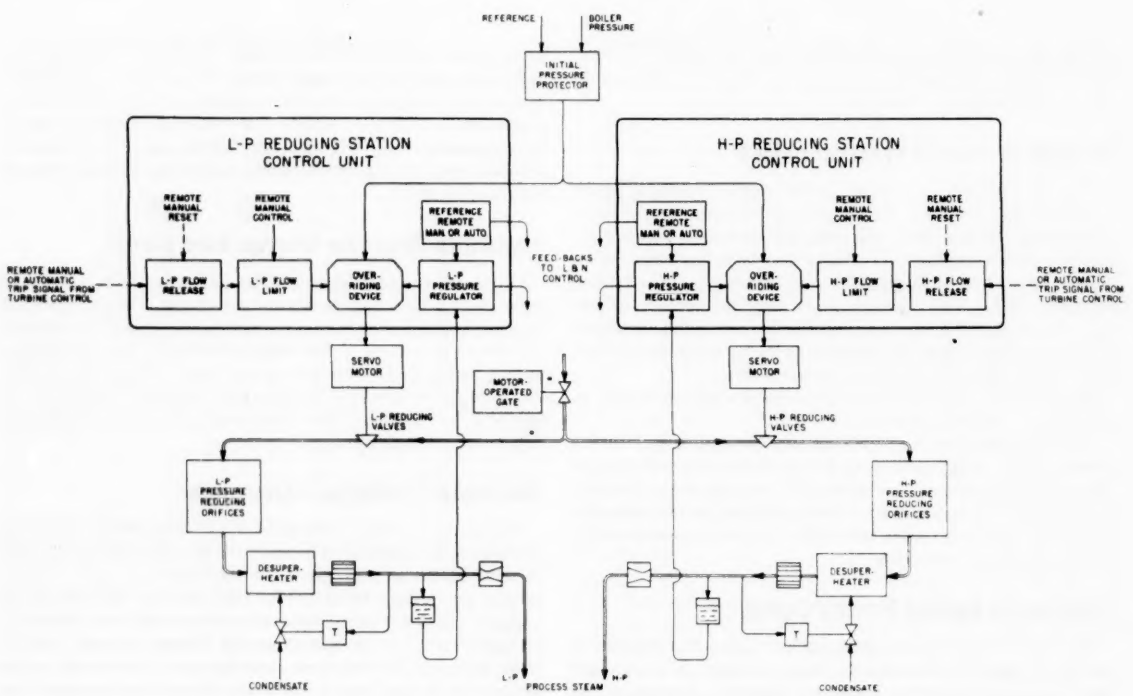

Fig. 8 Reducing station block control diagram

whereby the control input calling for the lowest position of the reducing valves will effectively control them. This system is shown in Fig. 8.

The steam which passes through the valves is further reduced in pressure across reducing orifices designed to limit the noise level; then it is desuperheated by controlled water injection (by Swartwout). Afterward the steam passes through a flow straightener and a flow-measuring nozzle. The sensing line for the pressure regulator is connected to the process-steam line between this flow straightener and the nozzle.

The Pressure Regulators

These reducing stations were to stand idle for extended periods of time during which the turbine would furnish the entire extraction flow. Special emphasis was therefore placed on control components which would not stick under such conditions. The pressure regulators are designed with an oil-jet pilot control instead of a conventional pilot valve. The principle of the stationary jet, influenced by a knife-blade-shaped jet deflector was patented in 1930 by Escher-Wyss of Zurich, Switzerland, and has since been widely used. A high-accuracy regulator of this type was built by the author's company in 1955, for the Turbine Development Lab. The regulators on these reducing stations represent the first industrial application of this principle in this country. A short description of the important features of the jet-relay pressure regulator can be found in Appendix 4.

The Flow Limit

This is a remote manually controlled device which permits operation of the valves from the control room. It overrides the pressure regulator toward the closed position of the valves. This device is used to manually control the reducing-station flow as long as neither the pressure regulator nor the flow release (to be described) is in control.

It is also used to transfer extraction flow to and from the reducing station in an orderly manner without sudden surges of steam flow.

The Flow Release (Stand-by Operation)

This mechanism was provided in order to make it possible to transfer steam flow to the reducing station automatically in case of sudden loss of extraction flow on the turbine. The flow-release mechanism will hold the reducing-station valves closed on stand-by operation. Upon an electrical signal from the turbine the release can be tripped, whereupon the respective valves will open quickly to the position given by the pressure regulator (or the flow limit). Since the pressure regulator is constantly readjusted to have a position corresponding to the extraction flow (by an L and N flow-positioning control) the valves will open to the proper position to provide the necessary process-steam flow automatically without any action of the operator.

The flow release can be reset and tripped manually from the control room.

Emergency Operation

While one reducing station is usually on stand-by operation the second reducing station is put on emergency operation by setting the references to both pressure regulators below the existing process-steam pressure. This will hold the valves closed by means of the position of the pressure regulators. The flow-release mechanism will be tripped and the flow limit run open to a position corresponding at least to the existing process flow in each line. If the extraction flow from the turbine should be lost and for any reason the stand-by station should fail to cut in, the pressure in the headers will drop sufficiently to open the valves of the emergency station which will then provide the flow at a preset lower pressure.

In order to keep the steam lines of both reducing stations hot while they are on stand-by or emergency operation, a small steam flow is maintained through both stations across small holes in the valve disks.

Fire-Resistant Operation Fluid

The operating fluid for the reducing stations is a fire-resistant lubricant of the phosphate-ester type. The particular type chosen was Monsanto OS-58-1 which was developed for steam-turbine service. It has a specific gravity of 1.3 and undergoes considerably more viscosity change with temperature than petroleum oils do. The fluid is an effective solvent and dissolves or softens most paints and varnishes. The hydraulic system for the reducing station was designed to accommodate these characteristics. Provision was made for heating the oil electrically in cold weather and cooling it with air-cooled heat exchangers in hot weather under thermostatic control to keep the fluid within a satisfactory range of viscosity. Because of the large specific gravity this fluid behaved quite differently from normal oils in the jet regulators where the flow in the jet nozzle was very close to the critical velocity. In order to assure consistent laminar flow, special care had to be taken to design the ejecting nozzle for disturbance-free inlet flow. The centrifugal pumps were designed to produce the desired pressure with a fluid having a specific gravity of 1.3, but the casings were made large enough for an impeller which would give the same pressure with turbine oil in case the fire-resistant fluid proved unsatisfactory. There has been no need to use this feature because the performance of the fluid has been entirely satisfactory. Early trouble with foaming of fluid has been eliminated.

Experiences With the Control System During Initial Start-Up

The complexity of this control system made it advisable to carry out an extensive test program during the start-up period in order to prove that the system would properly perform all functions for which it was designed.

Points of particular interest which had to be verified were:

1 Performance of the overheating protections over the entire load and extraction-flow range

2 Transfer of h-p and l-p extraction flow from any reducing station to the turbine manually or from the turbine to the reducing station manually or automatically

3 Stability of speed-load control

4 Stability of h-p and l-p extraction-pressure control by the turbine independently or in parallel with the pressure regulators of the reducing stations

5 Performance on loss of load

Performance of the Overheating Protections

After a small number of adjustments on the control system, the unit performed at temperatures very close to those predicted at low load and zero or low-extraction flows. Under normal conditions it is not expected that the operators will have to take steps to prevent overheating. For abnormal operating conditions which could not be anticipated, the operator still has the possibility of opening the bypass valves manually to obtain lower pressures in the extraction section if this should become necessary.

Transfer of Extraction Flow

Any time the turbine is started up while one of the reducing stations is supplying the process steam, it is necessary to transfer the flow from the reducing station to the turbine manually. This operation was quite easily performed and all equipment operated

as expected. The same is the case for manual transfer from the turbine back to one of the reducing stations.

The automatic transfer from the turbine to the reducing station which takes place when the load on the turbine is reduced suddenly or gradually was tried out several times, in particular at the occasion of load-dump tests which will be discussed later.

Stability of Speed-Load Control

The speed control at no load was originally slightly unstable. This was corrected by a change in slope of the cam of the *S*-valve. The large volumes between this valve and the first-stage nozzles of the h-p extraction and condensing turbine had a larger destabilizing effect than was anticipated. After an increase of the incremental regulation to about 12 per cent at the synchronizing point, the no-load control was stable.

The load control did not present any difficulty at any time.

Stability of Pressure Control

Artificial disturbances were introduced by changing the pressure references on one or simultaneously on two pressure regulators of the turbine or at a reducing station. Even more abrupt disturbances were imposed on the system by temporarily overpowering the pressure-sensitive elements of a regulator and then releasing it. Under all these conditions the control was stable and operated as expected.

Performance on Loss of Load

The load-dump tests were made to prove the adequacy of several devices:

1 Performance of speed control on fast acceleration
2 Performance of the cross-under safety valves
3 Performance of the automatic extraction-flow transfer equipment
4 Performance of the overheating protections

Several tests were made at loads ranging from 60 mw to 225 mw. The results of the full-load dump test (225 mw) were as follows:

1 The peak speed was very close to 109 per cent of rated speed (average of two independent speed measurements was 108.7 per cent, however, peak-speed measurements are always difficult to take accurately). The predicted peak speed was 108.9 per cent.

2 The cross-under safety valves opened for some 30 sec without any tendency to chatter or cycle. Their performance was excellent.

3 The extractions were automatically transferred to the stand-by reducing station with a pressure swing of about 20 psi in the h-p process-steam line and about 5 psi in the l-p line. These pressure dips were of such short duration that the refinery personnel did not even notice when the test was performed.

4 At no time during the load-dump tests was there any excessive temperature experienced in any part of the turbine.

Conclusion

The complexity of the problems which had to be solved for the design of this control system represented a real challenge to the designers. This fact is emphasized by the lack of any existing control system which could be used as a reference for this new design. It was, therefore, the desire of the authors to have this system fully checked out and in commercial operation which would prove its inadequacy before reporting on it.

It is believed that this system is a good example of what can be achieved with hydraulic mechanical controls of very high force level and response speeds. It also showed that computing functions of which some are given by limits rather than continuous functions, can be handled by an adequate lever system in conjunction with the necessary hydraulic amplifiers.

Another important consideration was the step toward automatic interconnection between the turbine-control system and the reducing stations. The builder of this interconnecting system, Leeds and Northrup, will report separately on that part of the installation.

Acknowledgments

The authors would like to express their appreciation to Public Service Electric and Gas Company for the opportunity to work out this unique system and also to Leeds and Northrup and Crosby Ashton for their co-operation in solving the common problems for this plant.

NOTE: When this paper was written the authors included information and expressed opinions believed to be correct and reliable. Because of the constant advance of technical knowledge, the widely differing conditions of possible specific application, and the possibility of misapplication, any application of the contents of this paper must be at the sole discretion and responsibility of the user.

APPENDIX 1

Acceleration-Responsive Intercept-Valve Control (Fig. 9)

The intercept valves are operated by the output of the pre-emergency control unit. This output has a position which is inversely proportional to speed (except for a small lag), and its rate of position change is, therefore, equivalent to acceleration. This rate of position change is compared to a constant rate of position change of an oil-filled dashpot, which can be adjusted to the desired value. As soon as the rate of change of the pre-emergency speed relay exceeds the set rate on the dashpot, the

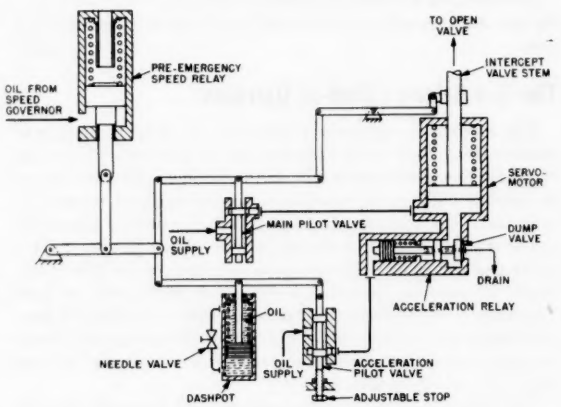

Fig. 9 Acceleration relay

"acceleration pilot valve" operated by a lever on the dashpot which computes the difference between the two rates, will open a dump valve on the servomotor for the intercept valves and will close them in less than 0.2 sec.

After the acceleration has subsided the dashpot will bring the acceleration pilot valve back in its normal position onto the stop. This will reclose the dump valve and make the intercept-valve servomotor responsive to movement of its main pilot valve for speed control again.

Extensive tests with this device have shown that its response to acceleration is very close to the expected performance.

APPENDIX 2

Special Balanced-Flow Servomotor

The control-valve servomotor design normally used by the authors' company is shown in Fig. 10. It is a double-acting type having a skirted piston with area B on the closing side equal to about one half of area A on the opening side. This difference in area is used to reduce by one half the oil flow required to close the valves in a given time. However, its use results in an unbalance in flow taken from and returned to the pump during motion of the operating piston.

During a closing stroke, for each gallon of oil fed into the servomotor 2 gal are discharged. If all of this oil were forced back into the main pump inlet, the inlet pressure would rise sufficiently to increase the servomotor-stroke time. Therefore a relief valve is added at the pilot-valve discharge to spill out the excess.

During an opening stroke, for each gallon fed into the servomotor, $^1/_2$ gal is returned to the pump inlet. This causes the pump-inlet pressure to fall and the result is a definite limit in servomotor-opening rate. With three large servomotors to feed, this limitation resulted in undesirably slow opening rates.

The balanced-flow servomotor shown in Fig. 11 was developed to overcome the limitations of the normal design. An additional piston having an area equal to A minus B is added, and either injects oil into the pilot-valve discharge line or takes oil away so as to equalize the net oil flows to and from the servomotor. On a closing stroke it absorbs the extra gallon discharged from the opening side of the servomotor and on an opening stroke it supplies the missing $^1/_2$ gal.

Both Figs. 10 and 11 show a shock-relief valve between the inlet and discharge headers for the servomotor. This protects against the oil hammer which would result when flow is suddenly stopped by reporting of the pilot valve or stopping of the operating piston at the limit of its stroke.

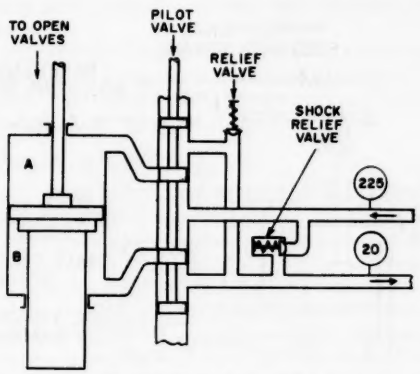

Fig. 10 Normal servomotor

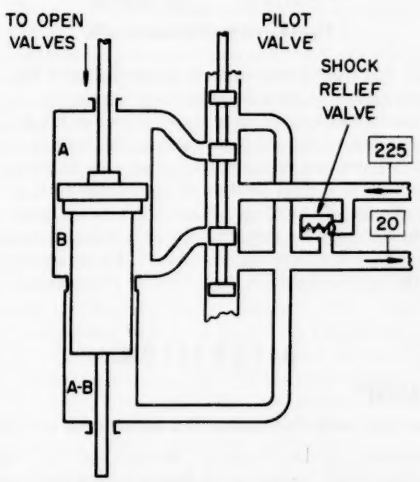

Fig. 11 Balanced-flow servomotor

APPENDIX 3

Hydraulic Shaft Position Detector (With Electrical Tripping of the Unit, Fig. 12)

By means of a follower piston, 1, this device continuously and accurately detects the axial position of the turbine shaft with respect to the thrust-bearing casing. The position of this follower piston is transmitted to the pilot valve, 2, which controls the pressure to two independent pressure switches, 6 and 7. The pilot-valve feed pressure is 200 psig, and the pressure switches 6 and 7 are set to trip at 50 psig. This results in a characteristic of the device which is shown in Fig. 13. The trip points shown are 42 mils to either side of the set point (neutral). Since the thrust-bearing clearance is usually 12 to 20 mils, this leaves about 30 to 35 mils as wear margin before the relay will trip the unit. The follower piston is a hydraulic force amplifier which is widely used in turbine-control systems of various manufacturers. It operates by means of a differential piston with a given area ratio (approximately 1:2). Operating oil is admitted to the small piston area and passes to the large area across a calibrated orifice O. From there the oil continues through a snout which rides on an oil film of constant thickness F against a collar C on the shaft. In order to obtain equilibrium on the follower piston, 1, the flow area F must be substantially equal to the orifice area O which is fixed. Thus F is, for all practical purposes, constant regardless of oil pressure and viscosity. A small spring S prevents the follower piston from rubbing against the shaft when oil is shut off.

The testing mechanism, 3, is capable of positioning the bushing, 4, axially so that the operation of the pilot valve and the pressure switches can be tested during operation. The displace-

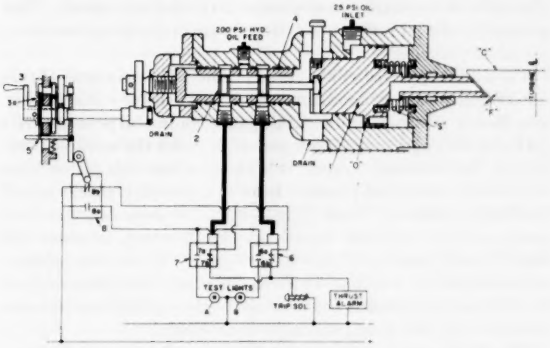

Fig. 12 Shaft-position detector

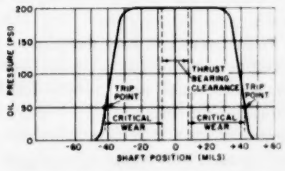

Fig. 13 Characteristic of shaft-position detector pilot valve

ment of bushing, 4, can be read accurately on a vernier dial, 3 (*a*), at the test station. In order to prevent tripping of the unit, while testing, a lock-out switch, 8, is used to open the trip circuit and to close the test-light circuit. This switch is operated by the locking lever, 5, which must be pulled to release the testing mechanism. The switch, 8, will reset automatically when the testing mechanism is returned to neutral position. The testing mechanism is also used to measure the thrust-plate wear by comparison of test records. Initially, the testing mechanism serves to set the device in correct position.

APPENDIX 4

Oil-Jet Relay Pressure Regulator

Principle. The heart of the oil-jet relay regulator is, as its name implies, an oil jet. This oil jet originates in an ejecting nozzle from which it proceeds across the free air to the receiving nozzle which is of the same diameter as the ejecting nozzle. Approximately in the middle, the free oil jet is influenced by a jet deflector in form of a knife edge, suspended on the pressure-sensitive element of the regulator. Fig. 14 illustrates the operation of the oil jet.

In Fig. 14(*a*) the oil jet is shown not deflected, Fig. 14(*b*) represents the oil jet approximately half-deflected, and Fig. 14(*c*) illustrates the jet entirely deflected whereby the jet is not hitting the receiving nozzle at all.

The ejecting nozzle is shown in Fig. 14(*d*).

The continuous characteristic of the oil jet illustrated in Fig. 14 in three steps is shown in Fig. 15 where the oil pressure of the receiving nozzle is plotted versus the active deflector travel in mils. At zero deflector travel a pressure of 95 psi exists in the receiving nozzle which is in other words an efficiency of 95 per cent of the transmission of pressure from the ejecting nozzle to the receiving nozzle. As the deflector approaches 5 mils the receiving-nozzle pressure starts falling off in a practically straight line, reaches 50 psi at approximately 9 mils, curves over to the other side at approximately 14 mils, and becomes zero at about 18 mils. The shape of this curve looks very much like a characteristic of a simple triode vacuum tube if current is plotted against negative grid voltage.

The oil stream exerts a small reaction force on the jet deflector. This force is essentially proportional to the deflector travel. The gradient of the jet reaction is extremely small and proportional to initial oil pressure.

The oil jet operates a differential piston. The area ratio of this differential piston is approximately 2 to 1 whereby the smaller area (below piston) is under the constant-control oil pressure (100 psi) and the larger area (above piston) is under the variable pressure of the receiving nozzle. It is obvious that this piston is at equilibrium when the pressure from the receiving nozzle is half the initial pressure. From Fig. 15 it can be seen that this happens at 9 mil deflector travel which, therefore, becomes the steady-state position of the jet deflector. If the jet-deflector travel is more or less than 9 mils the pressure on the large side of the differential piston is below or above the equilibrium pressure and therefore the piston will move accordingly.

Since the operation of the jet deflector requires very little force, the pressure-sensitive elements can be made relatively small. Bourdon tubes or bellows are used depending on the level of the controlled pressure.

Jet Relay With Proportional and Rate Feedback. For this application the basic components of the jet relay were used in combination with a proportional and a rate feedback. This is schematically shown in Fig. 16.

The proportional feedback is accomplished by a spring which exerts a force back onto the Bourdon tube proportional to relay-piston travel. The proportional feedback is necessary in order

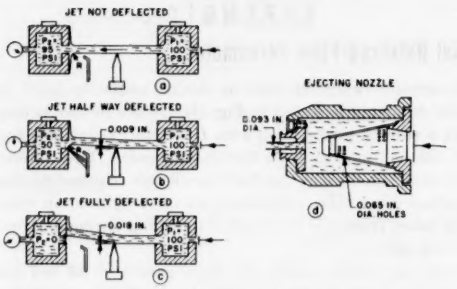

Fig. 14 Operation of oil jet

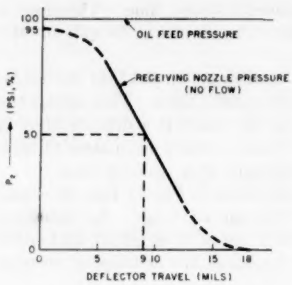

Fig. 15 Characteristic of jet

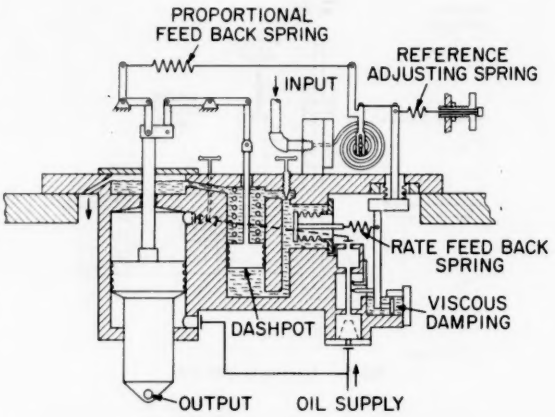

Fig. 16 Jet-regulator schematic

to permit this regulator to operate in parallel with the turbine-pressure regulator or with the other reducing station.

The rate feedback is obtained by a dashpot which is mechanically connected to the relay piston and will influence the rate feedback bellows and spring in the proper way to return the jet deflector back to normal position in accordance with the rate of position change of the relay. While the rate feedback was not obviously necessary for this application, it was still incorporated in order to have the necessary provisions if, for some unforeseeable reason, the control should be unstable with proportional feedback only.

DISCUSSION

W. C. Astley[1]

It has been said that praise of a paper does not constitute

[1] Philadelphia Electric Company, Philadelphia, Pa. Chairman, Joint AIEE-ASME Committee for Recommended Specifications for Prime Mover Speed Governing. Mem. ASME.

discussion. The writer fears that this is the situation we now face. The authors have given a detailed account of the solving of an intricate control problem. The solution is obviously well thought out and has been presented in a concise and lucid manner.

The performance of the control system upon sudden and complete loss of load is of interest. Because of the large quantities of steam involved and the small rotor inertia, the problem of controlling overspeed so that the unit will not trip out is extremely difficult. That this can be done within the time available (0.68 sec) is an accomplishment.

It is true that the Recommended Specification for Speed-Governing of Steam Turbines Intended to Drive Electric Generators Rated 500 Kw and Up, as issued in May 1, 1949, specified that upon the sudden and complete loss of turbine power output, the speed-governing system shall be capable of controlling the overspeed of the turbine to a value that is less than the specified setting of the emergency governor. A revision of that specification now being considered by ASME and AIEE contains the same provision. It is of interest to note that when the revision was presented at the AIEE Fall General Meeting in 1957, a representative of an operating company questioned the necessity for such a provision. Apparently opinion among operators is divided. Some operating companies require that the turbine-generator unit must satisfy this provision during the acceptance tests of the unit. Other operating companies shy away from a full-load dump test and use a simulated-load dump test when the machine is not connected to the bus. Still others do not test for this provision.

The authors deserve a great deal of credit for the design of this control system, for its satisfactory operation in meeting all the requirements of the Recommended Specification, and for the excellent paper they have presented.

J. D. Conrad, Jr.[2]

The authors are to be commended for an excellent presentation and a noteworthy contribution to the art of steam-turbine design.

The paper gives a very clear and concise picture of the many problems involved in designing a satisfactory control system for a double-automatic-extraction turbine of large capacity.

One of the problems, quite adequately handled, is that of finding a satisfactory turbine arrangement which will permit the high inlet steam flows for both large and small kilowatt loads and still allow the use of reasonably sized control components such as steam valves and valve-operating mechanisms.

With the use of higher steam temperatures and pressures and with the advent of more efficient generator-cooling methods, the capacities of turbine-generators have increased considerably while the moment of inertia WR^2 of the rotating parts has decreased. As brought out by the authors, this has increased the problem of overspeeding following a large loss of load. To combat this problem, acceleration-responsive relays similar to those used on the subject machine have become essential elements of the turbine-control system.

In line with the problem of overspeeding, it is important that the volume of entrapped steam be kept as low as possible thereby reducing the peak speed of the turbine following a complete load loss.

As stated by the authors, a necessary requirement of any automatic-extraction turbine is good load compensation. The consistency with which the authors' company has used the compound lever system as a computer for positioning steam valves is to be commended. However, with the advent of larger units with higher temperatures, it appears that expansion of linkage might present a problem. It would be interesting to know how the subject machine performed with respect to load compensation.

A seldom realized but important point regarding the large momentary demands on the main oil pump when fast servomotor action is required is brought out by the authors. The need for "balanced-flow" type servomotors has become a necessity in order to maintain a reasonably sized main oil pump and at the same time keep pump-pressure fluctuations at a minimum when fast servomotor action is required. This has been an industry-wide problem where large fast-acting multiservomotors are required and has been solved successfully in a somewhat similar manner.

In conclusion, the paper brings to light a field in which a public utility company and an industrial process company can cooperate to mutual advantage in producing both electric power and process steam, provided that they have an accurate knowledge of their requirements and a clear understanding of the limitations of steam-turbine designs.

L. W. Lemon[3]

The authors are to be complimented for a well-planned, concise presentation of this complex control problem. The principles of hydraulic control employed on No. 1 turbine-generator unit and the pressure-reducing stations at Linden testify admirably to the art of power-plant automation. It should be mentioned here that the control systems must be extremely reliable because the extraction turbine and associated pressure-reducing stations are the only sources of supply to a neighboring refinery.

Of particular interest is the authors' discussion of the following aspects of this problem:

1 Load and extraction-flow capabilities.
2 Provisions for starting the turbine-generator unit.
3 Automatic transfer of extraction from turbine to pressure-reducing station.
4 Provisions for remote operation of equipment.

A unique feature specified in the design of the machine is its ability to maintain 225,000 kw load when process-steam flow is reduced to zero. This is accomplished through the bypass control which automatically routes steam from the exhaust of the low-pressure extraction element to the condensing turbine.

Regarding the "Control Specification," we believe it is not the authors' intent in item 9 to infer that the control system places an arbitrary lower limit of 100,000 kw on machine output, which is determined by turbine-design characteristics.

Starting-up of this turbine-generator unit is usually accomplished against 150-psi back pressure in the low-pressure process header. For warming purposes, a motor-operated bypass valve from one 150-psi process line routes steam around the nonreturn valve and into the exhaust of the low-pressure extraction turbine.

The automatic transfer of extraction flow from the turbine to the reducing station has proved satisfactory. The pressure-regulating elements have demonstrated a regulation accuracy of $1^1/_2$ per cent in maintaining steam pressures at the property line.

The process-steam controls are designed for full automatic operation in response to pressure measurements at the property line or for remote manual operation from the central control room. Also there are at the turbine duplicate extraction-pressure regulators and flow-limit devices, with appropriate gages, to permit local operation of process-steam controls in the event of electric control-circuit failure.

Certain operating difficulties described in the following were encountered during initial operation of controls:

[2] Design Engineer, Westinghouse Electric Corporation, Philadelphia, Pa. Assoc. Mem. ASME.

[3] Mechanical Engineer, Electric Engineering Department, Public Service Electric and Gas Company, Newark, N. J. Mem. ASME.

1 Split-series-field control motors were specified for the reducing stations. The pressure-regulator motors were shunted heavily to reduce their speed to 200 rpm and avoid overshooting of the regulators. Two of these motors burned out as a result of cycling of the control which was not corrected until the dead band on the Leeds and Northrup controller was set up to 20 per cent. New lead screws built into the pressure-changer mechanism to permit higher motor speed, and motor-circuit interrupters permitted us to discard the speed-control resistors and decrease the field current to normal. This resulted in elimination of the 20 per cent dead band with good stability in the pre-positioning control.

2 The turbine-generator governing mechanism is run back if steam pressure in the low-pressure crossover pipes becomes excessive. Means for testing this protective device with the machine in service are provided. During one such test the contacts in the pressure switch were held closed by wiring under the switch cover which resulted in a run-back of load from 200,000 to 10,000 kw. Subsequent modification to the switch and enclosed wiring has eliminated this fault.

3 The pressure-reducing valves are enclosed by unheated, walk-in housings. The valves operate from a camshaft, rocker arm, and oil servo-arrangement similar to conventional turbine-control valves. The original camshafts of carbon steel were replaced with stainless-steel materials in an effort to eliminate corrosion and the threat of binding in their bearings, there having been some tendency of the camshafts to stick. Following the turbine-generator load dump described in (2), the operators attempted to cut in the reducing station manually, the automatic controls not being available at the time. The camshaft on the 750-psi valves stuck and had to be jacked free by hand before the valves would open. Sticking of the camshaft was remedied by General Electric Company after it was discovered that it was binding in its bearings and one intermediate bearing was removed.

The foregoing are considered to be no more than the usual difficulties which are usually found and must be overcome in putting new apparatus in operation.

We reiterate the authors' statements regarding the fine performance of the double-automatic-extraction-control system. The smoothness of transfer to pressure-reducing-valve operation on full-load drop on the turbine is testified to by the inquiry of refinery personnel some time after scheduled test: "Has the transfer taken place?" This was indeed the highest compliment that could be paid to the men who developed, designed, and now operate this control.

Author's Closure

Concerning Mr. Conrad's comment about expansion problems with respect to load compensation it can be said that a slow shift in load during starting may be encountered because of such phenomena. This seems unimportant because the load is intentionally varied (increased) during this period. In normal operation the expansions, though large, do not change much and, therefore, the load compensation is about as good as the lever system can make it.

With respect to Mr. Lemon's comment about the load specification (item 9), the mentioning of the 100,000 kw as lower limit refers to operation with maximum extraction flow which was thought to be inferred in the latter part of the sentence in item 9.

The difficulty with the split-series motors of the pressure changers at the reducing stations was due to heavy overloading of the fields of these motors due to the heavy shunting. This way of slowing down control motors seems definitely not advisable. The change of the lead screws was only a minor improvement; the intermittent contactor was the real corrective measure.

The authors of the paper would like to express their appreciation for the discussion offered by the three discussers. The widespread interest in this unconventional installation, manifested by a large circle of the power industry, was indeed gratifying.

Design of 321-Mw Cross-Compound Steam Turbine—River Rouge Unit No. 3

C. D. WILSON

Chief Turbine Design Engineer, Steam Turbine Department, Allis-Chalmers Manufacturing Company, Milwaukee, Wis. Mem. ASME

This paper discusses the design features and general arrangement of a 321-mw close-coupled cross-compound 3600/1800-rpm steam turbine-generator unit. The machine is designed for operation with subcritical pressures and with steam temperatures that permit using ferritic materials. It was the first machine to be ordered in the 300-mw size range and is installed in the River Rouge Station of The Detroit Edison Company.

Introduction

THE DETROIT EDISON COMPANY was the first public utility to order a steam turbine-generator unit in the 300-mw size range. This first machine has a nameplate capability of 321 mw and is installed as the No. 3 unit in the River Rouge Station. It is a close-coupled cross-compound design[1] similar to many smaller cross-compound units of the author's Company in service since 1953. However, the much larger rating of the River Rouge machine created many new design problems that required extensive study and investigation. Major problems included the efficient handling of the large volume steam flow, while keeping floor space requirements to a minimum. The preservation of the same degree of operating stability in a large machine that is presently available in the smaller conventional units had to be maintained as well as the ability to ship and service the larger components without difficulty. This paper describes how these requirements have been satisfied in the design of the No. 3 machine for River Rouge.

Operating Cycle

The River Rouge turbine is used in a seven-heater cycle, as shown in Fig. 1, with provision for extra extraction for air preheating at the No. 5 heater extraction point. The steam conditions are 2400 psig and 1050 F at the throttle, with single reheat to 1000 F. The 321-mw nameplate capability is based on a normal exhaust pressure of 1 in. Hg abs. The flat performance characteristic of the low-pressure steam path will give acceptable economy when slightly lower exhaust pressures are available during colder seasons of the year.

In establishing the steam conditions for River Rouge No. 3, the important basic concept was obtaining optimum performance with subcritical steam pressure and with steam temperatures that would permit using ferritic materials. Chrome-moly steels and Type 422 stainless steels are the ferritic materials that have been used in many of the high-temperature components.

General Arrangement

The close-coupled turbine arrangement, with the high-pressure and intermediate-pressure turbines on the 3600-rpm shaft and the two low-pressure turbines on the 1800-rpm shaft, is shown in Fig. 2. A single foundation is used to support both the high-speed and low-speed turbines. This design increases the transverse stability of the foundation because the supporting structures below the adjacent turbines act to reinforce each other. Very compact over-all space is required for the cross-compound machine because the two shaft systems are located close together on this single foundation. The over-all width of the unit at the floor line is 51 ft 6 in., and the over-all length, including exciters, is 88 ft $1^{6}/_{8}$ in.

The condenser is installed with its axis parallel to that of the

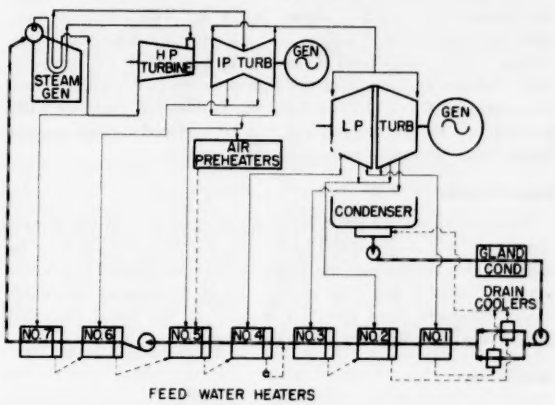

Fig. 1 Cycle diagram

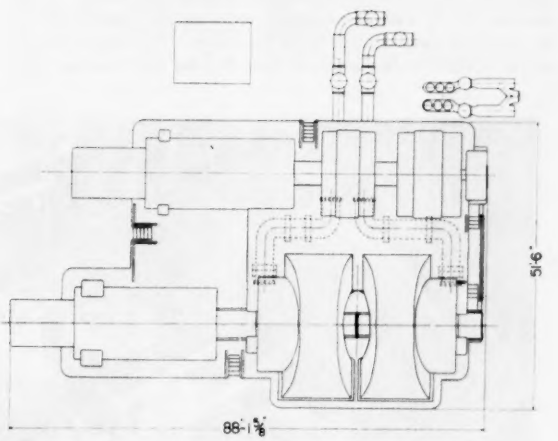

Fig. 2 General arrangement

[1] C. D. Wilson, "Large-Capability Steam-Turbine-Generator Units . . . made possible by compact close-coupled cross-compound arrangement," *Mechanical Engineering*, vol. 77, 1955, pp. 407–410. (Slight condensation of ASME Paper No. 54—A-182.)

Contributed by the Power Division and presented at the Semi-Annual Meeting, Detroit, Mich., June 15–19, 1958, of THE AMERICAN SOCIETY OF MECHANICAL ENGINEERS.

NOTE: Statements and opinions advanced in papers are to be understood as individual expressions of their authors and not those of the Society. Manuscript received at ASME Headquarters, March 11, 1958. Paper No. 58—SA-22.

low-pressure turbines. This eliminates the need for wide-span arches below the support feet on the side of the exhaust casing and makes it easy to provide substantial foundation support for turbine and condenser loading.

All high-temperature steam valves are located below the floor on the boiler side of the 3600-rpm turbines. The oil reservoir is located below the floor at the side of the 3600-rpm generator where it is separated from the high-temperature parts of the turbine.

The connecting steam piping between the 3600-rpm and 1800-rpm turbines is located above the foundation and below a platform between the two turbines.

Steam-Chest Assembly

The 2400-psi 1050-F throttle steam enters the turbine through the steam-chest assembly, shown in Fig. 3. This assembly contains two parallel stop valves and six governor-controlled inlet valves. The steam-chest assembly is supported by compensated hangers at the side of the high-pressure turbine and below the operating floor. In this location, it does not interfere with accessibility to the turbine and can be serviced by the powerhouse crane through a removable floor section.

Steam Strainers

Steam strainers are provided as an integral part of the steam-chest assembly at the inlets to the two parallel stop valves. In order to give the turbine continuous protection against the carry-over of harmful particles in the steam, permanent fine-mesh steam strainers were specified instead of the usual standard strainers with temporary fine-mesh screens.

Stop Valves

The two parallel stop valves are single-seat plug-type valves with pilot valve and back-seated valve stem. They are not throttling valves and are either fully open or fully closed. They are operated by a direct-connected hydraulic servomotor located in a shielded compartment below the valve. The strainer bodies and stop valve bodies are made from $2^1/_4$ per cent chrome, 1 per cent moly forgings, and they are shop-welded to each other and to two cast chrome-moly governor-valve-chest manifolds to form the complete steam-chest assembly. Equalizing passages above and below the stop-valve seats permit individual closing of the stop valves without interrupting steam flow to any of the six governor-controlled inlet valves.

Inlet Valves

The six governor-controlled inlet valves (Fig. 4) are cam-operated and are provided with a straight-line lift mechanism to avoid imposing side thrust on the valve-stem packing. Separately-mounted cam-shaft segments on each valve superstructure give more precise control of valve lift and a new design of tension-spring mechanism for closing the valve simplifies the valve superstructure and makes it easier to dismantle. Triple valve-stem leak-offs are used so that more efficient disposal of valve stem leakage steam can be provided.

Each inlet valve connects to a separate nozzle group in the turbine. The first two inlet valves open simultaneously to two nozzle groups that are located diametrically opposite from each other. This is done to balance the nozzle reaction forces on the relatively light spindle and to limit the pressure drop across the first stage blading. The governing stage, with this arrangement, has a total of five valve points.

Joints

The covers on the steam strainers, stop valves, and inlet valves are all provided with pressure-seal joints. Steamtight joints are thus obtained without requiring the use of massive flanges or highly stressed high-temperature bolting. The design of the pressure-seal joint used on the stop valve covers is shown in Fig. 5. A silver-plated expendable wedge-shaped seal ring is confined between the valve body and the cover plate. The area surrounding the seal ring is protected by a stainless-steel inlay. The cover plate is mechanically secured against the steam pressure forces by a segmented lock ring that is inserted in an annular groove in the valve body. The steam-tight seal is obtained by the internal steam pressure acting against the cover plate to compress the

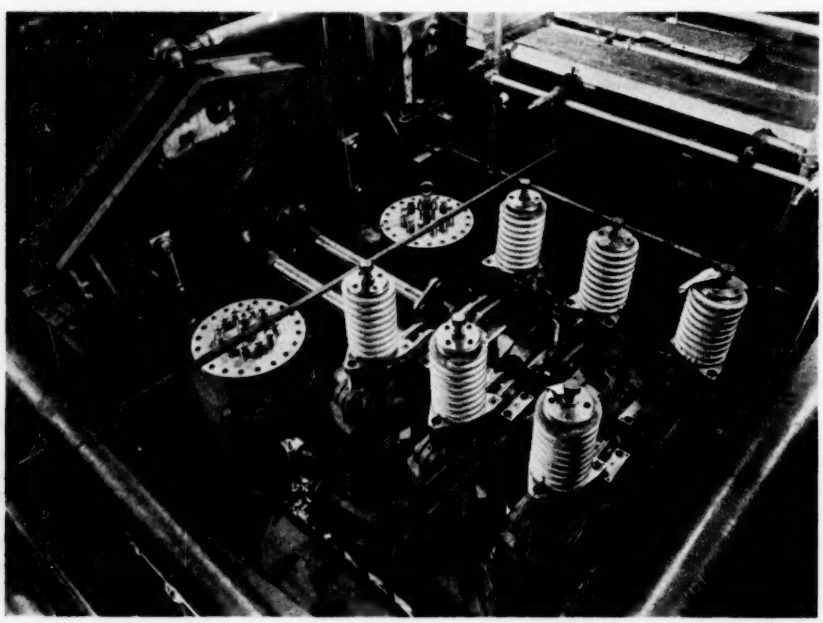

Fig. 3 Steam chest assembly on test

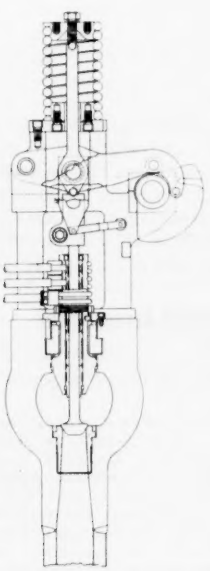

Fig. 4 Governor controlled inlet valve

wedge-shaped seal ring and expand it against the sealing surfaces. To assist in dismantling the joint, drilled holes are provided in the cover-plate so that compressed air can be blown through to cool the cover-plate and shrink it away from the seal ring. During the hydrostatic tests of the River Rouge components, these joints were subjected to hydrostatic test pressures of 11,000 psig without leakage.

High-Pressure Turbine

Flexible U-bends connect the inlet valves on the steam chest to the high-pressure turbine. The support for the steam-chest assembly is anchored in a longitudinal direction leaving the steam chest free to move in a vertical and horizontal direction with respect to the turbine axis. This freedom of movement in the steam chest permits automatic equalization of pipe expansion forces and moments and reduces force and moment reactions on the turbine cylinder.

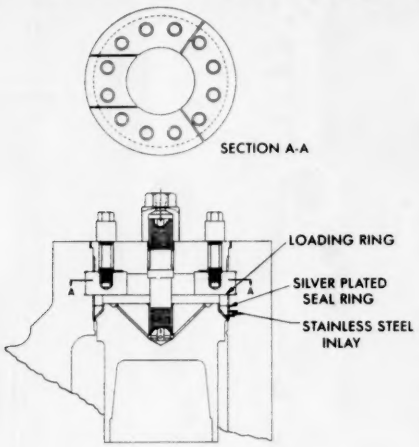

Fig. 5 Pressure seal joint

Inlet Connections

The inlet steam passes directly into the nozzle chambers of the high-pressure turbine without contacting either the outer or inner turbine cylinders. This is shown on the cross section through the high-pressure and intermediate-pressure turbines in Fig. 6. The inlet pipes are welded to forged chrome-moly sleeves which are grooved and fitted with a series of 13-chrome double-seal piston rings. These rings seal against a bore in the inner cylinder and a similar bore in the nozzle chest. A steam-tight joint is made with the outer cylinder by a bolted flange which seals against the moderate exhaust pressure of the high-pressure turbine. Differential expansions are taken care of by a welded extension neck between the pipe sleeve and the flange. A second extension neck on the opposite side of the flange has a sliding guide fit with the pipe sleeve to provide additional support and reduce bending stress in the welded connection.

Nozzle Chests

The nozzle chest design is a new development first used on 3600-rpm tandem-reheat machines. The new design retains the desirable separation between nozzle chest and turbine cylinder and, at the same time, offers a number of advantages over the divided separate nozzle chest design formerly used.

The nozzle chest (Fig. 7) is made in the form of two half-ring forgings that are bolted together at the horizontal joint to form a continuous ring. The nozzle ring has liberal radial clearance with the turbine cylinder so that distortions and thermal stresses caused by differential expansion between nozzle chamber and the cylinder are avoided. The nozzle ring is radially guided in the cylinder and this, plus its circular shape, gives it an expansion characteristic that closely matches the turbine shaft expansions. Shaft and nozzle-chest expansions occur with minimum change in radial alignment.

The ring shape of the nozzle chest permits using an almost

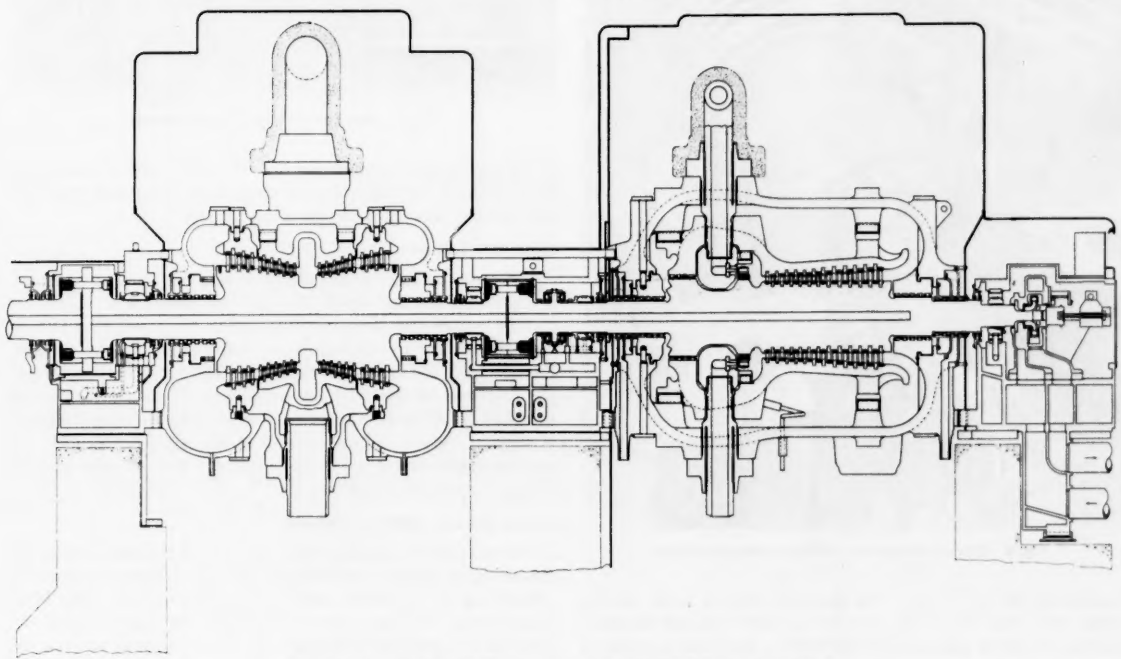

Fig. 6 Cross section of high-pressure and intermediate-pressure turbines

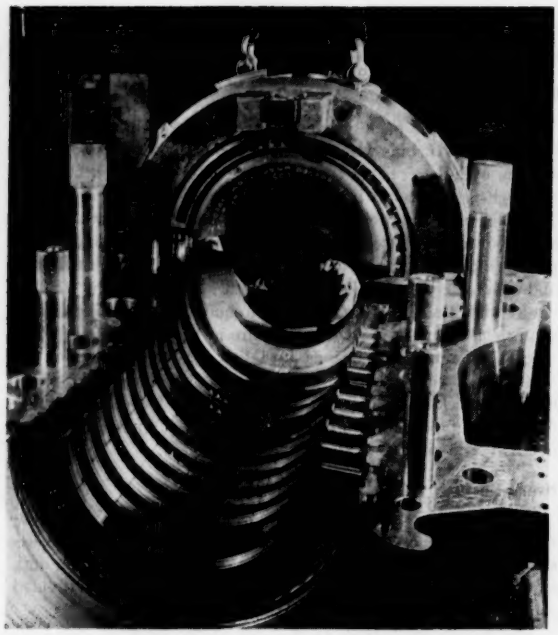

Fig. 7 Ring type nozzle chest

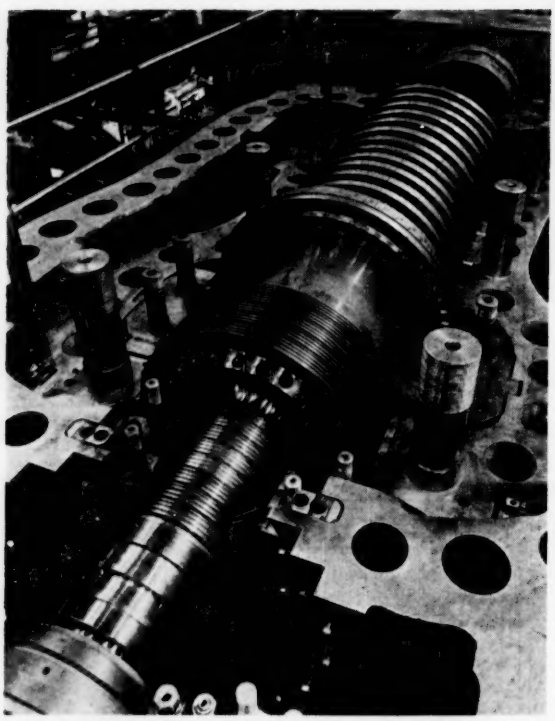

Fig. 8 Offset parting joint on high-pressure turbine

continuous arc of nozzles. On machines having large volume steam flow, the steam can thus be handled without excessive height for blades and nozzles and with a minimum number of circumferential interruptions to flow. The nozzle elements themselves are mechanically secured in a "T" slot groove in the nozzle chest without bolting. Tight-fitting dowel pins and keys are used to seal between adjacent nozzle groups.

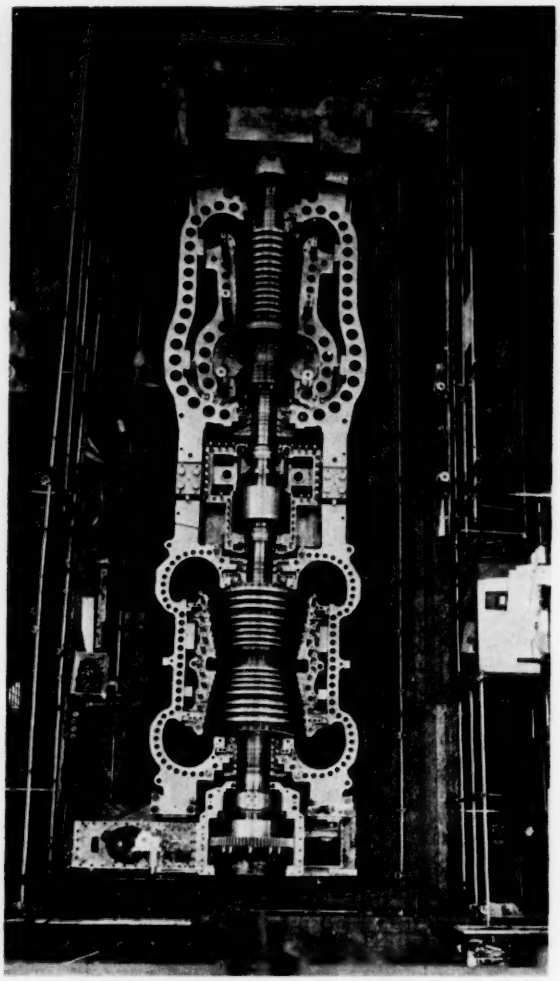

Fig. 9 Plan view of 3600-rpm turbines

Center-Line Support

The outer cylinder of the double-casing high-pressure turbine is made with the horizontal parting joint located 6 in. above the turbine center line (Fig. 8). This offset joint provides center-line support for the high-pressure turbine on all four corners. Extensions of the lower-half cylinder flange rest on hemispherical stainless-steel blocks which are self-aligning to adjust themselves to minor distortions in the outer cylinder. By locating the plane of support for the turbine cylinder at the exact center line, the vertical expansion of the cylinder support foot will not cause a change in vertical alignment.

Anchor Point for 3600-rpm Turbines

Steam enters the high-pressure turbine at the end nearest the intermediate pressure turbine and flows in a forward direction, exhausting to the return line to the reheat boiler. The high-speed thrust bearing is located between the high-pressure and intermediate-pressure turbines in the No. 2 pedestal which is anchored to the foundation. The turbine casings are also anchored

to this pedestal so that the cylinders and spindles of both high-temperature turbines each expand axially in a direction away from this common anchor point to minimize axial differential expansion.

Blading and Seals

Except for that in the first row or governing stage, all of the blading in the high-pressure and intermediate-pressure turbines is of the reaction type with stepped radial interstage seals. The seal strips are inserted in both cylinder and spindle so that there can be no direct contact of the sealing tips with either cylinder wall or spindle body in case of accidental rubbing. Spring-back radial seals are used on all balance pistons and steam-sealed glands. All radial seals are provided with liberal axial clearance so they can accommodate normal axial differential expansions without requiring critical attention from the operators. The only axial seal in the entire machine is in the governing stage. This seal is located relatively close to the thrust bearing where differential axial expansions are small.

Intermediate-Pressure Turbine

The flow of steam returning to the intermediate-pressure turbine from the reheat boiler is controlled by two parallel intercept valves backed up by reheat stop valves.

Four equally-spaced inlet connections are provided at the center of the double-casing intermediate-pressure turbine to obtain symmetrical entry of the high-temperature reheat steam. The connecting sleeves through the double casing are sealed with piston-ring seals similar to the design used in the high-pressure turbine inlet. The outer casing of the intermediate pressure turbine is provided with an offset horizontal parting joint and four-point center-line support similar to the high-pressure turbine.

Double-Flow Design

Inside the turbine, the steam flow divides and flows in opposite directions through duplicate opposed-flow steam paths (Fig. 9). The divided steam-flow design is used to advantage with large volumetric flows because blades of efficient proportions can be used on a small diameter shaft that is axially balanced without balance pistons. The maximum diameter of the intermediate-pressure spindle is $39^{1}/_{4}$ in. and the diameter at the entrance of the 1000-F reheat steam is $32^{13}/_{16}$ in.

Crossunder Piping

The intermediate-pressure turbine exhausts through two 38-in. pipes to two 1800-rpm low-pressure turbines (Fig. 2). The pipes are attached to the lower halves of each turbine so that connections do not have to be broken when lifting turbine covers. All piping is above the foundation and is short and direct so that there is a minimum volume of stored steam. Stainless-steel linked expansion joints in the "dog leg" pattern of the piping allow the pipes to flex and accommodate expansion movements. The links across the expansion joints confine the pressure forces acting on the joint so that the only force reactions transmitted to the turbines are the relatively small forces required to deflect the expansion joints in bending.

Low-Pressure Turbines

The two single-flow low-pressure turbines are mounted in tandem back-to-back so that they exhaust to a single condenser (Fig. 10). The cylinder section of each turbine is built as a spherical dished head and is bolted at a point of low pressure to the fabricated steel exhaust casing.

Spindles and Blading

Each of the low-pressure turbine spindles is supported on two bearings and a pivoted pad thrust bearing is combined with one of the journal bearings located between the turbines. All rotating blading is carried on disks shrunk on small diameter shafts. The exhaust blade is 46 in. long and was developed for application in machines of 300 mw and larger.

The resonant frequencies and modes of vibration of the 46-in. blades were established and studied analytically on IBM computers during the design stage. Following manufacture, finished blades were run up to overspeed in a special test stand designed for that purpose (Fig. 11). The actual running tests of the 46-in. blades in this test stand have confirmed that the points of resonance are well removed from the danger zones for 1800-rpm operation.

Exhaust Casings

The annulus of two rows of 46-in. blades is 267 sq ft and large exhaust casings are required to handle efficiently the large volume of steam. The connecting flange to the condenser is 25 ft wide by 26 ft 8 in. long (Fig. 12). The steam passage between the

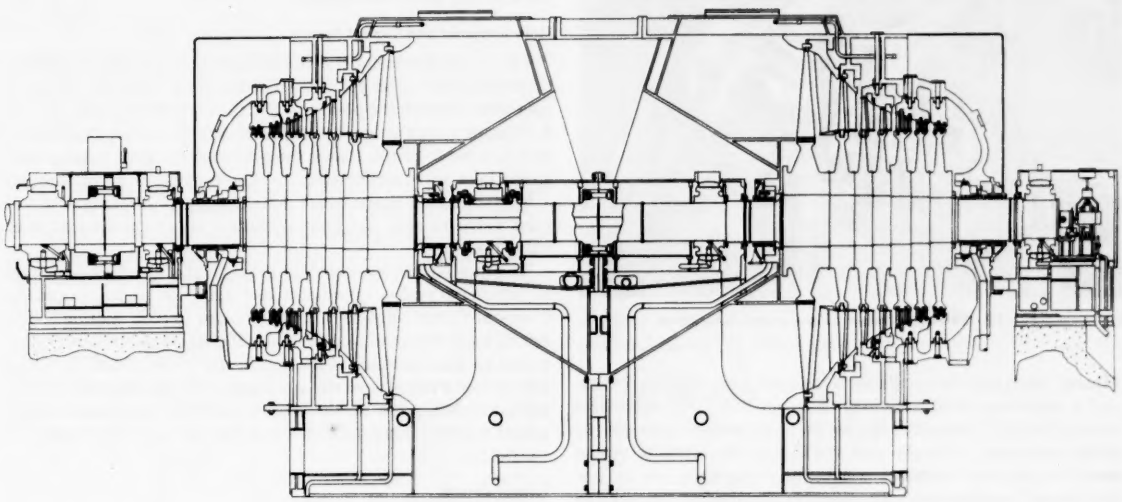

Fig. 10 Cross section of low-pressure turbines

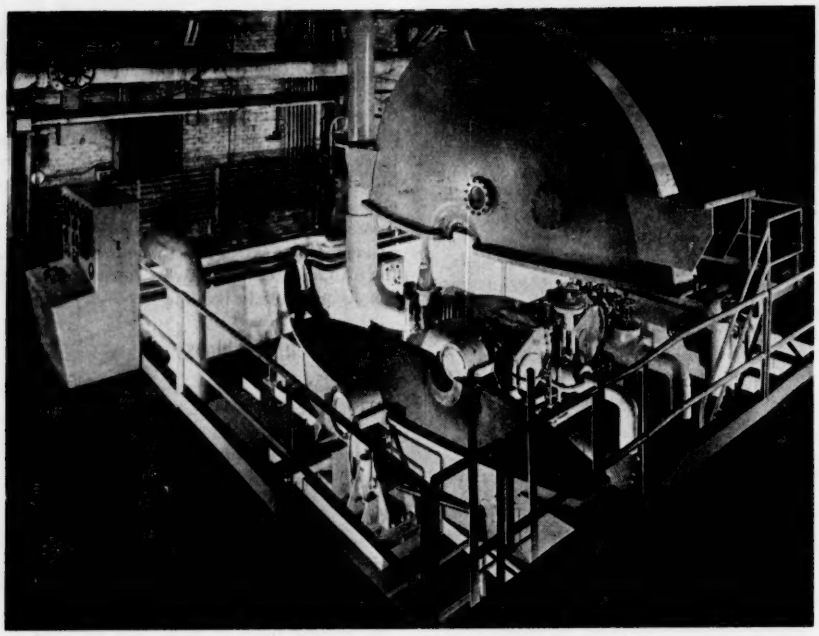

Fig. 11 Blade vibration test stand

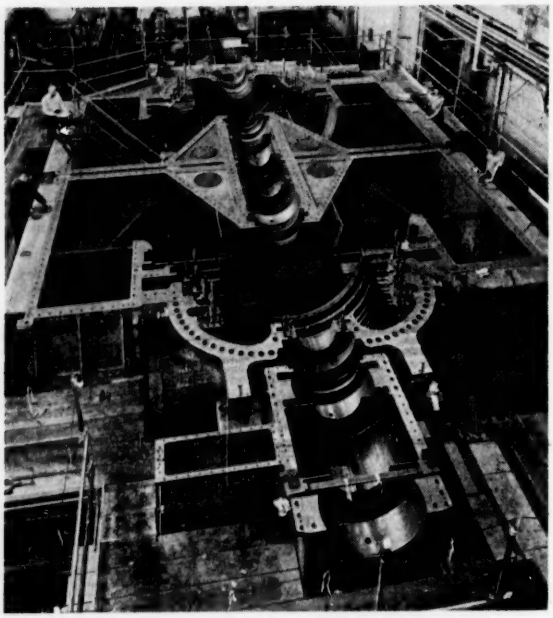

Fig. 12 Lower half view of low-pressure turbines

exhaust blade and the condenser is designed with controlled areas and a minimum of obstructions to steam flow. All extraction heater piping is external to this steam flow passage. In order to obtain necessary strength and rigidity in the exhaust casing structure without excessive weight, the flat walls are hollow double-wall construction with stiffening ribs welded between the walls.

Controls

The turbine operating controls are centralized in the 3600-rpm forward pedestal, and an illuminated panel is provided on the pedestal for the instruments and controls needed for normal operation. These include the speed changer, load limit and hand-trip controls, and associated indicator dials, as well as oil-pressure gages, starting gage, and electric tachometer indicator. The speed governor, shaft-driven main oil pump, and all relays and operating cylinders for the governor-controlled steam-inlet valves are located inside this pedestal. Like all the other separate pedestals on this machine, the 3600-rpm forward pedestal is of fabricated steel design and is nonsliding with bolts and keys anchoring it solidly to the foundation.

Main Governor and Control System

The major governors and controls are shown on the simplified schematic diagram of Fig. 13. The speed governor on the 3600-rpm shaft controls the positioning of the six governor inlet valves. A rotating sleeve valve, connected to this governor, controls oil flow to a servo-piston that is integral with the pilot valve of the steam inlet valve servomotor. The control oil flows through a hydraulic load limit which operates by positioning a small pilot valve to stop the flow of control oil at the desired inlet valve opening.

The mechanical lever system between the speed governor and the steam inlet valve servomotor does not transmit power and the levers are used only as a compensating return motion. The return motion is power-operated by the steam valve servomotor piston so that mechanical friction in the lever system does not influence the response of the governor. The lever system is connected to indicators on the turbine control panel which show actual valve opening position and actual setting of the load limit control.

Reheat Control

A second speed governor is provided on the low-speed shaft to

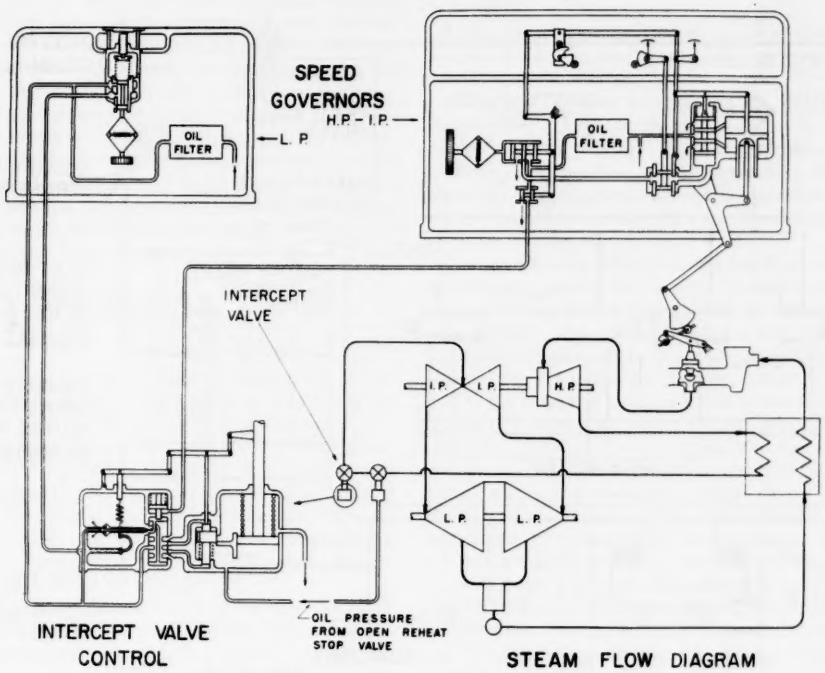

Fig. 13 Governor control diagram

close the reheat intercepting valves as soon as there is a slight increase above rated speed. This governor operates a pressure converter that sends out a control-oil pressure signal proportional to the speed of the 1800-rpm shaft. Askania controls on the intercepting valves start to close the valves at $1^1/_2$ per cent overspeed, and the valves are fully closed at 3 per cent overspeed.

For the remote possibility of the two generators becoming electrically separated, an auxiliary reheat control is provided on the 3600-rpm governor which closes the intercepting valves when the 3600-rpm shaft reaches 104 per cent speed. The closing action on the intercepting valves from both the main and reheat governors is reversible when normal speed is restored.

Overspeed

At 10 per cent overspeed, separate overspeed governors mounted on the 3600 and 1800-rpm shafts each act to trip closed the main and reheat stop valves, the inlet valves and reheat intercepting valves, and all power-operated nonreturn valves in the extraction lines.

Turning Gears

The turning gears on both the 3600 and 1800-rpm shafts are a new underslung design with the motor and gear train located at the side of the bearing cover and engaging the gear on the turbine coupling from below. This design of turning gear makes it unnecessary to remove or disconnect the gear when raising the turbine bearing covers.

Gland Sealing System

All of the shaft sealing glands on this machine are sealed with steam, and the simplified controls provided for the gland seal system are shown in Fig. 14. During normal operation, all gland sealing steam is supplied from the middle leak-off point on the governor-controlled inlet-valve-stem packings. Two separate regulators are used to maintain constant gland-steam supply pressure. When the manifold pressure drops below $3^3/_4$ psi, the high-pressure regulator admits steam to the system from the main inlet steam header. This source is required only when starting or stopping the unit or at very light loads. The second regulator comes into operation when the mainfold pressure exceeds 4 psi and discharges excess steam to the lowest pressure heater.

Hand bypass valves are provided around each regulator to take care of abnormal operating conditions. When the unit is started with low-steam pressure, the high-pressure regulator bypass is used and the bypass line orifice is sized to pass the required gland steam flow with the reduced starting pressure. Safety relief valves are provided that have adequate capacity to prevent excessive pressure in the gland supply manifold in case of any abnormal operation.

All of the glands take steam direct from the gland header with the exception of the two glands on the low-pressure exhaust. Here, the gland-steam supply piping is passed through the exhaust steam passage to cool the gland steam temperature to about 100 F above saturation temperature. The small vacuum in the gland exhauster system is obtained by using a conventional surface condenser equipped with a motor-driven exhauster fan. The gland condenser uses full-flow condensate as circulating water and maintains a vacuum of 12 in. of water at the connection to the exhauster manifold. For emergency operation, the gland exhauster flow can be diverted to a large water ejector which has capacity to maintain the required vacuum. Since the water ejector is intended for use only during emergencies, raw water is used and the ejector discharge is not recovered.

Shipping Provisions

Shipping clearance is a subject that must be considered on all types of machinery and it becomes especially important as the size of the machine becomes larger. The low-pressure exhaust casings on the River Rouge machine constitute the largest turbine components. The lower half of each low-pressure turbine

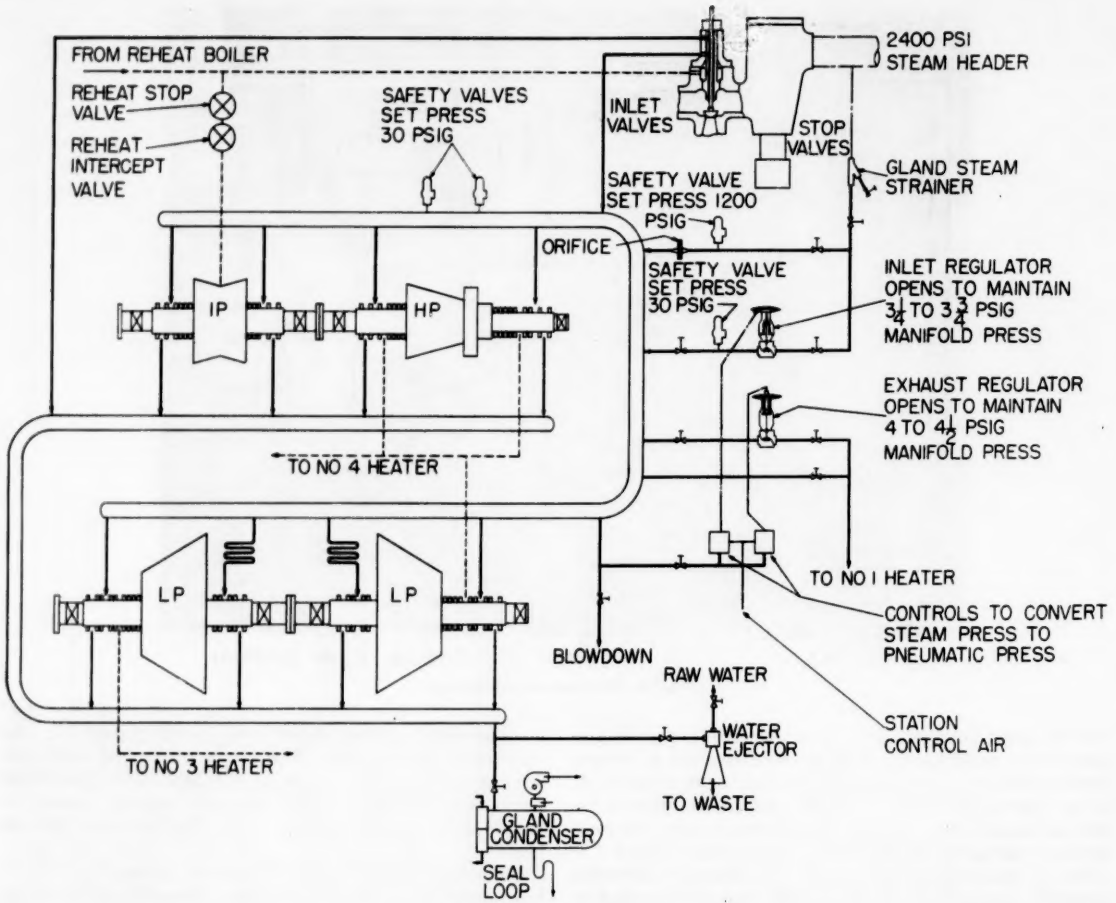

Fig. 14 Gland seal diagram

exhaust casing was designed to come just inside railroad shipping limits, and these parts were shipped separately, mounted on their sides.

The tip diameter of the bladed low-pressure spindles is 14 ft 11 in. and since this exceeds permissible shipping limits, the 46-in. blades were removed and shipped separately. The low-pressure spindles were completely assembled in the shop, including all blading, and the assembled spindles were statically and dynamically balanced (Fig. 15). The axial-entry blade attachment used on the 46-in. blades made it relatively easy to remove these blades for shipping and re-installation in the field. The low-pressure spindles, with shop-assembled spindle disks shrunk in place, could then be shipped without exceeding shipping limitations.

Conclusion

Steam turbine design is never static and the components developed for River Rouge are being applied to other machines, some of which operate under different steam conditions and have larger capability. One of the single-flow low-pressure elements developed for River Rouge is now being applied in the 150-mw turbine for the Enrico Fermi Atomic Power Plant of The Detroit Edison system. The high-speed elements of the River Rouge machine are adaptable to other large-capability turbine arrange-

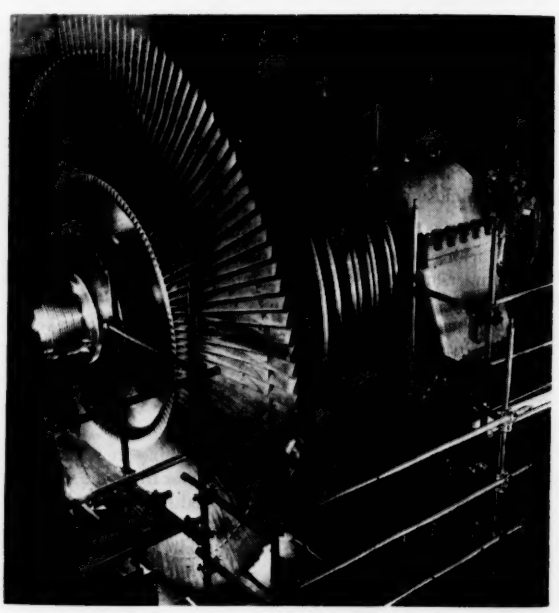

Fig. 15 (*Right*) Balancing low-pressure spindle

ments including all the 3600-rpm cross-compound designs.

The most significant items developed to handle efficiently the large volume steam flow on the River Rouge machine are the new nozzle chest design, the use of opposed-flow steam paths in the intermediate-pressure turbine, and the development of the 46-in. exhaust blade. The close-coupled arrangement with the cross-under piping located above the foundation has made it possible to build this machine with compact over-all dimensions. Refinements in turbine components have been described which will improve turbine operating stability and the over-all dimensions of the larger components have been controlled so that they can be handled and shipped without difficulty.

DISCUSSION

W. W. Brown[2]

The author has presented in an interesting fashion the unique features in this turbine-generator. It may be in order to explain why we arrived at such an odd rating (321 mw) for this unit. When bids were taken for this turbine-generator from three manufacturers, a maximum throttle flow of steam was given and requests made for bids at $3^1/_2$-in. Hg back pressure. The resulting unit size was 300 mw for $3^1/_2$ in. Hg. Since our turbine-generators are usually rated at 1-in. Hg back pressure, the corresponding rating for the unit quoted operating at 1-in. Hg back pressure was 321 mw.

The author referred to this unit being one of the first rated above 300 mw. The decision to install the large unit was based on two factors: (*a*) The economy of such a move must be worth while, and (*b*) the unit size should not exceed 10 per cent of our installed system capability. On the first point, the economy of going to 321 mw for this unit rather than repeating the size (260 mw) of the first and second units installed at River Rouge resulted in a saving of $15 per kw for the complete addition to the plant. On the second point, our installed system capability when this unit is in operation will be 3250 mw.

The close-coupling has resulted in a single turbine base for the two turbines with the condenser center line paralleling the turbine center line. This permits continuous walls flanking the condenser, resulting in a simple design void of arched openings necessary in a crosswise condenser layout.

As a matter of interest, the turbine heat rate for this unit at 321 mw 1-in. Hg back pressure is 7340 Btu per kwhr.

M. K. Drewry[3]

The manufacturer's first use of the close-coupled, cross-compound design at the Oak Creek plant, Milwaukee, has provided to date ten unit-years of experience.

Original selection of this design was encouraged by its higher thermal efficiency, its lesser evaluated cost, and its higher reliability. A lesser, but not minor, selection reason was that it appeared to represent the probable design of the distant future. A speed of 3600 rpm is positively necessary for high-pressure, high-temperature turbine sections. For the same exhaust-blade stresses of the low-pressure sections, 1800 rpm affords four times the exhaust area. Four times as many 3600-rpm exhaust rows also quadruples several rows of expensive low-pressure blading and in the case of large units requires cross-compounding.

No serious objection to the close-coupled design has been experienced during the ten unit-years of operation. Loss-of-load experiences have proved that the minimum amount and energy of steam entrapped in the short "cross-under" commends close-coupling.

[2] The Detroit Edison Company, Detroit, Mich. Fellow ASME.

[3] Chief Engineer of Power Plants, Wisconsin Electric Power Company, Milwaukee, Wis. Fellow ASME.

J. C. Spahr[4]

This excellent paper has been read with interest. The information presented has raised several questions which have provoked the following comments:

In opening the first two inlet valves simultaneously in the diametrically opposite nozzle groups, a double shock is produced on the first-stage blading. While it is recognized that due consideration must be given to the lateral forces created by partial admission on the governing stage, we question the advisability of alleviating this condition by a construction which subjects the first-stage blading to such severe duty.

The use of two half-ring forgings which are bolted together at the horizontal joint to form a nozzle chest consisting of a continuous ring seems to be a departure from the divided separate nozzle chest formerly used. It would appear that the continuous ring would not have the desirable feature of complete freedom of expansion of each nozzle chest under conditions of thermal changes. If it is the intention to operate the unit continuously with all nozzles wide open, then such a continuous ring would be entirely adequate. However, it would appear that operation at any valve position less than wide open would result in rather high thermal strains within the continuous nozzle chest. One of the advantages given in favor of the continuous-ring type of nozzle chest is the use of continuous arc of nozzles. By proper design considerations, it is possible to utilize the divided, separate nozzle chests and still not create circumferential interruptions to flow. In large machines operating with high temperatures and at variable loads, the divided, separate-nozzle-chest construction offers a solution for the severe thermal stresses which will exist as a result of load cycling.

Excellent results have been achieved in the exhaust-casing design and the structure appears to have one of the most obstruction-free flow areas that has ever been developed. In observing Fig. 12 of the paper, which shows the lower half view of the low-pressure turbines, it would appear that the physical size of each integral section presents rather large dimensional structures. The illustration is not clear as to how these sections are handled during shipping. In addition, no mention is made in the text as to how these particular pieces will be transported to the power-plant site.

The author is to be congratulated on a very complete and well-illustrated paper.

Author's Closure

W. W. Brown's discussion has added much interesting information to the paper, for which the author is duly grateful.

M. K. Drewry points out in his discussion the advantage of obtaining large exhaust area with a minimum number of exhaust flows when 1800-rpm low-pressure turbines are used. This is especially important and desirable for installations having large volume steam flow in the low-pressure turbine.

J. C. Spahr raises some important questions in his discussion which cover points that have to be carefully considered in the design of large turbines.

One of these, the opening of the first two inlet valves simultaneously in diametrically opposite nozzle groups, was applied on the River Rouge turbine to obtain more uniform heating of the turbine casing, to give equalized steam thrust from the first stage nozzles on the relatively light turbine spindle, and to limit, to a certain extent, the maximum steam loading of the first stage blading. The natural frequencies of the short rugged impulse blades are high, with the actual frequencies of individual blades falling in bands that cover several multiples of operating speed. It is, therefore, impossible to tune the blades to frequen-

[4] Manager, Large and Medium Turbine Engineering, Westinghouse Electric Company, Lester, Pa. Mem. ASME.

cies that avoid all high-order excitation. Instead, the blades are designed with high safety factors to withstand the vibratory stresses and shock loadings imposed. The shock loads remain the same for any given steam flow, and separating the nozzle groups to obtain other desirable benefits, changes only the number of impulses per revolution. Because the blades are designed to operate at stresses well below the endurance limit of the material, changes in the frequency of the cyclic load will not alter the life expectancy of the blades.

A second question in Mr. Spahr's discussion concerns the continuous separate ring nozzle chest design. We adopted this improved design after more than twenty years' experience in building separate nozzle chests on all our high temperature machines. The nozzle ring retains the desirable features of the separate chests and has the additional advantage of maintaining better alignment between nozzles and the rotating blading plus the ability to provide continuous arc of admission without restricting the steam passages to the nozzles.

The ring-type nozzle chest is completely separated from the cylinder casing so that the chest can expand freely without restraint when the more massive cylinder is at different temperature. The ring-type nozzle chest has relatively small mass and is completely surrounded by hot steam so that it heats quickly and uniformly. The temperature gradient between the steam inside and outside the nozzle chest is relatively small because a single row impulse stage is used. In addition, the inlet pipes to all unused valves are provided with warm-up bypasses. All of these factors result in small temperature differentials between different sections of the nozzle chest. The negligible distortion resulting from these small temperature differentials has been established by tests on full size nozzle chests where the individual chambers were subjected to much higher temperature gradients than anticipated in service. This has been further confirmed by actual operating experience on a number of machines.

To answer Mr. Spahr's question as to how the large exhaust components were shipped, a picture was shown when the paper was presented which showed the exhaust casing components loaded on railroad freight cars. It is regretted that lack of space made it impossible to include this picture in the printed paper.

W. C. BEATTIE
Mem. ASME
H. A. BAUMAN
J. M. DRISCOLL
Mem. ASME
P. T. ONDERDONK
Mem. ASME
R. L. WEBB
All of Consolidated Edison Company, New York, N. Y.

Five Years' Experience on the Consolidated Edison System With Protection of Turbine Generators and Boilers by Automatic Tripping

In 1953 the authors presented a paper entitled "Protection of Turbine Generators and Boilers by Automatic Tripping."[1] Consolidated Edison now has had five years experience with three 200 mw units so protected. This paper relates the actual shutdowns experienced as a result of the automatic trip system functioning. Troubles, design changes, and additions incorporated in the protection system on new units now being installed are also discussed.

OVER FIVE YEARS AGO the authors presented a paper[1] which described a new integrated automatic trip protection system for unit turbine-generators and boilers which had been placed in service for the first time at Consolidated Edison's Astoria Station, in 1953. The simplified diagram, Fig. 1, provided for tripping out the unit,[2] together with its major auxiliaries, to protect equipment against the following:

Damage from thrust-bearing failure.
Damage from excessive vibration.
Damage from excessive exhaust hood and condenser shell temperature.
Damage from loss of vacuum.
Damage from excessive overspeed.
Damage from failure of air supply for combustion.
Damage from complete interruption of all fuel.
Extensive damage from generator and transformer electrical failures.
Extensive damage from generator grounds.
Extensive system disturbance from loss of field in high or low-pressure generator.
Damage from generator motoring.
Extensive damage from auxiliary circuit electrical failures.
Extensive damage from 138-kv generator feeder failures.

At the time of presentation the consensus among several discussers, as related to the untried elements described, was that the protection system would be acceptable for alarming, but not for automatic tripping. Concern was expressed that false trips might occur too frequently and, besides affecting unit availability adversely, might at times produce major system emergencies.

The authors, with five years operating background with the protective system on these three units, feel that a further addition to the technical literature on the subject now could be made by presenting a paper relating the history of trip-outs during this operating period. This paper reviews the tripping experience on the three units including all "false" tripping cases, the changes to the original system, and further developments as now being applied to the new unit installations on the Consolidated Edison system.

Experience From 1953 to 1958 With Protective System

Electrical

Table 1 shows the record of electrical relay operations, two of which were false. It should be noted that this relay protection is conventional and has been used for many years for generator protection. While it is true that both cases were unusual and did not show protection relay design weaknesses, they do illustrate that minor items such as relay panel vibration can cause unanticipated trouble during the early days of shakedown operation. These relay operations will be discussed in more detail later in the paper.

Turbine

Table 2 gives the record of turbine-relay operations. The first item in this table is by far the one holding greatest interest. This machine is a cross-compound 3600/3600 unit with the high-pressure and the intermediate-pressure cylinders in tandem driving the high-pressure generator. The thrust bearing is located between the high-pressure and intermediate-pressure cylinders and was sized in its design to take the net thrust of the two spindles and was never intended to be capable of carrying the thrust load of each individual spindle. During the initial operating history of the unit when the reheater safety-valve settings were being checked with the unit operating under load, the pressure was being built up on the reheater by first closing completely one of the two intercept valves and then by closing gradually the second valve, when the latter suddenly went to total closure shutting off all steam to the intermediate-pressure cylinder. Steam continued to pass for seconds through the high-pressure turbine and one of the reheat safety valves until the unit was hand tripped. Under the unbalance which occurred, the thrust bearing failed and extensive damage was done to the tur-

---

[1] H. A. Bauman, J. M. Driscoll, P. T. Onderdonk, and R. L. Webb, "Protection of Turbine Generators and Boilers by Automatic Tripping," *Trans. AIEE*, vol. 72, part 3, 1953, pp. 1248–1260.

[2] Units 1 and 2 at Astoria Station and Unit 7 at East River Station, all approximately 200 mw in size and all designed as cross-compound, 3600/3600 units operating at 1800 psi, 1000/1000 F, the Astoria units being General Electric and the East River unit, Westinghouse.

Contributed by the Power Division of THE AMERICAN SOCIETY OF MECHANICAL ENGINEERS and presented at the ASME-AIEE Power Conference, Boston, Mass., September 28–October 1, 1958.

NOTE: Statements and opinions advanced in papers are to be understood as individual expressions of their authors and not those of the Society. Manuscript received at ASME Headquarters, July 17, 1958. Paper No. 58—Pwr-8.

bine. Investigation revealed that the reheat stop valve oil operating pressure had not been set quite properly and the valve suddenly closed as pressure differential increased. The thrust-bearing trip controller did not protect the unit in this instance and a study of the complete incident showed that the unit had been tripped by hand 20 sec after the closing of the second intercept valve, and that the multipoint trip controller was not monitoring the thrust-bearing temperature at the time of high thrust load. This incident immediately resulted in a temporary installation of additional multipoint trip controllers to approach continuous monitoring of the thrust bearing. There is some difference of opinion on whether or not the temperature relays would have had sufficient speed of response to trip the unit without having serious internal damage, had they been of the continuously monitoring type. As a result of this incident the turbine manufacturer developed a pressure-differential sensitive relay measuring pressure differential between the inlet pressures to the high-pressure and intermediate-pressure cylinders to trip the unit in the event of a similar occurrence.

Again referring to Table 2 the two cases of trip-outs caused by high thrust-bearing temperatures resulted from loss of salt water to the oil coolers. Both were caused by the loss of suction at the intake of the service pumps under unusual conditions; the first being caused by a sudden inflow of debris into the suction strainer and the second due to an operating condition where one of the two circulating water pumps supplying a very long water-supply line to the condenser, was shut down. This latter condition together with an extreme low tide resulted in loss of service water. In both cases the advance alarm on the temperature recorder sounded, but before the operators could take measures to restore the service pump, the trip controller functioned. In both these cases the protection system worked as intended.

The other two incidents shown in Table 2 are false trips due to incorrect multipoint trip-controller operation. As a result of these two trip-outs the complication of the prealarm was removed from the multipoint trip controller because such an alarm was also available from a turbine multipoint temperature recorder. Also the circuitry was modified as described later in the paper.

Boiler

The single case of incorrect relay operation, the first item in Table 3, will be discussed later.

Of the remaining two cases of loss of fuel-trip instances, one was initiated by low pressure due to fuel-oil-pump suction becoming partially air bound, and the other by closing of the main gas valve, the cause of which closing could not be explained.

The three out of four cases of high-pressure furnace trip on Astoria No. 2 that are listed in Table 3 were all caused by rup-

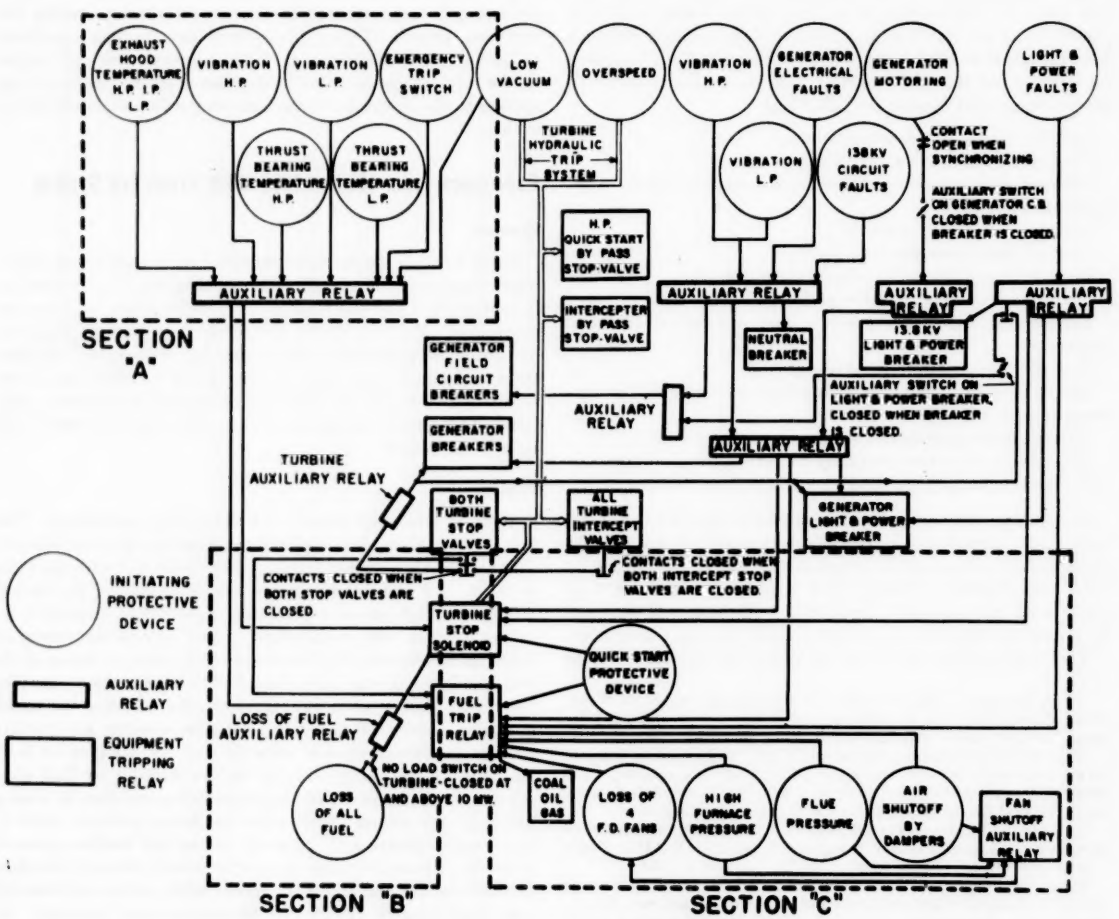

Fig. 1 Boiler-turbine-generator over-all protection

tures of a waterwall tube, two occurring at full load. The furnace-pressure trip was incorporated in the protection picture to guard against the possibility of overpressuring the furnaces which were the first pressurized furnaces to be installed in the country without induced-draft fans. The fourth case of high-pressure furnace trip at Astoria was caused by a puff due to the sudden opening of the forced-draft-fan dampers.

When the protection system functioned to remove the unit on rupture of a furnace wall tube for the first time, a little reflection brought out that an automatic trip-out is highly desirable for such cases, because automatic trip-out protects against:

1 Possible damage from carryover due to sudden reduction in boiler drum pressure.

2 Possible seizure of boiler feed pumps due to flashing in the suction from too rapid reduction in pressure in the deaerator.

3 Possible furnace puffs caused by reignition of the burner flame which had been quenched or smothered by steam and water.

The last case of automatic tripping listed under Table 3 happened on No. 70 Boiler at East River Station when there was a puff in the furnace due to too great an increase in fuel feed. When load was increasing on the unit and output was just above 100 mw and the operators were preparing to change from manual master to automatic master control, a sudden sag in steam pressure occurred for which a correction was attempted by manually increasing the master loading. Apparently the attempt was an extreme overcorrection; one which put too much fuel into the furnace. No furnace damage resulted.

Table 1 Electrical relay operations

STATION	PROTECTIVE RELAY	CAUSE OF TRIPPING	
ASTORIA 1	LOSS OF FIELD	CIRCUIT BREAKER OPENED ON PILOT EXCITER	(1)
ASTORIA 1	* GENERATOR DIFFERENTIAL	VIBRATION OF PANEL CAUSED OPERATION, DUE TO TOO SMALL CONTACT SEPARATION	(2)
ASTORIA 1	* CONTROL CIRCUIT SUPERVISORY	FAULT IN RELAY COIL	(3)
ASTORIA 2	PILOT WIRE	GENERATOR CABLE POTHEAD FAILURE	(4)
ASTORIA 2	LOSS OF FIELD	FAILURE OF EXCITATION SYSTEM BREAKER	(5)
EAST RIVER 7	MOTORING ON HIGH PRESSURE GENERATOR OF CROSS-COMPOUND UNIT	LOW AIR PRESSURE ON GENERATOR AIR BLAST CIRCUIT BREAKER CAUSED BREAKER TO OPEN	(6)
EAST RIVER 7	GENERATOR DIFFERENTIAL	FLASHOVER ON 69 KV INSULATOR	(7)
EAST RIVER 7	TRANSFORMER DIFFERENTIAL	FAULT IN GENERATOR TRANSFORMER	(8)

* INDICATES INCORRECT RELAY OPERATION
(1) FOR OUTAGE HOURS SEE TABLE IV

Table 2 Turbine relay operations

STATION	PROTECTIVE RELAY	REMARKS OR CAUSE OF TRIPPING	
EAST RIVER 7	INTERCEPTOR VALVE INTERLOCK	RELAY DID NOT OPERATE BECAUSE WIRING HAD NOT BEEN CONNECTED	(9)
	THRUST BEARING TEMPERATURE	RELAY WAS NOT CONTINUOUSLY MONITORING AND DID NOT OPERATE	
EAST RIVER 7	THRUST BEARING TEMPERATURE	LOSS OF SALT WATER TO OIL COOLERS	(10)
EAST RIVER 7	* THRUST BEARING TEMPERATURE	FAULTY MULTI - POINT TEMPERATURE RELAY	(11)
EAST RIVER 7	THRUST BEARING TEMPERATURE	LOSS OF SALT WATER TO OIL COOLERS	(12)
ASTORIA 2	* THRUST BEARING TEMPERATURE	FAULTY MULTI - POINT TEMPERATURE RELAY	(13)

* INDICATES INCORRECT RELAY OPERATION
(1) FOR OUTAGE HOURS SEE TABLE IV

Table 3 Boiler relay operations

STATION	PROTECTIVE RELAY	CAUSE OF TRIPPING	
ASTORIA 2	* LOSS OF FUEL	FAULTY CONTROL WIRING	(14)
ASTORIA 2	LOSS OF FUEL	LOSS OF FUEL OIL SUPPLY	(15)
ASTORIA 2	LOSS OF FUEL	CAUSE NOT KNOWN	(16)
ASTORIA 2	HIGH FURNACE PRESSURE	RUPTURE OF FURNACE WALL TUBE	(17)
ASTORIA 2	HIGH FURNACE PRESSURE	RUPTURE OF FURNACE WALL TUBE	(18)
ASTORIA 2	HIGH FURNACE PRESSURE	RUPTURE OF FURNACE WALL TUBE	(19)
EAST RIVER 7	HIGH FURNACE PRESSURE	HIGH FURNACE PRESSURE DUE TO A "PUFF"	(20)
ASTORIA 1	HIGH FURNACE PRESSURE	HIGH FURNACE PRESSURE DUE TO A "PUFF"	(21)

* INDICATES INCORRECT RELAY OPERATION
(1) FOR OUTAGE HOURS SEE TABLE IV

Outage Hours

In Table 4 there is listed chronologically by units, all cases of trips both true and false with the hours duration of outage which followed. The key numbers shown in parentheses are for the purpose of assisting the reader to correlate the cause of the trip in Tables 1, 2, and 3 with the date of occurrence and duration of outage hours.

Incident (2) under Astoria No. 1 Unit is recorded as a false trip with zero hours duration because the relay functioned after the unit had been intentionally hand tripped at 20 mw and the high-voltage circuit breaker had been opened by hand preparatory to a scheduled weekend shutdown in order to free-up control-valve stems. The vibration of the relay panel, mentioned earlier in the text, was corrected within the time required to accomplish the other planned work during the weekend outage and therefore no outage hours are chargeable.

Table 4 does not incorporate the East River No. 7 outage, shown on Table 2 (9) because the outage was initiated by manual tripping rather than by the automatic system. If the timing of the trip controller had been in synchronism with the accidental closure of the intercept valves, the automatic protection probably would have markedly reduced the outage time from that actually experienced.

In connection with restarting after outages of a few hours of short duration, it was found not necessary to use the control start bypass[3] because the automatic trip system cuts off fans so

[3] J. C. Falkner, "Quick-Starting of Large High-Pressure High-Temperature Boilers," TRANS. ASME, vol. 75, 1953, p. 1407.

Table 4 Outage hours after automatic tripping

ASTORIA 1 HOURS 1954-1958*				ASTORIA 2 HOURS 1954-1958				EAST RIVER 7 HOURS 1954-1958				TOTAL HOURS ALL STATIONS
DATE OF TRIP	TRUE	FALSE		DATE OF TRIP	TRUE	FALSE		DATE OF TRIP	TRUE	FALSE		
10-20-54	2		(1)	7-7-54	16		(4)	11-1-55	3		(10)	21
11-5-54		0	(2)	7-8-54		2	(14)	12-2-55	3		(6)	5
12-6-56		7	(3)	12-29-54	1		(15)	1-13-56	5		(7)	13
5-23-58	5		(21)	3-4-55	1		(16)	2-28-56		9	(11)	15
				5-25-55		1	(13)	3-11-56	3		(12)	4
				1-31-56	24		(17)	6-25-56	2		(20)	26
				3-7-56	33		(18)	1-28-57	10		(8)	43
				12-10-56	1		(5)					1
				9-25-57	144		(19)					144
TOTAL HOURS	7	7		TOTAL HOURS	220	3		TOTAL HOURS	26	9		272

KEY (1) FOR CAUSE SEE TABLES I, II AND III

* UP TO JUNE 1, 1958

Table 5 Outage hours caused by false automatic tripping

YEAR	ASTORIA 1	ASTORIA 2	EAST RIVER 7	TOTAL HOURS
1954	0	2	-	2
1955	0	1	0	1
1956	7	0	9	16
1957	0	0	0	0
TOTAL HOURS	7	3	9	19

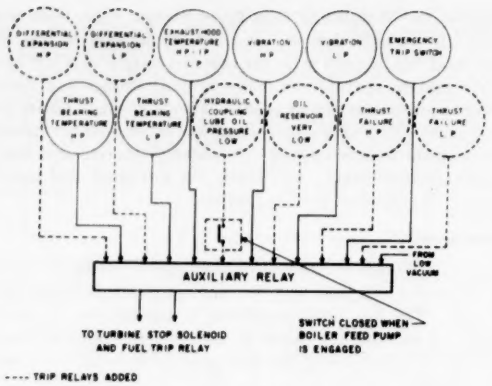
DIFFERENTIAL EXPANSION H P
DIFFERENTIAL EXPANSION L P
EXHAUST HOOD TEMPERATURE H P - I P
VIBRATION H P
VIBRATION L P
EMERGENCY TRIP SWITCH
THRUST BEARING TEMPERATURE H P
THRUST BEARING TEMPERATURE L P
HYDRAULIC COUPLING LUBE OIL PRESSURE LOW
OIL RESERVOIR VERY LOW
THRUST FAILURE H P
THRUST FAILURE L P
FROM LOW VACUUM
AUXILIARY RELAY
TO TURBINE STOP SOLENOID AND FUEL TRIP RELAY
SWITCH CLOSED WHEN BOILER FEED PUMP IS ENGAGED
---- TRIP RELAYS ADDED

Fig. 2 Revised section A of Fig. 1

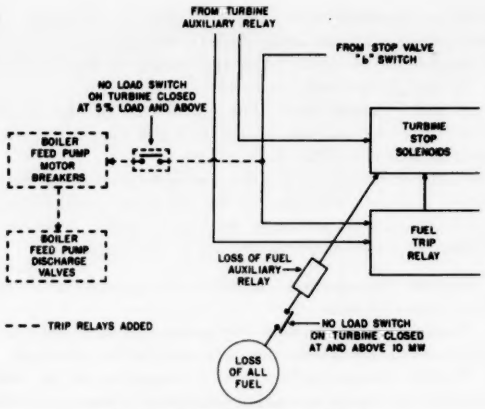
FROM TURBINE AUXILIARY RELAY
FROM STOP VALVE "b" SWITCH
NO LOAD SWITCH ON TURBINE CLOSED AT 5% LOAD AND ABOVE
BOILER FEED PUMP MOTOR BREAKERS
TURBINE STOP SOLENOIDS
BOILER FEED PUMP DISCHARGE VALVES
FUEL TRIP RELAY
LOSS OF FUEL AUXILIARY RELAY
TRIP RELAYS ADDED
NO LOAD SWITCH ON TURBINE CLOSED AT AND ABOVE 10 MW
LOSS OF ALL FUEL

Fig. 3 Revised section B of Fig. 1

quickly that there is no appreciable cooling of the superheater and reheater metals and good matching of steam and turbine metal temperatures is obtained in restarting. It is anticipated that, after Unit No. 3 Astoria Station goes into service this fall, one of Units No. 1 and 2 reported on here will be shut down nightly and control start bypassing will become routine.

Table 5 directs attention to the matter which concerned many engineers when the original paper was presented in 1953; namely, outages and their adverse effect on availability due to false trips. It is evident that experience with the system in three units over five years has proved these fears to be ungrounded. It is also of interest to note that over 50 per cent of the 19 outage hours were caused by growing pains with the thrust bearing trip controller.

Changes to Protective System Resulting From Experience

Electrical System

Table 1 lists two incorrect relay operations in the electrical protective relays. In the first of these a generator current differential relay, using $^1/_8$-in. contact gap, was affected by vibration in its supporting steel panel. The panel was resonant to vibration in the supporting steel which developed at partial speed when the unit was coasting down to turning gear engagement for scheduled maintenance. The relay would not repeat this performance every time. However, the relay contact gap was increased to $^1/_4$ in. with only a small increase in relay operating time for generator winding short circuits, and the panel was mounted on vibration dampeners.

The second incorrect operation shown in Table 1 occurred when a 125-volt relay coil, used to supervise the protective relay tripping circuit, caused loss of the machine to the system. Since this incident, all such relays have been equipped with an external resistor connected in series with the coil, having such ohmic value that a short circuited relay coil will not cause the tripping multicontact relay to function. This is an example of history repeating itself. Years ago we went through the same corrections in the case of the supervisory indicating lamp.

Turbine System

Table 2 shows faulty performance in a multipoint, automatic standardizing, thrust-bearing temperature controller used for tripping the unit. This device has been shown to have two major weaknesses. First, it is a poor application which requires the protective device to supervise 4 to 6 thermocouples, as described in the foregoing material and it is very likely to be on the wrong "point" when an abnormal temperature develops at one particular thermocouple. Second, the automatic standardizing circuit adds such complication and does little real good. We now know that by use of a suitable battery, standardizing can be done once every two weeks and this can be performed manually. These statements are not meant as a reflection on the trip controller manufacturer. In fact, he originally protested the adoption of his recorder to protective service. We felt it offered the best solution available at that time and that it should be modified for this purpose and so urged the manufacturer to furnish the equipment for our use as requested. The manufacturer has since worked with us to produce a single-point device which we now call a temperature relay. It has no provision for recording and it is set up for manual standardizing.

We began using turbine and generator bearing vibration protection[4] some years before the use of unit protection systems. Due to the mass of the bearing pedestals or standards, vibration amplitudes for the relay settings had to be held very low. Since our main concern is the behavior of the shaft, we have encouraged over an extended period the development of a vibration pickup to measure shaft vibration for relay purposes. This type of protective equipment will be used for the first time when the 335-mw Unit No. 3 turbine generator at Astoria Station goes into operation this Fall. The shaft pickup allows larger vibration amplitude settings of the relay with the same degree of protection than the pedestal type of pickup and makes the relay less susceptible to false operation due to nearby explosions or disturbances that may result in vibration being transferred to the turbine-generator through the foundation.

In all of the work associated with the development of protective relays our experience has indicated the desirability of utmost simplicity in circuitry and the use of the highest quality components. Considerable progress has been made in this direction with the co-operation of the manufacturers.

Also we have urged the development of better quality pickup magnets and coils such as are used for turbine supervisory instrumentation since we expect to use these "pickups" for protective elements in the future. Earlier designs were susceptible to loosening of the core iron and mounting bolts and also to coil damage from moisture, high temperature, and oil vapors. As a result of the manufacturer's co-operation, there are now available assemblies which are more rugged, capable of withstanding heat, moisture, and oil atmospheres, and have other improved design features. This work has resulted in a considerable advance in over-all reliability of turbine supervisory sensing devices and has made practical the use of additional turbine pro-

[4] R. L. Webb and C. S. Murray, "Vibration Protection for Rotating Machinery," *Electrical Engineering*, vol. 63, 1944, pp. 534–537.

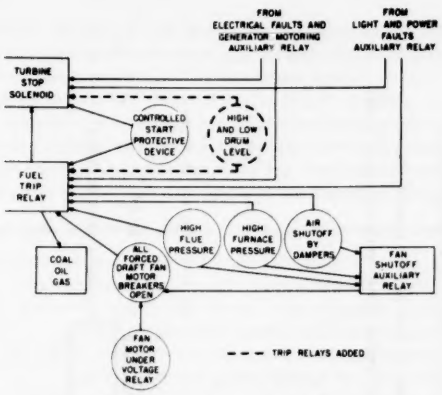
FROM ELECTRICAL FAULTS AND GENERATOR MOTORING AUXILIARY RELAY
FROM LIGHT AND POWER FAULTS AUXILIARY RELAY
TURBINE STOP SOLENOID
CONTROLLED START PROTECTIVE DEVICE
HIGH AND LOW DRUM LEVEL
FUEL TRIP RELAY
HIGH FLUE PRESSURE
HIGH FURNACE PRESSURE
AIR SHUTOFF BY DAMPERS
COAL OIL GAS
ALL FORCED DRAFT FAN MOTOR BREAKERS OPEN
FAN SHUTOFF AUXILIARY RELAY
FAN MOTOR UNDER VOLTAGE RELAY
TRIP RELAYS ADDED

Fig. 4 Revised section C of Fig. 1

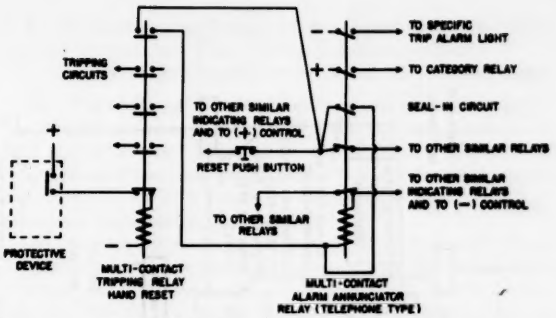
TRIPPING CIRCUITS
TO SPECIFIC TRIP ALARM LIGHT
TO CATEGORY RELAY
SEAL-IN CIRCUIT
TO OTHER SIMILAR INDICATING RELAYS AND TO (+) CONTROL
TO OTHER SIMILAR RELAYS
RESET PUSH BUTTON
TO OTHER SIMILAR INDICATING RELAYS AND TO (−) CONTROL
TO OTHER SIMILAR RELAYS
PROTECTIVE DEVICE
MULTI-CONTACT TRIPPING RELAY HAND RESET
MULTI-CONTACT ALARM ANNUNCIATOR RELAY (TELEPHONE TYPE)

Fig. 5 Basic diagram of trip and alarm wiring

tective relays not heretofore considered possible. These new type coils will be used for the first time on Unit No. 3 at Astoria.

Boiler System

Table 3 provides nothing for comment in regard to changes to the boiler protective devices excepting for the one instance on Astoria No. 2 unit where faulty control wiring on the motor-operated gas valve associated with the loss of fuel relay resulted in a trip-out of the unit. This and similar incidents in relation to wiring has led to improvements in types of cable and insulation employed for protective circuits.

Miscellaneous

The annunciator panel and the type of indications to be expected for any unit tripping operation were described in the original paper.[1] The electrical wiring of the system is quite simple as shown in Fig. 5. When a main protective device or relay operates, it closes several contacts directly or through an auxiliary relay. One of these initiates the annunciator by energizing a small relay at the rear of the panel. A separate such relay is assigned to each tripping device. When this annunciator panel relay operates it:

1 Energizes a "category" relay which indicates whether the boiler, turbine, or electrical system is involved by energizing a large white light.

2 Closes a contact which energizes a small red light to indicate the main protective device or relay which initiated the tripping operation.

3 Opens both polarities of a circuit which prevents the coils of any of the remaining annunciator relays being energized.

4 Seals itself in the "operated" position and holds this position until "reset" by a hand operated push-button.

This indication system has been very helpful to the station operators in analyzing the causes of tripping operations.

It might be of interest at this point to say that the relay trip-annunciator panel was wired originally to reset as soon as a boiler-draft fan is started following a trip-out. This has been found undesirable, since on some occasions a fan is restarted before the trip indication has been recorded. This wiring is now changed so that the operator must reset the trip-indication lights by hand.

Further Development of Protective System

Certain protective relays and tripping circuits have been added to the original protective system. This development has taken place as the result of a continuing study of those conditions which may occur under:

1 Excessive differential expansion.
2 Instantaneous thrust bearing failure under impact loading.
3 Very low level in the oil reservoir.
4 Loss of lubricating-oil pressure in the hydraulic coupling drive for a shaft driven boiler feed pump.
5 Trip of unit as related to motor-driven boiler feed pumps.
6 Excessively high and low boiler-water drum level.
7 Excessive rates of metal temperature change.

Damage From Excessive Differential Expansion

Occasions arise particularly under rapid steam-temperature changes or during starts from cold of a modern high-temperature unit when differential movement between rotor and casing may become excessive. Since this movement is not detected by any of the trip relays employed in the original protective system, a differential expansion trip relay has been added as shown in Fig. 2 to protect the unit against blade and other internal damage. The sensing element for this relay is a pair of coils which will be essentially a duplicate of and similarly mounted as the newly developed coils for the differential expansion recorder.

Damage From Thrust-Bearing Failure Under Impact Load

When impact loading is applied to the thrust bearing causing failure there is the possibility that the temperature rise in the metal shoe or plate would not be sufficiently fast to prevent the disintegration of the thrust face. Therefore to back up the temperature relay, each shaft is provided with a thrust babbitt failure protective relay of the hydraulic jet type as shown in Fig. 2. As now furnished by the turbine manufacturer this device senses axial movement, and the unit is tripped before extensive damage to the thrust runner and other parts of the turbine takes place.

Damage From Low Oil Reservoir Level

In view of the possibility of losing oil from the main oil reservoir through failure of some part of the lubrication system or, more particularly, through some improperly operated valved connection in the drain or filter system piping associated with it, a very low oil level switch is provided on the reservoir, Fig. 2, which is set to trip the unit when the oil level falls below the lowest point for satisfactory operation. It is expected that, when such an unusual loss of lubricating oil occurs, it will be possible to bring the unit to rest before bearing and other damage is experienced.

Damage From Loss of Hydraulic Coupling Lubricating-Oil Pressure

The first installation of a shaft-driven boiler feed pump will be placed in operation when Unit No. 3 at Astoria goes into service this Fall. Lubrication for this pump is provided from the hydraulic coupling through which this pump is driven. In order

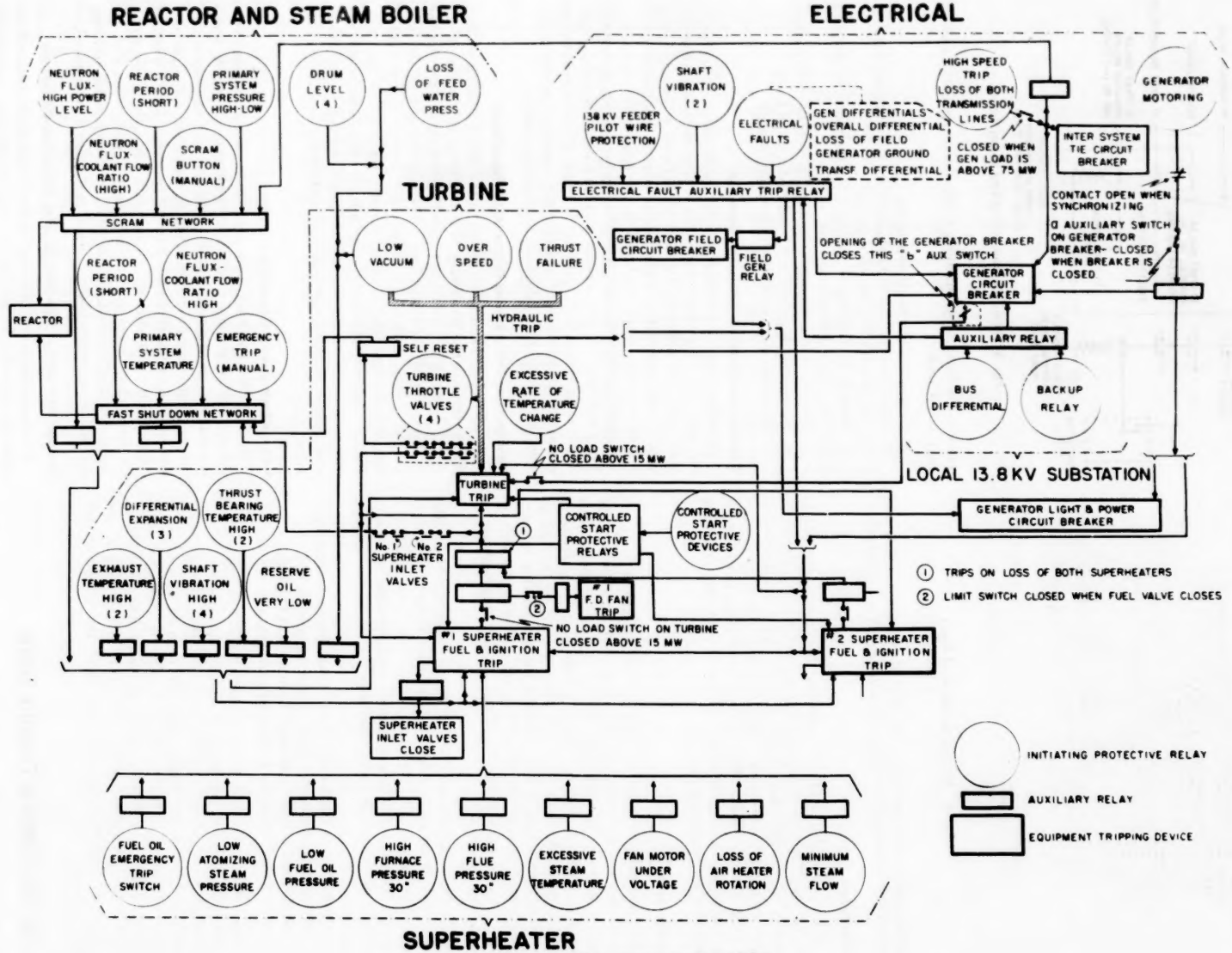

Fig. 6 Protection system—nuclear station

to prevent damage to the pump and coupling in the event of loss of lubricating-oil pressure a relay is provided to trip the unit whenever this pressure falls below a preset level.

Since a mechanical shear-type disconnect coupling is interposed between the outboard end of the generator shaft and the hydraulic coupling, an interlocking position switch is provided on the mechanical coupling as shown in Fig. 2 which interrupts this trip circuit whenever this coupling is in the disconnected position.

Damage From Excessively High or Low Boiler-Water-Drum Level

With extreme load swings occurring on a unit or with trouble on level control devices there can take place a transient level change of the water in the boiler drum. On occasion these level changes are so extensive that the water level is no longer visible in the gage glass. If the water rises to an excessively high level, water may be carried over and cause damage to the turbine. If the condition is such as to result in excessively low level, damage to the boiler may occur. To prevent either of these situations from arising contacts are provided on the drum-level indicating device, Fig. 4, to trip the unit when the boiler-water-drum level exceeds the range of the gage glass.

Damage From Loss of Boiler Feed Suction Pressure on Trip of Unit

On the three units whose history has been reviewed and on three additional 335-mw units now under construction, the boiler-feed suction is taken from a deaerating heater. When a sudden change in load occurs on such a feedwater-cycle arrangement there is rapid decay of deaerator pressure. Flashing of the stored water in the deaerator follows immediately. If the rate of load decrease is high enough there is flashing in the boiler feed pump which may result in seizure of the rotating and stationary pump parts. This is true for flexible-shaft-design pumps which constitute most of the feed pumps in operation today. With the automatic protection system, this hazard has been virtually eliminated where the operating condition calls for the automatic trip system to function. The improvement results from the automatic tripping, by undervoltage devices, of main condensate and boiler feed-pump motors in two to three seconds after the main unit is tripped. Tripping of the condensate pump halts the flow of cold condensate into the deaerator and arrests the condensing action and resulting pressure decay in the deaerator. Stopping the boiler-feed-pump motors prevents possible rubbing, galling, and ultimate seizure of rotating and fixed pump parts. A further improvement in this latter situation will be made on new trip systems by tripping the feed-pump motors directly on loss of the main unit as well as by undervoltage relays. Protection against reverse rotation of the boiler feed pumps will be provided in the event of main unit trip-outs by energizing to close the electrically operated fast-closing gate valves in the discharge. This feature serves as a back-up in case of failure of the discharge check valves. These additions are shown in Fig. 3.

Automatic Tripping System Applied to Nuclear Station

Fig. 6 shows the automatic protection system as now developed for application at Indian Point Station, with provisions for both fast reactor shutdowns and for scramming depending upon the initiating source of trouble.

Conclusions

1 The relay protection developed has proved to be reliable beyond expectations.

2 This system reduces the extent of serious boiler, turbine, and generator damage and also reduces repair outage time.

3 This relay protection system provides supervision which functions automatically under conditions which may not be immediately recognizable by the operator.

4 The protective equipment relieves the operator of a certain amount of strain and fatigue during abnormal conditions.

5 The cost of the protection is justified on the following bases:

(*a*) The additional cost of this over-all unit protection is only $^1/_2$ per cent of the installed cost of a 200-mw unit, exclusive of land and structures. This cost is justified because without this relay system at least one more operator would be required around the clock. Even with this extra operator the same quality of protection could not be obtained.

(*b*) Another approach to the cost matter is to consider it on an annual basis as one would pay annual premiums on insurance coverage and in that case the premium payment for the protection is on the same order per dollar of equipment investment as the premium on explosion insurance on the turbine-generator unit only.

6 The demonstrated reliability of the automatic protection system enhances the possibilities of the development of the remotely operated generating station.

DISCUSSION

J. F. Allen[5]

The authors have presented a very interesting and valuable description of the service performance of a modern power-plant protective scheme. New and improved equipment has been developed. It emphasizes the importance of care in the design and selection of components in any protective scheme. This raises an interesting question in regard to the application of control systems in nuclear power plants. Would the authors care to comment on the effect radiation levels in the reactor area may have on the selection of appropriate control apparatus and wiring?

The authors found that multipoint temperature trip devices did not provide protection because of the time interval required for scanning. Would the authors indicate what scanning interval (something more than continuous) would be short enough so that incipient thrust-bearing failure can be detected by a temperature measurement, or is the time constant of the bearing material so large that measurement of temperature is not satisfactory even on a continuous basis?

The authors point out that the protective system has not only eliminated one operator per shift but has improved system protection. This appears to imply that an operator would usually not take corrective action quickly enough to limit damage to the same degree as the automatic system. A rough order of magnitude of speed with which various corrective actions must be taken would be useful in determining the programming and scanning speed of supervisory control systems, especially where remote operation is contemplated.

The desirability of automatic protection is demonstrated by the system operating correctly sixteen out of twenty-one times with only 7 per cent total outage time attributable to faulty operation. The total outage time due to control system failure is a very small portion of the unit's service time. This fact, together with the large number of control elements involved, shows the extremely high average reliability of individual components.

P. G. Ipsen[6] and R. L. Jackson[6]

It is recognized that there have been many cases where immediate tripping would have reduced the amount of damage that resulted. Such cases are loss of lubricating oil, bearing failures, vibration, etc.

[5] Jackson & Moreland, Inc., Boston, Mass.

[6] Engineering Section, Large Steam Turbine-Generator Department, General Electric Company, Schenectady, N. Y. Mem. ASME.

There has been a reluctance on the part of operators to remove a unit from service until the external evidence is very pronounced and this is sometimes very late. Instruments can continuously monitor and function at a given value to give more positive protection.

The excellent record of reliability reported by the authors owes a great deal to the care and thoroughness which their company used in the details of engineering and design of the automatic tripping arrangements. During the design period, it was evident to the equipment suppliers that the Consolidated Edison Company engineers subjected each component to detailed study before accepting it for use, and that they often were unwilling to accept available products, requiring instead that new designs be developed to meet their requirements. It is presumed that equal attention was given to circuit design and wiring practices. This is the sort of approach that the power-plant designer must take to achieve satisfactory reliability for elaborate automatic control systems.

As a regular standard practice, the turbine manufacturer with whom the writers are associated requires a number of the tripping circuits which are described. Tripping on overspeed and low vacuum is provided for in the turbine control system. It is intended that the turbine solenoid trip be energized by any of the following devices:

1 Remotely located trip switch.
2 Thrust-bearing failure relay.
3 Generator differential and ground relays.

In addition, it is recommended that closure of the main and reheat stop valves open the generator circuit breaker.

Where the tripping is initiated by a mechanical malfunction, such as low vacuum, it is recommended that a sequential system be used; that is, the initiating device should energize the solenoid trip and the resulting closing of main and reheat stop valves should open the generator circuit breaker. This is recommended to avoid opening the breakers, if the turbine valves are stuck, because to do so would cause damage far more serious than that which started the tripping action.

The remainder of the tripping circuits on the Astoria machines were introduced at the initiation of the Consolidated Edison Company. The turbine manufacturer is willing to go along with these extra tripping circuits, provided that the sequential tripping scheme is used for mechanical faults, and that the device for detecting the fault can be installed in a reasonable manner and at reasonable cost.

We note with interest that an "excessive rate-of-temperature change" trip relay is being supplied on the Indian Point turbine. It has been our experience that the difference in temperature across a metal section in a critical area provides a more satisfactory measure of thermal stress.

Tripping of a turbine is in itself not harmful, since steam flow is cut off and temperatures decay and equalize rather slowly without large thermal stresses being set up. The difficulties occur on restarting when it has been usually impossible to get high steam temperatures and, in addition, large throttling temperature drops take place while bringing the turbine back up to speed.

Julius A. Lind[7]

We feel that additional automation can usually be justified in electric central stations as rapidly as reliable devices and systems are developed. The authors are to be congratulated for having pioneered a full scale automatic protection system. It was to be expected that some of the initial installation would be troublesome. They are to be commended for exploring and correcting the troubles rather than taking the easy way out of abandoning the troublesome items.

In our own stations we have waited for devices to be proved reliable before applying them to automatic trips. Through a step-by-step program we have reached the point that we trip units from many of the trouble indications cited in the paper. We do not yet use:

High positive furnace pressure.

Turbine supervisory instruments except:

1 "Squealer ring" temperature
2 Thrust direction movement indicated by hydraulic pressure of position sensing device.

Loss of fuel

Drum level

The paper accomplishes two important purposes. It shows from actual experience the extent of reliability we others can expect from future similar installations. It points out to both designers and suppliers the careful study and field follow-up necessary to make such systems acceptably dependable.

The final conclusion, hinting at remotely operated steam-generating stations, should not be taken lightly. Our efforts should always be in that direction. The installation described in the paper is a major contribution in that direction.

Robert L. Reynolds[8]

This paper presents a comprehensive history of the operating experiences on the tripping equipment on several units of the Consolidated Edison Company of New York's system. As such, it removes many of the misgivings formerly held by users of this equipment and, furthermore, serves as a valuable background for further advances in the study of automatic operation of steam turbine generators and boilers.

In this study of automatic control there are now two operating philosophies:

1 Use of automatic control equipment only to indicate and record important measurements and, when they reach undesirable levels, to actuate a signal so that the operator is alerted in sufficient time to take the necessary steps to protect the unit.

2 Use of automatic control equipment not only to alert the operator but also to carry through and perform the necessary functions to protect the unit.

In both cases, but particularly so in the second case, reliability of the automatic control instrumentation is absolutely essential. The results at East River and Astoria indicate that the tripping instruments are quite reliable, resulting in an average annual outage of only $1^1/_2$ hours per unit caused by false trips, but an even higher degree of reliability is required before it can be considered safe to dispense with operators and depend upon the instrument always to do the right thing at the right time. In addition, this equipment should be inspected, and if necessary adjusted, at scheduled intervals to make sure that it is maintained in proper working condition.

In the broader aspects of automatic operation, the various cycles should first be considered separately and then integrated into a complete whole covering all of the equipment in the station.

On the turbine generator unit the following cycles of operation must be considered:

1 Turning gear operation
2 Speed-increasing cycle
3 Synchronization
4 Minimum-load cycle
5 Load-increasing cycle

[7] Assistant Chief Mechanical Engineer, Niagara Mohawk Power Corporation, Buffalo, N. Y. Mem. ASME.

[8] Section Engineer, South Philadelphia Works, Westinghouse Electric Corporation, Lester, Pa. Mem. ASME.

6 Changes in load to suit system requirements
7 Automatic load and frequency control
8 Shutting-down cycle
9 Speed-reducing cycle
10 Automatic tripping, such as described in this paper

As pointed out in this discussion, each of these operating cycles should be thoroughly studied separately before applying it to a particular installation. For example, utility companies have expressed a desire for a fully automatic turning gear. By this is meant equipment which, when the unit comes to rest, will actuate a switch which will start the turning gear motor, (provided oil at an adequate pressure is being supplied to the bearings), will then operate a jogging mechanism and engage the turning gear teeth, and, finally, roll the shafts at the proper speed. All of this is to be done without any action on the part of the operator, but under the control of such monitoring equipment as to insure that the unit is in a suitable condition to be placed on the turning gear.

Work is now being done on the development of such a control, operating, and monitoring system for automatic turning gear operation. Furthermore, study is also being made of the other phases listed. It will be appreciated that the complete development of this automatic operating system is a tremendous undertaking, since it involves in some cases some or all of the equipment in the station. Furthermore, we repeat that each part of the system should be placed in service and operated for a considerable length of time under all sorts of operating conditions, to make sure that its reliability is maintained over extended periods of time.

In the paper, the authors question the ability of the thrust trip to anticipate a thrust-bearing failure sufficiently to prevent serious damage to the turbine. This device consists of a hydraulic jet directed against a disk or collar on the shaft. An axial movement of the shaft will change the pressure of this hydraulic jet, which is adjusted to trip the valves when this movement is excessive but still comfortably less than that which would cause serious failure.

In summary, we again wish to thank the authors for this comprehensive history of this automatic equipment and feel that it serves as a worth-while stepping stone along the path of the development of completely automatic operation of steam power plants.

Authors' Closure

In response to questions raised by the discussers of this paper, the authors wish to comment as follows:

In answer to Mr. Allen, although there is a limited background of experience in the application of instrumentation in reactor areas, it is anticipated that the problems presented can be coped with by proper selection of apparatus and wiring and also arranging it so as to subject it to a minimum exposure. While final decision has not yet been reached on the insulation for control wiring within the sphere at Indian Point, tests have shown that synthetic rubber compounds with lead sheath may be expected to have a life expectancy of 40 years or more in radiation intensities in the order of 160 R.

In any case solenoid coils in this area will be insulated with silicone rubber possibly reinforced with glass fibers, and motor windings shall be class H insulated.

For thrust bearing temperature relay protective circuits, or for that matter any relay protective circuit, continuous supervision should be provided. Earlier applications where scanning of multiple points was employed proved inadequate. Even with continuous supervision the paper points out in the case of the thrust bearing relay the possibility of insufficient rate of response for adequate protection. It is for this reason that the thrust babbitt failure protective relay of the hydraulic jet type as provided by several turbine builders is regarded as a valuable addition to the protective system.

In answer to Messrs. Ipsen and Jackson, as indicated by the protection diagrams shown in this paper, it is the practice of the Consolidated Edison System to trip the turbine and then the generator, except where certain electrical faults occur which leave little or no choice between sequential and simultaneous tripping. Where such an electrical fault is involved simultaneous tripping has been employed as shown by the diagrams in the paper. The excessive rate-of-temperature change protective relay has been introduced in the future Indian Point protective system to protect against the possibility of unusually large and extremely rapid steam temperature changes. This unit employs a separately oil-fired superheater in conjunction with the reactor with a considerably greater potential rate of temperature change than the conventional boiler and superheater combination. Under such conditions and particularly where heavy metal sections are encountered, the measure of temperature differences across these sections is not considered an adequate criterion for protection.

No particular difficulties have been encountered on restarting a unit which has been tripped out. Since the boiler and turbine are tripped simultaneously, with the usual short shutdown following a trip, there is no appreciable pressure decay and temperature conditions are re-established so rapidly that the degree of cooling to which the turbine parts are exposed is not considered excessive.

The authors concur with the viewpoint of Mr. Reynolds that any protective relay should be proved reliable before being accepted for this service. This applies not only to the relay itself but also to the circuitry associated with it. There are in general four basic requirements which should be met to attain this reliability. The design of the relay should be as simple as possible, the quality of the components should not be compromised, and the circuitry should be confined to the prime function of the protective relay, and it should be thoroughly tested before being used for unit protection.

It was not intended to imply in this paper that the thrust babbitt failure protective relay of the hydraulic jet type would not prevent serious damage to the turbine. On the contrary, this device is mentioned in the paper as functioning to trip the turbine before extensive damage to the thrust runner and other parts of the turbine takes place.

W. F. SCHALKWIJK

Philips Research Laboratories,
N. V. Philips' Gloeilampenfabrieken,
Eindhoven, Netherlands

A Simplified Regenerator Theory

Most regenerators encountered in practice have simple linear or exponential temperature fields in their central parts. This leads to the possibility of a simplified representation of the regenerator efficiency with sufficient accuracy for all practical cases. In the important "symmetrical" case, in which the parameters have the same value in both directions of gas flow, the efficiency can be represented by a single curve. This case is treated extensively in this paper. The results for the general case are given in an Appendix. Here also a reduction is achieved of the number of parameters needed to represent the efficiency.

1 GENERAL INTRODUCTION

Brief Outline

THE PRESENT WORK arose from the need for reliable and accurate values of the efficiency of regenerators, which had not yet been calculated with sufficient accuracy or were not yet known at all.

There are two ways of obtaining these figures: We can either derive a simple theory which would be approximately valid for the field of parameter values in which we are interested, or try to calculate the values we need from known values of η. However, both methods are based on the same fact; viz., that in "long" regenerators the temperature field in the central part can be represented by simple linear or exponential functions. This was discovered by Hausen,[1] who found that for long regenerators the temperature field in the central part of the regenerator could be represented in close approximation by his so-called "zeroth eigenfunction." He also sketched in his book a method of calculating approximately the complete temperature field in long regenerators from the calculated field in shorter regenerators. A formula for the efficiency was not given, however.

For the derivation of this formula we have made use of the idea of "enthalpy flux," which already had proved to be a powerful tool in other respects. By means of this concept the loss of the regenerator can be calculated from the zeroth eigenfunction and this enables us to calculate the loss of a longer regenerator from the known value of the loss of a shorter regenerator. The formula which is derived from these considerations proves to be in perfect agreement with numerical results obtained by other authors. It will be given completely for the symmetrical case in which the parameters in both directions of flow have the same values. It can be extended also, however, to the general case.

In Part 1 we shall give the differential equations which are needed for the derivation of the formulas for the zeroth eigenfunction. The formulas for the enthalpy flux also will be derived.

In Part 2 we proceed to apply these formulas to the symmetrical case, and compare the resulting formula with known numerical results. This formula takes the form of a new quantity, denoted by the symbol Ω, *which depends only on the dimensionless parameter* Π. The definition of Ω for the symmetrical case is

$$\Lambda + 2 - \frac{2}{1 - \eta} = \Omega(\Pi)$$

The function Ω is derived from numerical results up to a value of $\Pi = 20$. We wish to extrapolate this curve to all values of Π, however. This is done in Part 3 by means of a simple theory, which has only heuristic value. This part closes with a discussion of the results. To avoid confusion the results for the general case are presented only in very short form in the Appendix.

The Differential Equations (Symmetrical Case)

In this section we use the nomenclature introduced by Hausen.[1] Only his symbol for the dimensionless time co-ordinate is replaced by the symbol τ, to avoid confusion with the symbol for the efficiency of the regenerator η. We introduce (cf. also list of symbols given under Nomenclature):

[1] Helmuth Hausen, "Wärmeübertragung in Gegenstrom, Gleichstrom und Kreuzstrom, Springer Verlag, Berlin, Göttingen, Heidelberg, Germany, 1950, pp. 406–412.

Contributed by the Gas Turbine Power Division and presented at the Annual Meeting, New York, N. Y., November 30–December 5, 1958, of THE AMERICAN SOCIETY OF MECHANICAL ENGINEERS.

NOTE: Statements and opinions advanced in papers are to be understood as individual expressions of their authors and not those of the Society. Manuscript received at ASME Headquarters, June 24, 1958. Paper No. 58—A-135.

Nomenclature

Λ = dimensionless length of regenerator

Π = dimensionless period of regenerator

Γ = ratio of total thermal capacity of regenerator to total thermal capacity of gas flowing through regenerator

ξ = dimensionless co-ordinate of place in regenerator

τ = dimensionless time co-ordinate

H = total enthalpy transport during complete cycle of regenerator

C_g = total thermal capacity of gas flowing through regenerator in one direction (symmetrical case)

T_w = matrix temperature during period of flow in positive direction

T_w' = matrix temperature during period of flow in negative direction

T_g = gas temperature during period of flow in positive direction

T_g' = gas temperature during period of flow in negative direction

T_0 = temperature of gas entering at low-temperature side of regenerator

$T_0 + \Delta T_g$ = temperature of gas entering at high-temperature side of regenerator

F_0 = zeroth eigenfunction of matrix temperature (gas flowing in positive direction)

F_0' = zeroth eigenfunction of matrix temperature (gas flowing in negative direction)

η = efficiency of regenerator

ξ = dimensionless place co-ordinate; $0 \leqq \xi \leqq \Lambda$

Λ = dimensionless length of regenerator

τ = dimensionless time co-ordinate; $0 \leqq \tau \leqq \Pi$

Π = dimensionless length of period of flow in one direction

T_g = gas temperature during period of flow in positive direction

T_g' = gas temperature during period of flow in negative direction

T_w = matrix temperature during period of flow in positive direction

T_w' = matrix temperature during period of flow in negative direction

F_0 = zeroth eigenfunction of matrix temperature (positive direction)

F_0' = zeroth eigenfunction of matrix temperature (negative direction)

The parameters Λ and Π are related by the expression:

$$\Lambda = \Pi\Gamma \tag{1}$$

It should be noted that in both periods (positive and negative flow) the co-ordinate τ goes from 0 to Π. The differential equations, as derived by Hausen,[1] are

$$\frac{\partial T_g}{\partial \xi} = T_w - T_g; \quad \frac{\partial T_w}{\partial \tau} = T_g - T_w$$
$$\frac{\partial T_g'}{\partial \xi} = T_g' - T_w'; \quad \frac{\partial T_w'}{\partial \tau} = T_g' - T_w' \tag{2}$$

Boundary conditions

$$\xi = 0: \quad T_g = T_0; \quad \xi = \Lambda: \quad T_g' = T_0 + \Delta T_g \tag{2a}$$

Combining these equations into one differential equation for the matrix temperature yields

$$\frac{\partial^2 T_w}{\partial \xi \partial \tau} + \frac{\partial T_w}{\partial \xi} + \frac{\partial T_w}{\partial \tau} = 0$$
$$\frac{\partial^2 T_w'}{\partial \xi \partial \tau} + \frac{\partial T_w'}{\partial \xi} - \frac{\partial T_w'}{\partial \tau} = 0 \tag{3}$$

From these equations F_0 and F_0' can be obtained. When shifting from the "positive" period to the "negative" period, the matrix temperature does not jump to another value, as does the gas temperature. The following conditions therefore should be fulfilled for every value of ξ:

$$T_w(\xi, 0) = T_w'(\xi, \Pi)$$
$$T_w(\xi, \Pi) = T_w'(\xi, 0) \tag{4}$$

If we introduce as a reference temperature the constant temperature T_0 with which the gas enters the low-temperature side of the regenerator in the positive period at $\xi = 0$, we may write

$$F_0 = T_0 + A + B(\xi - \tau)$$
$$F_0' = T_0 + A + B(\xi - \Pi + \tau) \tag{5}$$

A and B are arbitrary constants. It can be verified easily that these equations satisfy both (3) and (4). They do not, however, satisfy the boundary conditions at both ends of the regenerator. In the vicinity of $\xi = 0$ and $\xi = \Lambda$ the temperature field will be different from (5). The difference between the actual temperature field and (5) will, however, decrease more or less exponentially toward the central part of the regenerator, so that here F_0 and F_0' represent a very good approximation of the actual temperature field. This is illustrated in Fig. 1. The actual temperature fields are drawn at the beginning of the positive and negative periods in

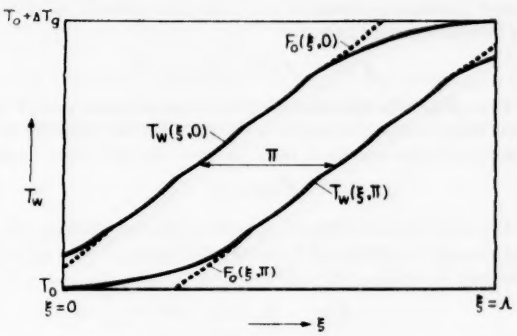

Fig. 1 Temperature field in regenerator matrix

full lines. F_0 and F_0' are indicated by dotted lines. We see that the curves coincide in the central part of the regenerator. Another fact is also indicated in this figure; viz., the horizontal distance through which F_0 and F_0' move. For example, this can be found from the equations:

$$F_0(\xi, 0) = F_0(\xi + \Delta\xi, \Pi)$$

We obtain

$$\Delta\xi = \Pi$$

From F_0' of course the same value is obtained. We also may ask what fraction this represents of the length of the regenerator. We obtain

$$\text{Fraction} = \frac{\Pi}{\Lambda} = \frac{1}{\Gamma}$$

It is to be expected that our approximation will only hold good if this fraction is small; i.e., that Γ fulfills the inequality

$$\Gamma \gg 1$$

In practice it turns out that $\Gamma > 2$ is completely sufficient, and that even good results are obtained if $\Gamma > 1$.

Enthalpy Flux

The first law of thermodynamics may be written for a fixed or varying volume V instead of for a fixed mass of gas. If U is the total amount of internal energy contained in the gas occupying this volume, and δH is the net enthalpy carried into V by the entering and leaving gas, we can write

$$\delta H + \delta Q = dU + pdV$$

We apply this formula to the gas in the regenerator contained between two arbitrary fixed cross sections 1 and 2, Fig. 2. We have $dV = 0$. If we consider only a stationary cycle of the regenerator, i.e., the temperature field repeats itself after each full

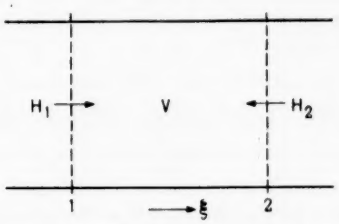

Fig. 2 Enthalpy flux in regenerator

period (containing a positive and a negative period), we obtain by integrating over this period

$$\oint \delta H + \oint \delta Q = \oint dU = 0$$

Here $\oint \delta Q$ is the total amount of heat supplied to the gas in V by heat transfer from the matrix to the gas. By the definition of a regenerator this amount is equal to zero. We thus have finally

$$\oint \delta H = 0$$

But this integral consists of two parts; viz., the enthalpy entering through 1 and through 2 during a full cycle. If we call these amounts H_1 and H_2, respectively, we have

$$\oint \delta H = H_1 + H_2 = 0$$

Hence

$$H_1 = -H_2 \tag{6}$$

Now H_1 is "flowing" in the positive direction and H_2 in the negative direction. But we may consider $-H_2$ to "flow" in the positive direction. As we considered arbitrary positions of cross section 1 and 2, (6) may be formulated in the following way:

During a full period the total amount of enthalpy flowing through a cross section in a specified direction is everywhere the same.

We shall denote this enthalpy flux by H. We shall make this more explicit by calculating H for a temperature field represented by F_0 and F_0'. In the regenerator theory with which we are concerned the amount of gas flowing through a cross section per unit time is supposed to be independent of time. If we denote by C_g the total heat capacity of the gas flowing through the regenerator in the positive period (and hence also in the negative period), we thus may write at once, as we consider an ideal gas with C_g independent of T_g

$$H = C_g \left[\frac{1}{\Pi} \int_0^{\Pi} T_g d\tau - \frac{1}{\Pi} \int_0^{\Pi} T_g' d\tau \right] \tag{7}$$

But F_0 and F_0' are given for the *matrix* temperatures. Therefore we must first calculate the corresponding gas temperatures. We do this with the aid of equations (2), which may be rewritten as follows:

$$T_g = T_w + \frac{\partial T_w}{\partial \tau}; \quad T_g' = T_w' + \frac{\partial T_w'}{\partial \tau}$$

Applying these formulas to (5) and substituting into (7) we obtain after an elementary calculation

$$H = -2C_g B \tag{8}$$

We see that H does not indeed depend on ξ, as we expected.

We also can relate H directly to the efficiency of the regenerator. We first introduce the symbol ΔT_g for the temperature difference between the gas stream entering the regenerator at the left-hand side during the positive period, and at the right-hand side during the negative period, Fig. 1. The total amount of heat which should be stored in the regenerator equals $C_g \Delta T_g$. The actual amount stored in the regenerator is, however, according to the definition of efficiency, equal to $\eta C_g \Delta T_g$. The difference between both amounts is equal to the loss of the regenerator. We can write therefore at once:

$$H = -(1 - \eta) C_g \Delta T_g \tag{9}$$

Comparing (9) with (8) shows that the general equation holds

$$(1 - \eta) \Delta T_g = 2B \tag{10}$$

We see that the loss of the regenerator is completely determined by the *slope* of the temperature field in the central part of the regenerator. This will play an important role in Part 2.

2 CALCULATION OF REGENERATOR LOSSES

General Theory

The basic idea of our method is to compare two regenerators of different lengths (Λ_1 and Λ_2) but with the same value of Π. We choose the gas-temperature differences ΔT_{g1} and ΔT_{g2} such that the value of B, and therefore, according to (8), also the value of H are the same in both regenerators. This enables us to calculate ΔT_{g2} from ΔT_{g1}, thereby establishing a relation between η_1 and η_2.

Consider two regenerators, which we shall call R_1 and R_2, Figs. 3 and 4. Their lengths are denoted by Λ_1 and Λ_2, the latter being the longer one. We assume that in the central part of R_1 the temperature field of the matrix is linear, which also can be formulated in this way, that the temperature field can be described in this part of the regenerator completely by the zeroth eigenfunction. In Fig. 3 we have drawn such a situation. The full lines indicate the temperature fields for $\tau = 0$ and $\tau = \Pi$, the dotted lines A_1A_2 and B_1B_2, F_0 (and F_0') for the same values of τ. We shall now prove the following statement:

By choosing a suitable value for ΔT_g in the second regenerator, the zeroth eigenfunction of the temperature field in this regenerator can be made exactly identical with the zeroth eigenfunction in the first regenerator

We recall that the formulas for the zeroth eigenfunction have the form (5)

$$\begin{aligned} F_0 &= T_0 + A + B(\xi - \tau) \\ F_0' &= T_0 + A + B(\xi - \Pi + \tau) \end{aligned} \tag{5}$$

We see that the formulas depend on the value of the parameter Π. Hence they can never be made identical in R_1 and R_2 if these regenerators have different values of Π. This obviates our condition to compare only regenerators with the same value of Π.

We must now show that it is possible to construct a temperature

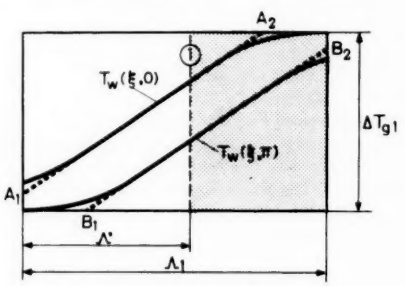

Fig. 3 Temperature field in shorter regenerator

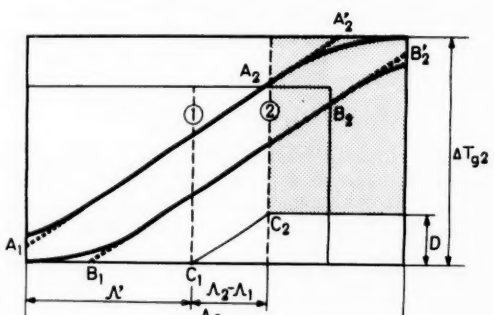

Fig. 4 Temperature field in longer regenerator

field in R_2 which satisfies all conditions. As identical eigenfunctions also must have an identical slope of the temperature lines, we proceed as follows:

We divide R_1 by a cross section 1 in two parts. This cross section is chosen at $\xi = \Lambda'$, where the temperature field is linear, Fig. 3. We "slide" the shaded part upward and to the right along A_1A_2 or B_1B_2 until it takes the position indicated by the shaded area in R_2, Fig. 4. The line C_1C_2 is drawn parallel to A_1A_2 and B_1B_2. We then see immediately

$$\begin{aligned} \Delta T_{g2} &= \Delta T_{g1} + D \\ D &= B(\Lambda_2 - \Lambda_1) \end{aligned} \tag{11}$$

Our new temperature field in R_2 is now supposed to be built up in the following way:

In the left-hand section (between $\xi = 0$ and $\xi = \Lambda'$) the temperature field is exactly equal to the temperature field in the corresponding section in R_1.

In the middle section the temperature field is represented by the same zeroth eigenfunction as in R_1.

In the right-hand section the temperature field is equal to the temperature field in the shaded area in R_1, to which only the constant D is added. We must show that this is consistent with the differential equations and the boundary conditions.

The matrix temperature in cross section 1 in R_1 is represented by [cf. (5)]:

$$\begin{aligned} T_w &= T_0 + A + B(\Lambda' - \tau) \\ T_w' &= T_0 + A + B(\Lambda' = \Pi + \tau) \end{aligned} \tag{12}$$

As we suppose F_0 and F_0' to be identical in R_2, this also represents the temperature fluctuation in cross section 1 in R_2. The temperature field in R_1 is of course supposed to be a solution of the differential equations; e.g., by numerical computation. Hence, as the boundary conditions in the corresponding sections in R_1 and R_2 are identical, the temperature fields also must be identical.

In the middle section of R_2 no difficulty arises, as F_0 and F_0' are solutions of the differential equations (cf. Part 1). In cross section 2 in R_2 according to our assumption the formulas (5) still hold, so the temperature fluctuation, acting as a boundary condition to the right-hand section, becomes [cf. (11)]:

$$\begin{aligned} T_w &= T_0 + A + B[\Lambda' + \Lambda_2 - \Lambda_1 - \tau] \\ &= T_0 + A + B(\Lambda' - \tau) + D \\ T_w' &= T_0 + A + B[\Lambda' + \Lambda_2 - \Lambda_1 - \Pi + \tau] \\ &= T_0 + A + B(\Lambda' - \Pi + \tau) + D \end{aligned} \tag{12a}$$

We see that this is exactly the temperature fluctuation represented by (12) with only the constant D added. However, we also added, according to (11), this same constant D to the temperature with which the gas enters the regenerator from the right-hand side. Hence the whole temperature field in the last section in R_2 can be considered to be equal to the corresponding section in R_1 with only the constant D added. This always represents a solution of the differential equations, as these equations are homogeneous.

By this reasoning we have shown that starting with the same zeroth eigenfunction in R_2 as in R_1 a new temperature field can be constructed which is consistent with the differential equations and all boundary conditions, provided the relations (11) hold. This is equivalent to our statement.

If (11) holds, we may write, according to (10):

$$(1 - \eta_1)\Delta T_{g1} = 2B = (1 - \eta_2)\Delta T_{g2}$$

Substituting these relations in (11) and rearranging

$$\Lambda_1 - \frac{2}{1 - \eta_1} = \Lambda_2 - \frac{2}{1 - \eta_2}$$

As the value of Λ_2 is arbitrary, we see that this combination of Λ and η is invariant for all regenerators having the same value of Π. This may be expressed in the form

$$\Lambda - \frac{2}{1 - \eta} = f(\Pi)$$

In practice $f(\Pi)$ turns out to be a monotonously increasing function of Π. For $\Pi = 0$, which corresponds with a finite value of Λ and an infinite value for Γ, we have the well-known equation

$$\eta = \frac{\Lambda}{\Lambda + 2}$$

Substituting, we obtain

$$f(\Pi = 0) = -2$$

As we may add a constant to $f(\Pi)$ without it losing its generality, we finally write

$$\Lambda + 2 - \frac{2}{1 - \eta} = \Omega(\Pi) \tag{13a}$$

Then Ω has positive values for all values of Π and is equal to zero only for $\Pi = 0$.

We recall that this expression is expected to hold only if the temperature field in the central part of the regenerator is linear. This will only be the case if the value of Γ is not too small. It turns out in practice that (13*a*) already holds to an exceedingly good approximation with the limits

$$2 < \Gamma < \infty \tag{13b}$$

Therefore we may say:

In the large majority of cases encountered in practice the value of η can be calculated to a high degree of accuracy from a single curve Ω, which is a function of Π only.

For the sake of convenience we rewrite (13*a*) to obtain as a function of Ω and Λ:

$$\eta = \frac{\Lambda - \Omega}{\Lambda - \Omega + 2} \tag{13c}$$

For $\Pi = 0$, Ω being then equal to zero, this coincides with the well-known formula. For other values of Π, Ω acts as a "correction" applied to the value of Λ.

Comparison With Numerical Results

The theory presented in the foregoing sections must now be compared with numerical results. We shall use the calculated values for η from a paper by Lamberton[2] as in that paper the values of η are claimed to be accurate to four figures. By interpolating carefully between these values Table 1 is obtained. Values of Ω are given as a function of Π and Γ. In the last column slightly rounded-off figures for the limiting figure of Ω for high values of Γ are given. These figures represent an estimation of these limiting values with the additional requirement that they represent a perfectly smooth function of Π. They also are plotted in Fig. 9. Table 1 bears out quite clearly that already for low values of Γ the value of Ω becomes practically independent of Γ. It is curious, however, that the limiting value of Ω seems to be approached in a slightly oscillatory manner. It is not clear

[2] T. J. Lambertson, "Performance Factors of a Periodic-Flow Heat Exchanger," TRANS. ASME, vol. 80, 1958, pp. 586–592.

Table 1 Values of Ω for different values of Π and Γ

Π/Γ	1.00	1.25	1.50	1.75	2.00	3.00	5.00	∞
1	0.0497	0.0555	0.0610	0.0654	0.0692	0.0784	0.0805	0.081
2	0.251	0.276	0.287	0.294	0.300	0.308	0.306	0.31
3	0.577	0.615	0.632	0.641	0.647	0.650	0.646	0.65
4	0.992	1.038	1.058	1.067	1.071	1.072	1.067	1.07
5	1.468	1.525	1.544	1.549	1.551	1.549	...	1.55
6	1.990	2.056	2.071	2.074	2.074	2.071	...	2.07
7	2.548	2.622	2.634	2.634	2.633	...	...	2.63
8	3.137	3.217	3.224	3.222	3.219	...	...	3.22
9	3.749	3.835	3.837	3.832	3.828	...	...	3.84
10	4.381	4.473	4.470	4.462	4.457	...	...	4.47
11	5.029	5.127	5.118	...	...	...	...	5.12
12	5.695	5.794	5.781	...	...	...	...	5.79
13	6.372	6.476	6.457	...	...	...	...	6.48
14	7.059	7.167	...	...	...	...	...	7.17
15	7.762	7.868	...	...	...	...	...	7.87
16	8.472	8.577	...	...	...	...	...	8.58
17	9.192	...	...	...	...	...	...	9.30
18	9.915	...	...	...	...	...	...	10.03
19	10.648	...	...	...	...	...	...	10.76
20	11.39	...	...	...	...	...	...	11.50

whether this is due to some systematic error in the values of η from which the values of Ω were calculated or whether this effect is real.

With increasing values of Π the value of Ω become more and more uncertain. Nevertheless, we sometimes encounter in practice values of Π of 40 or 50 or even higher. We shall therefore try to extrapolate the curve of Ω to these higher values of Π. In most cases, this need not be done very accurately, as in formula (13*a*) the *loss* $(1 - \eta)$ occurs, which in most cases need not be calculated with an accuracy higher than, say, 1 per cent. This is equivalent to an accuracy in Ω also of $\sim$1 per cent. An attempt is made to derive a simple theory for Ω in Part 3. However, first we will derive a general expression for Ω, which is independent of any assumption we make about the structure of the temperature field, except that this field is linear in the central part of the regenerator.

A General Formula for Ω

We consider the fluctuation of the matrix temperature at the point $\xi = \Lambda/2$ in the regenerator, Fig. 5. As this point is situated

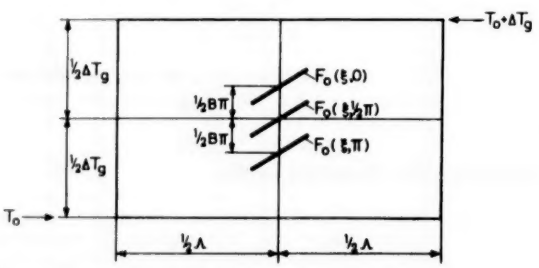

Fig. 5 Temperature fluctuation in middle of regenerator

in the central part of the regenerator, where the temperature field is linear, we may make use of (12)

$$T_w = T_0 + A + B\left(\frac{1}{2}\Lambda - \tau\right)$$

$$T_w' = T_0 + A + B\left(\frac{1}{2}\Lambda - \Pi + \tau\right)$$

We see that these temperatures "oscillate" symmetrically around the value

$$T_w\left(\frac{\Lambda}{2}, \frac{\Pi}{2}\right) = T_0 + A + \frac{1}{2}B(\Lambda - \Pi)$$

From considerations of symmetry it follows at once that this point also must lie symmetrically between the temperatures with which the gas enters the regenerator at both ends. These temperatures are T_0 and $T_0 + \Delta T_g$, respectively. Hence

$$T_0 + \frac{1}{2}\Delta T_g = T_0 + A + \frac{1}{2}B(\Lambda - \Pi)$$

$$\Delta T_g = 2A + B(\Lambda - \Pi)$$

Combining these equations with (10) yields an expression for $(1 - \eta)$, which can be substituted in (13*a*). We obtain finally

$$\Omega = \Pi + 2 - \frac{2A}{B} \tag{14}$$

We recall that again the only assumption is that the temperature field in the central part of the regenerator is linear. Otherwise this expression is completely general. We shall use it in Part 3.

3 EXTRAPOLATION OF Ω TO HIGHER VALUES OF Π

Simple Models

Formula (14) shows that a theory needs only to yield a value for the ratio between A and B, the constants occurring in F_0 and F_0', the zeroth eigenfunction. We try therefore to approximate the *whole* temperature field by this eigenfunction. We recall one of the results from an earlier section that the maximum horizontal distance over which F_0 and F_0' move, is equal to Π, independent of the slope of the lines. The simplest assumption which we can make is

$$A = 0$$

This situation is represented in Fig. 6. The temperature field sweeps to the right and the left across the shaded area over a distance Π. Formula (14) yields at once

$$\Omega_1 = \Pi + 2 \tag{15}$$

If we look at pictures of the actual temperature fields,[1] we see, however, that the slope of these lines is always less than the slope of the lines in Fig. 6. This seems to indicate that A is always

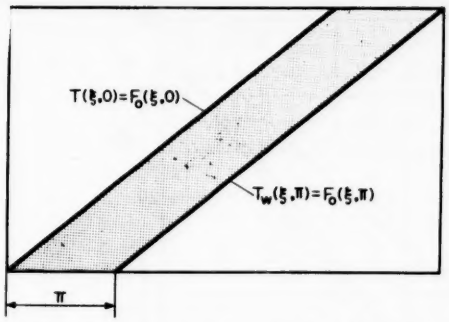

Fig. 6 First approximation to temperature field in regenerator

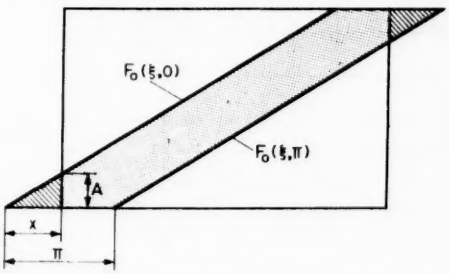

Fig. 7 Second approximation to temperature field in regenerator ($\Pi \geqq 2$)

positive, so that it seems quite reasonable to assume that Ω_1 represents an upper bound to the real values of Ω.

To obtain a more realistic picture of the temperature field, we assume A to have a positive value, as shown in Fig. 7. We try to fix the ratio of A and B by a consideration about the heat stored in the regenerator. It is obvious that this heat is proportional to the shaded areas in Figs. 6 and 7. The actual amount of heat stored in the regenerator is $\eta C_g \Delta T_g$, according to the definitions of these quantities. The maximum amount of heat that can be stored in a regenerator is $C_r \Delta T_g$, if C_r denotes the total thermal capacity of the regenerator. It is clear that this amount of heat is proportional by the same factor to the total area of Fig. 6 or Fig. 7. Hence

$$\frac{\text{Shaded area}}{\text{Total area}} = \frac{\eta C_g \Delta T_g}{C_r \Delta T_g} = \frac{\eta}{\Gamma},$$

$$\text{Shaded area} = \frac{\eta}{\Gamma};\ (\text{total area}) = \frac{\eta}{\Gamma}\,\Lambda \Delta T_g = \eta \Pi \Delta T_g$$

In Fig. 6 we had

$$\text{Shaded area} = \Pi \Delta T_g$$

Our first model corresponds therefore to a regenerator without any loss. In Fig. 7, however, we choose the shaded areas to be exactly equal to $\eta \Pi \Delta T_g$. Since

$$\text{Shaded area} + \text{total hatched area} = \Pi \Delta \tau_g,$$

we have

$$\text{Total hatched area} = (1 - \eta)\Pi \Delta T_g = XA$$

From the formula for F_0 it follows that

$$A = BX, \quad X = A/B$$

hence

$$XA = A^2/B$$

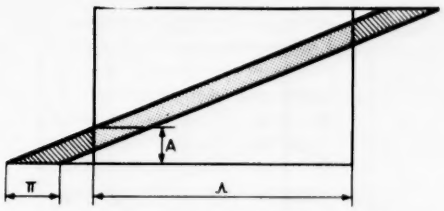

Fig. 8 Second approximation to temperature field in regenerator ($\Pi < 2$)

Substituting this in the foregoing equation and making use of (10) yields

$$A^2/B^2 = 2\Pi, \ A/B = (2\Pi)^{1/2}$$

Substituting this value into (14) yields finally

$$\Omega = \Pi + 2 - 2(2\Pi)^{1/2}$$

We also substitute the value of A/B into the formula for X

$$X = (2\Pi)^{1/2}$$

This shows that our formulas break down for $\Pi \leqq 2$, because then

$$X \geqq \Pi \quad \text{for} \quad \Pi \leqq 2$$

This is represented in Fig. 8. Also in this case the ratio of A to B can be calculated. We shall not go into details, as the computation is similar to the computation already performed. The result is

$$\Omega = 0, \quad \text{for} \quad 0 \leqq \Pi \leqq 2$$

Our model leads therefore to the following results (which will be denoted by Ω_2):

$$\begin{aligned} 2 \leqq \Pi < \infty: &\qquad \Omega_2 = \Pi + 2 - 2(2\Pi)^{1/2} \\ 0 \leqq \Pi \leqq 2: &\qquad \Omega_2 = 0 \end{aligned} \tag{16}$$

As the first formula for Ω_2 represents a curve which touches the axis at $\Pi = 2$, we see that no discontinuities arise at the point where both "branches" meet. The curves for Ω_1 and Ω_2 are represented in Fig. 9. There is some reason to expect that the values of Ω_2 represent a lower bound to the values of Ω. We compare them with numerical results in the next section.

Comparison With Numerical Results

In Table 2 the values of Ω_1, Ω_2, and Ω are given. For the values of Ω we use the estimated values from Table 1. Ω_1 and Ω_2 are given by (15) and (16). We see that as far as our table extends it is always true that

$$\Omega_1 > \Omega > \Omega_2 \tag{17}$$

This is also clearly seen in Fig. 9, where the three curves for Ω_1, Ω, and Ω_2 are plotted against Π.

We now wish to extrapolate our values for Ω to higher values of Π. We use as an asymptotic formula

$$\Omega_e = \Pi + 2 - 2.35\sqrt{\Pi} \tag{18}$$

Comparing (18) with (15) and (16) we see that

$$\Omega_1 > \Omega_e > \Omega_2$$

always holds for $\Pi > 2$. Hence condition (17) is fulfilled.

The values calculated for Ω with (18) are also shown in Table 2,

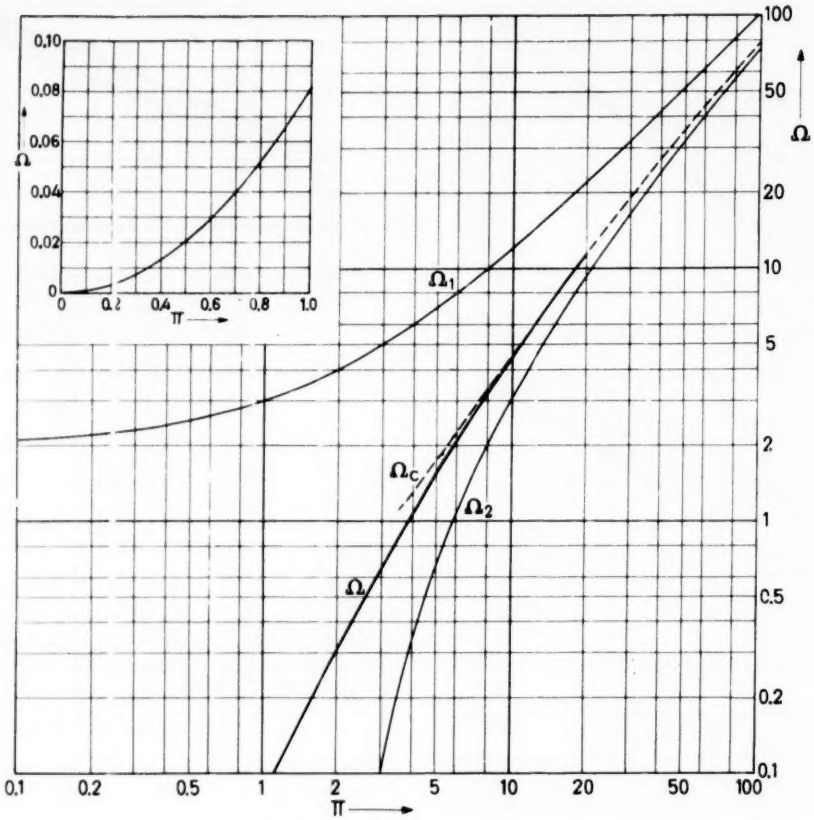

Fig. 9 Curves for Ω—symmetrical case

Table 2 Values of Ω

Π	Ω_1	Ω	Ω_2	Ω_c
0	2.00	0.00	0.00	...
1	3.00	0.081	0.00	...
2	4.00	0.31	0.00	...
3	5.00	0.65	0.10	0.93
4	6.00	1.07	0.34	1.30
5	7.00	1.55	0.68	1.75
6	8.00	2.07	1.07	2.24
7	9.00	2.63	1.52	2.78
8	10.00	3.22	2.00	3.35
9	11.00	3.84	2.51	3.95
10	12.00	4.47	3.06	4.57
11	13.00	5.12	3.62	5.21
12	14.00	5.79	4.20	5.86
13	15.00	6.48	4.80	6.53
14	16.00	7.17	5.42	7.21
15	17.00	7.87	6.05	7.90
16	18.00	8.58	6.69	8.60
17	19.00	9.30	7.34	9.31
18	20.00	10.03	8.00	10.03
19	21.00	10.76	8.67	10.76
20	22.00	11.50	9.35	11.49

and plotted as the dotted curve in Fig. 9. We see that this formula represents the values of Ω for higher values of Π with an astonishing accuracy. Besides, there are other indications that an asymptotic formula, representing Ω for high values of Π, will have a form which closely resembles (18). We therefore used this formula to extrapolate the values of Ω, calculated from numerical results, to higher values of Π in Fig. 9.

Discussion of Results

In practice, one is usually more interested in the loss of a regenerator than in its efficiency. For regenerators of high efficiency the loss is also far more sensitive to errors in the formula for the efficiency than the efficiency itself. We therefore rewrite (13c) in the following form:

$$1 - \eta = \frac{2}{\Lambda - \Omega + 2} \tag{13d}$$

The most important question is, how well the actual values of $(1 - \eta)$ are represented by (13d). To answer this question we calculate $(1 - \eta)$ with (13d) and the values of Ω from the last column in Table 1 for $\Gamma = 1$ and $\Gamma = 2$ as a function of Π, and compare them with the actual values. The relative error in the computed values are represented in Table 3, together with the values of Ω we used. We see that even for $\Gamma = 1$ the relative error is only of the order of magnitude of 1 per cent. For $\Gamma = 2$ this error is already much smaller and decreases with increasing value of Π. For higher values of Π, we recommended formula (18) for Ω:

$$\Omega = \Pi + 2 - 2.35\sqrt{\Pi} \tag{18}$$

We see from Table 2 that for values of Π in the vicinity of Π = 20 this formula represents the values of Ω to a very close approximation. Hence in this region the values of $(1 - \eta)$ calculated with (13d) and (18) have relative errors of the same order of magnitude as indicated in Table 3. For higher values of Π the ac-

Table 3 Relative error in $(1 - \eta)$, calculated with formula

Π	Ω	Relative error in $(1-\eta)$, per cent $\Gamma = 1$	$\Gamma = 2$
1	0.081	1.1	0.3
2	0.31	1.6	0.2
3	0.65	1.7	0.0
4	1.07	1.6	0.0
5	1.55	1.5	0.0
6	2.07	1.4	−0.1
7	2.63	1.3	0.0
8	3.22	1.2	0.0
9	3.84	1.3	0.1
10	4.47	1.2	0.1
11	5.12	1.2	...
12	5.79	1.2	...
13	6.48	1.3	...
14	7.17	1.3	...
15	7.87	1.2	...
16	8.58	1.1	...
17	9.30	1.1	...
18	10.03	1.2	...
19	10.76	1.1	...
20	11.50	1.1	...

curacy of $(1 - \eta)$ depends on the accuracy of (18), which in its turn depends chiefly on the accuracy of the constant 2.35. The relative error in this constant is expected to be of the order of magnitude of 1 per cent. We investigate the total error in $(1 - \eta)$ by substituting (18) in (13*d*) and taking into account that $\Lambda = \Gamma\Pi$:

$$1 - \eta = \frac{2}{(\Gamma - 1)\Pi + 2.35\sqrt{\Pi}} \tag{19a}$$

For $\Gamma = 1$ this takes the form:

$$1 - \eta = \frac{2}{2.35\sqrt{\Pi}} \tag{19b}$$

From Table 3 it is seen that (13*d*) represents $(1 - \eta)$ with a relative error of ~ 1 per cent for $\Gamma = 1$. As we expect the constant 2.35 to be in error only by ~ 1 per cent, the total relative error in $(1 - \eta)$ for $\Gamma = 1$ is expected to be of the order of magnitude of 1–2 per cent.

According to Table 3 we may assume that for this region of values of Π (13*d*) represents $(1 - \eta)$ already for $\Gamma = 2$ with a negligible error. Formula (19*a*) takes for $\Gamma = 2$ the form:

$$1 - \eta = \frac{2}{\Pi + 2.35\sqrt{\Pi}} = \frac{2}{\Pi\left[1 + \dfrac{2.35}{\sqrt{\Pi}}\right]} \tag{19c}$$

We see that for high values of Π a relative error of 1 per cent in the constant 2.35 introduces only a small error in $(1 - \eta)$; e.g., for $\Pi = 100$ an error of 0.1 per cent.

In practice $\Gamma \geq 1$ always holds, as otherwise the total thermal capacity of the regenerator would be less than the total thermal capacity of the gas. Hence we may say that (13*d*), combined with the numerically calculated values of Ω up to $\Pi = 20$ and with (18) for higher values of Π, represents $(1 - \eta)$ in all practical cases with sufficient accuracy. For $\Gamma > 2$ the values of $(1 - \eta)$ obtained in this way are even astonishingly accurate.

APPENDIX

General Case

The general case is characterized by the fact that the values of the parameters Λ and Π during the period of flow in the negative direction are different from their values during the positive period. These values for the negative period are therefore denoted by Λ' and Π'. In this case the zeroth eigenfunction takes the form of an exponential curve. Also in this case, however, most regenerators encountered in practice show temperature fields that consist in the central part of the regenerator only of the zeroth eigenfunction. Hence in these cases too, we can compare regenerators with identical eigenfunctions, which also lead to an

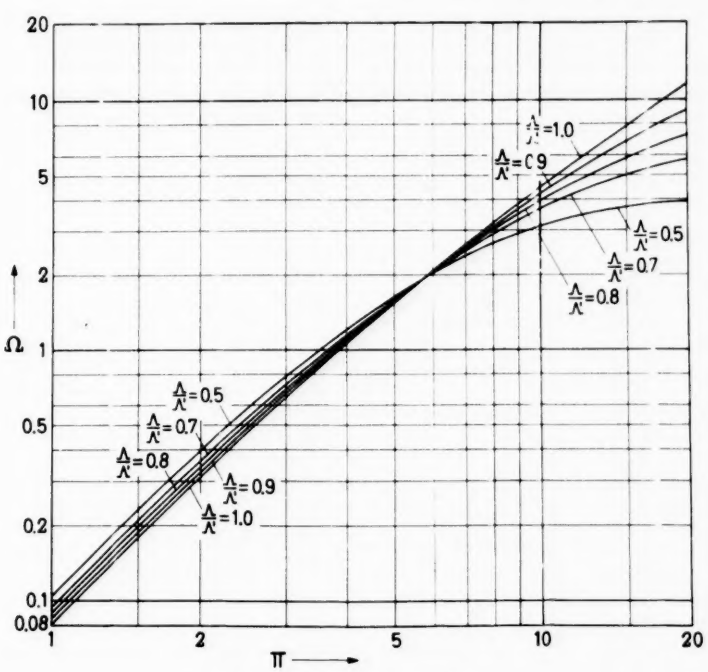

Fig. 10 Curves for Ω—general case

Table 4 Values of Ω for $\Pi' = \Pi$ and different values of Λ/Λ' and Π

$\Pi/\Lambda/\Lambda'$	1	0.95	0.90	0.80	0.70	0.50
1	0.081	0.083	0.085	0.089	0.094	0.105
2	0.31	0.32	0.33	0.34	0.36	0.40
3	0.65	0.66	0.67	0.70	0.73	0.78
4	1.07	1.09	1.10	1.12	1.15	1.22
5	1.55	1.56	1.57	1.59	1.60	1.64
6	2.07	2.08	2.07	2.06	2.05	2.04
7	2.63	2.61	2.59	2.54	2.49	2.38
8	3.22	3.17	3.12	3.02	2.91	2.67
9	3.84	3.74	3.66	3.48	3.30	2.92
10	4.47	4.33	4.19	3.92	3.66	3.13
11	5.12	4.92	4.72	4.35	3.99	3.31
12	5.79	5.52	5.25	4.76	4.29	3.45
13	6.48	6.11	5.77	5.14	4.56	3.56
14	7.17	6.71	6.28	5.50	4.80	3.65
15	7.87	7.30	6.78	5.84	5.02	3.72
16	8.58	7.89	7.26	6.15	5.21	3.77
17	9.30	8.48	7.74	6.44	5.38	3.81
18	10.03	9.06	8.20	6.72	5.53	3.85
19	10.76	9.64	8.65	6.97	5.66	3.88
20	11.50	10.21	9.08	7.20	5.78	3.90
∞	∞	40.00	20.00	10.00	6.67	4.00

invariant expression. The reasoning which leads to this result is quite analogous to the reasoning already presented in this paper, but more intricate. We shall only give the result, which is expressed in the following formulas:

$$\frac{2}{1 + \frac{\Pi'}{\Pi}} \frac{1}{a} [1 - e^{-a\Lambda}] + 2 - \frac{2e^{-a\Lambda}}{1 - \eta} = \Omega\left(\Pi, \frac{\Lambda'}{\Lambda}, \frac{\Pi'}{\Pi}\right) \quad (20)$$

$$a = \frac{\frac{\Lambda'}{\Lambda} - \frac{\Pi'}{\Pi}}{1 + \frac{\Pi'}{\Pi}}$$

We see that in this general case Ω not only depends on Π, but also on Λ'/Λ and Π'/Π. The symmetrical case, which we have treated in this paper, is characterized by:

$$\frac{\Lambda'}{\Lambda} = 1; \quad \frac{\Pi'}{\Pi} = 1$$

If we substitute this in (20), we see that $a \to 0$. We then have

$$\lim_{a \to 0} \frac{1}{a} [1 - e^{-a\Lambda}] = \Lambda$$

Hence it is easily seen that (20) becomes

$$\Lambda + 2 - \frac{2}{1 - \eta} = \Omega(\Pi, 1, 1)$$

This equation is identical with the expression for Ω represented by formula (13a). In this way it is seen that this formula is a special case of the general formula (20). Numerical values for Ω could only be obtained for $\Pi' = \Pi$. In this case it turns out that for $\Gamma \gg 1$

$$\lim_{\Pi \to \infty} \frac{e^{-a\Lambda}}{1 - \eta} = 0$$

Substituting this into (20) and rearranging yields

$$\lim_{\Pi \to \infty} \Omega = \Omega_\infty = \frac{2}{1 - \frac{\Lambda}{\Lambda'}}$$

This limiting value of Ω, denoted by the symbol Ω_∞, is shown in Table 4, in which the value of Ω is obtained from Lambertson,[2] are shown. The values of the symmetrical case ($\Lambda' = \Lambda$) have been entered also, to show the continuous variation of Ω as a function of Λ/Λ'. The values are also shown in Fig. 10.

We may rewrite (20), using the symbol Ω_∞:

$$1 - \eta = \frac{2}{e^{a\Lambda}(\Omega_\infty - \Omega) + 2 - \Omega_\infty}$$

We see that for high values of Π the numerator contains the product of a very small and very large quantity. Hence for these values of Π the formula yields rather uncertain values of $(1 - \eta)$. The value of $(1 - \eta)$ is, however, very small for these values of Π, so in practice usually no very accurate values are needed.

J. R. SCHNITTGER

Chief Engineer, Gas Turbine Department, Swedish Turbine Company Ljungström (STAL), Finspong, Sweden

Development of a Smooth Running, Double-Spool, Gas-Turbine Rotor System

Bearing stability difficulties of a 10,000-kw gas-turbine plant comprising three independent shafts (those of the low-pressure compressor, the high-pressure compressor, and the power-turbine rotors) are discussed. The bearing design changes which finally resulted in a solution of this instability problem are outlined, followed by a theoretical discussion of dynamic shaft and bearing performance which explains the experimental findings.

Description of Bearing Arrangements

THE GENERAL arrangement of the 26-ton gas-turbine unit considered here is shown in Fig. 1. The entire assembly is supported by one front support and by two rear supports at positions indicated in Fig. 1. The rear supports are firmly connected with the concrete base while the front support is hinged at the bottom to allow for thermal expansion. Air enters at the left and passes in turn through the low and high-pressure compressors, the combustion chambers, and the several turbine stages. The output power is produced in the 3000-rpm power turbine.

The low-pressure compressor and intermediate-pressure turbine are attached to the same shaft which is supported by journal bearings 1, 2, and 8. The high-pressure compressor and high-pressure turbine are attached to a second concentric shaft supported by bearings 3, 4, and 6. The two shafts are coupled by relative bearings 5 and 7. The sleeves of these latter two bearings are housed in the high-pressure compressor shaft rather than being fixed in space. The low-pressure compressor-shaft speed N_1 has a maximum value of 5250 rpm while the high-pressure compressor-shaft speed N_2 has a maximum value of 6400 rpm in the same direction. The variation of speeds N_1 and N_2 with power output is shown in Fig. 2. The power turbine is supported by bearings 9 and 10 and its speed is designated N_3. Thrust load is supported by one bearing on each shaft designated A1, A2, and A3.

Test Results

Table 1 reviews the sequence of test runs undertaken during the course of development, while Table 2 gives the design and operational characteristics of the bearings originally used (test series A) at 4 mw. During this A series of tests with the original bearings some vibration was experienced and the following observations could be made:

1 There existed a speed limit above which smooth operation ceased, at which the amplitude of the casing vibration increased from about 0.0005 in. to between 0.002 and 0.003 in. At 4 mw this limiting speed usually corresponded to low and high-pressure compressor-shaft speeds of 4250 rpm and 5800 rpm, respec-

Contributed by the Gas Turbine Power Division and presented at the Annual Meeting, New York, N. Y., November 30–December 5, 1958, of THE AMERICAN SOCIETY OF MECHANICAL ENGINEERS.

NOTE: Statements and opinions advanced in papers are to be understood as individual expressions of their authors and not those of the Society. Manuscript received at ASME Headquarters, September 15, 1958. Paper No. 58—A-197.

Nomenclature

a = constant of generalized co-ordinate
a_{ij} = constant of oil-film resilience ($i = 1, 2$; $j = 1, 2$)
C = radial clearance
D = journal diameter
E = eccentricity of high-pressure rotor mass
F_x = reaction force of journal
F_y = reaction force of journal
g = acceleration due to gravity
K = low-pressure compressor rotor elastic spring constant
K_2, K_2' = oil-film spring constant (force in x-direction per unit displacement in x-direction)
K_3, K_3' = oil-film spring constant (force in x-direction per unit displacement in y-direction)
K_2, K_2'' = oil-film spring constant (force in y-direction per unit displacement in y-direction)
K_3, K_3'' = oil-film spring constant (force in y-direction per unit displacement in x-direction)
l = center distance of bearing halves in modified design
L = length of bearing
M = equivalent mass of high-pressure compressor rotor, dimension $ML^{-1}T^2$
N_1 = shaft rpm of low-compressor rotor
N_2 = shaft rpm of high-pressure compressor rotor
N_3 = shaft rpm of power-turbine rotor
N_{crit} = first critical frequency ppm of rotor system
P = specific bearing load
R = radius of journal
r = polar co-ordinate
$S = \left(\frac{R}{C}\right)^2 \frac{\mu N}{P}$ sec/min, Sommerfeld number
W = weight or absolute load on journal
w = incremental beam load
x = co-ordinate
y = co-ordinate
α = damping decrement
β = experimental correction factor of damping force
δ = local beam deflection
ϵ = $l/2C$ dimensionless displacement (eccentricity) of bearing halves in stabilized, film located design
ξ = $x + ay$ generalized co-ordinate
η = $x + ay$ generalized co-ordinate
θ = angle, polar co-ordinate
λ = complex argument of characteristic equation
μ = absolute viscosity
φ = phase angle of whipping rotor mass
ω = frequency of oil whip
ω_{crit} = $[(K_2' + K)/M]^{1/2}$ first critical frequency of rotor system
ω_s = $(K/M)^{1/2}$ shaft frequency
ω_2 = $(K_2'/M)^{1/2}$ bearing frequency
ω_3 = $(K_3/M)^{1/2}$
Ω = shaft rps or rpm

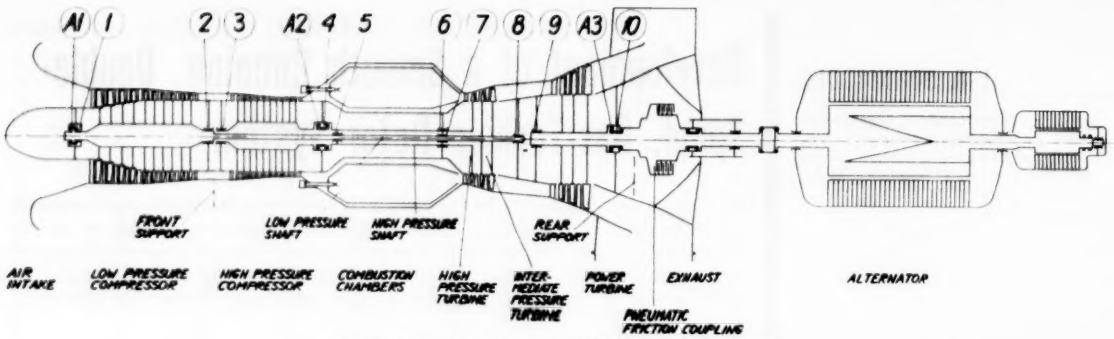

Fig. 1 General arrangement of 10,000-kw gas-turbine unit

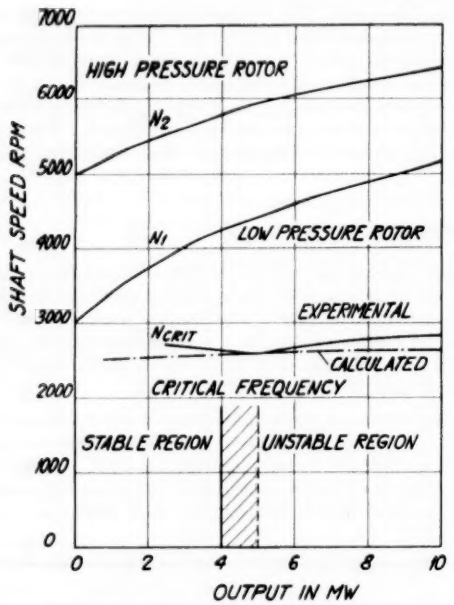

Fig. 2 Shaft speed as function of power output. Critical frequency N_{crit} of test C.

tively. Fig. 3 gives the maximum amplitude distribution observed in the structure adjacent to bearings 1, 2, 4, and 6.

2 Frequencies corresponding to all three shaft speeds N_1, N_2, and N_3 were recorded, but a resonance was not observed in any of these cases. A fourth frequency designated N_{crit}, proved to be the important one. With normal operation N_{crit} was hardly discernible, but in the unstable region of operation roughness was observed and N_{crit} was equal to 2600 ppm.

3 The first critical speed for the low-pressure compressor rotor, calculated neglecting any oil-film elasticity, was found to be 1670 ppm without either relative bearing. With relative bearing 5 present this became 3400 ppm and 7460 ppm with both relative bearings 5 and 7 present. The first critical speed of the high-pressure compressor rotor was estimated to be 10880 ppm.

4 No fundamental resonance frequency or structural or aerodynamic origin, corresponding to N_{crit}, could be found theoretically or experimentally.

5 Some influence on vibrations of lubricant oil-inlet temperature was found.

It was concluded that this was a case of high-speed bearing instability and that the relative bearings were the most likely ones

Table 1 List of test runs

Test	Bearing design	Note
A..	Original design	Excessive vibrations
B..	Relative bearings 5 and 7 of tilting-pad type	Improvement
C..	Bearing 1 with film-located design	Improvement in front end
D..	Bearings 4 and 6 with film-located design	Only normal unbalance vibrations left; stable operation

Table 2 Design data and operational characteristics of original journal bearings at 4 mw with oil having viscosity of 17 CP at 122 F

Bearing no.	Speed, rpm	Diam, in.	Radial clearance $\times 10^{+3}$, in.	Length/diam ratio L/D	Specific bearing-load P, psi	Sommerfeld number S
1	4250	3.94	5.74	0.85	57.0	21.7
2	4250	6.30	7.10	0.63	37.0	52.3
3	5800	6.30	7.10	0.63	29.8	86.0
4	5800	6.50	7.30	0.54	37.0	70.5
5	10050	4.72	7.88	0.84	10.0	228
6	5800	9.45	9.45	0.46	31.3	104
7	10050	4.72	7.88	0.92	21.3	104
8	4250	3.69	5.35	0.89	44.0	26.5

to be unstable. Tilting-pad bearings, Fig. 4, which generally are considered to be inherently stable, were therefore substituted for the inner parts of relative bearings 5 and 7. The radial clearance of the tilting pads in concentric position was made but 0.004 in. (diameter of bearing = 4.72 in.). The outer part of both relative bearings was of the sleeve variety, but the bearing length was reduced to half the values used in the A tests. The outer sleeve of bearing 7 provided the needed cooling path for the thermal energy to be removed from this bearing. After this modification, test B was run and whereas some improvement was noted, the general trouble was still present, Fig. 3.

Since vibration was still greatest at the front end, it was next decided to modify bearing 1.

The new bearing of Fig. 5 provides two cylindrical bearing halves with displaced centers, thus creating two pressure-producing oil wedges. With this new front end bearing it was possible to perform a 50-hr continuous test (C) over the entire load range, which in itself demonstrates improved bearing stability. Rough running above a load of about 5 mw was still obtained, although the point of greatest vibration was shifted from the vicinity of bearing 1 to the vicinity of bearing 4, Fig. 3. Fig. 6 shows the manner in which the vibrational amplitude of the casing varies with load at the positions of bearings 1 and 4. Figs. 7 and 8 show the amplitudes corresponding to frequencies N_1, N_2, N_3, and N_{crit} at bearing 1 for different values of power level, and for tests B and C, respectively. The significant improvement at bearing 1 due to the change rendered in this bearing is clearly evident.

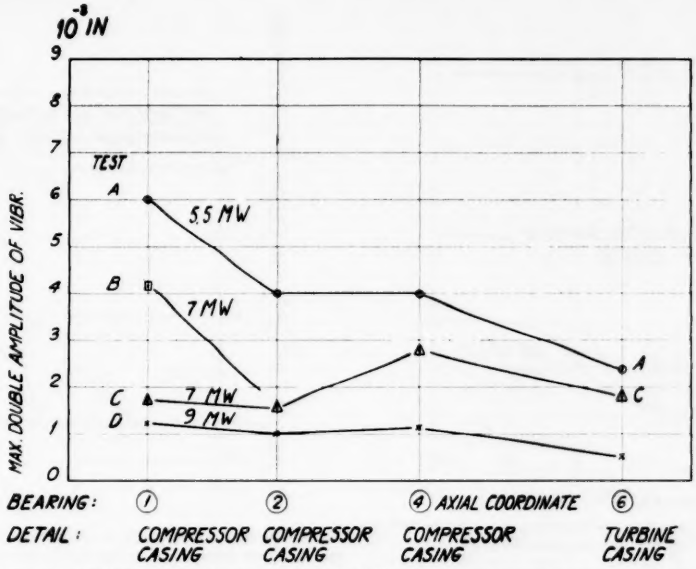

Fig. 3 Distribution of maximum amplitudes of vibration in gas-generator structure during various test runs

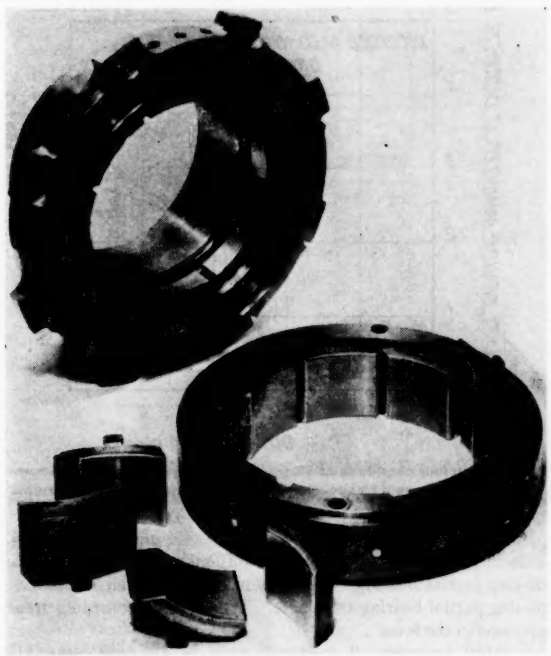

Fig. 4 Tilting-pad bearing design applied to relative bearings 5 and 7

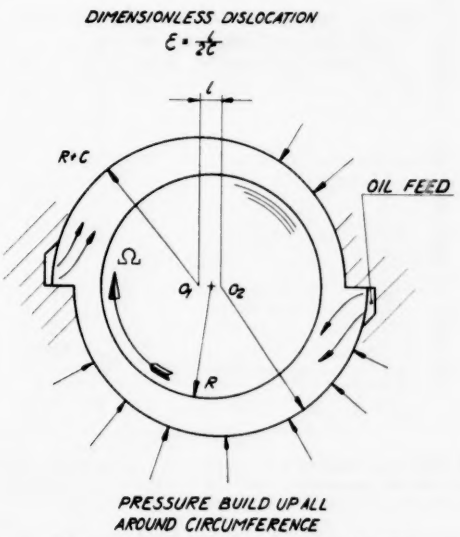

Fig. 5 Stabilized bearing with displaced halves

Fig. 9 is the counterpart of Fig. 8, but measured at bearing 4. It is evident that, while the stabilization of bearing 1 has improved the situation in the vicinity of this bearing, it has little influence upon vibrational amplitude in the vicinity of bearing 4.

Calculation of First Critical Speed of Rotor System

Since the experiments showed that introduction of stable relative bearings caused no change in N_{crit}, the relative bearings do not appear to be responsible for the main difficulty. The stable new bearing of the exposed front end did remove the unstable speed range at this end. It would thus appear that the fixed bearings of the high-pressure rotor are the critical ones.

Next, consider the high-pressure rotor mass to ride on the low-pressure shaft with a constant eccentricity E. This creates a new situation. If the high-pressure bearings had infinite spring constants, there would be no interaction, since the high-pressure rotor then could not move in a plane perpendicular to the axes and accordingly the low-pressure rotor could be considered to be coupled to the ground through bearings 5 and 7. However, when the elasticity of the oil films of bearings 4 and 6 is taken into account a different result is obtained. Because of the rigidity of the low-pressure compressor (LC) between bearings 1 and 2, the actual system may be simplified to a beam of constant thickness

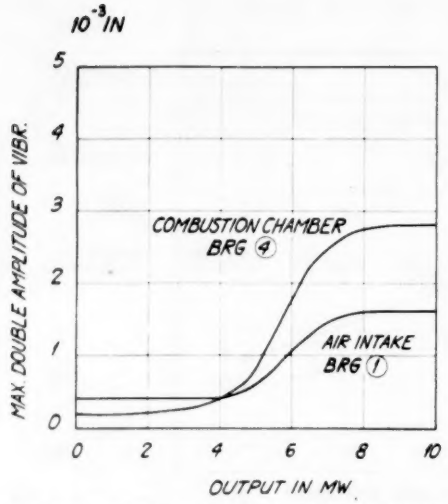

Fig. 6 Maximum amplitudes of vibration in casing at air intake and at combustion chamber in test C as function of power output

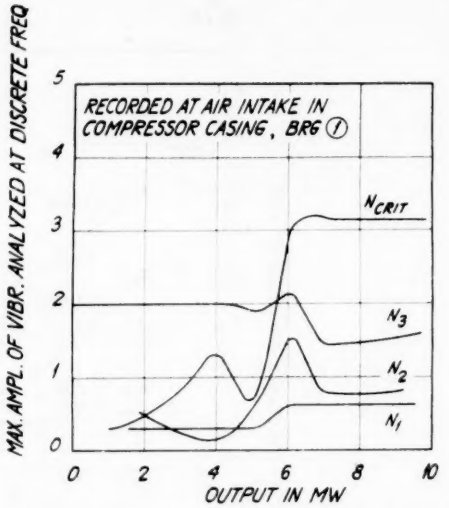

Fig. 7 Maximum amplitude of vibration in casing at air intake at different discrete frequencies in test B as function of power output

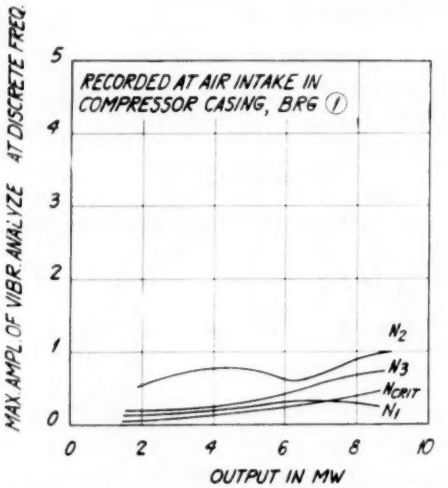

Fig. 8 Maximum amplitude of vibration in casing at air intake at different discrete frequencies in test C as function of power output

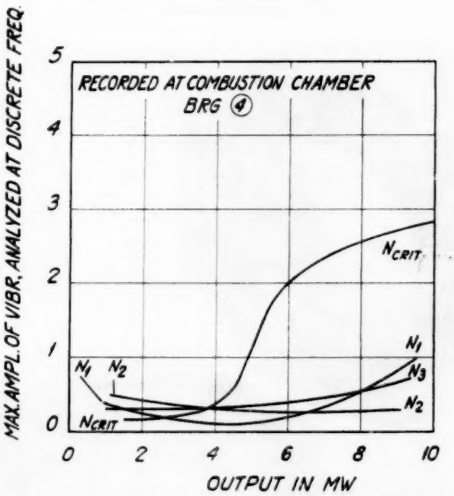

Fig. 9 Maximum amplitude of vibration in casing at combustion chamber at different discrete frequencies in test C as function of power output

with fixed left end and freely supported right end, Fig. 10. The equivalent beam is loaded with approximately $^1/_2$ the weight of the high-pressure compressor (HC) at bearing 4 and the whole weight of the high-pressure turbine (HT) at bearing 6. The weight of the intermediate-pressure turbine (IT) is divided between bearings 6 and 8. The beam deflections due to these weights may be obtained at any point along the beam from equations given in textbooks on elementary elasticity [1].[1] For the mode of static loading assumed, the sum of displacements at bearings 4 and 6 is subject to the two additional boundary conditions, that the net deflections are compatible with the spring constants of the bearings at these points. Then the first critical speed ω_{crit} may be computed readily by Rayleigh's method [2]:

$$\omega_{crit}^2 = g \frac{\Sigma(w, \delta)}{\Sigma(w, \delta^2)} \quad (1)$$

[1] Numbers in brackets designate References at end of paper.

For the spring constants of the bearings 4 and 6 the author chose the minimum values quoted by Hagg and Sankey [3] for a 150-deg partial bearing, which resembles fairly well the actual 180-deg partial bearing used here. These spring constants were expressed in the form

$$k = \frac{W}{C} f(\mathbf{S}) \quad (2)$$

where **S** is the Sommerfeld number and the values used in these computations are those of Table 2. (Note the accepted practical definition of **S** with dimension sec per min according to given nomenclature.) The result of these computations is shown in Fig. 11, where N_{crit} is plotted against bearing resilience (proportional to inversed bearing oil-film elasticity). The original bearing had a resilience value of 1.64 according to Fig. 11 rendering N_{crit} equal to 2580 ppm, which is to compare with the experimentally observed N_{crit} = 2600 ppm as previously mentioned. The low-

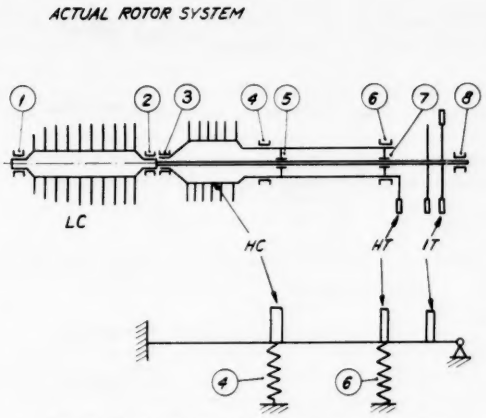

Fig. 10 Analytical model of vibrating rotor system

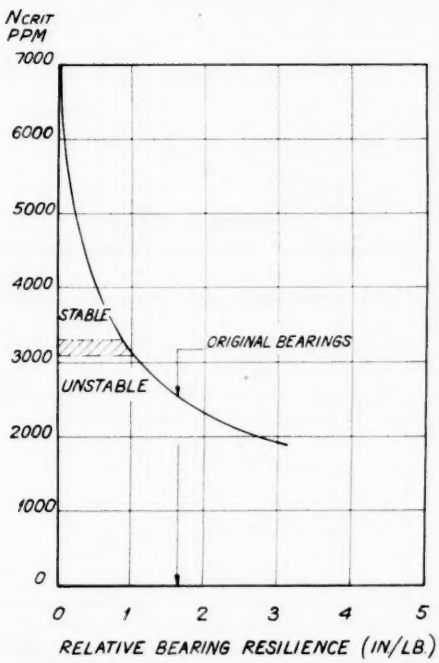

Fig. 11 First critical speed of rotor system as function of resilience of high-pressure rotor bearings 4 and 6

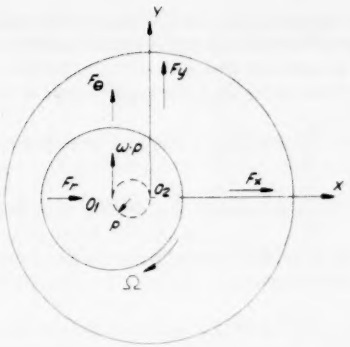

F_r = RADIAL OIL FILM FORCE
F_θ = TANGENTIAL OIL FILM FORCE
F_x, F_y = OIL FILM FORCES IN RECTILINEAR COORDINATES
ρ = RADIUS OF ORBITAL MOTION

Fig. 12 Bearing nomenclature

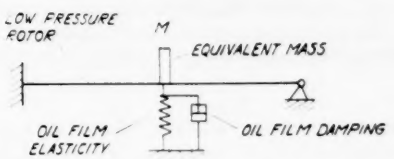

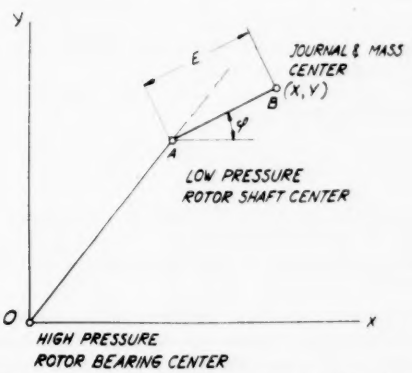

Fig. 13 Equivalent mechanical rotor system for study of bearing dynamic stability

pressure rotor is vibrating in its fundamental bending mode, but that mode is not independent of the presence of the high-pressure rotor.

Dynamic Stability of High-Pressure Compressor Rotor

To clarify the rotor behavior with respect to experimental load (or shaft speed) we must consider the dynamic stability of the equivalent rotor system in its relevant journal bearings.

The analysis by Boeker and Sternlicht [4], partly built on the mathematics of Poritsky [5], seem to provide the most satisfactory analytical expressions available with respect to compatibility of journal motion and oil flow continuity. (See also references [6, 7, 8].)

According to Boeker and Sternlicht one may express the forces on the journal of vertically mounted bearings, possessing a high degree of symmetry with respect to their axes (which is approximately the case for the bearings originally employed here), in the following form, Fig. 12:

$$F_x = -\frac{2K_3}{D}\dot{x} - K_2 x - K_3 y \tag{3}$$

$$F_y = -\frac{2K_3}{\Omega}\dot{y} - K_2 y + K_3 x \tag{4}$$

An equivalent mechanical system for study of the stability characteristics is given in Fig. 13. The equivalent mass M is influenced by inertia forces, bearing forces from Equations (3) and (4) and the shaft elastic forces $K(x - E\cos\varphi)$; $K(y - E\sin\varphi)$. The center of mass (journal center) (x, y) is located eccentrically with respect to the shaft (E is of the order of magnitude of the radial bearing clearance C). For high-speed bearings the steady-state

position of the journal center will be close to the bearing center. If we assume for the time being that Equations (3) and (4) may be used even though they were derived for vertical bearings, a summation of forces yields the following equations of motion:

$$M\ddot{x} + \frac{2K_3}{\Omega}\dot{x} + K_2x + K_3y + K(x - E\cos\varphi) = 0 \quad (5)$$

$$M\ddot{y} + \frac{2K_3}{\Omega}\dot{y} + K_2y - K_3y + K(y - E\sin\varphi) = 0 \quad (6)$$

Generalizing the elastic constants K_2 and K_3 for nonsymmetrical bearings one may write

$$M\ddot{x} + \frac{2K_3}{\Omega}\dot{x} + (K_2' + K)x + K_3'y = KE\cos\varphi \quad (7)$$

$$M\ddot{y} + \frac{2K_3}{\Omega}\dot{y} + (K_3'' + K)y - K_3''x = KE\sin\varphi \quad (8)$$

K_3', K_3', K_2'', and K_3'' may all have different values. Damping constant $(2K_3/\Omega)$ may be assumed equal in both x and y-directions and in turn equal to the value for the symmetrical system [4, 7, 8]. If the latter assumption is not adopted, a fourth-order problem results [4, 7, 8]. The simple x and y-co-ordinates are replaced by the generalized co-ordinates of Lagrange. Thus we assume for these new co-ordinates:

$$\xi = x + a_1y \quad (9)$$

$$\eta = x + a_2y \quad (10)$$

In order to determine constants a_1 and a_2 we multiply Equation (8) by a and add Equations (7) and (8), which results in a single equation of motion:

$$M\ddot{\xi} + \frac{2K_3}{\Omega}\dot{\xi} + [(K_2' + K) - aK_3'']\xi = KE(\cos\varphi + a\sin\varphi) \quad (11)$$

and the condition for a follows:

$$a = \frac{a(K_2'' + K) + K_3'}{(K_3' + K) - aK_3''} \quad (12)$$

The second-order equation (12) results in two values of a, corresponding to generalized co-ordinates ξ and η, respectively. Depending on the nature of these values two fundamentally different motions may result. Thus:

1 If a has two real values, the journal center will move along two unrelated straight lines through the origin of x-y-co-ordinates. This is the case of Cameron's stable motion, with damping neglected [6].

2 If a has two complex values, motion takes place in two opposite directions along a generally elliptical path described by

$$\xi = x + (A + iB)y$$
$$\eta = x + (A - iB)y \quad (13)$$

Only one of these will usually have physical significance. Fig. 14 illustrates the orbital motions of symmetrical and asymmetrical bearings.

It is seen in the foregoing analysis how it is possible to retain the inherent simplicity of polar co-ordinates even when dealing with asymmetric bearings. The r-co-ordinate is then replaced by the generalized ξ-co-ordinate in the x-y-system. The relevant stability problem then involves solution of second-order Equation (11) by elementary methods.

Having outlined the solution of the general, asymmetrical bearing we may once more concentrate on the actual symmetric case. Since the solution will contain complex quantities, it amply

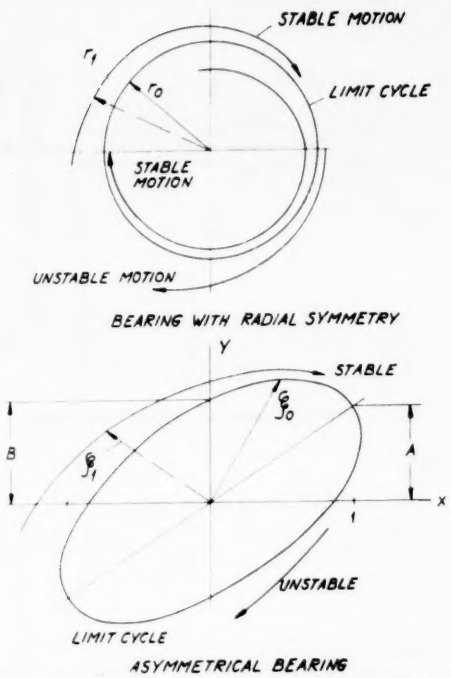

Fig. 14 Orbital motions of symmetrical and asymmetrical bearings

demonstrates the general approach. Equation (11) becomes

$$M\ddot{\xi} + \frac{2K_3}{\Omega}\dot{\xi} + [(K_2 + K) - iK_3]\xi = KEe^{i\varphi} \quad (14)$$

With $\varphi = \omega t$ it is seen that ξ has a limit cycle ξ_0 and a deviation ξ_1 from this. The limit cycle is obtained by putting

$$\xi = \xi_0 e^{i\omega t} \quad (15)$$

$$\xi_0 = \frac{\omega_s^2}{(\omega_{crit}^2 - \omega^2) + \left(2\frac{\omega}{\Omega} - 1\right)\omega_3^2 i}E \quad (16)$$

$\xi_0 = x + iy$ is complex and represents a circular orbit. That ξ is complex in terms of eccentricity E merely shows that motion of the journal center B (x, y) is slightly out of phase with respect to shaft center A. In other words, the extension of line O-A in Fig. 13 does not coincide with A-B. The orbital frequency ω of the system under consideration in Fig. 13 is essentially determined from the homogeneous part of Equation (14), that is

$$\ddot{\xi} + 2\frac{\omega_3^2}{\Omega}\dot{\xi} + [\omega_{crit}^2 - i\omega_3^2]\xi = 0 \quad (17)$$

$$\xi = \xi_1 e^{\lambda t}$$

The following values for the deviatory solution from the limit cycle are obtained:

$$\lambda_{1,2} = \frac{-\omega_3^2}{\Omega} \pm i\left[\omega_{crit}^2 - \left(\frac{\omega_3^2}{\Omega}\right)^2 - i\,\omega_3^2\right]^{1/2} \quad (18)$$

The stability limit is obtained, when λ is a pure imaginary quantity $i\omega$. Solving Equation (18) by moving $-\omega_3^2/\Omega$ to the left and squaring gives for the stability limit

$$\omega = \omega_{crit}$$
$$\omega = \Omega/2 \quad (19)$$

Studying the denominator of Equation (16) for ξ_0 one will find that it tends to zero when Ω approaches $2\omega_{crit}$. Under such conditions ξ_0 tends to infinity.

Similar results would follow from an antisymmetrical bearing solution. The practical purpose of this section was to determine the behavior of the bearing with respect to shaft speed, and Equation (18) enables this to be done. We shall apply the formula to test C, the N_{crit} values of which are shown in Fig. 2. By definition

$$\omega_{crit}^2 = \omega_s^2 + \omega_2^2 \tag{20}$$

The Hagg and Sankey tests [3] indicated that in our range of Sommerfeld numbers it is justified to let

$$\omega_3 = \omega_2 \tag{21}$$

The "shaft frequency" ω_s is obtained by considering the original equivalent system of Fig. 10 as being without any high-pressure rotor bearings. This computation was performed in conformity with the method of the last section and yielded

$$\omega_s = 1100 \text{ ppm}$$

and

$$\omega_{crit} = 2600 \text{ ppm}$$

Hence one obtains

$$\omega_2 = \omega_3 = 2360 \text{ ppm}$$

The stability limit occurs for $\Omega = 5900$ rpm. Obviously, the quantity 2 is the damping coefficient of Equation (17) must not necessarily be an integer in practical bearings. The ratio $\Omega/\omega_{crit} = 2.27$ indicates that one should apply a correction factor β and replace 2 by $2 \times \beta$, letting β equal 1.135. A complete computation with normal slide-rule accuracy gives $\beta = 1.14$. The bearing behavior is characterized by the damping α and the variation of whip frequency ω. Both may be obtained from the following set of equations, resulting from elementary theory of complex numbers:

$$\left.\begin{aligned} A &= 1 - B^2\left(\frac{\omega_3}{\omega_{crit}}\right)^2\left(\frac{\omega_3}{\Omega}\right)^2 \\ B &= -\left(\frac{\omega_3^2}{\omega_{crit}}\right) \\ z &= (A^2 + B^2)^{1/4} \\ \tan\varphi &= \frac{B}{A} \\ \frac{\alpha}{\omega_{crit}} &= \left[-\beta\left(\frac{\omega_3}{\omega_{crit}}\right)\left(\frac{\omega_3}{\Omega}\right) \pm z \sin\frac{\varphi}{2}\right] \\ \frac{\omega}{\omega_{crit}} &= z\cos\varphi/2 \end{aligned}\right\} \tag{22}$$

From the foregoing values the final results in Table 3 are obtained.

Table 3 Calculated characteristic values of bearing stability for test C as a function of the high-pressure rotor speed

Ω	5200	5900	6400
$\frac{\alpha}{\omega_{crit}}$	−0.049	0	0.027
$\frac{\omega}{\omega_{crit}}$	0.978	1.000	1.010

Table 3 verifies the essential characteristics of test C, except for the somewhat irregular drop of N_{crit} with increasing output in the subcritical range. Thus it is seen:

1 That there exists one subcritical and one critical rpm range Ω or N_2 in the actual machine, indicated by the shift in sign of the damping quantity

$$\alpha/\omega_{crit} \text{ at } \Omega = 5900 \text{ rpm}$$

2 That the frequency of vibration ω will rise slowly with the exciting speed Ω. This is indicated by the magnitudes of the (ω/ω_{crit})-values.

3 That the foregoing findings have been obtained neglecting the complete influence of Ω on the constants in the most general equation of motion for a bearing [9], which might explain minor differences which still exist between observed and calculated values.

4 That the foregoing results appear to explain not only the experimental findings on the actual gas turbine unit, but also form the basis for an understanding of recent research work in the United States reported by Pinkus [10], who found the same extended stability range and the same slight rise of ω with exciting rpm Ω.

5 That a redesign of high-pressure rotor bearings for increased stiffness would raise the critical speed of the equivalent rotor system and thus constitute the best solution to the present problem.

Experiments to Determine Spring Constants for Modified Bearings

High-pressure rotor bearings of the design of Fig. 5 were given an offset of $\epsilon = 0.53$ between upper and lower bearing halves. The following discussion is concerned with the determination of "spring constants" for the new design applied to high-pressure compressor-rotor bearings 4 and 6.

Consider a rectilinear co-ordinate system with origin at the bearing center, Fig. 15. An unloaded journal will have a balanced force system, when the bearing center (x_0, y_0) is at origin $x_0 = 0$, $y_0 = 0$. At a steady-state force F_y, the loaded journal will be in

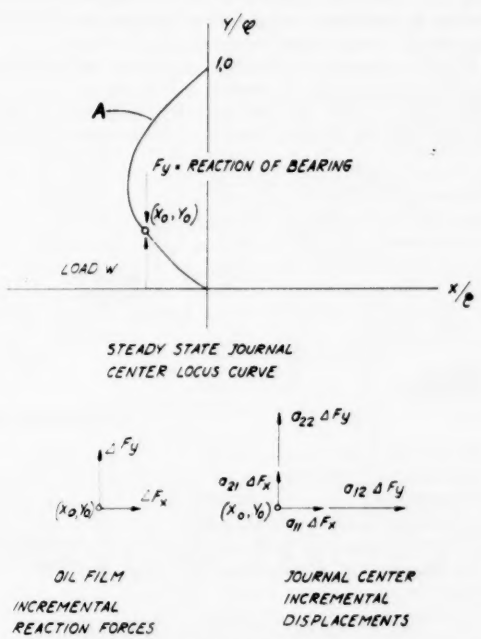

Fig. 15 Geometry of experimental force system

static equilibrium when bearing center (x_0, y_0) is at rest at the proper point along the "steady-state locus curve" (A). If we apply an additional steady-state force ΔF_y, the bearing center (x_b, y_0) moves to a new position along curve (A) and in general this causes motion in both the x and y-directions. The same is true, if we apply a similar free ΔF_x in the x-direction. We may express the foregoing statements as follows:

$$\Delta x = \Delta x_{11} + \Delta x_{12} \tag{23}$$

$$\Delta y = \Delta y_{21} + \Delta y_{22} \tag{24}$$

Assuming linear relationships we may write:

$$\Delta x = a_{11}\Delta F_x + a_{12}\Delta F_y \tag{25}$$

$$\Delta y = a_{21}\Delta F_x + a_{22}\Delta F_y \tag{26}$$

A linear transformation gives

$$F_x = -K_2'x - K_3'y \tag{27}$$

$$F_y = K_3''x - K_2''y \tag{28}$$

If

$$\left.\begin{aligned} D &= a_{11}a_{22} - a_{21}a_{12} \\ K_2' &= -\frac{a_{22}}{D} \\ K_3' &= \frac{a_{12}}{D} \\ K_2'' &= -\frac{a_{11}}{D} \\ K_3'' &= -\frac{a_{21}}{D} \end{aligned}\right\} \tag{29}$$

The test arrangement to determine oil-film resilience is shown in Fig. 16. The exact position of the rotating journal in two directions is determined by inductive pickups in a calibrated bridge circuit. Some typical results are given in Figs. 17 and 18 Fig. 17 is for a conventional 180-deg bearing with concentric bearing halves, whereas Fig. 18 presents similar results for the new design when $\epsilon = 0.53$. In these tests the journal was turning at 2000 rpm and the oil-inlet temperature was 100 F. All dependent variables are included in the Sommerfeld number **S**. The lower diagrams in terms of x_0 and y_0 are merely another way of giving the locus of the journal. The upper curves give the constants of resilience a_{11}, a_{21}, a_{12}, and a_{22} required in the analysis previously presented and are expressed in (micron/kg)(1 micron/kg = 1.82×10^{-4} in/lb). The bearings of Figs. 17 and 18 represent fairly closely the original and modified bearings of the high-pressure compressor rotor, respectively. A Sommerfeld number of 100 approximates the operating conditions of Table 2 and from Figs. 17 and 18 we obtain the values of Table 4.

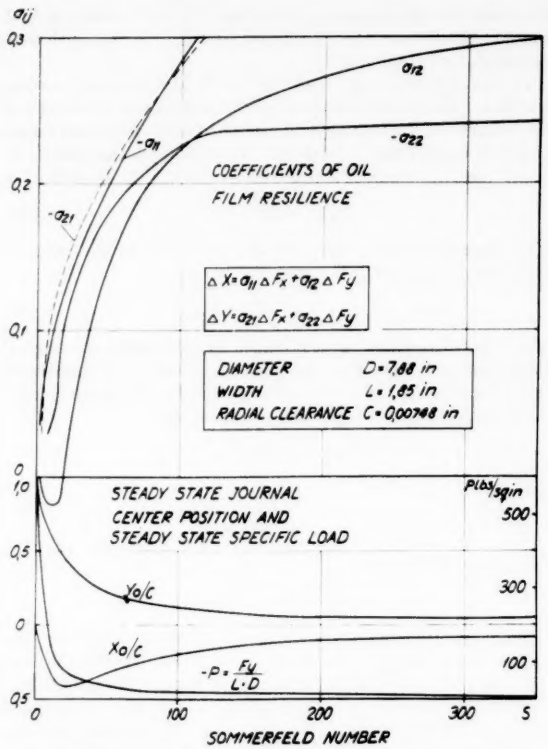

Fig. 17 Displacement of journal for steady-state loads F_y. Resilience coefficients a_{11}, a_{21}, a_{12}, and a_{22} for plain sleeve bearing with $\epsilon = 0$, and two axial feed slots in the horizontal plane.

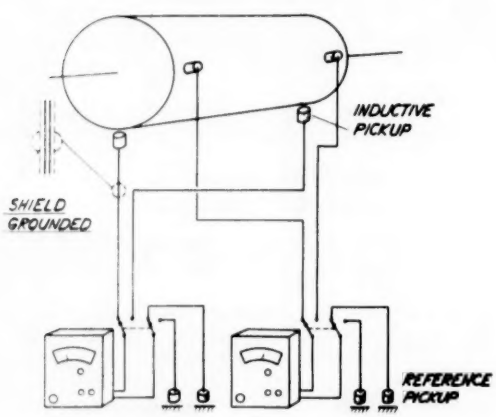

Fig. 16 Bearing test arrangement

Table 4 Experimental values of oil-film resilience at S = 100

Original bearing, micron/kg	Modified bearing, micron/kg
$a_{11} = -0.29$	$a_{11} = -0.04$
$a_{21} = -0.29$	$a_{21} = -0.04$
$a_{12} = 0.23$	$a_{12} = 0.007$
$a_{22} = -0.23$	$a_{22} = -0.115$

Table 5 Experimental values of oil-film spring constant

Original bearing, kg/micron	Modified bearing, kg/micron
$K_2' = 1.72$	$K_2' = 23.4$
$K_3' = 1.72$	$K_3' = 1.43$
$K_2'' = 2.17$	$K_3'' = 8.15$
$K_3'' = 2.17$	$K_3'' = 8.15$

When the values of a_{ij} in Table 4 are applied to Equation (29) the values of Table 5 result. It is seen that even the original bearing with its two inlet holes (180-deg partial bearing) in the horizontal plane has a certain asymmetry, since $K_2' \neq K_2''$ and $K_3' \neq$

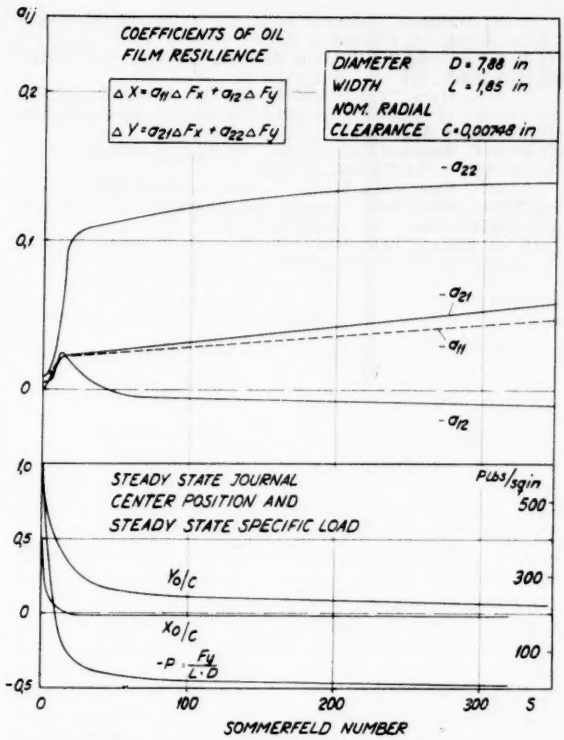
COEFFICIENTS OF OIL FILM RESILIENCE
DIAMETER D = 7,88 in
WIDTH L = 1,85 in
NOM. RADIAL CLEARANCE C = 0,00748 in
STEADY STATE JOURNAL CENTER POSITION AND STEADY STATE SPECIFIC LOAD
SOMMERFELD NUMBER

Fig. 18 Displacement of journal for steady-state loads F_y. Resilience coefficients a_{11}, a_{21}, a_{12}, and a_{22} for modified bearing design with $\epsilon = 0.53$, and two axial feed slots in the horizontal plane.

K_3''. The degree of asymmetry is even greater for the modified bearing.

First Critical Speed of Equivalent Rotor System Based on Experimentally Derived Spring Constants

The critical speed for the equivalent rotor system, from Equation (11), is

$$\omega_{crit}^2 = \frac{K_2' + K - \text{Real}(aK_3'')}{M} \tag{30}$$

The results of Table 6 are obtained from Equations 11 and 30.

Table 6 Values of constant a, and of natural frequency ω_{crit} of equivalent rotor system

	Original bearing	Modified bearing
Constant a.....	$a_{1,2} = -0.104 \pm 0.882i$	$a_1 = 0.1$ $a_2 = 1.76$
Natural frequency ω_{crit}	2690 ppm	$\omega_1 = 5100$ ppm $\omega_2 = 7950$ ppm

An interpretation of the values of Table 6 may be made based on Equations (11) and (13). The results of such an analysis follow:

1 The original bearings are inherently unstable above a certain speed N_2 of the high-pressure rotor. The whipping rotor system describes a slightly elliptical orbit, since the constant a is not an entirely imaginary quantity.

2 The large increase in natural frequency of the modified bearing at first may appear somewhat surprising since resilience coefficient a_{22} of the weakest mode has only been reduced by a factor of 2. However, this depends on the fact that the increase in stiffness in the x-direction almost neutralizes the bearing deflection in that direction for the F_y force.

3 The modified bearing no longer exhibits natural modes of vibration of an orbital character. Instead one obtains two inherently stable, unrelated rectilinear motions. Motions take place along two straight lines at an angle that is generally different from 90 deg. This is derived from the fact that constant a of Equation (12) now assumes two discrete, real values.

4 Forced vibrations of the modified bearing caused by external unbalance forces may still take place in elliptical paths at shaft frequency. These orbits, however, are immediately resolved into the two aforementioned rectilinear damped motions, should the exciting unbalance force be removed. Thus no danger of unstable motion over an extended speed range can occur.

5 Since even infinitely stiff bearings cannot raise the critical frequency of the system above 7450 ppm, it is evident that the influence of greatly increased stiffness of the high-pressure compressor-rotor bearings, i.e., of the natural frequency of the system, is overemphasized. This stems from the fact that with the approach toward fixed bearings one no longer may neglect low-pressure rotor inertia, as was done for the simplified system of Fig. 13.

We may easily make a rough estimate of the error committed by neglecting rotor inertia. By use of Fig. 11 we shall compare frequencies for the weakest mode. From the computation of Equation (30) the complete bearing spring constants follow:

Original bearing: $(K_2' - \text{Re}[aK_3''])$ = 1.87 10^3 kg/m
Modified bearing: $(K_2 - \text{Re}[aK_3''])$ = 9 10^6 kg/m
Stiffness ratio: 9/1.8 = 4.8

From Fig. 11 a resilience of 1.64 is seen to correspond to an ω_{crit} of 2580 ppm, which frequency is in close agreement with previous calculations for the original bearing. For the modified bearing, we obtain a reduced resilience of 1.64/4.8 = 0.342, which gives a critical frequency of 4600 ppm, instead of the 5000 ppm found previously.

Final Results

When the gas-turbine unit was ultimately tested (test D), there were only parasitic harmonics left in the frequency spectrum, besides the three shaft speeds N_1, N_2, N_3. Further, it was found that the turbine operates in an entirely stable manner over the whole load range. The remaining vibration is due entirely to normal unbalance, which caused the amplitudes shown indicated in Fig. 3 for test D. In the vicinity of bearing 1, the amplitude of harmonic N_1 rose with speed, which is natural for this relatively flexible overhung condition. However, in the vicinity of bearing 4 no such increase was found in the N_1 harmonic. This seems to corroborate the general bearing analysis presented in this paper.

Acknowledgments

The author wishes to thank the General Manager of the STAL company, Mr. Curt Nicolin, for his support and permission to publish this paper. Mr. Eric Östmar, head of the design section, was responsible for the several design modifications, while gas-turbine tests were made by Messrs. Paul Persson and Folke Arvidsson. The careful laboratory investigation was carried out by Mr. Agnar Skog, assisted by Messrs. Nils Lier, Sonny Karlsson, and Carl-Johan Wahren. To Prof. Milton C. Shaw many thanks are due for his valuable criticism and kind assistance in transforming the original report into the present paper.

References

1 R. J. Roark, "Formulas of Stress and Strain," McGraw-Hill Book Company, Inc., New York, N. Y., second edition.

2 C. B. Biezeno and R. Grammel, "Technische Dynamik," Springer Verlag, Berlin, Göttingen, and Heidelberg, Germany, 1953, pp. 155–222.

3 A. C. Hagg and G. O. Sankey, "Some Dynamic Properties of Oil-Film Journal Bearings With Reference to the Unbalance Vibration of Rotors," *Journal of Applied Mechanics*, vol. 23, TRANS. ASME, vol. 78, 1956, p. 302.

4 G. F. Boeker and B. Sternlicht, "Investigation of Translatory Fluid Whirl in Vertical Machines," TRANS. ASME, vol. 78, 1956, p. 13.

5 H. Poritsky, "Contribution to the Theory of Oil Whip," TRANS. ASME, vol. 75, 1953, p. 1153.

6 A. Cameron, "Oil Whirl in Bearings," *Engineering*, February 25, 1955, p. 237.

7 A. C. Hagg, "The Influence of Oil-Film Journal Bearings on the Stability of Rotating Machines," *Journal of Applied Mechanics*, vol. 13, TRANS. ASME, vol. 68, 1946, p. A-211.

8 A. C. Hagg and P. C. Warner, "Oil Whip of Flexible Rotors," TRANS. ASME, vol. 75, 1953, p. 1339.

9 M. C. Shaw and E. Macks, "Analysis and Lubrication of Bearing," McGraw-Hill Book Company, Inc., New York, N. Y., 1949, pp. 190–196, 357–366.

10 O. Pinkus, "Experimental Investigation of Resonant Whip," TRANS. ASME, vol. 78, 1956, p. 975.

G. R. FUSNER

Supervisor, Stress Analysis and Vibration Unit, Gas Turbine Department, General Electric Company, Schenectady, N. Y. Mem. ASME

D. L. NEWHOUSE

Supervisor, Forgings Development Subunit, Materials and Process Laboratory, Large Steam Turbine-Generator Department, General Electric Company, Schenectady, N. Y.

M-252 Alloy for Heavy-Duty Gas-Turbine Buckets[1]

In order to apply safely a turbine-bucket alloy which has been successful in short-life high-temperature aircraft gas turbines to long-life heavy-duty gas turbines, it was necessary to make many laboratory tests. These included tensile, rupture, creep, fatigue, damping, oxidation, and corrosion tests. Many of these tests were made on specimens which had been aged for 5000 and 10,000 hr. Rupture data were obtained to 15,000 hr. Operating experience has confirmed laboratory tests and now M-252 is destined to become a standard bucket material for heavy-duty gas turbines.

In 1954, when a turbine was being designed to operate with a turbine-inlet temperature of 1500 F and a corresponding first-stage bucket temperature of 1250 F, a number of superalloys were considered for the first-stage bucket material. The most promising material was vacuum-melted M-252, which had been used successfully in aircraft gas turbines. When used in this type of service, the alloy operated at high temperatures for short periods of time, contrasted to the lower temperatures and long-time service required in heavy-duty machinery. Most of the laboratory data on this alloy were obtained to determine its suitability as an aircraft gas-turbine material. However, the limited amount of data taken at 1200 F and the stress-rupture characteristics to approximately 1000 hr were encouraging. Since high reliability is required in heavy-duty gas turbines, a laboratory evaluation program was conducted on the alloy to make sure that it had the necessary properties. Most of the data obtained in this investigation are presented in this paper.

M-252 is a nickel-base alloy. The chemical compositions of the seven heats used in the tests are indicated in Table 1. In general, the variations in the amounts of the elements are small.

All of the material used in the tests was manufactured by the vacuum-melting process described in [1].[2] This process is responsible for many of the good properties exhibited by this alloy because they are not obtained when it is air-melted.

Heat-Treatment

The heat-treatments used in this investigation are listed in Table 2. Table 3 describes these heat-treatments in greater detail and presents a code used in subsequent tables of test results to identify heat number, heat-treatment, and aging treatment.

The first number of the code identifies the heat, the second series of one letter and two numbers identifies the heat-treatment, and the final group of three numbers indicates stress, temperature, and time for any aging cycle applied. For example, 1-A64-012 denotes heat 1, solution-treated 1950 F—4 hr—air-cooled, first-aging treatment 1675 F—24 hr—air cooled, second-aging treatment 1400 F—15 hr—air cooled; aged without stress for 2000 hr at 1050 F. Similarly 1-A64 or 1-A64-000 indicates the same heat-treatment without subsequent long-time aging.

The principal heat-treatment, used on the material tested, con-

Table 1 Chemical composition

Element	Weight percentage						
Heat no.	1	2	3	4	5	6	7
Carbon	0.15	0.14	0.21	0.15	0.14	0.18	0.14
Chromium	19.2	19.2	19.4	19.1	19.5	19.9	17 5
Molybdenum	9.3	9.7	9.6	9.6	9.4	9.7	10.5
Cobalt	9.4	9.4	9.6	9.7	9.4	9.2	9.3
Iron	2.2	Nil	3.0	2.2	5.0	2.5	3.1
Manganese	0.5	0.5	0.5	0.05	0.07	0.05	0.5
Silicon	0.5	0.5	0.35	0.2	0.12	0.09	0.57
Phosphorus	0.017	N	N	N	N	N	0.005
Sulfur	0.010	N	N	N	N	N	0.022
Aluminum	0.86	0.81	1.10	0.84	1.1	0.87	1.1
Titanium	2.25	2.35	2.68	2.45	2.45	2.35	2.2
Boron	N	N	N	N	N	0 001	0
Nickel	B	B	B	B	B	B	B

B—Balance N—Not determined

Table 2 Solution and aging temperatures

Treatment code	Heat-treatment: Solution temp, deg F	First aging temp, deg F	Second aging temp, deg F
A40	1950	1400	None
A54	1950	1550	1400
A64	1950	1675	1400
A74	1950	1750	1400
B64	2050	1675	1400
B74	2050	1750	1400

[1] Any views or opinions expressed in this paper are those of the authors. The authors and the General Electric Company make no warranty or representation and shall have no liability with respect to this paper or any of its contents nor with respect to any use thereof, nor with respect to whether any such use will infringe the rights of others.

Contributed by the Gas Turbine Power Division and presented at the Annual Meeting, New York, N. Y., November 30–December 5, 1958, of The American Society of Mechanical Engineers.

Note: Statements and opinions advanced in papers are to be understood as individual expressions of their authors and not those of the Society. Manuscript received at ASME Headquarters, August 27, 1958. Paper No. 58—A-191.

[2] Numbers in brackets designate References at end of paper.

Table 3 Identification code for material and heat-treatment; heat-treatment code

Heat Code	Code	Solution treatment	Code	First aging treatment	Code	Second aging treatment
1	A	1950 F 4 hr AC[a]	4	1400 F 15 hr AC	0	None
2	B	2050 F 4 hr AC	5	1550 F 24 hr AC	4	1400 F 15 hr AC
3			6	1675 F 24 hr AC		
4			7	1750 F 24 hr AC		
5						
6						
7						

Long-time aging code

Code	Stress, psi	Code	Temp, deg F	Code	Time, hr
0	None	0	None	0	None
7	17,500	1	1050	2	2000
		2	1250	5	5000
		4	1400	10	10000

[a] AC—air cooled.

sisted of solution-treating at 1950 F—4 hr—air cooled, followed by a single 1400 F—15 hr—air-cooled aging treatment (A40). An intermediate aging treatment at 1550 F—24 hr was added to improve rupture ductility for some heats (A54). Other treatment variables explored were intermediate aging treatments at 1675 and 1750 F followed by the usual 1400 F final age, again with the purpose of optimizing rupture ductility; and a higher solution temperature, 2050 F (A64, A74, B64, B74) for improved rupture strength.

To provide data on the effect of long service times at operating temperatures on properties of M-252, test bars were aged at several operating temperatures (1050, 1250, and 1400 F) for times up to 10,000 hr, some with and some without tensile loading to simulate bucket loads. Creep measurements were made on some of the specimens during the stress-aging at 17,500 psi.

Tensile Tests

Tensile tests, smooth and notched, were conducted at room temperature and at elevated temperatures as described in Table 4

Table 4 Tensile test results

Material and Condition Code	Material Form	Specimen Size	Specimen Type	Test Temperature -F	Tensile Strength -psi	0.02% Yield Strength -psi	Elongation -%	Reduction in Area -%
1-A40-000	Bar	.505	Smooth	75	186,250	115,000	24.5	28.5
1-A40-000	Bar	.505	Smooth	75	188,500	116,500	24.0	32.5
1-A40-000	Bar	.505	Smooth	75	188,000	112,000	24.5	28.5
1-A40-000	Bar	.505	Smooth	500	175,000	115,000	28.5	28.0
1-A40-000	Bar	.505	Smooth	1000	168,000	104,000	24.0	26.0
1-A40-000	Bar	.505	Smooth	1200	164,000	100,000	16.0	16.0
1-A40-000	Bar	.505	Smooth	1350	132,000	92,000	12.0	15.0
1-A40-000	Bar	.505	Smooth	1350	126,200	105,000	9.0	7.8
1-A40-000	Bar	.505	Smooth	1500	96,000	76,000	25.0	43.0
1-A40-000	Bar	.505	Notched	75	225,500	--	--	--
1-A40-000	Bar	.505	Notched	75	228,000	--	--	--
1-A40-000	Bar	.505	Notched	500	218,000	--	--	--
1-A40-000	Bar	.505	Notched	1000	208,000	--	--	--
1-A40-000	Bar	.505	Notched	1200	202,000	--	--	--
1-A40-000	Bar	.505	Notched	1350	163,000	--	--	--
1-A40-000	Bar	.505	Notched	1500	150,000	--	--	--
1-A40-000	Bucket	.160	Smooth	75	174,800	105,300	24.0	35.8
1-A40-000	Bar	.125	Smooth	75	180,000	112,000	24.5	28.5
1-A40-715	Bar	.125	Smooth	75	189,000	122,200	22.0	32.4
1-A40-7110	Bar	.125	Smooth	75	192,500	119,800	22.0	30.4
1-A40-722	Bar	.125	Smooth	75	200,000	141,000	18.0	22.7
1-A40-725	Bar	.125	Smooth	75	186,000	122,500	10.0	8.9
1-A40-7210	Bar	.125	Smooth	75	185,000	110,100	17.0	18.1
1-A40-742	Bar	.125	Smooth	75	179,200	107,200	8.0	3.0
1-A40-745	Bar	.125	Smooth	75	188,000	121,000	10.0	11.2
1-A40-7410	Bar	.125	Smooth	75	162,000	82,900	11.0	13.5
1-A40-0210	Bar	.505	Smooth	75	178,000	113,000	11.0	12.0
2-A40-000	Bar	.505	Smooth	75	179,500	107,500	25.0	27.5
2-A40-000	Bar	.505	Smooth	1350	127,800	103,500	12.0	8.5
2-A40-000	Bucket	.160	Smooth	1350	120,900	--	16.0	22.5
2-A40-0210	Bar	.505	Smooth	75	180,000	114,000	12.5	16.6
2-A40-0210	Bar	.505	Smooth	1350	125,000	104,000	16.5	19.6
4-A40-000	Bucket	.160	Smooth	1350	127,000	--	24.0	21.0
5-A40-000	Bucket	.160	Smooth	1350	117,000	--	10.0	16.0
6-A74-000	Bar	.437	Smooth	1350	127,500	90,000	10.0	9.5
6-A64-000	Bar	.437	Smooth	1350	119,000	--	25.0	32.2
6-A40-000	Bar	.437	Smooth	1350	145,000	100,600	11.9	17.5
6-A40-000	Bar	.437	Smooth	1500	102,400	87,500	20.8	19.0
6-B40-000	Bar	.437	Smooth	1350	157,600	103,000	22.7	35.0
6-B40-000	Bar	.437	Smooth	1500	108,000	65,000	46.0	44.0
7-A74-000	Bar	.437	Smooth	1350	121,000	71,000	17.2	15.9
7-A64-000	Bar	.437	Smooth	1350	127,000	88,000	11.0	12.4

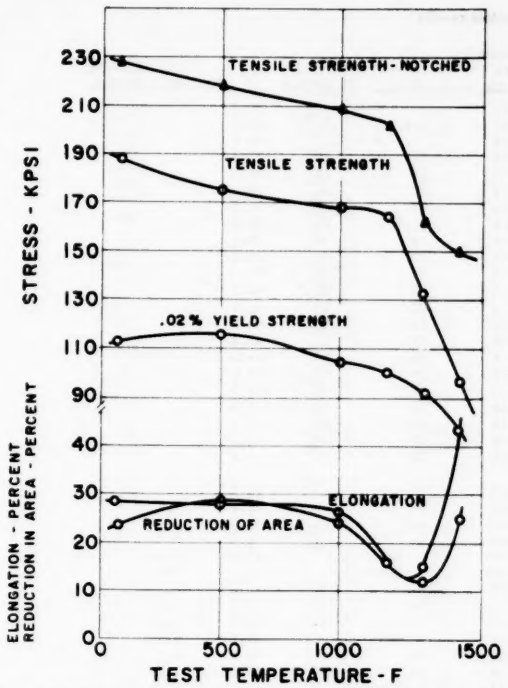

Fig. 1 Tensile properties versus temperature for M-252 material and condition code 1-A40

for several heats of material. Specimens with reduced diameters were required in some cases due to size of material. This was particularly true of specimens machined from forged buckets, where bar diameters of 0.125 and 0.160 in. were required. The notched bars had 60-deg V-circumferential notches prepared by grinding with a major diameter of 0.714 in., a minor diameter of 0.505 in., and notch-root radii of 0.023 in.

Results of tensile tests are tabulated in Table 4 and a plot of tensile properties versus temperature is presented in Fig. 1. Yield strength and tensile strength are maintained at high levels up to approximately 1200 F, above which temperature the tensile strength falls off more rapidly. A pronounced minimum value of ductility is apparent at approximately 1300 F. Under conditions of tensile testing, this material was notch-ductile since the notch-bar strength was well above smooth-bar strength.

Aging under 17,500-psi tensile stress produced appreciable changes in strength and ductility. At 1050 and 1250 F aging temperatures, tensile strength and yield strength were increased as compared with preaged properties (1-A40-000), while ductility (reduction in area) at 1250 F seems to go through a minimum value at 5000 hr at 1250 F (1-A40-725). Aging at 1400 F first produced an increase in strength and a decrease in ductility at 3000 and 5000 hr, followed by overaging at 10,000 hr. The effect of stress on after-aged properties was not conclusive (1-A40-0210 versus 1-A40-7210). In boron-containing M-252, an intermediate age of 1675 F as opposed to a 1750 F age results in a large improvement in 1350 F tensile ductility.

Stress-Rupture Tests

The stress-rupture properties of M-252 were investigated extensively because of their relevance to bucket design and performance. Rupture tests on both smooth and notched bars were conducted over a wide range of temperature and stress. Major dimensions of test specimens used are given in Table 5. Specimens were notched by grinding a 60-deg V-notch.

Table 5 Dimensions of rupture-test specimens

Material source	Specimen type	Gage length, in.	Minor diam, in.	Major diam, in.	Root radius, in.
Bar	Smooth	2	0.253	...	...
Bar	Notched	...	0.253	0.357	0.005
Buckets	Smooth	1	0.159	...	...
Buckets	Notched	...	0.159	0.226	0.005
Stress aging specimens	Smooth	1.5	0.160	...	...
Stress aging specimens	Notched	...	0.160	0.253	0.003

Rupture-test results are given in Table 6, identified by a code which gives the heat number, heat-treatment, material form, and type of specimen. Test temperature, stress in thousands of pounds per square inch (Kpsi), rupture time, elongation, and reduction of area are listed in order of increasing test temperature and decreasing stress. Where notched and smooth-bar tests were run at the same temperature and stress, the ratio of their rupture lives is given as a measure of notch ductility. In this paper, a material is termed notch-ductile if the notched-bar rupture life exceeds the smooth-bar life, giving a ratio of notched to smooth-bar life greater than one.

The time-temperature parameter $T(20 + \log t)$ for rupture stresses as described by Larsen and Miller [4] was used to correlate and interpret the rupture-strength data, and values for this parameter are listed for each test under the heading P_{20}. Twelve tests in Table 6 exceeded 5000 hr in life. These long-time tests either were as good or better than the predictions which were based on short-time data.

Fig. 2 shows a plot of rupture stress versus the rupture parameter for 1-A40 material from both bar stock and forged buckets and both smooth and notched specimens. A scale is provided showing temperature for 100,000-hr life. This plot shows the forged buckets to be stronger than the bar stock. Fig. 3 shows a similar plot for 2-A40, with the curve for 1-A40 and a typical curve for S-816, a well-known cobalt-base bucket super-alloy, superimposed for comparison. The curves for the heats of M-252 are quite similar in strength. It can be seen that the M-252 offers

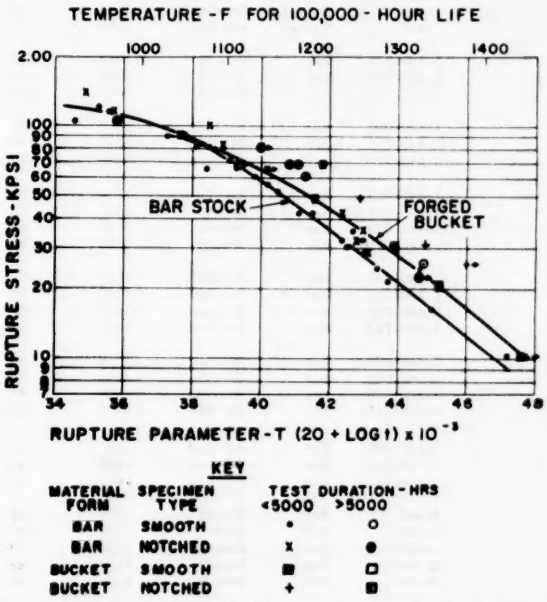

Fig. 2 Smooth-bar and notched-bar rupture strength versus rupture parameter for M-252 bars and forged buckets, material and condition code 1-A40

Table 6 Stress-rupture test results

Code	Material Form	Specimen Type	Test Temperature-F	Stress Kpsi	Rupture Time Hours	Elongation -%	Reduction in Area-%	P_{20}	Time - Notched / Time - Smooth
1-A40	Bar	Smooth	1050	120	2348	B.I.T.		35.3	
1-A40	Bar	Smooth	1050	115	3925	3.4	9.3	35.6	
1-A40	Bar	Smooth	1050	105	773	B.I.T.		34.6	
1-A40	Bar	Smooth	1200	90	323	7.9	17	37.3	
1-A40	Bar	Smooth	1200	80	1770	14	17	38.5	
1-A40	Bar	Smooth	1250	68	1063	30	41	39.3	
1-A40	Bar	Smooth	1250	68	1283	14	37	39.5	
1-A40	Bar	Smooth	1250	65	304	38	51	38.4	
1-A40	Bar	Smooth	1250	60	2022	19	48	39.8	
1-A40	Bar	Smooth	1300	70	186	19	35	39.1	
1-A40	Bar	Smooth	1300	52	1135	36	47	40.5	
1-A40	Bar	Smooth	1350	55	185	19	46	40.2	
1-A40	Bar	Smooth	1400	42	134	22	55	41.1	
1-A40	Bar	Smooth	1400	35	902	16	44	42.7	
1-A40	Bar	Smooth	1400	32	632	35	51	42.4	
1-A40	Bar	Smooth	1400	28	1344	46	64	43.0	
1-A40	Bar	Smooth	1400	22	9174	18	52	44.6	
1-A40	Bar	Smooth	1500	30	48	34	59	42.5	
1-A40	Bar	Smooth	1500	24	144	30	61	43.4	
1-A40	Bar	Smooth	1550	21	58	--	67	43.7	
1-A40	Bar	Smooth	1600	16	66	30	68	45.0	
1-A40	Bar	Smooth	1650	10	206	31	41	47.2	
1-A40	Bar	Notched	1050	122	100	--	--	33.2	
1-A40	Bar	Notched	1050	115	4322	--	--	35.7	1.1
1-A40	Bar	Notched	1050	105	5002	--	--	35.8	
1-A40	Bar	Notched	1200	100	1605	--	--	38.5	
1-A40	Bar	Notched	1200	80	13540+	Removed		40.0+	7.7+
1-A40	Bar	Notched	1250	65	3539+	Removed		40.2+	10+
1-A40	Bar	Notched	1250	68	6707	--	--	40.8	5.7
1-A40	Bar	Notched	1250	68	8021	--	--	41.0	6.9
1-A40	Bar	Notched	1250	60	15040	--	--	41.3	7.4
1-A40	Bar	Notched	1400	32	902+	Removed		42.8+	1.4+
1-A40	Bar	Notched	1400	35	1310	--	--	43.0	1.5
1-A40	Bar	Notched	1400	28	1435	--	--	43.1	1.1
1-A40	Bar	Notched	1400	22	9174+	Removed		44.6+	1.0+
1-A40	Bucket	Smooth	1200	90	568	68	9.7	37.7	
1-A40	Bucket	Smooth	1300	68	238	14	31	39.3	
1-A40	Bucket	Smooth	1400	48	249	16	32	41.6	
1-A40	Bucket	Smooth	1500	30	240	30	56	43.9	
1-A40	Bucket	Smooth	1600	20	86	25	62	45.2	
1-A40	Bucket	Smooth	1650	10	324	-	54	47.6	
1-A40	Bucket	Notched	1200	90	615	-	-	37.8	1.08
1-A40	Bucket	Notched	1300	68	5018	-	-	41.8	21.1
1-A40	Bucket	Notched	1400	48	1234	-	-	42.9	5.0
1-A40	Bucket	Notched	1500	30	728	-	-	44.8	3.0
1-A40	Bucket	Notched	1600	25	217+	Load Bar Broke		46.0+	2.5+
1-A40	Bucket	Notched	1650	10	451+	Threads Stripped		47.8+	1.4+
1-A40-000	Bar	Smooth	1050	140	86.0	5.7	8.0	33.1	
1-A40-715	Bar	Smooth	1050	140	94.9	5.3	15.0	33.2	
1-A40-7110	Bar	Smooth	1050	140	4.4	12.2	14.4	29.7	
1-A40-000	Bar	Notched	1050	140	1283	-	-	34.9	14.9
1-A40-715	Bar	Notched	1050	140	2632	-	-	35.5	27.8
1-A40-7110	Bar	Notched	1050	140	623	-	-	34.4	141
1-A40-000	Bar	Smooth	1250	82	206	13.0	18.0	38.1	
1-A40-722	Bar	Smooth	1250	82	342	12.8	26.0	38.5	
1-A40-725	Bar	Smooth	1250	82	80	32.0	44.0	37.4	
1-A40-7210	Bar	Smooth	1250	82	36	36.1	47.6	36.8	
1-A40-000	Bar	Notched	1250	82	579	-	-	38.9	2.8
1-A40-722	Bar	Notched	1250	82	4766	-	-	40.5	13.9
1-A40-725	Bar	Notched	1250	82	33	-	-	33.4	.4
1-A40-7210	Bar	Notched	1250	82	2379	-	-	39.9	66.2
1-A40-000	Bar	Smooth	1400	42	221	30.0	46.0	41.5	
1-A40-742	Bar	Smooth	1400	42	373	36.0	49.0	42.0	
1-A40-745	Bar	Smooth	1400	42	72	29.0	57.0	40.6	
1-A40-7410	Bar	Smooth	1400	42	180	47.4	42.4	41.4	
1-A40-000	Bar	Notched	1400	42	620	-	-	42.4	2.8
1-A40-742	Bar	Notched	1400	42	2903	-	-	43.6	7.8
1-A40-7410	Bar	Notched	1400	42	1182	-	-	42.9	6.6
2-A40	Bar	Smooth	1050	98	12888+	Still Running 8/6/58		36.5+	
2-A40	Bar	Smooth	1200	100	329	53	12	37.3	
2-A40	Bar	Smooth	1200	93	417	9.2	14	37.5	
2-A40	Bar	Smooth	1200	80	1304	13	16	38.3	
2-A40	Bar	Smooth	1250	44	12864+	Still Running 8/6/58		41.3+	

Table 6 (*Continued*)

	Code	Material Form	Specimen Type	Test Temperature -F	Stress Kpsi	Rupture Time Hours	Elongation -%	Reduction in Area-%	P_{20}	Time-Notched Time-Smooth
	2-A40	Bar	Smooth	1300	68	266	22	25	39.4	
	2-A40	Bar	Smooth	1400	50	81	15	48	40.7	
	2-A40	Bar	Smooth	1400	17	10872	11	56	44.8	
	2-A40	Bar	Smooth	1500	38	37	26	50	42.3	
	2-A40	Bar	Smooth	1500	30	12	40	59	43.2	
	2-A40	Bar	Smooth	1600	20	36	38	67	44.4	
	2-A40	Bar	Smooth	1650	10	45	B.I.T.		45.7	
	2-A40	Bar	Notched	1200	100	117	-	-	36.6	.36
	2-A40	Bar	Notched	1200	93	7336	-	-	39.6	17.6
	2-A40	Bar	Notched	1200	80	8179	-	-	39.7	6.3
	2-A40	Bar	Notched	1300	68	2939	-	-	41.2	11.0
	2-A40	Bar	Notched	1500	30	170	-	-	43.5	14.2
	2-A40	Bar	Notched	1600	20	86	-	-	45.2	2.4
	2-A40	Bar	Notched	1650	10	231	-	-	47.2	-
	4-A40	Buckets	Smooth	1500	38	64.8	15.2	20	42.8	
	4-A54	Buckets	Smooth	1500	38	47	15.0	25	42.5	
	4-A40	Buckets	Smooth	1200	100	158	7.2	14	36.9	
	4-A54	Buckets	Smooth	1200	100	35	22.0	25	35.8	
	4-A40	Buckets	Notched	1200	100	1296	-	-	38.5	8.2
	4-A54	Buckets	Notched	1200	100	536	-	-	37.8	15.3
	5-A40	Buckets	Smooth	1200	100	958	6.6	11	38.2	
	5-A54	Buckets	Smooth	1200	100	188	10.3	21	37.0	
	5-A40	Buckets	Notched	1200	100	17	-	-	35.3	.018
	5-A40	Buckets	Notched	1200	100	11	-	-	35.0	.012
	5-A54	Buckets	Notched	1200	100	651+	Bar Removed		37.9+	3.5+
	6-A64	Bar	Smooth	1050	120	902	5.7	9.3	34.6	
	6-A64	Bar	Smooth	1350	80	19	16.4	29	38.5	
	6-A64	Bar	Smooth	1450	50	22	33.2	42	40.8	
	6-B64	Bar	Smooth	1050	120	1825	9.7	14	35.1	
	6-B64	Bar	Smooth	1350	80	25	17	42	38.7	
	6-B64	Bar	Smooth	1450	50	46	34	50	41.4	
	6-B64	Bar	Smooth	1600	20	175	36	54	45.7	
	6-A74	Bar	Smooth	1050	120	1216	7.0	7.2	34.8	
	6-A74	Bar	Smooth	1350	80	24	26	28	38.6	
	6-A74	Bar	Smooth	1450	50	20	36	42	40.7	
	6-A74	Bar	Smooth	1600	20	98	33	47	45.4	
	6-B74	Bar	Smooth	1050	120	2665	8.3	9.3	35.3	
	6-B74	Bar	Smooth	1350	80	30	24	39	38.8	
	6-B74	Bar	Smooth	1450	50	49	27	20	41.4	
	6-B74	Bar	Smooth	1600	20	136	23	50	45.4	
Boron Free	(7-A64	Bar	Smooth	1050	120	364	8.3	12	34.1	
	(7-A64	Bar	Smooth	1250	80	121	8.6	12	37.7	
	(7-A64	Bar	Smooth	1350	50	118	6.8	12	39.9	
	(7-A64	Bar	Smooth	1550	20	68	5.7	23	43.9	
	(									
	(									
	(7-B64	Bar	Smooth	1050	120	538	12	12	34.3	
	(7-B64	Bar	Smooth	1250	80	207	9.2	11	38.1	
	(7-B64	Bar	Smooth	1350	50	318	7.5	8.5	40.6	
	(7-B64	Bar	Smooth	1550	20	179	20	29	44.7	
	(7-A74	Bar	Smooth	1050	124	28	8.2	15	33.9	
	(7-A74	Bar	Smooth	1250	80	202	12	15	38.1	
	(7-A74	Bar	Smooth	1350	50	172	10	14	40.2	
Boron Free	(7-A74	Bar	Smooth	1550	20	56	21	24	43.7	
	(									
	(7-B74	Bar	Smooth	1050	120	877	11	10	34.6	
	(7-B74	Bar	Smooth	1250	80	227	3.5	11	38.2	
	(7-B74	Bar	Smooth	1350	50	255	35	11	40.5	
	(7-B74	Bar	Smooth	1550	20	168	17	25	44.7	

B.I.T. - Broke in threads

\+ - Test incomplete or discontinued. Rupture life would be greater than value indicated.

P_{20} - $T\ (20 + \log t) \times 10^{-3}$, where T = absolute temperature in degrees R and t = time in hours.

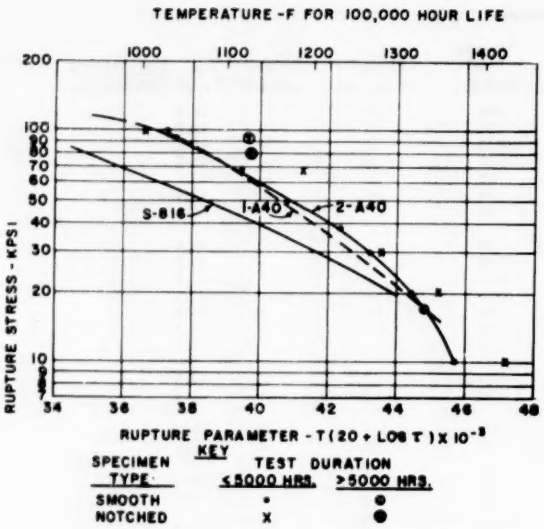

Fig. 3 Smooth-bar and notched-bar rupture strength versus rupture parameter for M-252 bar (2-A40) compared with smooth-bar strength of material 1-A40 and S-816

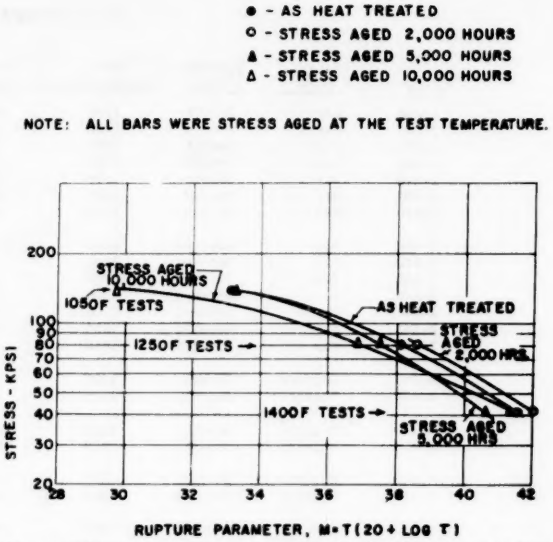
● - AS HEAT TREATED
○ - STRESS AGED 2,000 HOURS
▲ - STRESS AGED 5,000 HOURS
△ - STRESS AGED 10,000 HOURS
NOTE: ALL BARS WERE STRESS AGED AT THE TEST TEMPERATURE.
STRESS AGED 10,000 HOURS
1050F TESTS
AS HEAT TREATED
STRESS AGED 2,000 HRS.
1250F TESTS
1400F TESTS
STRESS AGED 5,000 HRS.
STRESS - KPSI
RUPTURE PARAMETER, M=T(20+LOG T)

Fig. 4 Rupture stress versus rupture parameter showing effects of stress aging of M-252, material and treatment 1-A40 at 17,500 psi, on subsequent rupture life

a large strength advantage over S-816 at most temperatures. At a strength of 36,000 psi, which is the material strength required for the first bucket to which M-252 was applied, a bucket made of M-252 material can be operated at a 60 F higher temperature than one made of S-816 material with the same margin of safety.

From Table 6 and Figs. 2 and 3, it can be noted that all tests above 1050 F on 1-A40 and 2-A40 tested as heat-treated are notch-ductile. At 1050 F, two bars broke in the threads indicating low ductility and the 1-A40 notched bar tested at 122,000 psi ran a shorter time than a smooth bar if it were loaded to the same stress.

The effect of stress-aging on rupture strength and ductility may be seen in Table 6 where, in the series 1-A40-000 to 1-A40-7410, stress has been held constant at each of three testing and aging temperatures while varying aging time from 0 to 10,000 hr. Generally, rupture life was decreased by aging while ductility tended to increase, with a few exceptions. Results are plotted in Fig. 4.

Heat 5-A40 was definitely notch-brittle with a single-aging treatment. An intermediate-aging treatment of 1550 F (5-A54) lowered smooth-bar strength but increased ductility and notch-rupture life so that with this treatment, Heat 5 was notch-ductile. The same treatment applied to the more ductile heat 4-A40 reduced both the smooth-bar and notched-bar strength while further increasing the margin of notch ductility. This treatment has been adopted for production buckets to achieve consistent notch ductility and improved stability of engineering properties for long periods of time.

A series of tests made with Heats 6 and 7 explores the effect of the presence or absence, respectively, of a trace of boron on rupture strength and ductility. The tabulated data and Fig. 5 show that Heat 6 containing boron is stronger than Heat 7 without boron and that the 2050 F solution-treatment significantly improves rupture strength over that for the 1950 F treatment. These gains are not accompanied by serious loss of ductility and there is little difference between the two aging treatments in

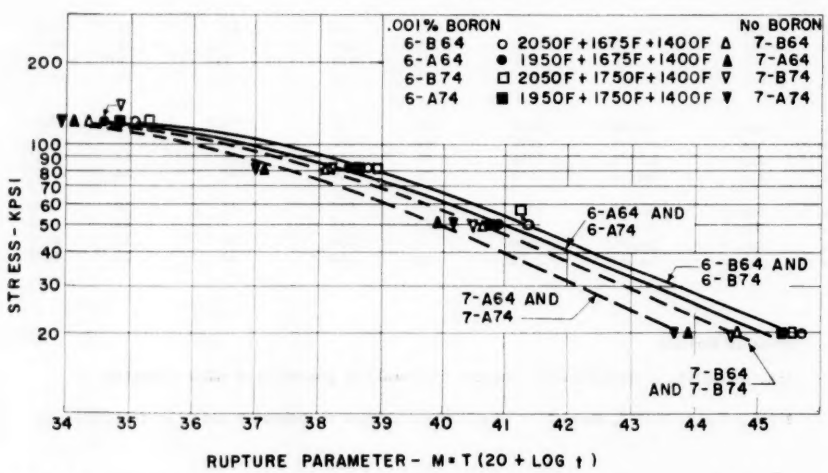

Fig. 5 Rupture stress versus rupture parameter for a boron-free heat and a boron-containing heat of M-252 showing effects of boron, solution temperature, and intermediate aging temperature

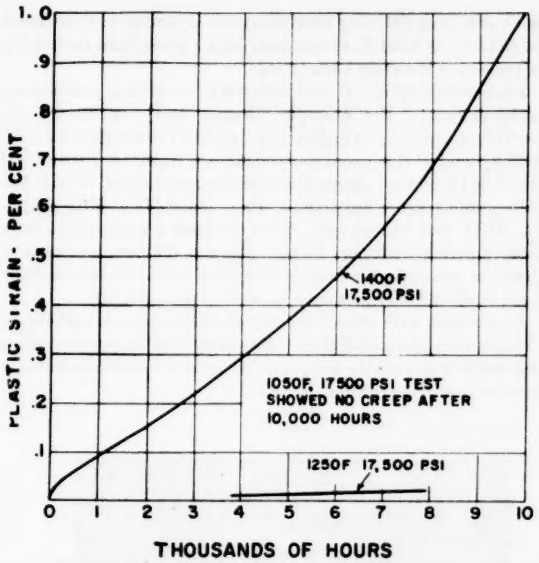

Fig. 6 Creep (plastic strain) measured during stress aging of M-252, material and condition code 1-A40

their effect on strength and ductility. Judging from the rupture properties of the boron-free Heat 7, all of the other heats probably contained some boron which was absorbed from the crucible during melting.

The rupture data as a group show that very satisfactory levels of rupture strength and ductility can be maintained after testing and exposure times extending to 10,000 hr at temperatures in the operating range of first-stage heavy-duty gas-turbine buckets. Boron additions which increase ductility at temperatures above 1050 F and higher solution temperatures having little effect on ductility are effective in increasing the rupture strength of M-252.

Creep Tests

The results of creep measurements obtained during aging at 17,500-psi tensile stress at 1050 F, 1250 F, and 1400 F are shown in Fig. 6. Virtually no creep occurred at 1050 or 1250 F, while at 1400 F the curve shows an increasing creep rate after approximately 2000 hr, with plastic strain reaching 1 per cent at 10,000 hr.

Phase and Structure Studies

Metallographic examinations were conducted on selected rupture specimens using mixed acids, 92 per cent HCl, 5 per cent H_2SO_4, 3 per cent HNO_3, for etching. Minor-phase identification was accomplished by first separating precipitates from the matrix using electrolytic cells with 10 per cent HCl electrolyte at low-current density (0.2 amp per sq in.); then analyzing the residue with a General Electric XRD-3 x-ray machine under cobalt K radiation before and after treating in boiling 50 per cent HCl. The details of techniques used and results are contained in a discussion by Becht and Tammanian of a paper by Beattie and Ver Snyder [5]. Phases identified from x-ray patterns of electrolytic residues from selected rupture-test specimens are listed in Table 7.

The complex carbide M_6C and the face-centered cubic hardening phase γ' (Ni_3Al) were predominant in the initial residues, making identification of less plentiful phases difficult. After selective solution of the γ' by HCl treatment, the complex carbide $M_{23}C_6$, titanium carbide (TiC), and the hexagonal phase η (Ni_3Ti), were identified and the complete removal of γ' was verified. Spectrographic analysis of the HCl treated residue showed the absence of aluminum, also indicating complete removal of γ'.

Analysis of the filtrate obtained after HCl treatment, containing practically pure γ' showed 11.9 per cent Ti and 6.2 per cent Al, indicating solution of Ti in these proportions. An x-ray

Table 7 Results of phase-identification studies conducted on broken rupture-test specimens

Exposure			Identified phases	
Temp, deg F	Stress, psi	Time, hr	Initial residue	After HCl treatment
1300	68000	5018	M_6C, $Ni_3(AlTi)$ ($M_{23}C_6$) (TiC)	M_6C, $M_{23}C_6$, TiC
1400	48000	1234	M_6C, $Ni_3(AlTi)$	M_6C, $M_{23}C_6$, TiC
1500	30000	728	M_6C, $Ni_3(AlTi)$	M_6C, $M_{23}C_6$
1600	20000	217	M_6C, $Ni_3(AlTi)$	M_6C, $M_{23}C_6$
1650	10000	457	M_6C, $Ni_3(AlTi)$	M_6C, Ni_3Ti

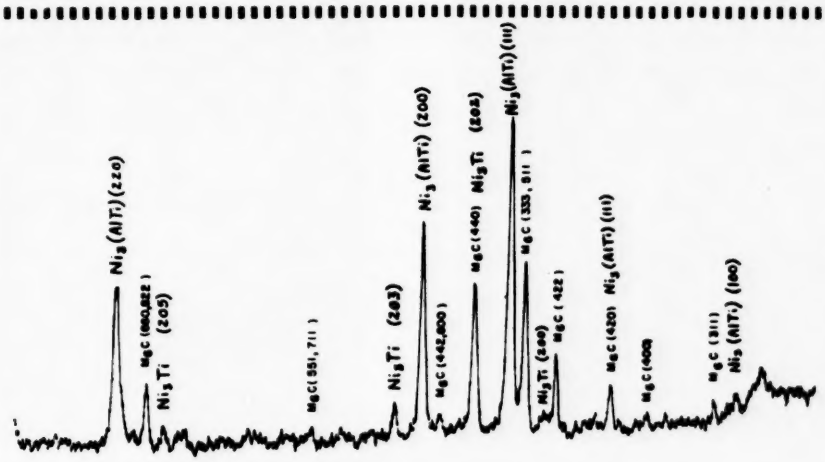

Fig. 7 Diffraction pattern of electrolytic residue of M-252 after 457 hr at 1650 F. Cobalt Kα radiation logarithmic recorder.

emission analysis of the solution showed only nickel and cobalt. Hence the use of the term $Ni_3(AlTi)$ in place of Ni_3Al in Table 7.

A typical x-ray pattern obtained on the electrolytic residue from a 1650 F exposed sample indicating the presence of both hardening phases γ' and η and the carbide M_6C is shown in Fig. 7. These phase studies show, as exposure temperature is increased, first, the disappearance of TiC above 1400 F, of $M_{23}C_6$ above 1600 F, and the appearance of Ni_3Ti at 1650 F.

Metallographic changes during rupture tests are shown on the selected photomicrographs of Fig. 8. They show a general distribution of globular M_6C within the grains and the growth of γ' with increasing temperature within the grains. Angular TiC disappears at 1500 F, globular M_6C at 1650 F. Grain boundary $M_{23}C_6$ increases at 1500 F, is much less prominent at 1600 F, and based on the x-ray identification is replaced by M_6C at the grain boundaries after 1650-F exposure. Ni_3Ti platelets start to appear at the highest temperature. The structure prior to long-time aging or testing following heat-treatment is similar to that shown for 5013 hr at 1300 F, except that $M_{23}C_6$ precipitate should not be present at the grain boundaries.

Phase relationships are affected greatly by melting practice and heat-treatment. For example, Beattie and Ver Snyder [5] found sigma phase, but no $M_{23}C_6$, γ', or Ni_3Ti in air-melted M-252 with 8.5 and 11.0 per cent molybdenum. However, Beattie and Hagel [6] found no sigma phase in vacuum-melted M-252, but with various aging treatments, they found TiC, M_6C, $M_{23}C_6$, γ', Ni_3Ti, and Mu phases. They propose a rationalization of these differing behaviors based upon the different amounts of titanium available for carbide reactions which is substantially lower in air-melted heats than in vacuum-melted heats.

In common with all other complex alloys, some metallurgical changes take place with time. However, with proper processing the stability is entirely adequate for service conditions encountered in first-stage turbine buckets.

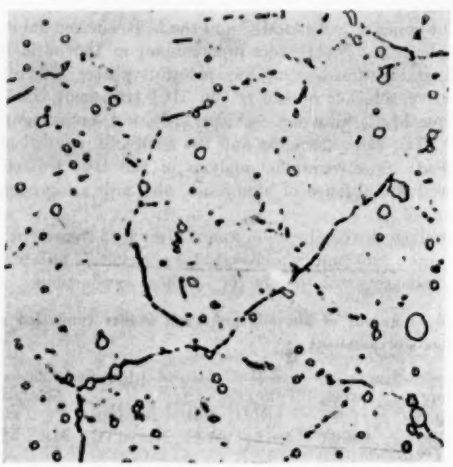

5013 hours at 1300 F; dispersion of M_6C globules; angular TiC; $M_{23}C_6$ probably at grain boundaries

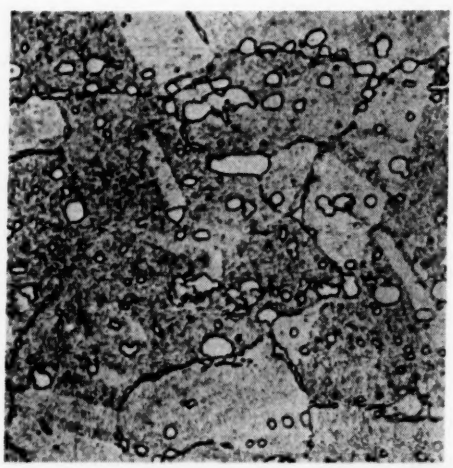

728 hours at 1500 F; visible precipitation of γ' [$Ni_3(AlTi)$]; growth of M_6C in grains and $M_{23}C_6$ in grain boundaries. Disappearance of TiC.

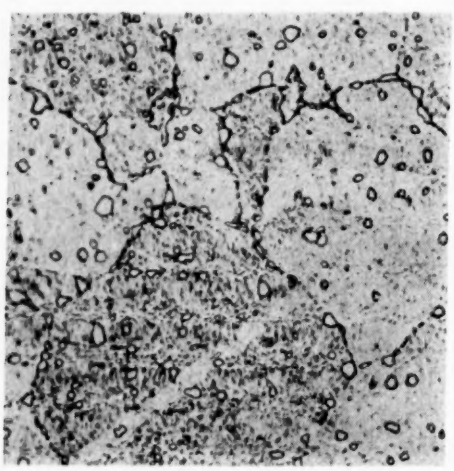

217 hours at 1600 F; increase in size of γ'. Decrease in $M_{23}C_6$ in grain boundaries.

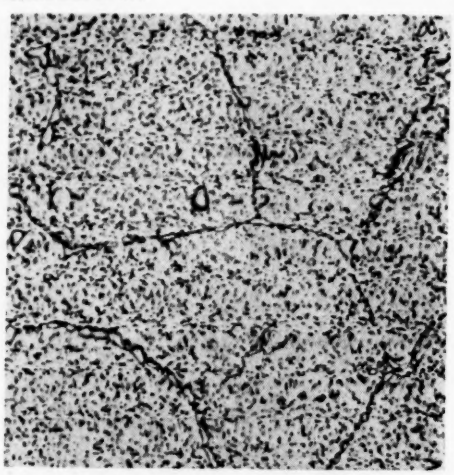

457 hours at 1650 F; further growth of γ', visible precipitation of $\eta(Ni_3Ti)$ platelets. Disappearance of globular M_6C in matrix.

Fig. 8 Structural changes during rupture tests

Note: All photos at 1000X; etchant mixed acids 92:5:3

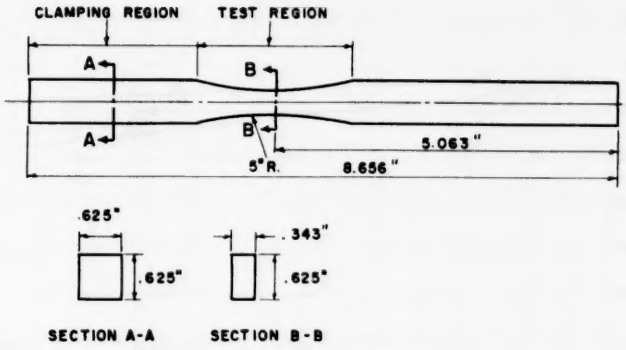

Fig. 9 Smooth fatigue-test specimen

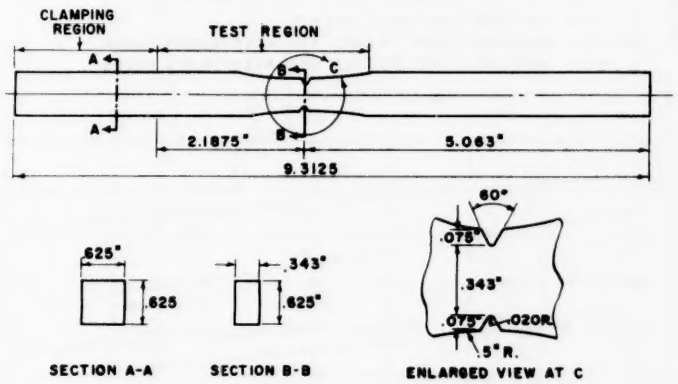

Fig. 10 Notched fatigue-test specimen

Table 8 Summary of fatigue test conditions

Specimen shape	Surface condition	Stress-free aging treatment Temp, deg F	Stress-free aging treatment Time, hr	Test temp, deg F
Notched	Shotpeened	Unaged		1050
Notched	Shotpeened	1050	5000	1050
Notched	Shotpeened	1050	10000	1050
Notched	As machined	Unaged		1250
Notched	As machined	1250	10000	1250
Notched	Shotpeened	Unaged		1250
Notched	Shotpeened	1250	5000	1250
Notched	Shotpeened	1250	10000	1250
Smooth	As machined	Unaged		1250
Smooth	As machined	1250	10000	1250

Fatigue Tests

Fatigue tests were conducted at temperatures of 1050 and 1250 F in pneumatic vibrating-cantilever equipment at a frequency of approximately 10,000 cpm. Both smooth and notched specimens, as delineated in Figs. 9 and 10, were tested. Some of the notched specimens also were shotpeened. In order to study the effect of temperature for long periods of time on the fatigue characteristics, some samples were also aged for 5000 and 10,000 hr without stress. Table 8 summarizes the conditions under which *S-N* curves were obtained.

Since the gas-turbine buckets are attached to the wheels with pine-tree dovetails which have relatively small fillets at the roots of the hooks, the fatigue program emphasized the testing of notched specimens. *S-N* curves plotted from data taken during the fatigue program are presented in Figs. 11 and 12. From these curves the fatigue strength at one hundred million cycles for the material in various conditions is summarized in Table 9.

Table 9 Summary of fatigue strengths at one hundred million cycles

Test and aging temperature, deg F	Physical condition	Fatigue strength, psi — Unaged	Aged 5000 hr	Aged 10000 hr
1050...	Notched and shotpeened	53200	47500	45100
1250...	Smooth	74500	...	59000
1250...	Notched	19000	...	27000
1250...	Notched and shotpeened	41500	47000	31000

A study of Table 9 and Figs. 11 and 12 reveals some interesting characteristics of M-252 material. The material appears to be more notch-sensitive in fatigue than other high-temperature materials such as S-816, Nimonic 80A, and Crucible 422. However, it responds much better than these alloys to shotpeening treatment. Data in Table 9 indicate that the unaged fatigue strength more than doubles when shotpeened. As a result, M-252 has a higher fatigue strength in the notched and shotpeened condition at 1250 F than S-816.

The beneficial effects of shot-peening, in general, decrease with time at temperature. At 1050 F, a 15 per cent decrease in fatigue strength was noted after 10,000 hr aging. At 1250 F the decrease was 25 per cent for the same period of time compared to a 20 per cent decrease for the smooth-bar specimens. After 10,000 hr of aging at 1250 F, the notched and shotpeened fatigue strength is still greater than the notched specimens which also were aged for 10,000 hr. The exact amount between the two values is clouded by the fact that the notched fatigue strength increased with time at temperature. This surprising change may have been due to the fact that the aging released unfavorable residual

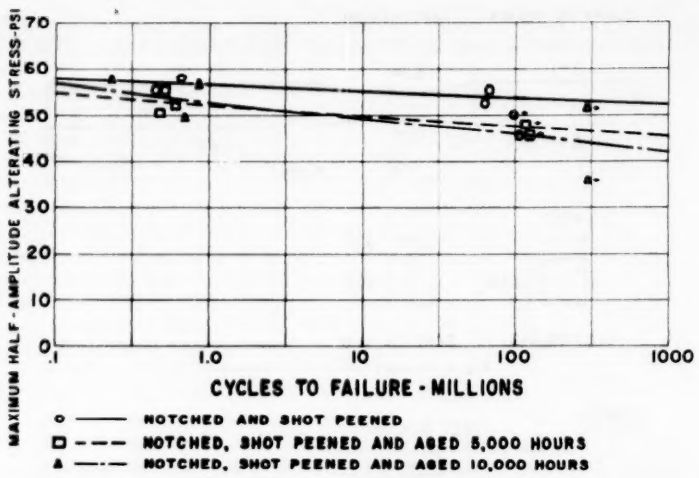

Fig. 11 *S-N* curves at 1050 F

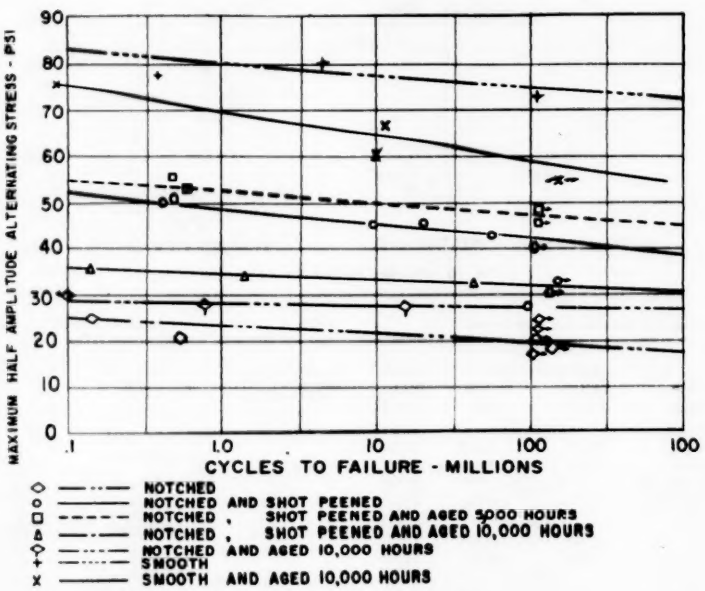

Fig. 12 *S-N* curves at 1250 F

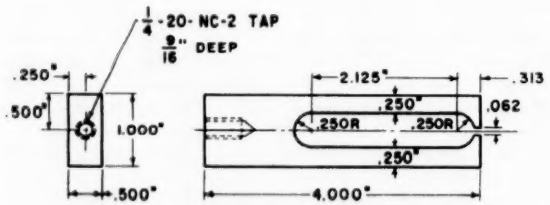

Fig. 13 Tuning fork used for damping measurements

stresses left in the specimens by the machining. It was encouraging to find that the effects of shotpeening remain significant for relatively long periods of time. During initial operation of a turbine, when the high local stresses in the fillet regions of the bucket dovetails are being redistributed, it is important to have the high fatigue strength which the shotpeening imparts to the material. After the material has yielded and the local stresses have been reduced, a reduced fatigue strength still gives long service life.

Damping Tests

A tuning fork, delineated in Fig. 13, was machined from M-252. It was vibrated and damping data were obtained in accordance with the method discussed in [2] at temperatures of 800, 1050, 1350, and 1500 F. Results of the tests are plotted in Fig. 14. The values of material internal damping are low and are comparable with data obtained on other austenitic alloys.

Oxidation and Oil-Ash Corrosion Tests

Samples were exposed in moving air at temperatures of 1200, 1350, and 1500 F to determine the oxidizing characteristics of the

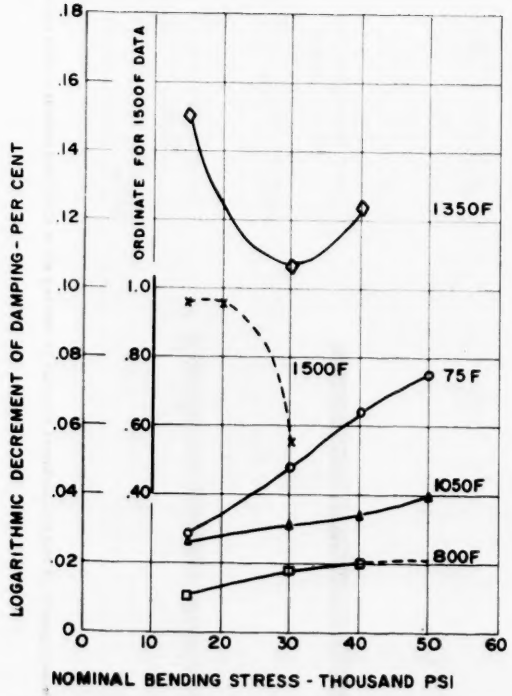

Fig. 14 Logarithmic decrement of damping versus nominal bending stress

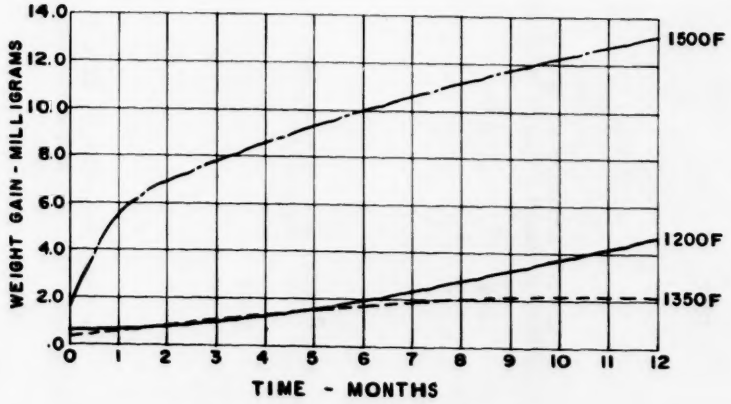

Fig. 15 Oxidation test weight gain versus time

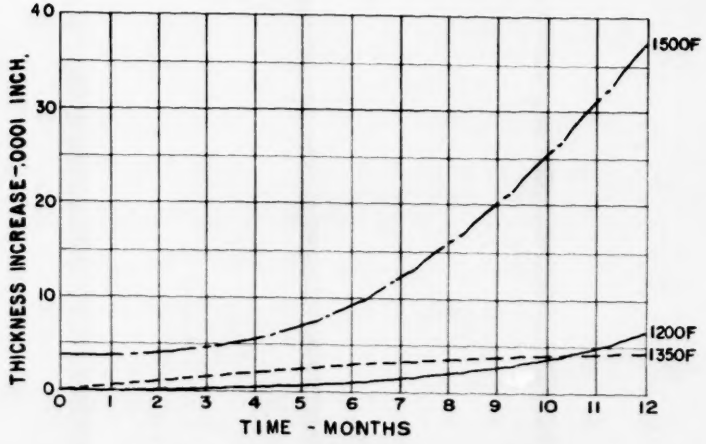

Fig. 16 Oxidation test thickness increase versus time

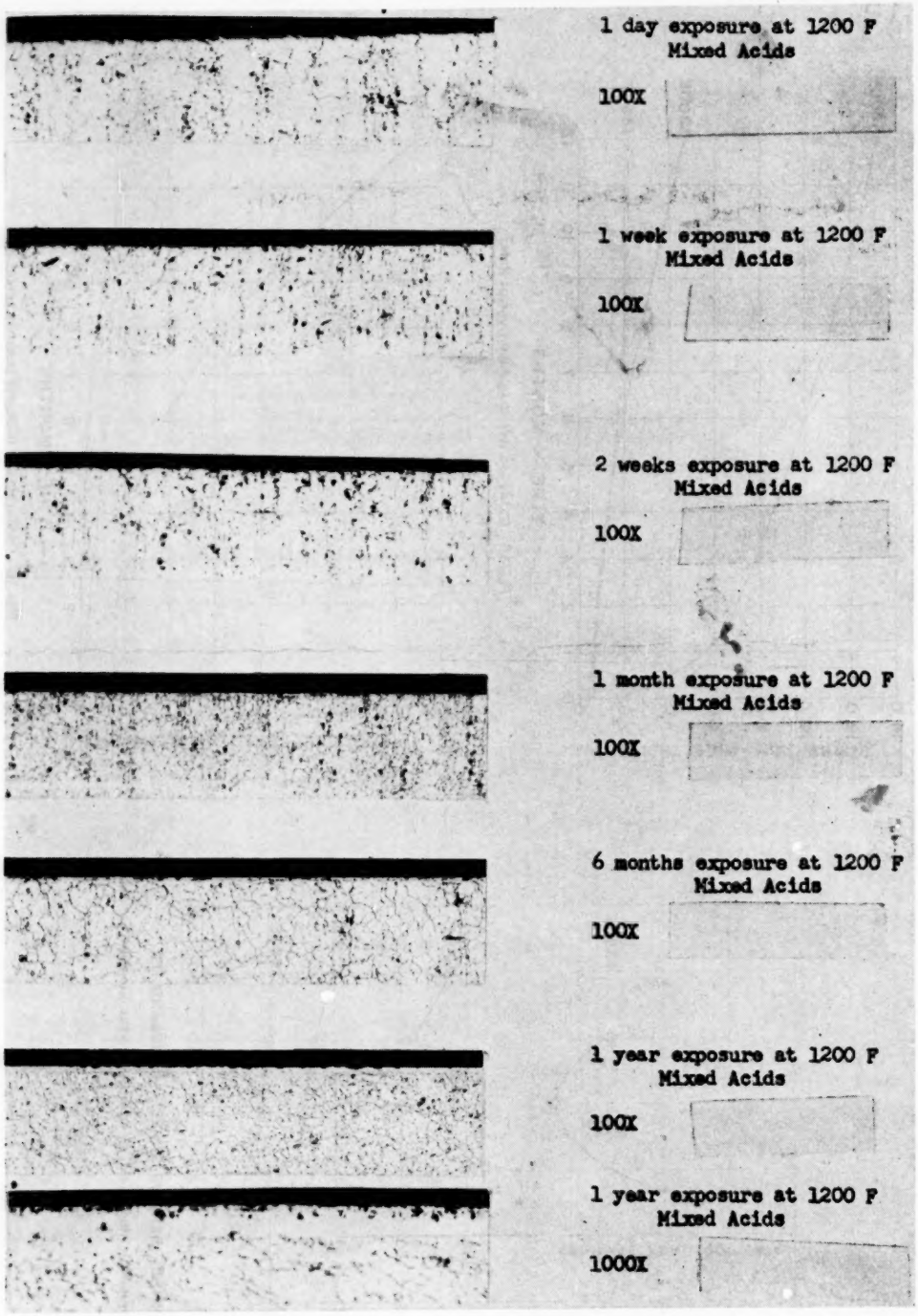

Fig. 17 Photomicrographs of M-252 specimens exposed to moving air at 1200 F for periods of time up to one year

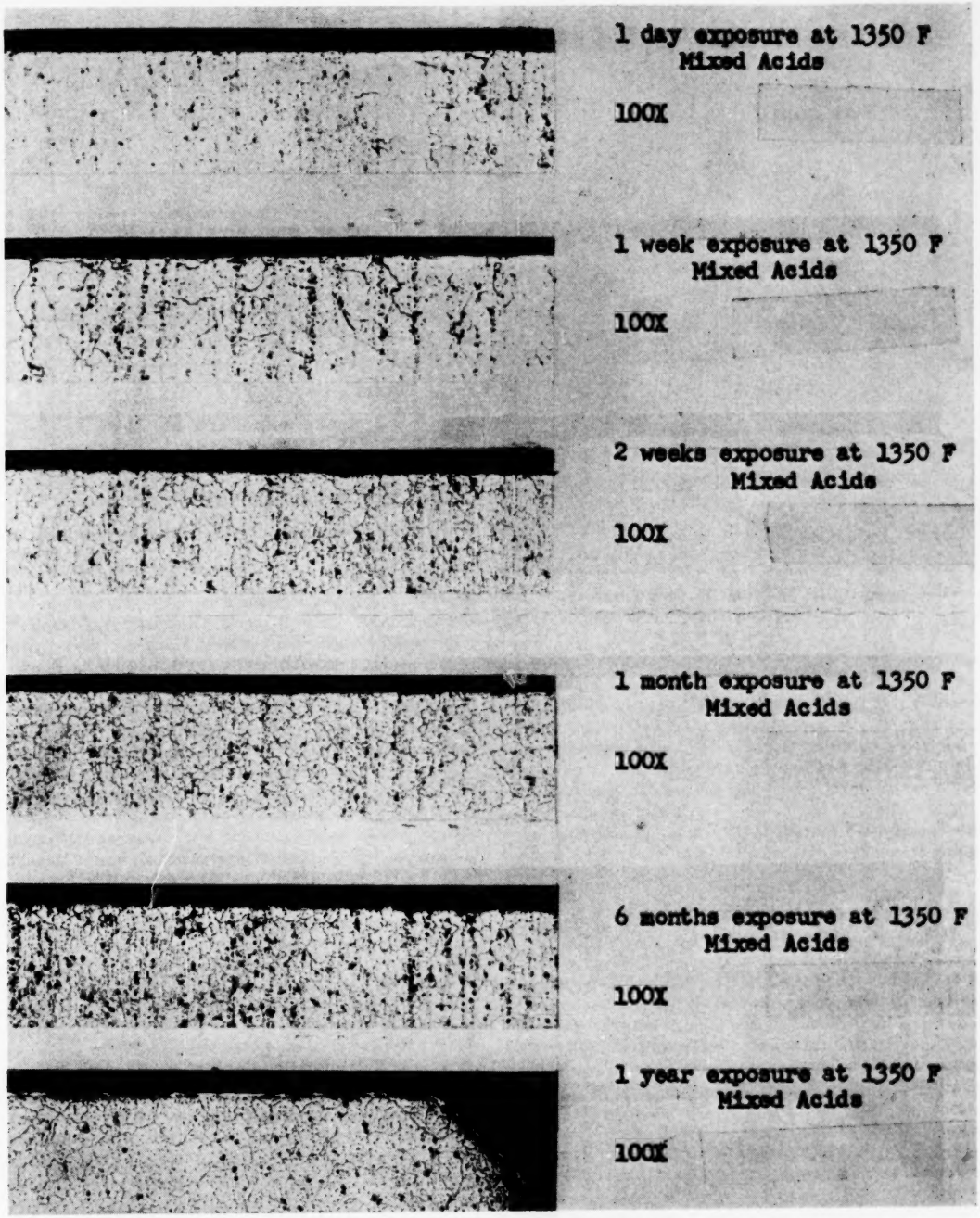

Fig. 18 Photomicrographs of M-252 specimens exposed to moving air at 1350 F for periods of time up to one year

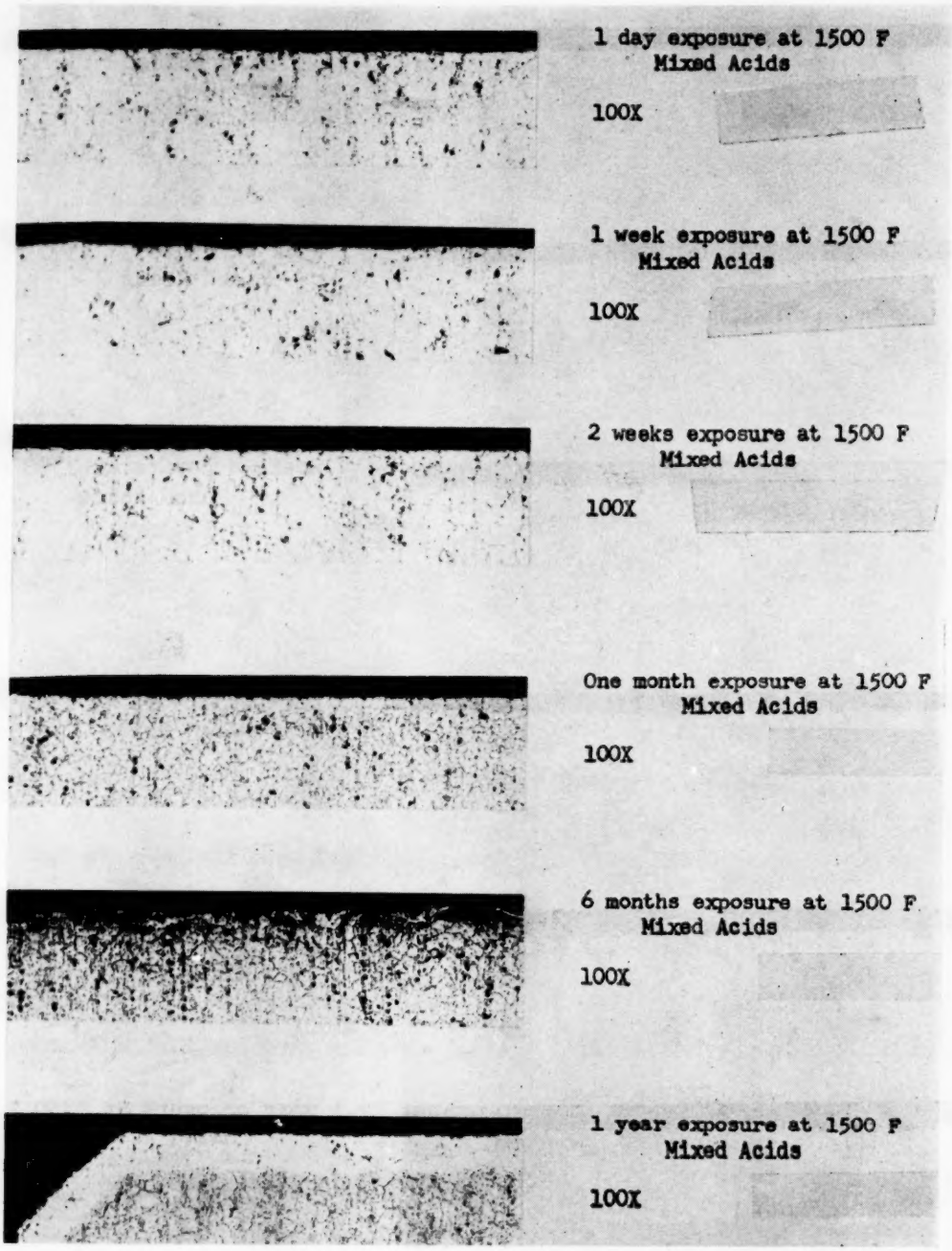

Fig. 19 Photomicrographs of M-252 specimens exposed to moving air at 1500 F for periods of time up to one year

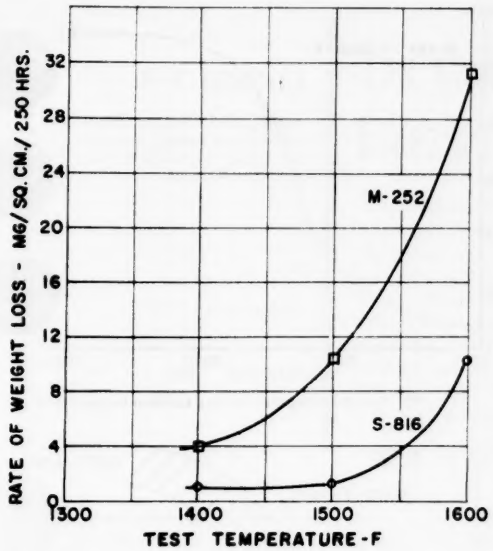

Fig. 20 Resistance of M-252 and S-816 to combustion products of Bunker C fuel

material in an atmosphere which contains large amounts of air like the products of combustion in a gas turbine. After exposures of 1 day, 1 week, 2 weeks, 1 month, 6 months, and 1 year, each specimen was weighed, its thickness was measured, and a photomicrograph was taken. These specimens were $^3/_4$ in. wide, $^1/_2$ in. high, and $^1/_4$ in. thick. The results are summarized in Fig. 15 which indicates the weight gain and Fig. 16 which indicates the thickness change. Photomicrographs of the specimens etched with mixed acids are exhibited in Figs. 17, 18, and 19.

At 1200 and 1350 F the amount of oxidation to the end of the one-year test period is insignificant. The curves for the 1350-F test suggest the formation of a protective layer after 6 months. Examination of the photomicrographs for the 1200 and 1350-F tests reveals a transformed area and some shallow pitting after 6 months of exposure.

The samples tested at 1500 F gained weight rapidly for the first month and then decreased their rate of oxidation for the remainder of the test. However, at the end of the one-year period there is no sign of a limit being reached. A structural change at the surface is indicated on the photomicrographs after exposures of one month at 1500 F. At the end of a year at this temperature there is evidence of slight intergranular attack.

The oxidation rates of approximately 0.004 in. per year at 1500 F and less than 0.001 in. per year at 1200 and 1350 F are very satisfactory for service in heavy-duty gas turbines.

A small-burner test, described in [3] was used to determine the resistance of M-252 to the products of combustion of bunker C fuel oil. Washed and treated high-vanadium residual-fuel oil was used for the test. It contained 400 ppm of vanadium, 6 ppm of sodium, and 1200 ppm of magnesium. The original specimens weighed approximately 11 gr and had a frontal area of 12.6 sq cm. Tests were conducted for 250 hr at 1400, 1500, and

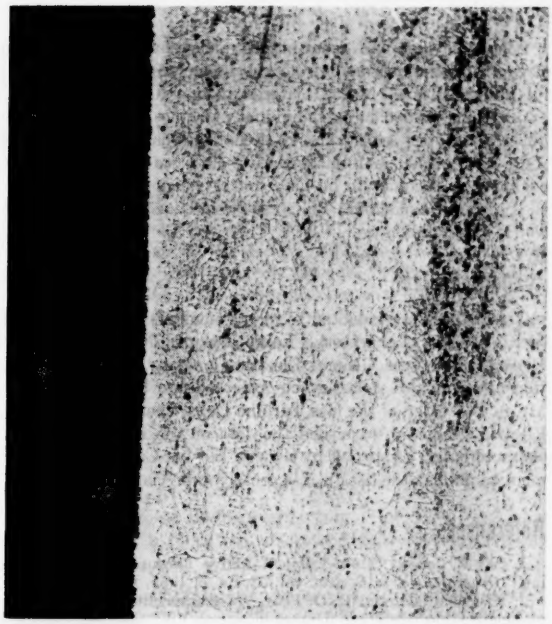

Fig. 21 Photomicrograph of surface of M-252 turbine bucket after 14,539 hr of operation—magnification 100×

1600 F. For comparison purposes, S-816 material was tested under similar conditions.

The results of the tests are plotted in Fig. 20. These data indicate that M-252 has a corrosion rate which is three to four times greater than that of S-816. However, in view of these results and the satisfactory service experience with S-816, M-252 should also give satisfactory long service if the bucket temperature is limited to 1400 F.

To date, the application of M-252 has been limited to gas turbines which burn gaseous fuels. No evidence of corrosion or oxidation has been found on these buckets.

Operating Experience

Sample buckets from two machines have been removed for examination after operation. One machine had 2046 hr of service and the other had 14,539 hr of operation on natural-gas fuel. One rupture sample was machined from each bucket. The results of the rupture tests are given in Table 10.

These results indicate that the material has not decreased in strength during service. The values of time and parameter for the 100,000-psi stress and 1200-F temperature are near the maximum values obtained during the evaluation program. Ductility of the material also remained at a high level. Metallographic examination of the buckets revealed that the structure was normal. Recrystallization, typical of buckets made from nickel-base alloys, was noted at the surfaces of the vanes. A typical area is shown in Fig. 21. No evidence of oxidation or corrosion was found.

Table 10 Rupture-test results from buckets after service

Length of service, hr	Temp, deg F	Stress, psi	Time, hr	Elongation, per cent	Reduction in area, per cent	P_{20}
14539	1200	100000	160.0	20.6	21.0	36.8
14539	1200	100000	155.8	19.4	22.0	36.8
2046	1200	100000	565.0	1.82	23.0	37.7

Conclusion

Long-time tests and operating experience have confirmed the strength predictions made from short-time tests. The successful performance of M-252 material in operating gas turbines, approaching 20,000 hr in individual machines at the time this paper was written, clearly indicates that this material will become a standard bucket material for heavy-duty gas turbines. It has enabled gas turbines to be fired hotter which greatly increases the output of a machine. This results in benefits to the user as well as the manufacturer.

Acknowledgment

The authors are indebted to many members of the Materials and Processes Laboratory, Large Steam Turbine-Generator Department of the General Electric Company. Messrs. E. F. Becht and H. M. Priestley co-ordinated the laboratory work. Mr. A. D. Foster, of the Gas Turbine Department of the General Electric Company, furnished the data on the fuel-oil corrosion characteristics. Approval by General Electric Company management to publish the data is also greatly appreciated.

References

1 W. E. Jones, "More Efficient Alloys Through Vacuum Melting," *General Electric Review*, vol. 58, no. 5, 1955, pp. 23–27.

2 C. Schabtach and R. O. Fehr, "Measurement of the Damping of Engineering Materials During Flexural Vibrations at Elevated Temperatures," *Journal of Applied Mechanics*, vol. 11, TRANS. ASME, vol. 66, 1944, pp. A-86–92.

3 B. O. Buckland, C. M. Gardiner, and D. G. Sanders, "Residual Fuel-Oil Ash Corrosion," ASME Paper 52—A-161.

4 F. R. Larson and James Miller, "A Time-Temperature Relationship for Rupture and Creep Stresses," TRANS. ASME, vol. 74, 1952, pp. 765–775.

5 H. J. Beattie, Jr., and F. L. Ver Snyder, "The Influence of Molybdenum on the Phase Relationships of a High-Temperature Alloy," *Trans. ASM*, vol. 49, 1957, pp. 883–904.

6 H. J. Beattie, Jr., and W. C. Hagel, "Observations on the Formation of Geometrically and Topologically Close Packed Phases in Commercial Superalloys," paper presented by Mr. Beattie at the Conference on Precipitation Processes in Steels, Sheffield, England, July, 1958.

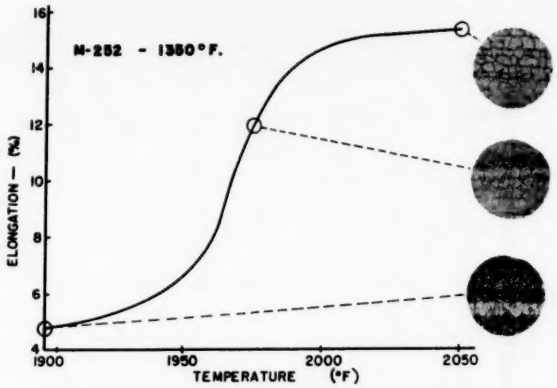

Fig. 22 Tensile elongation versus solution temperature

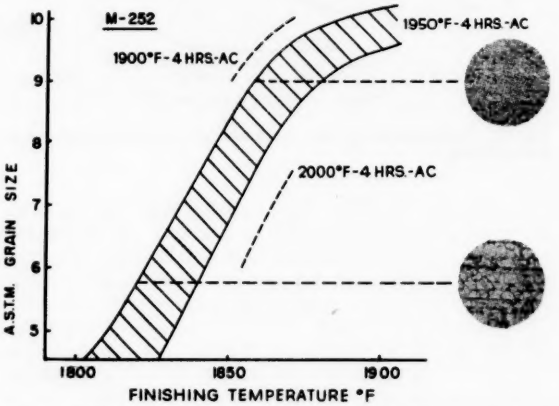

Fig. 23 Grain size (solution treated) versus finish rolling temperatures for indicated solution treatments

DISCUSSION

R. J. Stuligross[3]

In some of our work we have found that both finishing and solutioning temperatures have a significant influence on the properties of this alloy. The hot tensile ductility seems to be the property most significantly affected.

Fig. 22 shows the influence of the solution treating temperature on the tensile elongation of material tested at 1350 F. The bar stock material which was used in this investigation was finish rolled at 1890 F and aged at 1400 F for 16 hours and had a boron content of 0.0015 per cent.

The tensile elongation is influenced by grain size which in turn is influenced by the solution treating temperature. Since the fracture in the short-time tensile test at 1350 F is transgranular the larger grained material would exhibit a higher ductility.

Material finish rolled at 1825 F will produce a grain size of 5 to 6 when solution treated at 1950 F. Material finish rolled at 1900 F will produce a grain size of 9 to 10 for the same condition, Fig. 23.

Finishing temperatures higher than 1890 F will decrease the tensile elongation while finishing temperatures below 1890 F will increase the tensile elongation.

[3] Speciality Alloys Engineering, Metallurgical Products Department, General Electric Company, Detroit, Mich.

R. P. BENEDICT

Development Engineer, Steam Division, Westinghouse Electric Corporation, Lester, Pa.
Assoc. Mem. ASME

The Calibration of Thermocouples by Freezing-Point Baths and Empirical Equations

A calibration system is described which is based on the use of a few precisely determined experimental values obtained from freezing-point baths. Characteristics of the individual thermocouples at intermediate points are obtained by passing empirical equations of prescribed form through the test values. A program is reviewed, by which a high-speed digital computer accomplishes the necessary conversions, curve fittings, comparisons of individual characteristics with arbitrary reference tables, and the printing out of a table of differences. Test results for a series of iron-constantan thermocouples, over the temperature range 32–1225 F, are presented to illustrate the use of the system and the uncertainties involved. Comparisons are drawn between these results and those obtained by other methods.

In 1821 Seebeck [1][1] discovered that a closed circuit formed of two dissimilar metals generated a net EMF which induced a continuous electric current, so long as the junctions were maintained at different temperatures. Since that time, thermocouples (as these two-junction, thermally-dependent, EMF generators are called) have been recognized as providing a most useful means for sensing temperatures or, more properly, temperature differences.

However, since the EMF generated by an arbitrary combination of materials does not, of itself, define a satisfactory temperature scale, the signal of a thermocouple must be related to that of some other device which does serve to define temperature. Calibration is the term generally applied to this process of comparison. In the case of a thermocouple, calibration most often defines the process of comparing the signal from a test couple with that of a standard instrument in an attempt to establish a unique temperature-EMF relationship which is tacitly assumed to exist for each individual thermocouple and its associated system.

Of course we may proceed no further without reference to the text of the International Temperature Scale [2, 3] which, for the purposes of this paper, defines both temperature and the standard instruments used for realizing temperature. Briefly, this scale is based upon six fixed and reproducible equilibrium states to which are assigned numerical values corresponding to the respective thermodynamic Celsius temperatures, and upon four equations for relating the indications of standard interpolating instruments to temperatures between the fixed points. Limiting our interest for the remainder of the paper to the temperature range 25–1225 F, we note specifically that a standard platinum-resistance thermometer together with the Callendar equation defines temperature from the ice point (32.0 F) to the antimony point (1166.9 F), while a standard platinum/platinum-10 per cent rhodium thermocouple with an appropriate quadratic equation defines temperature from the antimony point to the gold point (1945.4 F).

Apparently, in our range of interest, we need only compare (directly or indirectly) each test couple with either a standard resistance thermometer or a standard thermocouple to obtain the desired valid T-EMF relationship. But three problems are encountered immediately which tend to thwart our calibration efforts:

1 In a practical sense, it is impossible to determine enough experimental points of comparison to define completely a unique T-EMF relationship. This means an interpolation scheme must be employed to define a continuous T-EMF characteristic.

2 The two independent measurements, upon which each calibration point is based, are not without their experimental uncertainties, a reality which makes more nebulous a unique T-EMF relationship. This means a weighting scheme must be employed to minimize effects of poor experimental points.

3 Finally, it is generally impossible to present temperatures and EMF on scales large enough to be useful, when at the same time the scales must extend over a large range of the variables. This means the test data must be compared with some judiciously chosen reference so that only differences need be shown.

In this paper, we will attempt to answer the following questions from a practical viewpoint:

1 How best to obtain a finite number of reliable calibration points?

2 How best to interpolate between these test points in such a manner as to minimize the uncertainties associated with the measurements?

3 How best to present the thermocouple characteristics, while preserving all the accuracy justified by the experiment?

Nomenclature. The following symbols are used in the paper:

E, EMF = electrical potential, volts or millivolts
I-C = iron-constantan
R = electrical resistance, ohms
t = time, min or sec
T = empirical temperature, deg F

Obtaining Reliable Calibration Points

The calibration of thermocouples has been divided conveniently into two general classes, depending upon the method of determining the temperature of the measuring junction [4].

Class I concerns comparison tests, wherein the measuring junction of the test couple and the sensing element of the standard instrument are both exposed simultaneously to an environment whose temperature is determined by the standard instrument. In this connection, we would list the circulating oil

[1] Numbers in brackets designate References at end of paper.

Contributed by the Power Test Codes Committee and presented at the Annual Meeting, New York, N. Y., November 30–December 5, 1958, of The American Society of Mechanical Engineers.

Note: Statements and opinions advanced in papers are to be understood as individual expressions of their authors and not those of the Society. Manuscript received at ASME Headquarters, August 29, 1958. Paper No. 58—A-175.

baths,[2] molten salt baths,[3] liquid metal baths,[4] as well as the various types of air furnaces,[5] as the comparators in common use.

Class II concerns fixed-point tests, wherein the measuring junction of the test couple is exposed to an environment which, under certain prescribed conditions, naturally exhibits a state of quasi-thermal equilibrium, and whose temperature is established by reference to the International Temperature Scale. Here, of course, we are speaking of the boiling, freezing, and triple-point baths of various substances.

Each of the foregoing methods of calibration is described in detail elsewhere [4, 5, 6]; but let us note that peculiarities and limitations exist for each. Specifically, the controllable-temperature environments have control and response problems which require large investments of time for each satisfactory test point. On the other hand, control and response problems are avoided in the fixed-point method which makes use of various reproducible temperature-time plateaus, each signifying the coexistence of two or more phases of a substance, and each obtained and maintained by nature. Thus the fixed-point baths appear deserving of more attention in our quest for reliable calibration points.

Of the three types of fixed-point baths, i.e., the liquid-solid, liquid-vapor, and liquid-solid-vapor baths, the triple-point type is commercially available for water only, and will be considered no further.

Boiling points are strongly pressure dependent. Such baths are elaborate in construction detail and, for inexperienced personnel, difficult to use. With this last premise anyone who has attempted the routine determination of the steam point will agree. The precise determination of the temperature of equilibrium between liquid sulfur and its vapor presents an even greater challenge [7]. Because of these difficulties, this type of bath likewise will be discussed no further. The search narrows rapidly.

Freezing points are virtually independent of barometric pressure variations [8]. Such baths are relatively simple in construction detail, Fig. 1, are commercially available,[6] and may be used by uninitiated personnel without great difficulty. The cooling curves for all materials used in freezing-point baths are characterized by a plateau (of approximately zero slope) in the temperature-time plot. To wax historical, we might quote Prof. Joseph Black [9], who in 1760 gave the first description of this phenomenon, ". . . when we freeze a liquid, a very large quantity of heat comes out of it, while it is assuming a solid form, the loss of which heat is not to be perceived by the common manner of using the thermometer . . . ." In Fig. 2 several cooling curves for tin illustrate this idea of a plateau. These curves further indicate that freezing does not occur at a fixed temperature under all conditions, and that the plateau varies in extent. Such variables as purity of material, initial temperature (above melting) from which cooling begins, first heat versus reheat, immersion of thermometer, induced versus normal cooling, and so on, all influence the observed freezing-point temperature, and the duration of the plateau [10]. In routine work, this variation in freezing-point temperature may be on the order of ±0.5 deg F.

[2] The oil should be of an electrically nonconducting variety such as Dow-Corning 550 synthetic oil, which has a flash point of about 580 F.

[3] Lavite, a heat-treating and tempering salt supplied by the Bellis Company, Bradford, Conn., is often used. It melts at 400 F.

[4] Tin, which melts at 450 F, is one example.

[5] Thermocouple checking furnaces, as manufactured by Leeds and Northrup Company, are useful up to 1800 F.

[6] Ram Industries, Inc., New York, N. Y., manufactures a selection of satisfactory freezing-point baths.

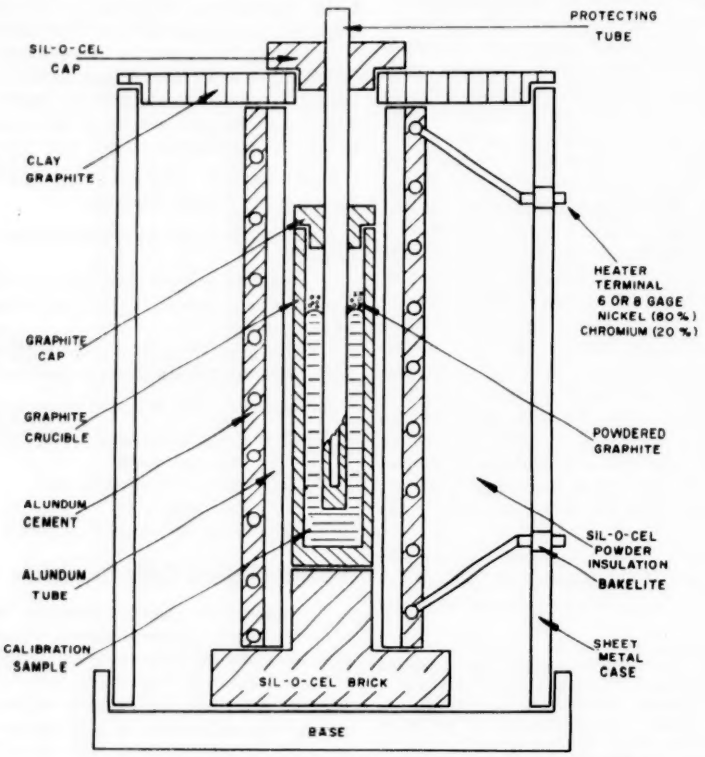

Fig. 1 Freezing-point bath according to National Bureau of Standards

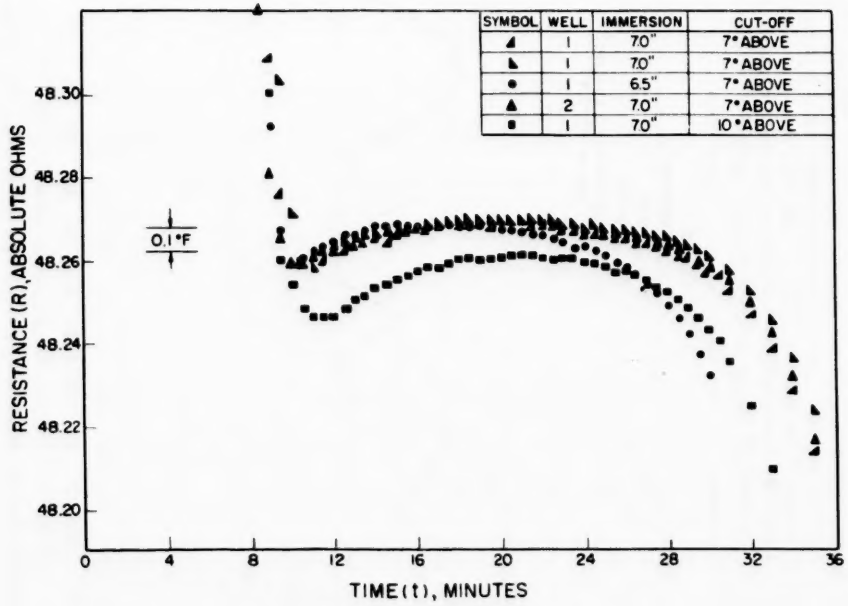

Fig. 2 Detailed cooling curves for tin

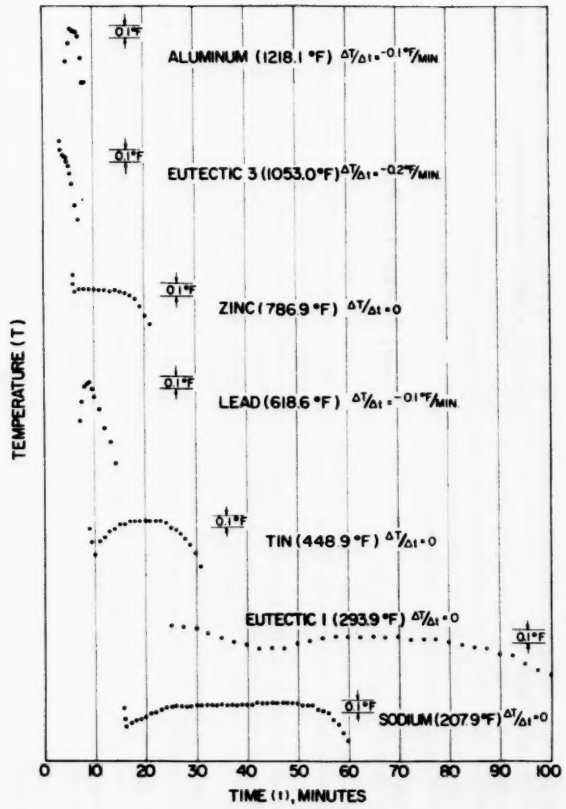

Fig. 3 Nominal cooling curves for various freezing-point baths

A comparison of the nominal cooling characteristics of seven freezing-point baths is given in Fig. 3.

With the foregoing in mind, we define a method for obtaining a finite number of reliable calibration points, which encompasses both the Class I and the Class II methods, and which involves a minimum of time, effort, and experimental uncertainty:

1 Certain freezing-point baths are used to provide calibration environments at discrete temperature levels:

(*a*) At present, nine baths are used. These are ice, sodium, eutectic 1, tin, lead, zinc, eutectic 3, aluminum, and a room-temperature oil bath.

(*b*) Rapid heating and reheating of the baths is assured because of the relatively small masses of calibration materials involved.

2 A standard temperature instrument is inserted in each bath, together with the test couples, and serves to indicate the temperature of the bath:

(*a*) Uncertainties associated with variations in the freezing-point temperature are avoided because of the simultaneous measurement of a standard temperature along with the output of a test couple.

3 Comparisons between standard and test instruments are made only when the calibration material exists in two phases:

(*a*) Response errors are avoided because measurements are taken only on the temperature-time plateau. The plateau is recognized when the indication of the standard or test instrument (whichever has the smallest time constant) changes with time by an amount less than that consistent with the accuracy required. A change of 1 deg F/4 min would insure a negligible response error in most cases.

(*b*) Immersion errors are avoided because of the uniform temperature zone (of approximately 6 in.) which exists within the two-phase calibration material. If no observable change in the EMF of a test couple occurs, when it is raised $^1/_2$ in. within the bath, a negligible immersion error is assured in most cases.

(*c*) Control problems are avoided because the plateau is maintained naturally.

The first question has been answered.

Reading Between Test Points

Granted, n reliable test points; interpolation is required to obtain a continuous T-EMF relationship. We now face the question: Which form of empirical equation will best fit the data and, more important, the thermocouple characteristic?

True, all n points may be used indiscriminately, and the Lagrange polynomial of $(n - 1)$ degree forced through the data. But, heedless of the premise that all measurements are in error, this practice weighs all measured values equally; avoids all semblance of averaging; and exaggerates the effect of a poor test point. In addition, this practice assumes (unreasonably) that the form of the fit depends upon the number of points observed.

Alternately, some selective weighting may be accomplished, and an empirical fit of undetermined form may be obtained by plotting all n points (provided a large enough graph) and then passing a smooth curve through the data. But this practice likewise detracts from the uniqueness of the thermocouple characteristic, for the result is clearly dependent upon the artistic ability of the draftsman and upon the French curves available, and no expression for the fit is forthcoming.

Surely, experimental data speak most succinctly when represented mathematically, in a manner which coldly, but consistently, considers each point; weighs its relative value according to the laws of probability; and then passes a precisely determined equation of prescribed form through the data. The well-known least-squares principle for treating data (see Appendix) fulfills the foregoing requirements most practically for industrial cali-

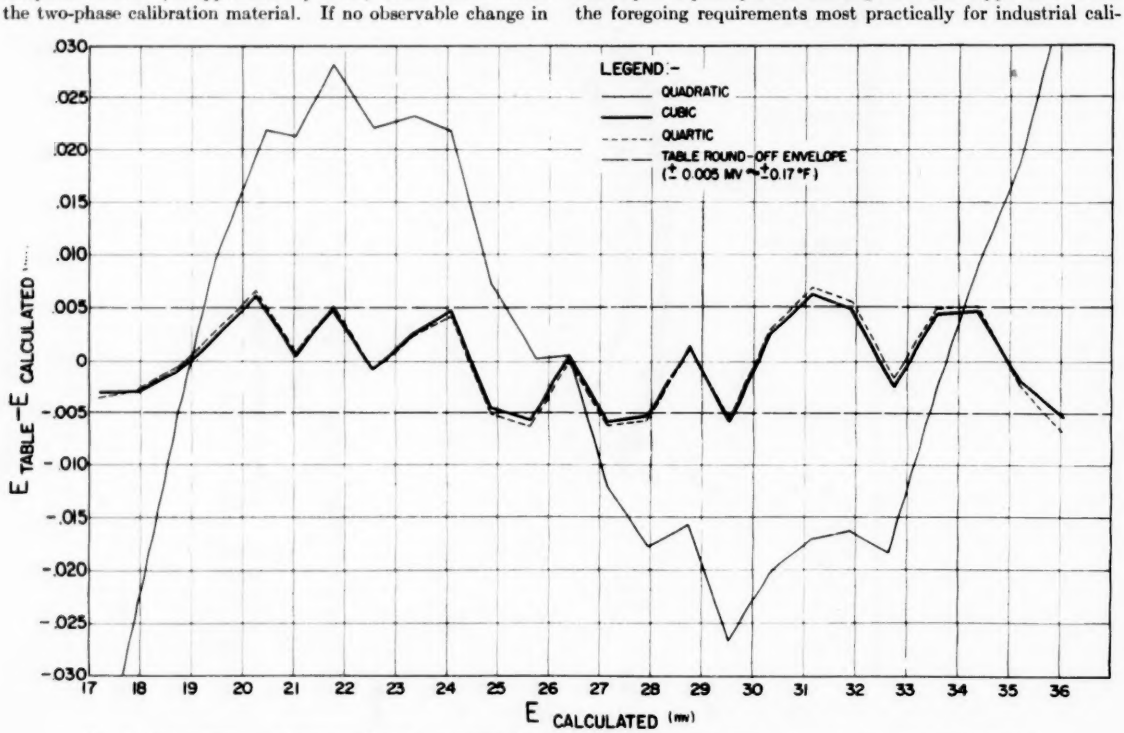

Fig. 4 Iron-constantan reference table, as represented by empirical equations of various form, in the range 600–1225 F

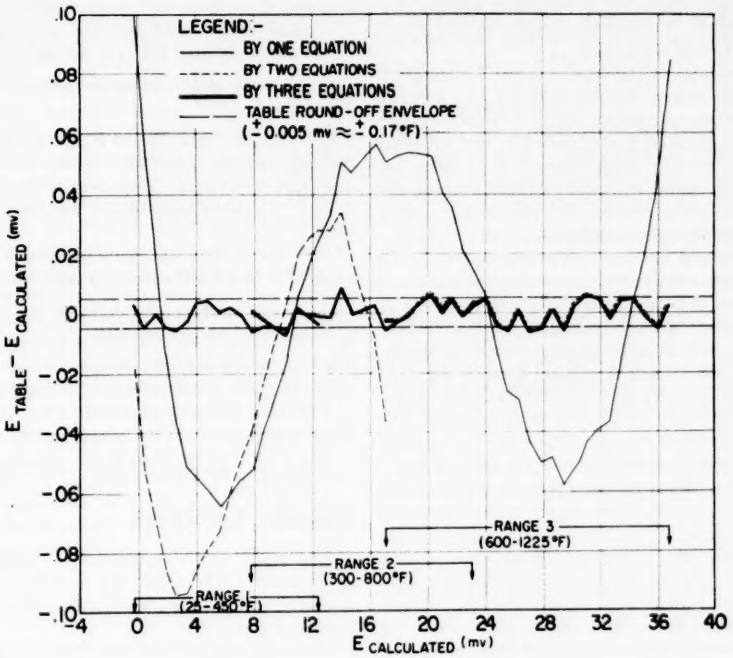

Fig. 5 Iron-constantan reference table, as represented by empirical equations of cubic form, over various ranges

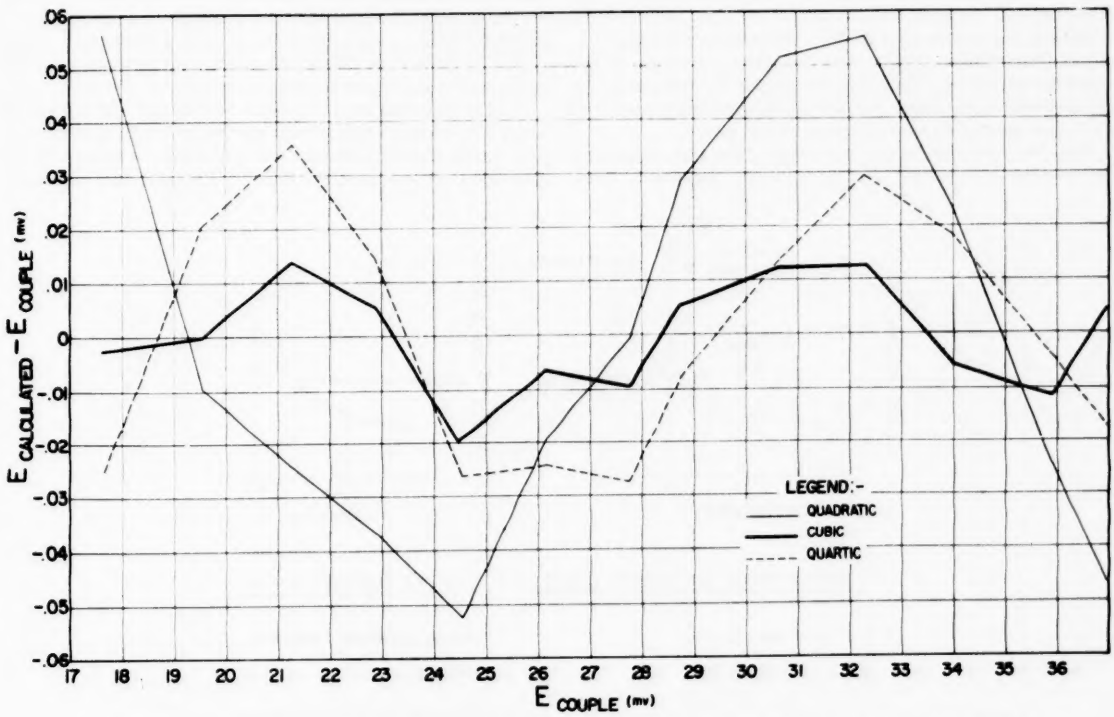

Fig. 6 Iron-constantan thermocouple, as represented by empirical equations of various form, in the range 600–1225 F

bration work. With this choice of a weighting scheme, the second question reduces to: Which form of equation shall determine the fit; i.e., linear, quadratic, cubic, . . . ?

Recall again the structure of the International Temperature Scale. It appears more than fortuitous that the two defining parabolas, each constrained to pass through but three points in the range 0–2000 F, should conform so closely [11] with all other points on the thermodynamic temperature scale. Thus we also might expect to find simple empirical relations between the voltage outputs of base-metal couples and temperatures, over limited ranges, within acceptable uncertainties.

One clue as to the form of the equation sought may be found in the appropriate thermocouple reference table, as published by the National Bureau of Standards. Such tables, of course, cannot concern particular couples; but they do list T-EMF values which represent, in form and magnitude, nominal characteristics of particular thermocouple types. Considering only iron-constantan couples in this paper, we note that the corresponding reference-table values [12] are fit equally poorly by a quadratic and a cubic in the range 25–1225 F (i.e., to ±0.060 mv). However, on dividing the over-all range in two, we find a decided advantage of the cubic over the quadratic for the upper subrange (600–1225 F), with no improvement gained by going to a fourth-order fit, Fig. 4. In the lower subrange (25–600 F), the fit remains about as poor as before. Finally, on dividing this lower subrange in two, i.e., using three overlapping subranges, namely, 25–450 F, 300–800 F, 600–1225 F, we find that the cubic fits the iron-constantan reference-table values over the entire range of interest to ±0.005 mv. The latter is nothing more than the round-off in the tabulated values. Fig. 5 summarizes these various attempts to fit the I-C reference table values by cubics.

These demonstrations certainly suggest that cubics likewise might best fit any individual iron-constantan thermocouple characteristic. Experimental tests confirm this. In all three subranges, the least-squares cubic best represents individual I-C couple characteristics within the uncertainty inherent in the experimental values. Fig. 6 illustrates this for one particular thermocouple in the range 600–1225 F by comparing quadratic, cubic, and quartic fits through experimental data.

With the foregoing in mind we define, for iron-constantan thermocouples, a method for interpolating between a finite number of reliable calibration points, which best represents individual couple characteristics, and which minimizes the uncertainties associated with the measurements:

1 Consider all the calibration points available in a given range of interest:

(*a*) In the range 25–450 F, the baths available are ice, oil, sodium, eutectic 1, and tin. In the range 300–800 F, the baths available are eutectic 1, tin, lead, and zinc. In the range 600–1225 F, the baths available are lead, zinc, eutectic 3, and aluminum.

(*b*) The calibration points considered should include several pairs of T and EMF-values for each bath in the given range.

2 Pass a least-squares cubic of the form $E = A + BT + CT^2 + DT^3$ through these data.

(*a*) If more than one range is to be considered, then more than one cubic will be used to represent the couple characteristic.

(*b*) The resulting equation gives the most probable T-EMF values throughout the range [13].

The second question has been answered.

Presenting Test Results

Granted, a precise mathematical representation of the most probable T-EMF values for a particular thermocouple; we seek the method for presenting this information in its most accessible form.

The cubic representing the thermocouple characteristic could be solved at appropriate intervals and the results tabulated or plotted. If the interval were small enough, a linear interpolation could be applied between the computed values. The method is quite sound in principle but would require excessive work both in computing and in presenting results. In addition, the results would be bulky. Eight pages are required to tabulate the results of a cubic solved every 5 deg F, over a 1200-deg-F range. A plot of these same values, on scales large enough to discern 0.2 deg F, would require a 25-ft-square map.

A more practical way to present results, and one commonly used, is to compare values from the thermocouple characteristic with values from an arbitrary reference table, retaining only the differences for examination, Fig. 7. Naturally, greater reada-

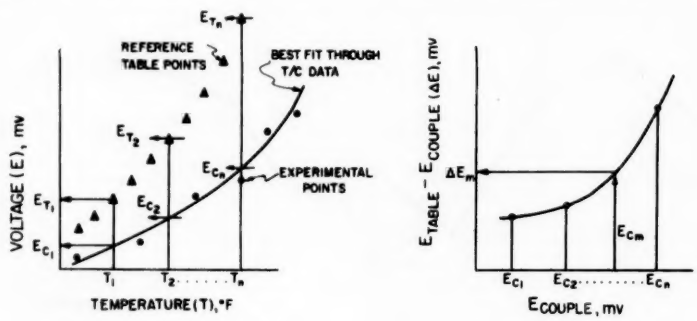

CONSTRUCTION OF DIFFERENCE CURVE

1. AT ANY T, READ E_C & E_T
2. PLOT $(E_T - E_C)$ vs E_C

USE OF DIFFERENCE CURVE

1. AT ANY E_{Cm} (MEASURED) READ ΔE_m
2. COMPUTE E_T (WHERE $E_T = \Delta E_m + E_C$)
3. ENTER REFERENCE TABLE WITH E_T AND READ T

Fig. 7 Construction and use of difference curves for representing thermocouple characteristics

bility is achieved by reducing data of large magnitudes to differences of small magnitudes (say ±4 deg F). Such differences can be presented to indicate any justifiable degree of readability (say ±0.1 deg F) and are plotted or tabulated against some quantity which indicates temperature level. This latter need not be specified in great detail (every 5 deg F is sufficient), since differences will not change rapidly with level when reference values agree closely in form and magnitude with thermocouple values (as is certainly the case with iron-constantan).

It should be noted that, to avoid confusion when comparing data from various sources, empirical equations are not used to define reference values. Instead, printed tables, the values of which are taken to be exact, serve as the reference. As a consequence, the difference curve, obtained by comparing a smooth cubic (the couple characteristic) with the table values (known to deviate from a smooth curve), must necessarily exhibit random fluctuations whenever results are presented on a scale which looks at quantities of the order of the uncertainties involved.

Choosing the difference curve as the best means for presenting thermocouple data, the third question reduces to: How often must differences be defined to preserve the accuracy justified by the experiment, while at the same time, the system is kept practical? It has been indicated before that rapid changes in slope should be absent from difference curves because the I-C reference table is of the same form as individual I-C couple characteristics. It is now maintained that the lengthy practice of plotting or tabulating differences based on solutions of the cubic at intervals of 25, 10, or even 5 deg F, is not more advantageous than using differences defined at the bath points only. Fig. 8 bears out this assertion, for here are compared the various means for representing the same I-C thermocouple data in the form of difference curves.

With the foregoing in mind, we define a method for presenting the characteristics of individual I-C thermocouples, which preserves all the accuracy justified by the experiment, and which involves a minimum of plotting time and effort:

1 Solve the least-squares cubic, representing the individual I-C couple characteristic, at temperatures corresponding to the nominal freezing points of the baths pertinent to the range of interest:

(*a*) This means there will be 4 or 5 weighted solutions per range.

2 Form the differences between these solutions and the appropriate printed values of the I-C reference table published by the NBS [12]:

(*a*) That is, $\Delta E = E_{\text{table}} - E_{\text{couple}}$, where E_{table} is the printed value and E_{couple} is the calculated value at the given temperature.

3 Plot or tabulate these differences (ΔE) versus level (E_{couple}), using linear interpolation between these weighted differences to obtain differences at points intermediate to the bath points.

The third question has been answered.

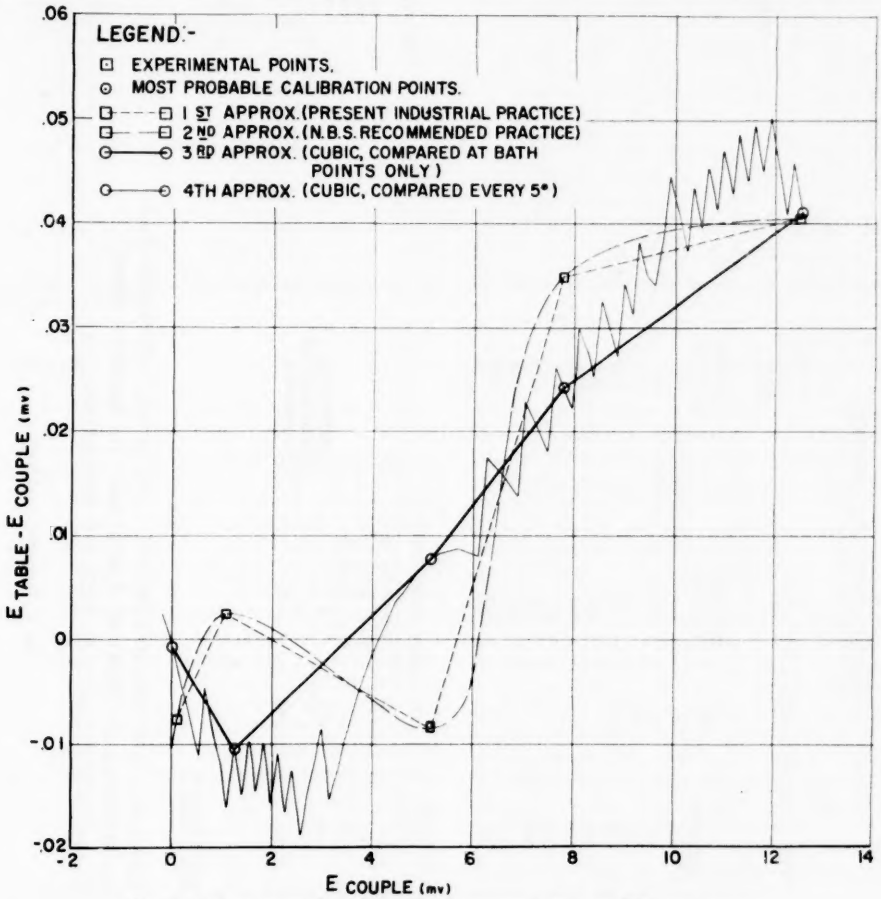

Fig. 8 Various means for representing thermocouple data on difference curves

THERMOCOUPLE CALIBRATION

TITLE THERMOCOUPLE 5-RUN 1

CHARGE _____
SENT BY _____
DATE _____

STORAGE LOCATION	E_S	STORAGE LOCATION	R_S	STORAGE LOCATION	E_m
001	0	011	57.3954	021	17.950
002	0	012	65.4400	022	22.860
003	4.6765	013	0	023	30.000
004	5.5788	014	0	024	35.180
005		015		025	
006		016		026	
007		017		027	
008		018		028	
009		019		029	
010		020		030	

STORAGE LOCATION	ADDITIONAL INFORMATION		
041		25 - 450 °F	
042		300 - 800 °F	
043	✓	600 - 1225 °F	
044	1.493	β	RESISTANCE THERMOMETER CONSTANTS
045	25.517	R_0	
046	10.0196	$R_{100} - R_0$	

NOTATION:-

E_S = VOLTAGE GENERATED BY STANDARD $P_t/P_t - 10\% R_h$ THERMOCOUPLE (mv)
R_S = RESISTANCE OF STANDARD P_t RESISTANCE THERMOMETER (OHMS)
E_m = VOLTAGE GENERATED BY TEST I-C THERMOCOUPLE (mv)

Fig. 9 Computer input form

THERMOCOUPLE 5-RUN 1

(STANDARD COUPLE VOLTAGE) mv	(STANDARD THERMOMETER RESISTANCE) ABS OHMS	(STANDARD TEMPERATURE) °F
0	57.3954	625.000
0	65.4400	784.993
4.6765	0	1015.014
5.5788	0	1174.985

COEFFICIENTS OF CURVE

A	-2.9682180×10^{0}
B	3.7870962×10^{-2}
C	$-9.8168080 \times 10^{-6}$
D	4.4403705×10^{-9}

CHECK OF FIT

(STANDARD TEMPERATURE) °F	(TEST COUPLE VOLTAGE) mv	(CALCULATED VOLTAGE) mv	(RESIDUALS) mv
625.000	17.950	17.950532	-5.320×10^{-4}
784.993	22.860	22.858883	1.117×10^{-3}
1015.014	30.000	30.000918	-9.180×10^{-4}
1174.985	35.180	35.179665	3.350×10^{-4}

TABLE OF DIFFERENCES

(ACTUAL TEMPERATURE) °F	(TABLE VOLTAGE) mv	(CALCULATED VOLTAGE) mv	(DIFFERENCE) mv
618.0	17.74	17.734818	0.0052
787.0	22.92	22.920432	-0.0004
1053.0	31.21	31.209409	0.0006
1218.0	36.62	36.618592	0.0014

Fig. 10 Computer print-out form

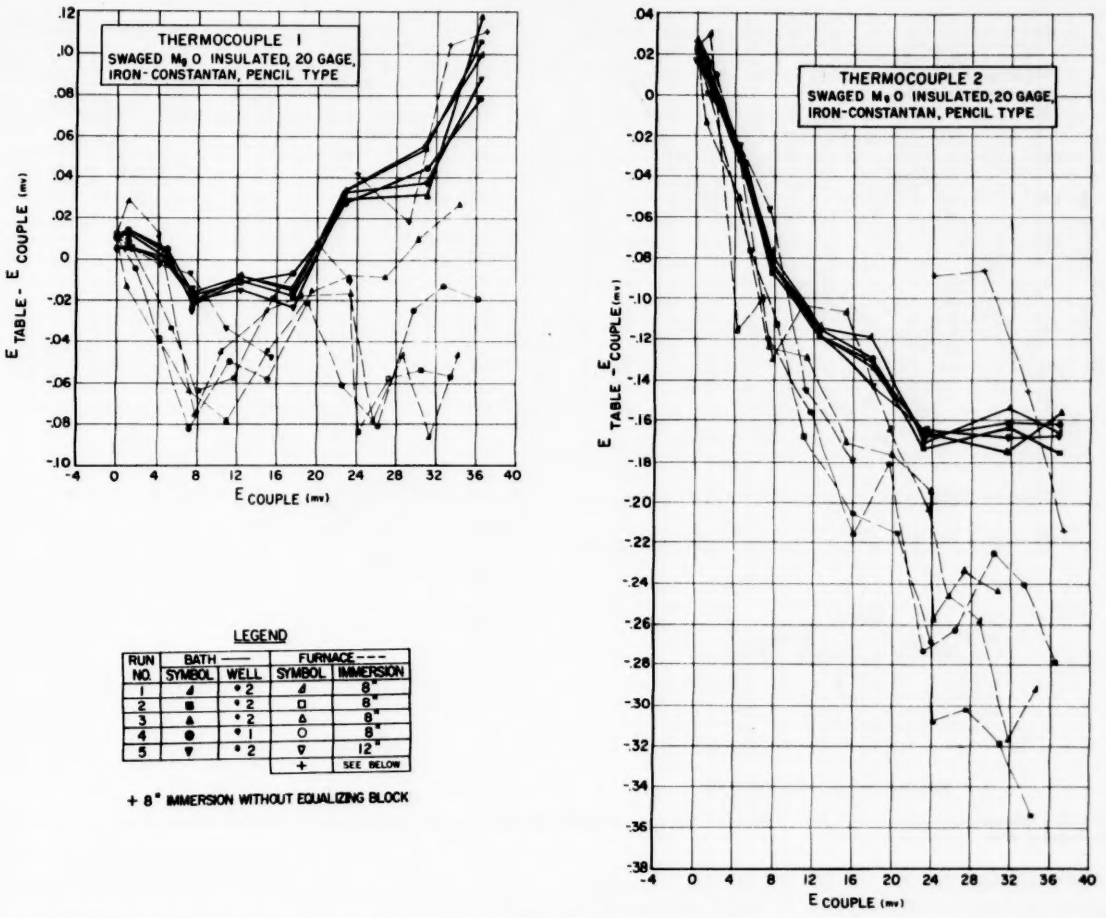
THERMOCOUPLE 1
SWAGED MgO INSULATED, 20 GAGE, IRON-CONSTANTAN, PENCIL TYPE
E TABLE - E COUPLE (mv)
E COUPLE (mv)
THERMOCOUPLE 2
SWAGED MgO INSULATED, 20 GAGE, IRON-CONSTANTAN, PENCIL TYPE
E TABLE - E COUPLE (mv)
E COUPLE (mv)
LEGEND
RUN NO. | BATH SYMBOL | BATH WELL | FURNACE SYMBOL | FURNACE IMMERSION
1 | | 2 | | 8"
2 | | 2 | | 8"
3 | | 2 | | 8"
4 | | 1 | | 8"
5 | | 2 | | 12"
+ | SEE BELOW
+ 8" IMMERSION WITHOUT EQUALIZING BLOCK

Fig. 11 Thermocouple calibration curves, indicating variation between results based on freezing-point-bath data (computer-processed) and on air-furnace data (hand-calculated)

A Computer Program

Our questions have been answered, but the system has not yet been presented in its most practical form. A great amount of routine calculation work is involved in the routine calibration of thermocouples by the proposed methods; a situation for which the application of a high-speed digital computer is well suited.

By means of a program, the computing machine is taught to do all of the computations. An input sheet is completed by the experimenter during the test, Fig. 9. This calls for readings from the standard instruments (E_s or R_s), readings from the test couple (E_m), and for certain other information used in the program. The computer, operating on these data, prints out a sheet, Fig. 10, which includes the conversion of standard instrument readings (E_s and R_s) to temperature (T_s) via the proper interpolating equations, the coefficients of the least-squares cubic through the experimental data, a check of the fit, the solutions of the cubic at the nominal bath points, and a comparison of these solutions with corresponding NBS reference-table values to obtain the differences.

Test Results

Six iron-constantan thermocouples of various pedigrees were chosen at random to test the proposed methods. Thermocoupel variables include wire gage, insulation, and type of measuring junction. In addition, the couples have various case histories; some are new, while others have been in use for years.

The tests consist of obtaining calibration points alternately by the freezing-point baths (the proposed method), and by a conventional air furnace used with a proportional controller (the present method). A zone-box circuit [14] was used with an ice-bath reference junction. The selector switch box served as the uniform temperature zone. A K-2 type precision potentiometer was used to indicate the voltage output of the standard thermocouple. A G-2 type precision Mueller bridge was used to indicate the resistance of the standard resistance thermometer. A Speedomax semi-precision potentiometer was used to indicate the voltage output of the test couples. Two independent runs were taken in each freezing-point bath for each of the five calibrations. These readings were processed by the digital computer. Three readings were taken at each temperature level of the furnace for each of these five calibrations. These latter readings were averaged arithmetically by hand calculations in conformance with present industrial practice.

The results from all of these tests are plotted in Figs. 11, 12, and 13, in the form of difference curves. Two outstanding features will be noted:

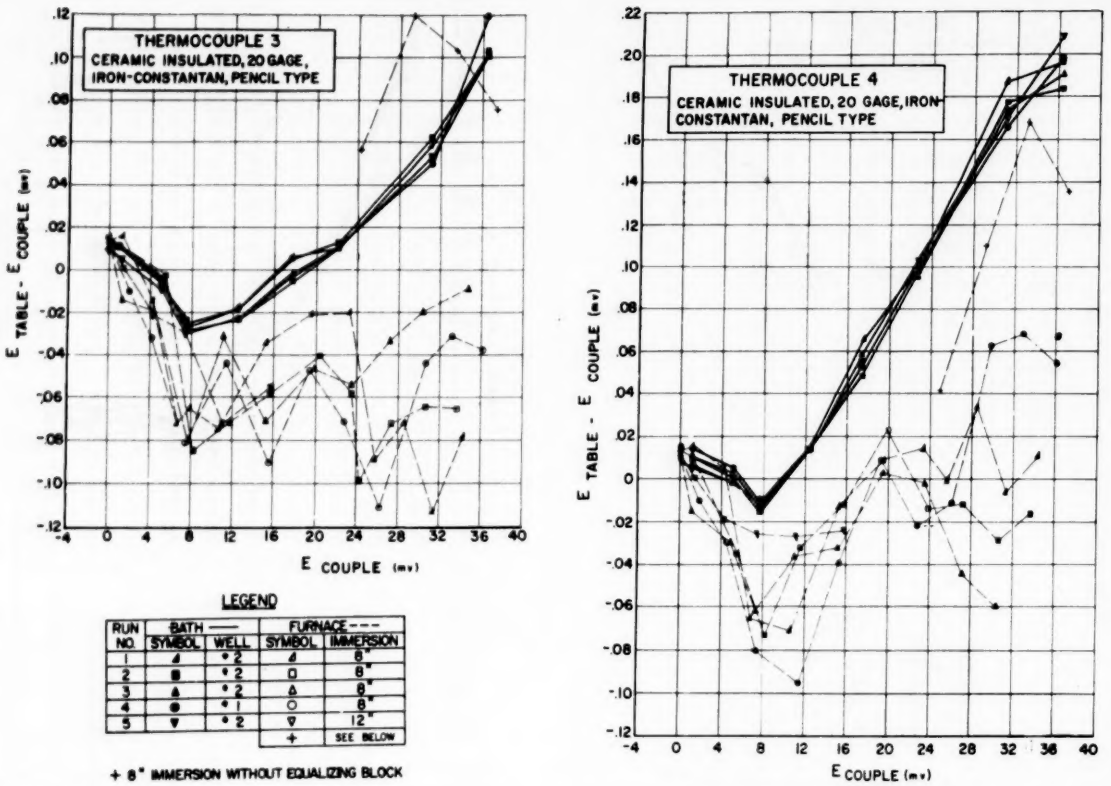

Fig. 12 Thermocouple calibration curves, indicating variation between results based on freezing-point-bath data (computer-processed) and on air-furnace data (hand-calculated)

1 The uncertainties involved in the freezing-point calibrations are on the order of ±0.4 deg F at all levels, while the uncertainties in the usual furnace calibrations are on the order of ±1.0 deg F.

2 The corrections by the freezing-point bath method are consistently more positive than those of the furnace method.

The latter may be explained by the minimum response, immersion, and positioning errors associated with the freezing-point baths, as compared with known deviations from these sources in the furnace points. To check this explanation, one set of points was obtained in the furnace at the high range without the use of the equalizing block which is conventionally used. The thought was to eliminate radial temperature gradients encountered in the block. In Figs. 11, 12, and 13 it may be seen that for this case the difference curves are in much better agreement. One cannot fail to note the great uncertainty which must be associated with calibrations obtained by usual methods.

Conclusions

The following have been shown to result in calibration curves which exhibit uncertainties of ±0.4 deg F from 25 to 1225 F for iron-constantan thermocouples:

1 Using certain freezing-point baths to provide calibration environments at discrete temperature levels

2 Using standard temperature instruments inserted in each bath with the test couples to indicate bath temperature

3 Comparing standard and test instruments only when calibration material exists in two phases

4 Considering at least two pairs of T-EMF values for each bath

5 Passing a least squares cubic through this data

6 Solving this cubic at temperatures corresponding to the nominal freezing points of the baths involved

7 Forming differences between these solutions and appropriate printed values of the NBS I-C reference table

8 Plotting these differences versus level, using linear interpolation between these points.

In addition, substantial savings in time and effort are realized by the use of this proposed system of calibration.

Acknowledgments

The author acknowledges the valuable assistance of Mr. L. M. Lazar who formulated the program for the IBM-650 digital computer, of Mrs. J. C. Spengler who helped with most of the calibration tests, and who constructed all of the figures used in this paper, and of Mr. A. C. DeSerio who helped evaluate the freezing-point baths.

APPENDIX

Principle of the least-squares fit, as applied to a third-order equation of the form, $E = A + BT + CT^2 + DT^3$:

1 For an exact fit:

$$E - A - BT - CT^2 - DT^3 = 0$$

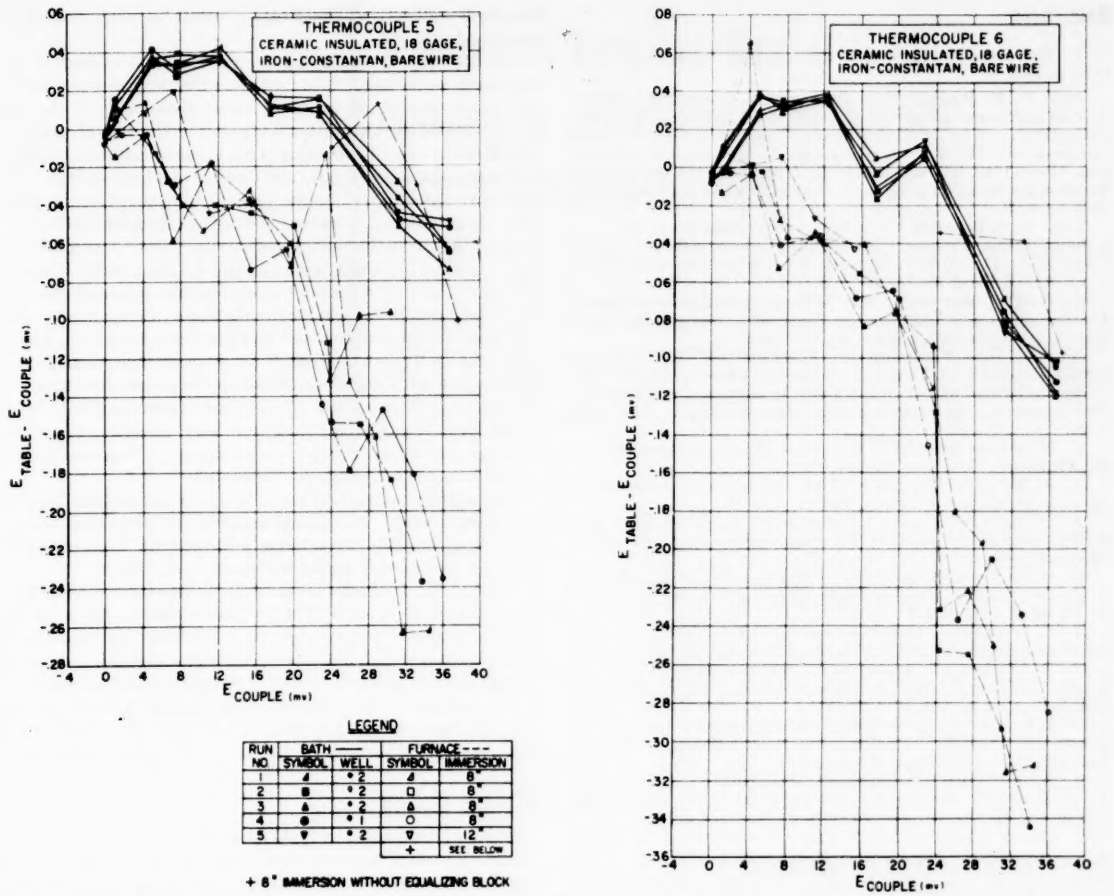

Fig. 13 Thermocouple calibration curves, indicating variation between results based on freezing-point-bath data (computer-processed) and on air-furnace data (hand-calculated)

2 For a misfit:

$$E - A - BT - CT^2 - DT^3 = r, \text{ a residual}$$

3 From the Gaussian law of error, the probability of obtaining the given values is a maximum when the sum R of the squares of the residuals r^2 is a minimum:

$$R = \Sigma(r^2) = f(A, B, C, D)$$

$$= \sum_{i=1}^{N} (E - A - BT - CT^2 - DT^3)^2 = \text{minimum}$$

4 The necessary conditions for a minimum R are:

$$\frac{\partial R}{\partial A} = 2\Sigma(E - A - BT - CT^2 - DT^3)(-1) = 0$$

or

$$\Sigma E = AN + B\Sigma T + C\Sigma T^2 + D\Sigma T^3 \qquad (1)$$

where N = number of points considered

$$\frac{\partial R}{\partial B} = 2\Sigma(E - A - BT - CT^2 - DT^3)(-T) = 0$$

or

$$\Sigma ET = A\Sigma T + B\Sigma T^2 + C\Sigma T^3 + D\Sigma T^4 \qquad (2)$$

$$\frac{\partial R}{\partial C} = 2\Sigma(E - A - BT - CT^2 - DT^3)(-T^2) = 0$$

or

$$\Sigma ET^2 = A\Sigma T^2 + B\Sigma T^3 + C\Sigma T^4 + D\Sigma T^5 \qquad (3)$$

$$\frac{\partial R}{\partial D} = 2\Sigma(E - A - BT - CT^2 - DT^3)(-T^3) = 0$$

or

$$\Sigma ET^3 = A\Sigma T^3 + B\Sigma T^4 + C\Sigma T^5 + D\Sigma T^6 \qquad (4)$$

5 Simultaneous solution of equations (1), (2), (3), (4) yields the desired coefficients A, B, C, D.

References

1 T. J. Seebeck, "Fundamental Principles," Pogg. Ann., vol. 6, 1826, p. 133.

2(*a*) G. K. Burgess, "The International Temperature Scale," *Journal of Research*, National Bureau of Standards, July-December 1928, RP 22, p. 635; (*b*) H. F. Stimson, "The International Temperature Scale of 1948," *Journal of Research*, National Bureau of Standards, March 1949, RP 1926, p. 209; (*c*) J. A. Hall, "The International Temperature Scale," *Temperature*, Reinhold Publishing Corporation, New York, N. Y., vol. 2, 1955, p. 116.

3(*a*) R. P. Benedict, "The Temperature Standard at the Westinghouse Steam Division," Westinghouse Steam Division Report 1318, 1957, p. 17; (*b*) R. P. Benedict, "Review of Practical Thermometry," ASME Paper 57—A-203, p. 8.

4 W. F. Roeser and S. T. Lonberger, "Methods of Testing Thermocouples and Thermocouple Materials," National Bureau of Standards Circular 590, February 6, 1958, p. 3.

5 P. H. Dike, "Thermoelectric Thermometry," Technical Publication EN-33A (1a), Leeds and Northrup Company, 1955, p. 59.

6 R. P. Benedict, "Temperature Measurement by Means of Thermocouples," Westinghouse Steam Division Report 1298, 1956, p. 20.

7 H. B. Lancaster and A. W. Brunot, "Thermocouples," *General Electric Review*, November, 1942, p. 649.

8 A. W. Grosvenor, editor, "Basic Metallurgy," American Society for Metals, vol. 1, 1954, p. 260.

9 D. Roller, "The Early Development of the Concepts of Temperature and Heat," Harvard University Press, Cambridge, Mass., 1950, p. 32.

10 H. Preston-Thomas, "The Zinc Point as a Thermometric Fixed Point," *Temperature*, Reinhold Publishing Corporation, New York, N. Y., vol. 2, 1955, p. 171.

11 J. A. Beattie, "Gas Thermometry," *Temperature*, Reinhold Publishing Corporation, New York, N. Y., vol. 2, 1955, p. 91.

12 H. Shenker, J. I. Lawritzen, R. J. Corruccini, and S. T. Lonberger, "Reference Table for Thermocouples," National Bureau of Standards, Circular 561, 1955, p. 75.

13 I. S. and E. S. Sokolnikoff, "Higher Mathematics for Engineers and Physicists," McGraw-Hill Book Company, Inc., New York, N. Y., second edition, 1941, p. 536.

14 W. F. Roeser, "Thermoelectric Thermometry," *Temperature*, Reinhold Publishing Corporation, New York, N. Y., vol. 1, 1941, p. 202.

DISCUSSION

Lowell A. Holcomb[7]

The author has made a very distinct contribution to the art of reliable temperature measurement by means of thermocouples.

The discusser's company has the requirement of calibrating all thermocouples used in the engineering laboratories and in the production test equipment every 90 days. This involves time-consuming disassembly of elaborate test stands and calibration of the thermocouple in a standards measurement laboratory, or else movement of the test stand where possible to the standards measurement laboratory where the thermocouple is partially removed from the test stand and calibrated relatively in place by comparison against the appropriate laboratory temperature standards and accessories. The temperature standards in use are the platinum resistance thermometer and precision ASTM liquid-in-glass thermometers. We intend to increase our temperature range above 1000 F by the use of platinum/platinum-10 per cent rhodium thermocouples which will become National Bureau of Standards certified at the freezing points of zinc, antimony, silver, and gold.

The best way of simplifying our thermocouple calibration requirement would be to "field" calibrate the thermocouples in the test stand without movement or major disassembly of the test stand. Based on the author's experience the use of portable commercially available freezing point baths to calibrate installed thermocouples appears to be very feasible and time saving. The thermocouple would, of course, have to be removed from the test stand plumbing and immersed in the freezing point bath a sufficient distance during actual calibration. Prior test stand design consideration could make this partial disassembly a simple matter. The test stand thermocouple indicator and recorder would be compared or adjusted to the finite freezing points using the same electrical system and lead junctions and switches as in actual use in the environment of actual use. The freezing point variation of ± 0.5 deg F mentioned in the paper plus the use of the complete thermocouple temperature system as it is installed in the test stand should result in very reliable calibrations. Damage and wear caused by repeated major disassembly and assembly would be practically eliminated.

This calibration method might be just what the missile flight test people need. This should make it relatively easy to calibrate thermocouple telemetering systems with their respective block house recorders during the missile count-down.

The one drawback appears to be the limited temperature range. High temperatures up to 1218.1 F (aluminum freezing point) are well covered, but temperature below 207.9 F (sodium freezing point) were not shown in the paper. The discusser's company needs thermocouple calibrations at temperatures below 207.9 F as well as above. Is the freezing point concept possible at temperatures below the sodium freezing point and above the ambient temperature? The author's comments would be appreciated.

[7] Test Engineer, Engineering Department, Convair/Pomona, Convair Division of General Dynamics Corporation, Pomona, Calif. Assoc. Mem. ASME.

Author's Closure

The author wishes to thank Mr. Holcomb for his generous remarks concerning the paper and to second his suggestion as to the use of the freezing-point bath—empirical equation method of thermocouple calibration in various field test applications.

On the question of the limited number of baths available in the lower temperature range (i.e., from the sodium point to ambient) two statements can be made:

1 We have demonstrated in the paper that the least-squares cubic based on 4 or 5 bath points well describes individual thermocouple characteristics in a particular range of interest. In the range under consideration (i.e., 25–450 deg F) the ice, oil, sodium, eutectic 1, and tin baths have been found sufficient to provide a continuous calibration curve. The uncertainty of such a curve is of the same order as the uncertainty in the freezing-point temperatures of the individual baths, when such baths are used without standard temperature-sensing instruments (as would be the case in field calibrations).

2 If, for reasons other than the requirement of a continuous calibration curve, additional freezing-point baths are desired, these can be procured. One example is the Glauber salt bath (nominally, the transition temperature of this sodium sulfate decahydrate is 90.28 F) which has a temperature-time plateau of over an hour in extent.

Theoretical Stresses Near a Circular Opening in a Flat Plate, Reinforced With a Cylindrical Outlet

EVERETT O. WATERS

Professor of Mechanical Engineering, Yale University, New Haven, Conn. Mem. ASME

Formulas are derived for stresses in the neighborhood of a circular hole in a flat plate, when the opening is reinforced with a cylindrical outlet such as a pipe or nozzle. The plate is loaded in tension, either uniformly in all directions, or with transverse and longitudinal tensions in the ratio of 2:1 as is the case in cylindrical pressure vessels. Consideration is given to the possibility of "balanced reinforcement" by adding material on both sides of the plate. Tables and graphs are included for the use of designers who wish to find the stress-concentration factors for different combinations of plate thickness, outlet-wall thickness, and outlet diameter.

A STUDY of the stress patterns around openings in pressure vessels, to which branches are attached, involves basically the problem of two intersecting cylindrical shells, or an intersecting cylinder and sphere, depending upon the location of the attachment in the side wall or the head of the vessel. As a logical first approximation from the theoretical angle, it is proposed to investigate the distribution of stress at the junction of a cylindrical shell (the branch connection) with a flat plate (the shell or header) when the plate is subjected to tension. This is the limiting case of the problem, when the diameter of the main shell, or the radius of the head, increases indefinitely in comparison with the diameter of the branch. It has the disadvantage of eliminating from consideration all lateral loads on the plate, whether from internal pressure, nozzle and side-branch connections, or other causes. Nevertheless, it provides a great simplification of the analysis, and the results should prove useful in establishing limiting values of stress-concentration factors for various practical constructions involving the welded connection of branches to headers, tanks, containers for chemical processes, and other pressure vessels. Moreover, it does permit the inclusion of pressure effects on the wall of the branch.

Studies of this type have been carried out by many investigators in the past, and references to the literature will be found in most if not all pressure-vessel bibliographies [1].[1] However, practically all of the analyses are based on a plane-stress approach, which ignores the loss in value of reinforcing material as it is located further from the middle plane of the pierced plate, or the bending moment introduced by reinforcement placed entirely on one side of the plate. In some instances, investigators have succumbed to the vision of 100 per cent, or "neutral" reinforcement; meaning reinforcement that maintains the pierced plate in the same state of stress and strain that it would have if no opening existed. Consider for example a circular hole, at the center of a large plate that is subjected to uniform all-around tension. This may be given neutral reinforcement theoretically—on a plane-stress basis—by a ring welded to the edge of the hole. However, if Young's modulus for this ring is no greater than that of the plate, then its cross section must have an area equal to half that of the material removed in forming the hole. Obviously, such an area cannot be

Contributed by the Power Division and presented at the Annual Meeting, New York, N. Y., November 30–December 5, 1958, of THE AMERICAN SOCIETY OF MECHANICAL ENGINEERS.

NOTE: Statements and opinions advanced in papers are to be understood as individual expressions of their authors and not those of the Society. Manuscript received at ASME Headquarters, September 4, 1958. Paper No. 58—A-171.

[1] Numbers in brackets designate References at end of paper.

Nomenclature

D = flexural rigidity, $Et^3/12(1 - \nu^2)$
d_c = mean diameter of cylinder
E = modulus of elasticity
K = stress-intensification factor (max normal stress criterion)
L = length of cylinder
M_r = radial bending moment in plate, per unit circumferential distance
$M_{r\theta}$ = twisting moment on unit element of plate
M_x = axial bending moment on right circular section of cylinder, per unit circumferential distance on middle surface
$M_{x\theta}$ = twisting moment on unit element of cylinder
$M_{\theta p}$ = circumferential bending moment in plate, per unit radial distance
$M_{\theta c}$ = circumferential bending moment in cylinder, per unit axial distance
N_c = axial membrane tensile force in cylinder, per unit circumferential distance on middle surface
p = internal pressure
Q_r = shear force on circular section of plate, in x-direction, per unit circumferential distance
Q_x = radial shear force on right circular section of cylinder, per unit circumferential distance on middle surface
$Q_{x\theta}$ = tangential shear force on right circular section of cylinder, per unit circumferential distance on middle surface
Q_{Mc} = "effective" radial shear force on a right circular section of cylinder, per unit circumferential distance on middle surface
R_c = radius to middle surface of cylinder
R_p = radius of hole in plate
R_{avg} = average of R_c and R_p
r = arbitrary radius
S = tensile stress in plate, at infinity
T_r = tangential shear force theoretically applied to surface of hole in plate, per unit circumferential distance

(Continued on next page)

concentrated at the edge of the hole, and only that element of the ring that lies at this edge can have full reinforcing value. It is safe to say that, in this case, neutral reinforcement can only be attained by tapering the plate in thickness, radiuswise as one moves outward from the edge of the hole; and the taper must be so gradual that the postulates of plane-stress distribution are not violated seriously.

Statement of the Problem

The problem of the flat plate of large extent, having a central circular hole, and supporting an arbitrary system of loads, is certainly well known. The same is true of the cylindrical shell. The present problem is simply one of adjusting the forces and displacements at the junction surfaces of these two elements so as to secure their mutual equality. The various constants that are determined by this requirement may then be used to solve for the stresses and displacements at any point in the combined structure.

In detail, the quantities that must be equated are:

1 Tangential shear force around circumference of hole in plate = tangential component of shear force on end of cylinder.

2 Radial force on plate, at edge of hole = radial component of shear force on end of cylinder.

3 Transverse shear force on plate, at edge of hole = axial force on end of cylinder.

4 Radial bending moment in plate, at edge of hole = longitudinal bending moment at end of cylinder.

5–7 Radial, tangential, and lateral displacements of plate at edge of the hole, and on side of the plate that is joined to cylinder = corresponding displacements of end of cylinder.

8 Angle of dish at edge of hole in plate = angle of flare in cylinder, at its junction end.

The forces listed in the foregoing are the forces per unit of circumference of the hole, or of the middle surface of the cylinder, suitable correction being made for the difference between the lengths of the two circumferences. We have classified the eight conditions that must be satisfied as of "zero order," meaning that they are unvarying around the circumference of the hole and cylinder, or of "second order," meaning that they are symmetrical about an axis in the plane of the plate, drawn through the center of the hole, and therefore proportional to cos 2θ (see Fig. 2). The zero-order conditions apply when the plate is under uniform tension in all directions in its plane; conditions 1, 3, 6, and 7 then disappear. If the plate is under uniform tension in one direction only, both the zero and second-order conditions are applicable. As long as the plate is pulled uniformly in one direction only, or in two perpendicular directions, no higher orders enter the problem.

The following assumptions, commonly found in studies of this nature, have been made:

All deformations are purely elastic; stresses and strains at all points are within the proportional limit.

The wall-to-mean-diameter ratio of the cylinder is small enough so that, when squared or raised to higher powers in the theoretical development, it may be neglected.

The effect of forces acting in the plane of the plate—tension, compression, or shear—on bending of the plate, is small enough to be neglected.

The simplified thin-shell or thin-plate theory is used, according to which the middle surface is the neutral surface, membrane stresses are uniformly distributed across the wall thickness, bending stresses are proportional to their distance from the middle surface, and normal stresses in a direction perpendicular to the middle surface are neglected.

Since linearity of stresses and displacements is assumed, we may employ superposition to obtain the stresses and displacements caused by a 1:1/2 biaxial loading of the plate, corresponding to the typical loading of the side wall of a cylindrical pressure vessel. Likewise, a 1:1 biaxial loading, corresponding to the condition at the crown of a pressure-vessel head, may be obtained by superposition, although it is of course much simpler to use the zero-order conditions alone. With 1:1 biaxial loading, the superposed second-order relationships nullify each other.

Definitions of Symbols. Most of the symbols and notations are illustrated in Figs. 1 and 2 and are listed in the nomenclature. Subscripts p and c refer to plate and cylinder, respectively. Likewise, subscripts 0 and 2 refer to zero-order and second-order quantities. Subscript e denotes a traction or displacement at the edge of the hole in the plate, or on the faying surfaces of plate and cylinder. Note that the positive direction of radial displacements in the plate w_p is outward, but that radial displacements of the cylinder w_c are positive toward the center of the opening. It should be noted that the zero and second-order solutions are entirely independent and mutually exclusive; accordingly, a symbol for a quantity in the one case is in no wise interchangeable with its duplicate in the other.

Plate Under Uniform Tension in All Directions: Cylinder on One Side of Plate. This is the zero-order case. The conventional plane-stress analysis, with constants of integration evaluated to make the normal stress at infinity equal to S_0 in all directions, and the radial stress at the edge of the hole equal to σ_{re} gives the pattern of membrane stress and displacement throughout the plate. Since the reaction of the one-sided reinforcement provided by the cylinder induces bending, the conventional analysis for plates subjected to transverse loads, shears, and bending moments also

Nomenclature

t = thickness of plate or cylinder
u = axial displacement, positive direction same as x, Fig. 1
V_{xe} = effective shear force on surface of opening in plate, in x-direction, per unit circumferential distance
v = tangential displacement, positive direction as indicated for θ in Fig. 2
w = radial displacement of middle surface of plate or cylinder
$\beta^4 = 3(1 - \nu^2)/R_c^2 t_c^2$
λ = exponential coefficient in the solutions of the second-order displacement equations for u, v, w
ν = Poisson's ratio, assumed as 0.3 in numerical examples and graphs
σ_r = radial component of membrane stress
σ_{xc} = longitudinal component of membrane stress, in cylinder
σ_θ = tangential component of membrane stress
$\tau_{r\theta}$ = shear stress, acting in r and θ-directions on planes normal to surface of plate

Edge Coefficients

U = axial displacement of cylinder at faying surface, per unit traction denoted by subscript
V = tangential displacement of cylinder at faying surface, per unit traction denoted by subscript
W = radial displacement of cylinder at faying surface, per unit traction denoted by subscript
η = angle of flare of cylinder at faying surface, per unit traction denoted by subscript

Edge-Coefficient Subscripts

M = axial bending moment M_{xe}/R_c
Q = effective radial shear force Q_{Mce}
Q' = tangential shear force $Q_{x\theta e}$
N = axial tensile force N_{ce}

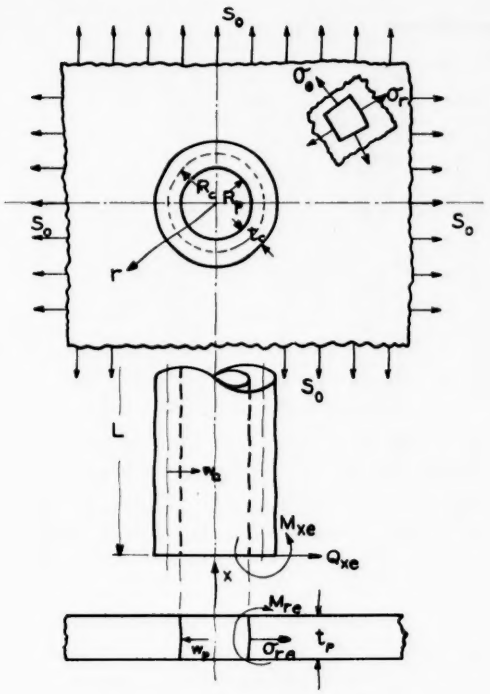

Fig. 1 Symbols for zero-order loading

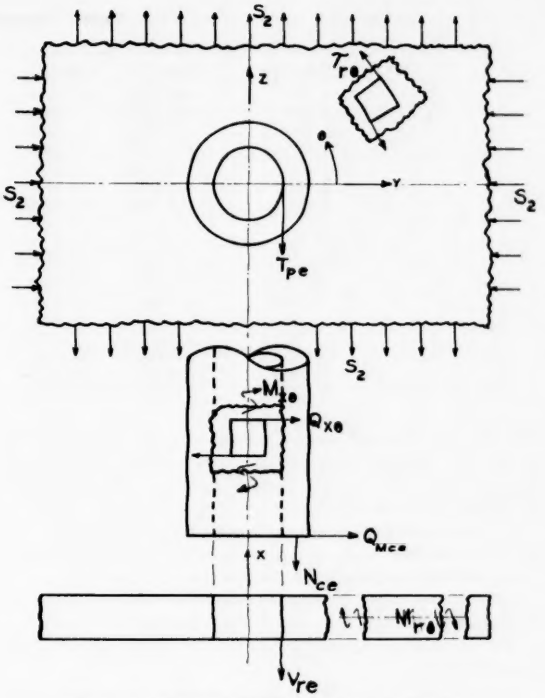

Fig. 2 Additional symbols for second-order loading

must be applied. For simplicity, it is assumed that because the plate is initially flat there is no interaction between the membrane and bending forces; actually tension in the plate tends to reduce any incipient bending, so that the assumption is on the side of safety. Detailed formulas resulting from these analyses are in the Appendix.

Coming now to the cylinder, the well-known fourth-order equations relating radial displacement w to foundation modulus β and internal pressure p, are the clue to the stress pattern. The solution is given in the Appendix, with constants evaluated to accommodate any requisite conditions of bending moment, transverse shear, radial displacement, and angle of dish, at the faying surfaces of plate and cylinder. It also takes care of either of two possible conditions at the far end of the cylinder; namely (*a*) free end, with zero bending moment and shear, (*b*) fixed end, with zero radial displacement and zero flare. These constants, be it noted, all appear as functions of βL, or $1.81784\ L/(d_c t_c)^{1/2}$ for steel with $\nu = 0.3$, and the displacement and flare at the faying surface of the cylinder are

$$\left.\begin{aligned} w_{ce} &= c_5 \frac{M_{xe}}{2D_c\beta^2} + c_6 \frac{Q_{xe}}{2D_c\beta^3} + c_9 \frac{pR_c^2}{Et_c} \\ (dw/dx)_{ce} &= c_7 \frac{M_{xe}}{2D_c\beta} + c_8 \frac{Q_{xe}}{2D_c\beta^2} + c_{10} \frac{\beta pR_c^2}{Et_c} \end{aligned}\right\} \quad (1)$$

where values for c_5, c_6, etc., may be found in Table 1. Case 1 and Case 2 in the table refer, respectively, to the free and fixed conditions at the far end of the cylinder.

The parameter $L/(d_c t_c)^{1/2}$, or effective foundation modulus, is easily visualized by making the simple construction of Fig. 3. Comparison of the last two rows in Table 1 proves that a length of cylinder more than 50 per cent in excess of $(d_c t_c)^{1/2}$ has no practical effect on conditions at the junction of cylinder and plate.

We may now write the four conditions for continuity at the faying surfaces in equation form, using the equivalents derived

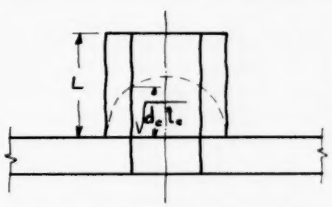

Fig. 3 Effective foundation modulus

for w_p, $(du/dr)_p$, w_c, and $(dw/dx)_c$ in equations (7) and (8) in the Appendix and equation (1), and noting that $Q_x = Q_{Mc}$ since there are no twisting moments:

$$\left.\begin{aligned} &(2) \quad (\sigma_{re}t_p + pt_p)R_p = Q_{Mce}R_c \\ &(4) \quad M_{re}R_p = \left(M_{xe} - \frac{1}{2}Q_{Mce}t_p\right)R_c \\ &(5) \quad [2S_0 - (1-\nu)\sigma_{re}]R_p + 6(1+\nu)M_{re}R_p/t_p^2 \\ &\quad = \left(-c_6M_{xe} - \frac{c_6Q_{Mce}}{\beta}\right)\frac{[12(1-\nu^2)]^{1/2}R_c}{t_c^2} - c_9pR_c^2/t_c \\ &(8) \quad -12(1+\nu)M_{re}R_p/t_p^3 \\ &\quad = (c_7\beta M_{xe} + c_8Q_{Mce})\frac{[12(1-\nu^2)]^{1/2}R_c}{t_c^2} + c_{10}\beta pR_c^2/t_c \end{aligned}\right\} \quad (2)$$

The number in parentheses that precedes each equation identifies it with the corresponding basic condition in the list of requirements set forth in the statement of the problem. Solution of the set of four equations gives the stresses σ_{re}, $6M_{re}/t_p^2$, $6M_{xe}/t_c^2$, and Q_{Mce}/t_c, in terms of the given plate tension S_0, pressure p, and dimensional parameters t_c/R_c, t_c/t_p, and $L/(d_c t_c)^{1/2}$. Then, any component of stress or displacement at any point in the plate or

Table 1 Zero-order edge coefficients

$L/(d_c t_c)^{1/2}$	c_5 Case (1)	c_5 Case (2)	c_6 Case (1)	c_6 Case (2)	c_7 Case (1)	c_7 Case (2)
0.125	−58.3559	−0.0516	−8.8390	−0.0078	513.7006	0.4542
0.250	−14.5360	−0.2040	−4.4001	−0.0618	64.2136	0.9012
0.500	−3.6320	−0.6869	−2.1745	−0.4112	8.5067	1.6087
1.000	−1.1758	−0.9506	−1.0644	−0.8606	2.2472	1.8830
1.500	−0.9885	−0.9560	−0.9858	−0.9533	1.9758	1.9114
2.000	−1.0012	−0.9957	−1.0006	−0.9950	2.0058	1.9930
∞	−1.0000	−1.0000	−1.0000	−1.0000	2.000	2.000

$L/(d_c/t_c)^{1/2}$	c_8 Case (1)	c_8 Case (2)	c_9 Case (1)	c_9 Case (2)	c_{10} Case (1)	c_{10} Case (2)
0.125	60.3559	0.0516	−1	−0.0013	0	0.00778
0.250	14.5360	0.2040	−1	−0.1167	0	0.1566
0.500	3.6320	0.6868	−1	−0.2812	0	0.4046
1.000	1.2615	1.0201	−1	−1.0559	0	0.8192
1.500	1.0032	0.9702	−1	−1.1656	0	0.3960
2.000	1.0012	0.9956	−1	−1.0931	0	0.04422
∞	1.0000	1.0000	−1	−1.0000	0	0.00000

cylinder is obtainable from equations (7), (8), and (9) in the Appendix. This will prove to be a tedious process, and to save labor, some useful solutions of equations (2) may be read directly from Fig. 4, for the special case where $p = 0$ and $L \gg (d_c t_c)^{1/2}$.

A close scrutiny of equations (2) reveals the fact that the solutions for the case of $S_0 = 1$, $p = 0$, as shown in Fig. 4, bear a linear relation to the solution for the case of $S_0 = 0$, $p = 1$, so that the curves of Fig. 4 apply to both cases. The rules for finding the solutions when $S_0 = 0$, $p = 1$, are as follows:

For σ_{rs}, multiply σ_{rs} in Fig. 4 by $0.65 - [R_c^2/t_c(2R_c - t_c)]$ and then subtract 1.

For $6M_{rs}/t_p^2$, $6M_{zs}/t_c^2$, and Q_{Mcs}/t, multiply the corresponding values in Fig. 4 by $0.65 - [R_c^2/t_c(2R_c - t_c)]$.

The designer is primarily interested in the location, magnitude, and nature of the greatest stresses associated with a reinforced opening. In the present case, the maximum tensile stress is at the intersection of the surface of the hole in the plate with the plate surface that is opposite the reinforcement, and is a combination of the membrane hoop stress $\sigma_{\theta p}$ and bending stress $6M_{\theta p}/t_p^2$ at the radius $r = R_p$; from equations (7) and (8) of the Appendix,

$$\sigma_{\theta \max} = 2S_0 - \sigma_{rs} - 6M_{rs}/t_p^2 \tag{3}$$

and the factor of stress intensification is

$$K_0 = 2 - (\sigma_{rs}/S_0) - (6M_{rs}/t_p^2 S_0) \tag{4}$$

If, by analogy with beams, the shear-stress distribution across the interface between plate and cylinder is taken as parabolic, then

$$\tau_{\max} = \frac{3}{2}(Q_{Mcs}/t_c) \tag{5}$$

Probably the stress-intensification factor K_0 as given by equation (4) is of greatest interest. Values of K_0, for various t_c/R_c and t_c/t_p ratios and zero pressure, are plotted in Fig. 5(*a*).

Example 1. A 4-in-ID, $5^1/_2$-in-OD nozzle, 12 in. long, is welded to a $1^1/_4$-in. plate at the point where the latter is pierced with a 4-in. opening; $p = 150$ psi, and the plate tension, at a distance from the nozzle, = 12,000 psi in all directions. What are the stresses at the opening?

$t_c/R_c = 0.316$, $t_c/t_p = 0.600$, $(d_c t_c)^{1/2} = 1.88$, L (excluding the plate thickness) = 10.75 in. Since $L \gg (d_c t_c)^{1/2}$, Table 1 gives $c_5 = c_6 = c_9 = -1$, $c_7 = 2$, $c_8 = 1$, $c_{10} = 0$. From Fig. 4, estimated values of the four boundary stresses, for $p = 0$, $S_0 = 12{,}000$ psi, are

$\sigma_{rs} = 1870$ psi	$6M_{rs}/t_p^2 = -6040$ psi
$6M_{zs}/t_c^2 = -970$ psi	$Q_{Mcs}/t_c = 2630$ psi

For $S_0 = 0$, $p = 150$ psi, using Fig. 4 combined with the rules of the preceding paragraphs,

$\sigma_{rs} = -180$ psi	$6M_{rs}/t_p^2 = 93$ psi
$6M_{zs}/t_c^2 = 15$ psi	$Q_{Mcs}/t_c = -40$ psi

Algebraic solution of equations (2) gives $\sigma_{rs} = 1700$ psi, $M_{rs} = -1551$ lb, $M_{zc} = -89$ lb, $Q_{Mcs} = 1947$ lb per in. From the last three of these, the maximum bending stresses and the mean shear stress are obtained:

$$6M_{rs}/t_p^2 = -5956 \text{ psi}, \quad 6M_{zs}/t_c^2 = -949 \text{ psi}, \quad Q_{Mcs}/t_c = 2596 \text{ psi}$$

As is readily seen, the results as read from Fig. 4, when combined for the effect of S_0 and p, show satisfactory agreement with those obtained by calculation.

The circumferential membrane stress in the plate, at the edge of the hole, is by the second of equations (7) (Appendix) 22,300 psi, and the maximum bending stress has already been determined as 5956 psi, making the total 28,256 psi and giving a stress intensification of 2.35. This is higher than the factor 2.00 for an unreinforced hole, the excess being caused by the bending stress which is 21 per cent of the total. A glance at the curves for σ_{rs} and $6M_{rs}/t_p^2$ in Fig. 4 indicates that the most direct way to improve the situation is to increase σ_{rs}. For a given R_c and t_p, this can be done most readily by increasing the cylinder-wall thickness t_c—an obvious common-sense conclusion that could have been reached without benefit of lengthy mathematical analysis. If, in this example, t_c is increased to a value 40 per cent greater than t_p, K_0 then drops to 1.96 (neglecting the effect of pressure, which is minor). Unfortunately, this is little better than a completely unreinforced hole, and the curves of Fig. 5(*a*) force us to the conclusion that no attachment of this type can be expected to give a substantial degree of reinforcement, if localized bending stresses in the plate are included in the determination of stress intensification. However, if the materials of construction and conditions of operation are such that it is considered safe to neglect the bending stresses, a much more optimistic picture results, as may be seen from Fig. 5(*b*). On this basis, the stress-concentration factor drops to 1.86.

The computed maximum hoop stress in the cylinder occurs at the interface and equals 12,113 psi, according to equation (10) of the Appendix. The maximum shear stress at the interface is, from equation (5), 3894 psi; this has no great significance.

Balanced Reinforcement. The foregoing example suggests that a more promising method of reducing K_0 is to minimize the eccentricity of the pull of the cylinder on the stressed plate. This pull results in a high bending stress that can be brought under control to a considerable degree by balancing the external cylinder with an internal cylinder, presumably of the same diameter and wall thickness and having a length within the conventional limits of reinforcement. The method of calculation resembles that for eccentric reinforcement, with modifications to accommodate the

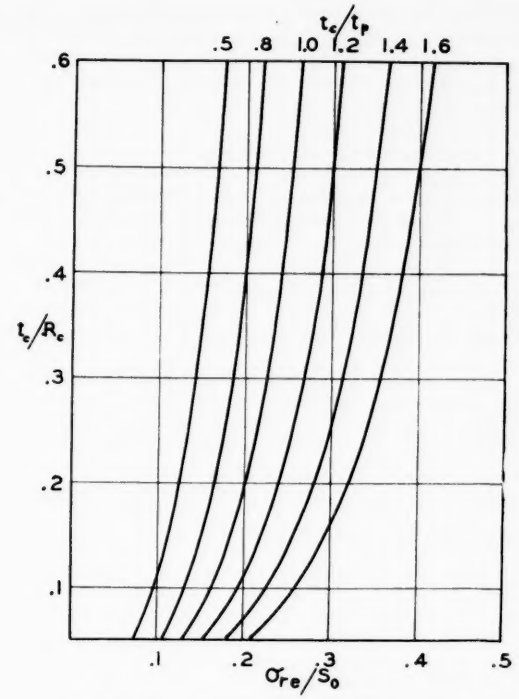

Fig. 4(a) Stress coefficients for zero-order loading

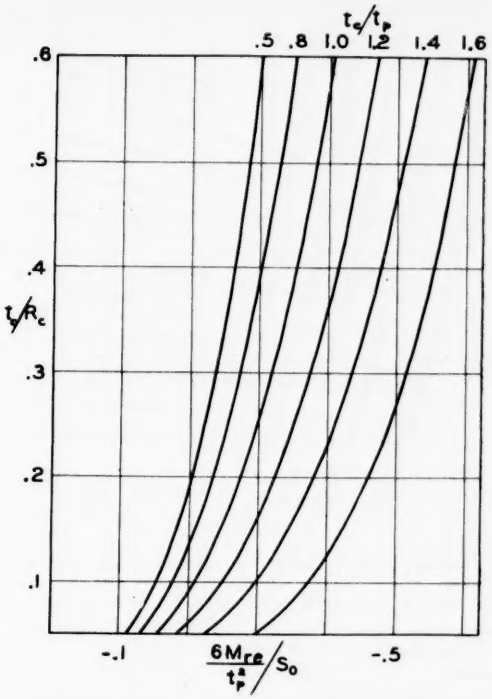

Fig. 4(b) Stress coefficients for zero-order loading

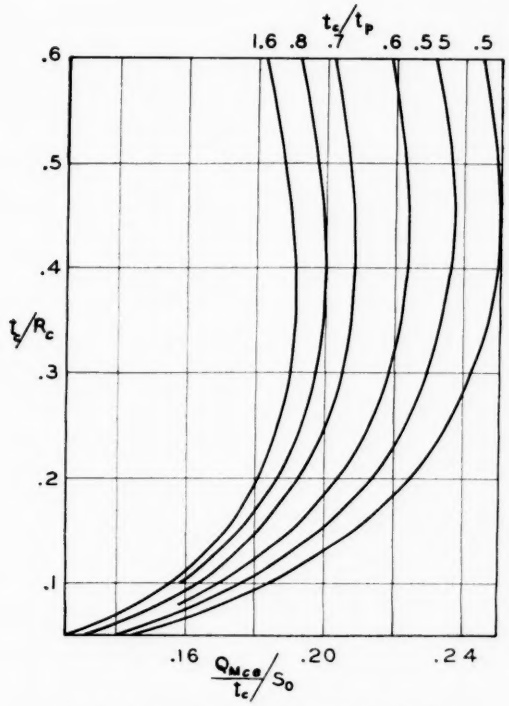

Fig. 4(c) Stress coefficients for zero-order loading

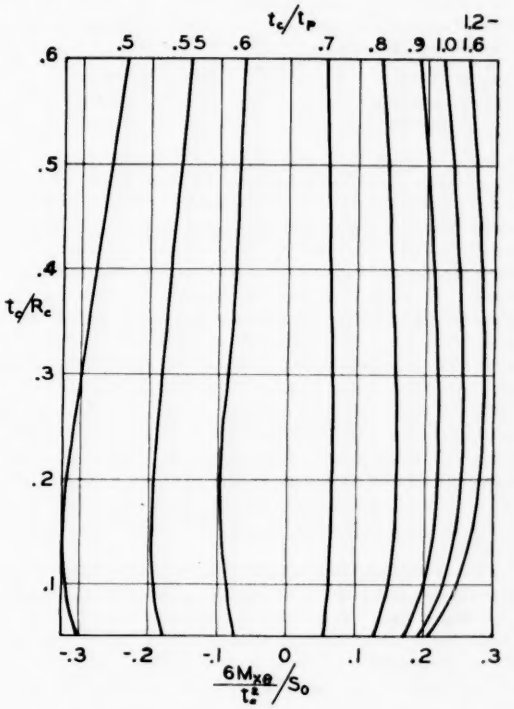

Fig. 4(d) Stress coefficients for zero-order loading

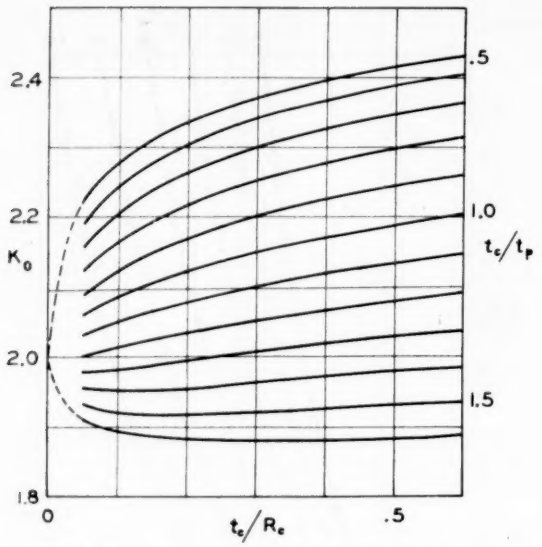

Fig. 5(a) Stress-concentration factors for zero-order loading

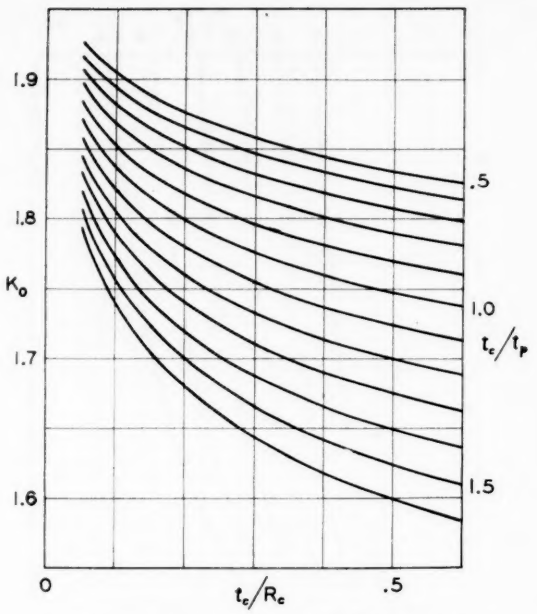

Fig. 5(b) Stress-concentration factors for zero-order loading

connections on both sides of the plate. Fig. 6, which is comparable with Fig. 1 for eccentric reinforcement, illustrates the forces that must be equated at the faying surfaces.

Example 2. The plate and nozzle of example 1 are reinforced with a ring on the opposite side of the plate, having the same ID and OD as the nozzle and a thickness of $^{15}/_{16}$ in. What is the stress concentration factor?

$L/(d_c t_c)^{1/2} = 0.497$ for the ring; use values in Table 1 for $L/(d_c t_c)^{1/2} = 0.50$. Substituting known values in equations (11) of the Appendix, and replacing displacements and rotations with forces and moments by means of equations (7), (8), and (1), gives a set of six simultaneous equations with the following solution:

$\sigma_{re} = 6782$ psi	$M_{re} = -159$ lb
$M_{xe} = -1793$ lb	$M_{xf} = -1645$ lb
$Q_{Mce} = 3636$ lb per in.	$Q_{Mcf} = -3660$ lb per in.

The 4-fold increase of σ_{re} over the value in example 1, with the accompanying drop in $\sigma_{\theta e}$, points up the beneficial effect of the balancing ring on the membrane stress in the plate, while the lower value of M_{xe} shows that bending of the plate has been almost eliminated. The combination of reduced membrane hoop stress and reduced bending gives a K_0-factor of 1.486, when computed for the same location as in example 1. This compares extremely well with the previous value of 2.35. However, that is not the whole story. Since the reinforcement is now more effective, it follows logically that it must carry a greater share of the load; this shows up as a greater stretching of the reinforcing members at the two faying surfaces. In the present case, the hoop stress in the reinforcing ring rises to 18,700 psi at the faying surface, so that the revised K_0-factor is 1.56. This is still a great improvement over the result obtained with one-side reinforcement.

The maximum shear stress at the interface between plate and balancing ring is, from equation (5), 7320 psi, which is again insignificant.

Plate Under Uniform Tension S_2 in $\theta = 0$ and 180-Deg Directions, and Uniform Compression S_2 in $\theta = 90$ and 270-deg Directions; Long Cylinder on One Side of Plate. This is the second-order case. With this type of loading, the plate tends to bend toward the cylinder along one axis of symmetry, and away from the cylinder along the other axis of symmetry, and the cross section of the cylinder becomes elliptical. Consequently, we have shear stresses and twisting moments that are nonexistent in the zero-order case, and all eight of the conditions for continuity listed in the statement of the problem must be observed. The corresponding eight equations, written in the same order as the conditions of continuity that they represent, are as follows, after replacing displacements and rotations in the plate by their equivalents in forces and moments as given by equations (12) and (13) of the Appendix, and remembering that r is now equivalent to R_p:

$$
\left.
\begin{aligned}
T_{pe}R_p &= -Q_{x\theta e}R_c \\
\sigma_{re}t_pR_p &= Q_{Mce}R_c \\
V_{re}R_p &= -N_{ce}R_c \\
M_{re}R_p &= \left(M_{xe} - \frac{1}{2}\,Q_{Mce}t_p\right)R_c + \frac{1}{2}\,V_{re}t_cR_{\text{avg}} \\
\left[-4S_2 - \frac{5-\nu}{3}\,\sigma_{re} + \frac{2}{3}\,(2-\nu)\tau_{re}\right]R_p & \\
+ \frac{2(1+\nu)(3-\nu)}{(3+\nu)t_p^{\,2}}\,M_{re}R_p - \frac{2\nu(1+\nu)}{(3+\nu)t_p^{\,2}}\,V_{re}R_p^{\,2} & \\
= E\left(-\bar{V}_M\,\frac{M_{xe}}{R} - \bar{V}_QQ_{Mce} - \bar{V}_{Q'}Q_{x\theta e} - \bar{V}_NN_{ce}\right) & \\
\left[4S_2 + \frac{2}{3}\,(2-\nu)\sigma_{re} - \frac{5-\nu}{3}\,\tau_{re}\right]R_p & \\
= E\left(\bar{V}_M\,\frac{M_{xe}}{R_c} + \bar{V}_QQ_{Mce} + \bar{V}_{Q'}Q_{x\theta e} + \bar{V}_NN_{ce}\right) & \\
\left[\frac{\nu}{3(3+\nu)(1-\nu)}\,M_{re}R_p^{\,2} - \frac{3-\nu}{12(3+\nu)(1-\nu)}\,V_{re}R_p^{\,3}\right] & \\
= D_p\left(U_M\,\frac{M_{xe}}{R_c} + U_QQ_{Mce} + U_{Q'}Q_{x\theta e} + U_NN_{ce}\right) & \\
\left[-\frac{3-\nu}{3(3+\nu)(1-\nu)}\,M_{re}R_p + \frac{\nu}{3(3+\nu)(1-\nu)}\,V_{re}R_p^{\,2}\right] & \\
= D_p\left(\eta_M\,\frac{M_{xe}}{R_c} + \eta_QQ_{Mce} + \eta_{Q'}Q_{x\theta e} + \eta_NN_{ce}\right) &
\end{aligned}
\right\} \quad (6)
$$

To find the complete stress pattern for this second-order "antisymmetrical" loading, we solve equations (6) for the eight edge tractions, and then substitute the results in equations (12) to get the pattern of membrane stresses in the plate, and in equations (13) for the bending stresses in the plate. The last four of equations (6), when solved, give firm values for sufficient numerical data to evaluate the constants of integration w_1, w_2, w_3, and w_4. Then, using equations (14), of the Appendix, the components of displacement in the cylinder along with their derivatives can be written with numerical coefficients, and the complete pattern of stress in the cylinder worked out using equations (15) and (16).

The maximum normal stress is found to be the combination of tangential membrane and bending stress in the plate, located at the edge of the hole and on either axis of symmetry, where $\cos 2\theta = \pm 1$.

Combination of Zero-Order and Second-Order Solutions. For a biaxial loading of the plate in any ratio other than 1:1, the problem is solved by using a mixture of the zero-order and second-order formulations in the proper proportion. For example, taking the familiar case where the ratio is 1:1/2, let us assume that the tension far from the hole along the line $\theta = 90$ and 270 deg is S, and along the line $\theta = 0$ and 180 deg is $\frac{1}{2}S$. Then we take $S_0 + S_2 = S$, $S_0 - S_2 = \frac{1}{2}S$, giving $S_0 = \frac{3}{4}S$, $S_2 = \frac{1}{4}S$, work out the solutions for S_0 and S_2 independently, and add the results.

It is readily seen that the computations for a complete stress analysis demand a formidable amount of labor, and it is certain that few if any designers would care to undertake the task. However, it is thought that the values of stress-intensification factors would have considerable interest; accordingly, a graph, Fig. 7, has been prepared which displays these factors for a plate-cylinder combination with 1:1/2 biaxial loading, and a range of t_c/R_c and t_c/t_p-values covering the same field as in Fig. 5. These curves give the ratio of the combined membrane and bending stresses in the plate at the edge of the hole and on an axis of symmetry, to the major membrane stress at infinity; they approach the limiting value 2.50 as the cylinder is decreased in size relative to the plate.

To illustrate the possibilities of the method of computation detailed in this paper, we conclude with a fairly complete stress analysis of a plate 0.75 in. thick, having a 1.1875-in. hole and an attached cylinder with ID flush with the hole and 2.1875 in. OD. The loading per square inch is S in the 90–270 deg direction and $1/2S$ in the 0–180 deg direction. This corresponds dimensionally, with respect to outlet diameter and wall and plate thickness, to a photoelastic test by C. E. Taylor[2] on a cylindrical vessel and nozzle.[2]

Example 3. Assuming the dimensions in the preceding paragraph, $R_p = 0.59375$ in., $t_c = 0.50$ in., $R_c = 0.84375$ in., $t_c/R_c = 0.59259$, $t_c/t_p = 0.66667$. For 1:1/2 biaxial loading, $S_0 = 3/4\,S$ and $S_2 = 1/4\,S$. $D_c = 0.0114469E$, and $D_P = 0.0386333E$.

First Order. Solution of equations (2) gives $M_{re} = -0.054048\,S_0$, $Q_{Mce} = 0.103428S_0$, $\sigma_{re} = 0.195968S_0$, $M_{xe} = 0.0007512S_0$. From equations (7), the membrane stresses in the plate are

$$\sigma_{rp} = (1 - 0.804032R_p^2/r^2)S_0$$

$$\sigma_{\theta p} = (1 + 0.804032R_p^2/r^2)S_0$$

$$\tau_{r\theta p} = 0$$

The bending stresses in the plate surface, on the side opposite the cylinder, are, from equations (8)

[2] Fifth Quarterly Report on Contract NObs 72069, Department of Theoretical and Applied Mechanics, University of Illinois, Jan. 10, 1957.

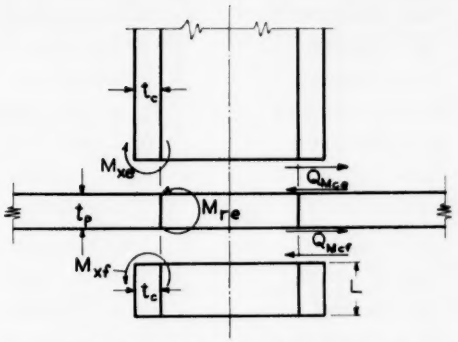

Fig. 6 Symbols for balanced reinforcement

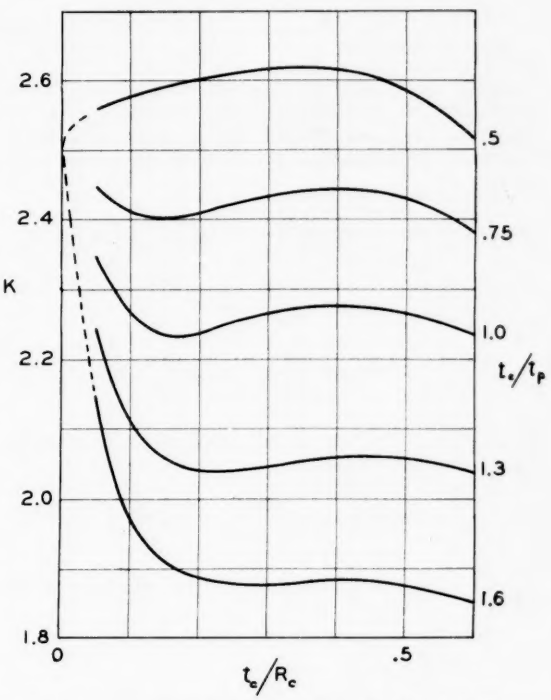

Fig. 7 Stress-concentration factors for 1:1/2 biaxial loading

$$6M_{rp}/t_p^2 = -10.666667 \times 0.054048(R_p^2/r^2)S_0 = -0.576512(R_p^2/r^2)S_0$$

$$6M_{\theta p}/t_p^2 = -6M_{rp}/t_p^2 = 0.576512(R_p^2/r^2)S_0$$

By means of equations (1) and (9) it is found that the circumferential membrane stress in the cylinder is

$$-Ew_c/R_c = e^{-\beta x}(0.591251\cos\beta x - 0.008378\sin\beta x)\frac{S_0}{0.84375}$$

and the axial bending stress on the inside surface is

$$6M_{xc}/t_c^2 = 24 \times 0.0896634e^{-\beta x}(0.008378\cos\beta x + 0.591251\sin\beta x)S_0$$

The circumferential bending stress on the inside surface is $6\nu M_{xc}/t_c^2$.

Second Order. Calculation of the compatibility equations for u, v, and w gives the set of values

$\lambda_1 = -2.789762$ $\quad \lambda_2 = -0.932523$

$u_1 = 0.055582$ $\quad u_2 = 0.421870$

$v_1 = -0.020835$ $\quad v_2 = 0.805163$

$\bar{W}_M = -6.565230/E$ $\quad \bar{W}_Q = -0.742206/E$

$\bar{C}_M = 0.827200/E$ $\quad \bar{C}_Q = 0.894862/E$

$\bar{V}_M = -1.473028/E$ $\quad \bar{V}_Q = -3.550282/E$

$R_c\eta_M = 22.026237/E$ $\quad R_c\eta_Q = 8.432702/E$

$\lambda_3 = -1.034842$ $\quad \lambda_4 = -0.526422$

$u_3 = -0.188226$ $\quad u_4 = -0.439970$

$v_3 = 0.599742$ $\quad v_4 = -0.141874$

$\bar{W}_{Q'} = -4.558378/E$ $\quad \bar{W}_N = 1.294376/E$

$\bar{C}_{Q'} = 1.121216/E$ $\quad \bar{C}_N = -1.890294/E$

$\bar{V}_{Q'} = -3.879444/E$ $\quad \bar{V}_N = 1.171068/E$

$R_c\eta_{Q'} = 4.296670/E$ $\quad R_c\eta_N = -1.844278/E$

Solution of equations (6) gives $\tau_{r\theta_c} = 0.934358S_2$, $\sigma_{r_c} = -0.038028S_2$, $V_{r_c} = 0.296134S_2$, $M_{r_c} = 0.132942S_2$, $Q_{x\theta_c} = -0.493134S_2$, $Q_{M_{c_x}} = 0.020070S_2$, $N_{c_\theta} = -0.208390S_2$, $M_{x_c} = 0.038012S_2$. From equations (12), the membrane stresses in the plate are

$$\sigma_{r_p} = \left(-1 + 2.207340\frac{Rp^2}{r^2} - 1.169312\frac{Rp^4}{r^4}\right) S_2 \cos 2\theta$$

$$\sigma_{\theta_p} = \left(1 + 1.169312\frac{Rp^4}{r^4}\right) S_2 \cos 2\theta$$

$$\tau_{r\theta_p} = \left(1 + 1.103670\frac{Rp^2}{r^2} - 1.169312\frac{Rp^4}{r^4}\right) S_2 \sin 2\theta$$

From equations (13), the bending stresses in the plate, on the side opposite the cylinder, are

$$\frac{6}{t_p^2} M_{r_p} = 10.666667\left(0.040156\frac{R_p^2}{r^2} + 0.092786\frac{R_p^4}{r^4}\right) S_2 \cos 2\theta$$

$$\frac{6}{t_p^2} M_{\theta_p} = 10.666667\left(0.133852\frac{R_p^2}{r^2} - 0.092786\frac{R_p^4}{r^4}\right) S_2 \cos 2\theta$$

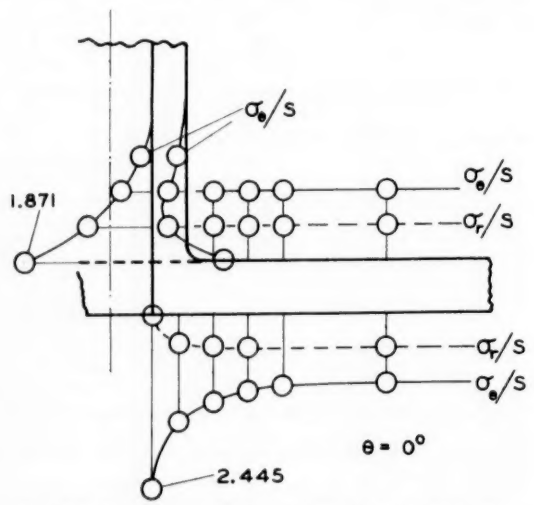

Fig. 8(a) Typical stress distribution with 1:1/2 biaxial loading

The solution of equations (6) determines four edge traditions each of which is a function of w; hence the four constants of integration for w may be evaluated, and we find that

$$w_c = [e^{\lambda_1\xi}(-0.5588 \cos \lambda_2\xi + 0.2476 \sin \lambda_2\xi) + e^{\lambda_3\xi}(2.0858 \cos \lambda_4\xi - 0.4896 \sin \lambda_4\xi)] \frac{S_2 \cos 2\theta}{E}$$

$$u_c = [e^{\lambda_1\xi}(0.0734 \cos \lambda_2\xi + 0.2494 \sin \lambda_2\xi) + e^{\lambda_3\xi}(-0.1772 \cos \lambda_4\xi + 1.0098 \sin \lambda_4\xi)] \frac{S_2 \cos 2\theta}{E}$$

$$v_c = [e^{\lambda_1\xi}(0.2111 \cos \lambda_2\xi + 0.4447 \sin \lambda_2\xi) + e^{\lambda_3\xi}(1.3203 \cos \lambda_4\xi + 0.0023 \sin \lambda_4\xi)] \frac{S_2 \sin 2\theta}{E}$$

These displacements and their derivatives determine, by means of equations (15) and (16), all the pertinent tractions throughout the cylinder. Accordingly, the circumferential membrane stress is

$$\frac{N_\theta}{t_c} = [e^{\lambda_1\xi}(0.5533 \cos \lambda_2\xi + 0.2953 \sin \lambda_2\xi) + e^{\lambda_3\xi}(0.2394 \cos \lambda_4\xi + 0.0994 \sin \lambda_4\xi)] \frac{S_2 \cos 2\theta}{0.50}$$

The axial membrane stress is

$$\frac{N_x}{t_c} = [e^{\lambda_1\xi}(-0.0933 \cos \lambda_2\xi - 0.2833 \sin \lambda_2\xi) + e^{\lambda_3\xi}(-0.1183 \cos \lambda_4\xi - 0.6447 \sin \lambda_4\xi)] \frac{S_2 \cos 2\theta}{0.50}$$

The circumferential bending stress on the inside surface of the cylinder is

$$\frac{6M_\theta}{t_c^2} = [e^{\lambda_1\xi}(-0.0303 \cos \lambda_2\xi - 0.0207 \sin \lambda_2\xi) + e^{\lambda_3\xi}(0.0863 \cos \lambda_4\xi - 0.0187 \sin \lambda_4\xi)]24S_2 \cos 2\theta$$

The axial bending stress on the inside surface of the cylinder is

$$\frac{6M_x}{t_c^2} = [e^{\lambda_1\xi}(0.0286 \cos \lambda_2\xi - 0.0738 \sin \lambda_2\xi) + e^{\lambda_3\xi}(0.0094 \cos \lambda_4\xi + 0.0333 \sin \lambda_4\xi)]24S_2 \cos 2\theta$$

Combination of First and Second Orders. This is simply done by

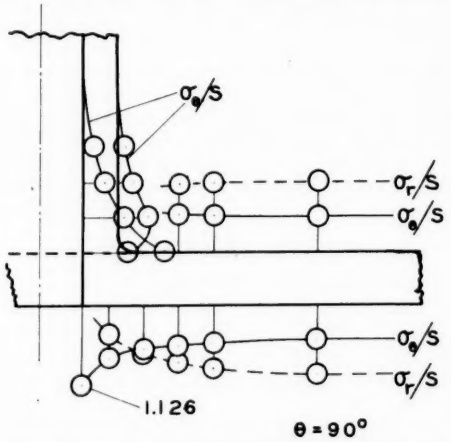

Fig. 8(b) Typical stress distribution with 1:1/2 biaxial loading

adding 75 per cent of the first-order stresses to 25 per cent of the second-order stresses. The results are plotted in Fig. 8 in terms of the major tensile stress S. For the stress intensification, take the values of the circumferential stresses, both membrane and bending, at the edge of the hole, on the inner surface of the plate, and on the axis of symmetry for which $\theta = 0$ or 180 deg. Thus

$$(1.8040 + 0.5765)S_0 + (2.1693 + 0.4380)S_2 = (2.3805 \times 0.75S) + (2.6073 \times 0.25S) = 2.4372S;\ K = 2.44$$

If the computations are made to include the effect of internal pressure on the cylinder, K is increased. For example, if the tension S is 4.2 times the internal pressure, which is approximately the hoop stress/internal pressure ratio in the photoelastic test previously referred to, $K = 2.6$.

Conclusions

As a result of this theoretical analysis, it may be concluded:

1 The location of the point of maximum stress is on the inside surface of the plate, in the longitudinal plane, and at the edge of the hole. This agrees with that found in practically all tests, both on photoelastic models and full-scale steel vessels, except possibly those where the outlet diameter approaches that of the main vessel.

2 A large proportion of the stress intensification around an opening with unbalanced reinforcement is due to bending. This is shown very clearly, for the case of uniform all-around tension, by contrasting the K_0-values given by Fig. 5(b) with those given by Fig. 5(a). For the case of 1:1/2 biaxial loading, consider the computations in the final paragraphs of Example 3. If the terms for bending stress are omitted, we have

$$1.8040S_0 + 2.1693S_2 = (1.8040 + 0.75S) + (2.1693 \times 0.25S)$$

and $K = 1.90$, as against 2.44 in Example 3 where bending is included.

3 The conclusion stated in the preceding paragraph suggests the need for further study of current proposals to classify conditions of service and materials of construction according as (a) all types of stress have major significance, or (b) moderately high but localized bending stresses may safely be given less weight than those stresses that are substantially uniform across a section.

4 A plain cylindrical outlet attached to one side of a vessel wall may induce a K-factor greater than that caused by a simple round opening, provided the vessel/outlet diameter ratio is large, so that the vessel is effectively a flat plate. This is shown in Fig. 7, where the line $K = 2.5$ represents the stress intensification for an unreinforced plate under 1:1/2 biaxial tension. A similar situation exists under uniform all-around tension, as evidenced by Fig. 5(a).

5 According to Figs 5(a), 5(b), and 7, stress conditions are improved by increasing the outlet-wall thickness relative to the plate thickness (t_c/t_p ratio). At the same time, Fig. 3 and the related explanation in the text show that material in the outlet has little or no effect on stress, beneficial or otherwise, unless it is close to the plate. In reconciling these two conclusions, it follows that reinforcement can best be attained by (a) increasing the outlet-wall thickness close to the plate (e.g., tapered nozzle), or (b) fitting a collar around an otherwise thin-walled outlet (pad reinforcement or insert-type nozzle with thick skirt).

6 It must be understood clearly that the formulas and curves in this paper are applicable to pressure-vessel design only when the head radius, or vessel diameter, is very large in relation to the outlet diameter. Comparison of the K-values herein with those obtained experimentally indicate that K increases as the outlet diameter approaches that of the main vessel. The true relationship of K to this diameter ratio is now receiving further study.

Acknowledgments

The author wishes to express his thanks to D. L. Caudill, who performed many exploratory computations on a desk calculating machine; to W. R. Burrows, who programmed and directed the computation of the exponential coefficients λ on the 705 IBM digital computer of the Standard Oil Company of Indiana, and to N. C. Lind, who saved the author much time by solving many of his 4 × 4 simultaneous equations. The work embodied in the paper as a whole has been sponsored by the Pressure Vessel Research Committee of the Welding Research Council, as part of a broad investigation of openings in pressure vessels.

References

1(a) E. O. Waters, "Reinforcement of Openings in Pressure Vessels," Welding Research, vol. 23, 1958, pp. 277–288. (b) M. B. Hogan, "A Survey of the Literature Pertaining to Stress Distribution in the Vicinity of a Hole and the Design of Pressure Vessels," Bulletin of the University of Utah, vol. 41, 1950, (c) W. A. Nash, "Bibliography on Shells and Shell-Like Structures," David Taylor Model Basin Report 863, 1954.

2(a) W. Flügge, "Statik und Dynamik der Schalen," Springer, Berlin, 1934, p. 118. (b) A. E. H. Love, "A Treatise on the Mathematical Theory of Elasticity," Dover Publications, New York, N. Y., fourth edition, 1944, p. 582. (c) S. Timoshenko, "Theory of Plates and Shells," McGraw-Hill Book Company, New York, N. Y., 1940, p. 440. The somewhat simpler formulation of Timoshenko has been used in this paper.

3 S. Timoshenko, "Theory of Plates and Shells," McGraw-Hill Book Company, Inc., New York, N. Y., 1940, pp. 354, 355, 439.

APPENDIX

Zero-Order Stresses in Plate. The five equations (7) satisfy the Airy stress function for symmetrical loading about a pole, and the desired boundary conditions $\sigma_{r_p} = \sigma_{\theta_p} = S_0$ at infinity, $\sigma_{r_p} = \sigma_{r_e}$ when $r = R_p$:

$$\left.\begin{aligned} \sigma_{r_p} &= S_0(1 - R_p^2/r^2) + \sigma_{r_e}R_p^2/r^2 \\ \sigma_{\theta_p} &= S_0(1 + R_p^2/r^2) - \sigma_{r_e}R_p^2/r^2 \\ \tau_{r\theta_p} &= 0 \\ Ew_p &= S_0[(1 - \nu)r + (1 + \nu)R_p^2/r] - \sigma_{r_e}(1 + \nu)R_p^2/r \\ Ev_p &= 0 \end{aligned}\right\} \quad (7)$$

The differential equation for bending of the plate $\nabla^2\nabla^2 u = 0$ is satisfied by the solution given in the following, and at the same time the bending moment $M_{r_p} = M_{r_e}$ and $u = 0$ at the edge of the hole

$$\left.\begin{aligned} u &= [M_{r_e}R_p^2/(1 - \nu)D_p] \ln (R_p/r) \\ du/dr &= -M_{r_e}R_p^2/(1 - \nu)D_p r \\ M_{r_p} &= D_p\left(\frac{d^2u}{dr^2} + \frac{\nu}{r}\frac{du}{dr}\right) = M_{r_e}R_p^2/r^2 \\ M_{\theta_p} &= D_p\left(\nu\frac{d^2u}{dr^2} + \frac{1}{r}\frac{du}{dr}\right) = -M_{r_e}R_p^2/r^2 \end{aligned}\right\} \quad (8)$$

Zero-Order Stresses in Cylinder. The equation $d^4w_c/dx^4 + 4\beta^4 w_c = -p/D_c$ has the solution and derived formulas

$$
\left.
\begin{aligned}
w_c &= e^{-\beta x}(c_1 \cos \beta x + c_2 \sin \beta x) \\
&\quad + e^{\beta x}(c_3 \cos \beta x + c_4 \sin \beta x) - \frac{pR_c^2}{Et_c} \\
dw_c/dx &= \beta e^{-\beta x}[(-c_1 + c_2) \cos \beta x + (-c_1 - c_2) \sin \beta x] \\
&\quad + \beta e^{\beta x}[(c_3 + c_4) \cos \beta x + (-c_3 + c_4) \sin \beta x] \\
M_{xc} &= -D_c d^2 w_c/dx^2 = 2D_c\beta^2[e^{-\beta x}(c_2 \cos \beta x - c_1 \sin \beta x) \\
&\quad + e^{\beta x}(-c_4 \cos \beta x + c_3 \sin \beta x)] \\
M_{\theta c} &= \nu M_{xc} \\
Q_{xc} &= -D_c d^3 w_c/dx^3 \\
&= 2D_c\beta^3\{e^{-\beta x}[(-c_1 - c_2) \cos \beta x + (c_1 - c_2) \sin \beta x] \\
&\quad + e^{\beta x}[(c_3 - c_4) \cos \beta x + (c_3 + c_4) \sin \beta x]\} \\
\sigma_{\theta c} &= -Ew_c/R_c \pm 6\nu M_{xc}/t_c^2 \\
\sigma_{xc} &= \pm 6M_{xc}/t_c^2
\end{aligned}
\right\} \quad (9)
$$

To evaluate c_1, c_2, c_3, and c_4 and obtain equations (1) in the body of the paper, we proceed thus for case 1 (free end): (*a*) In the foregoing equations for M_{xc} and Q_{xc}, substitute $M_{xc} = M_{xe}$ and $x = 0$, $M_{xc} = 0$ and $x = L$, $Q_{xc} = Q_{Mce}$ and $x = 0$, $Q_{xc} = 0$ and $x = L$; (*b*) solve these four equations for $c_1 \ldots . c_4$ in terms of M_{xe}, Q_{Mce}, and the dimensional parameters; (*c*) substitute these values in the foregoing equations for w_c and dw_c/dx; (*d*) let $w_c = w_{ce}$, $dw_c/dx = (dw_c/dx)_e$, $x = 0$, and rearrange the terms. For case 2 (fixed end) the procedure is the same except that in step (*a*) substitute $w_c = 0$ and $x = L$ in the first of equations (9), $dw_c/dx = 0$ and $x = L$ in the second, $M_{xe} = M_{xe}$ and $x = 0$ in the third, and $Q_{xc} = Q_{Mce}$ and $x = 0$ in the fifth. These linear transformations occur frequently in the literature and need not be detailed here. For the purposes of the present paper, applicable results are given in Table 1.

The maximum hoop stress in the cylinder is at the plate-cylinder interface, where $x = 0$. Accordingly, from the first and sixth of equations (9),

$$
\sigma_{\theta c\max} = -[(c_1 + c_3)E/R_c] + (pR_c/t_c) + |6\nu M_{xe}/t_c^2|
$$

or, using the derived constants c_5, c_6, c_9 of Table 1, and equations (1)

$$
\left.
\begin{aligned}
\sigma_{\theta c\max} &= -\frac{E}{R_c}\left(c_5 \frac{M_{xe}}{2D_c\beta^2} + c_6 \frac{Q_{xe}}{2D_c\beta^3} + c_9 \frac{pR_c^2}{Et_c}\right) \\
&\quad + |6\nu M_{xe}/t_c^2| \\
&= -\frac{2[3(1-\nu^2)]^{1/2}}{t_c^2}\left(c_5 M_{xe} + c_6 \frac{Q_{Mce}}{\beta}\right) \\
&\quad - c_9 \frac{pR_c}{t_c} + |6\nu M_{xe}/t_c^2|
\end{aligned}
\right\} \quad (10)
$$

Balanced Reinforcement. Equations (9) are valid for both the main cylinder and balancing ring. To define the conditions of force and displacement that must be continuous at the faying surfaces, subscript e may be used as heretofore for the main cylinder, and subscript f for the balancing ring. Then for continuity of shears,

$$
(\sigma_{re} + p)t_p R_p = (Q_{Mxe} - Q_{Mxf})R_c
$$

moments,

$$
M_{re}R_p = \left[M_{xe} - M_{xf} - (Q_{Mxe} + Q_{Mxf})\frac{t_p}{2}\right]R_c
$$

radial displacements,

$$
w_{pe} - \left(\frac{du}{dr}\right)_e \frac{t_p}{2} = -w_{ce}
$$

rotations,

$$
\left.
\begin{aligned}
w_{pe} + \left(\frac{du}{dr}\right)_e \frac{t_p}{2} &= -w_{ef} \\
\left(\frac{du}{dr}\right)_e = \left(\frac{dw}{dx}\right)_e &= \left(\frac{dw}{dx}\right)_f
\end{aligned}
\right\} \quad (11)
$$

(*Cont'd*)

When the foregoing displacements and rotations are replaced by their equivalents in forces and moments, using equations (7), (8), and (1) exactly as for the unbalanced reinforcement, a set of simultaneous equations is obtained with six, instead of four, unknowns. Solutions of this set is the key to the determination of stresses throughout the assembly. It must be noted that pressure has no effect on the balancing member, and there are sign changes in c_6 and c_7.

Second-Order Stresses in Plate. The following five equations satisfy the Airy stress function for antisymmetrical loading about a pole, and the following boundary conditions at an infinite distance from the pole: $\sigma_y = -S_2$, $\sigma_z = S_2$, $\tau_{yz} = 0$. Also, $\sigma_{rp} = \sigma_{re}\cos 2\theta$ and $\tau_{r\theta p} = \tau_{r\theta e}\sin 2\theta = T_{pe}/t_p$, when $r = R_p$ (see Fig. 2 for directions of y and z co-ordinates):

$$
\left.
\begin{aligned}
\sigma_{rp} &= \left[S_2\left(-1 + 4\frac{R_p^2}{r^2} - 3\frac{R_p^4}{r^4}\right)\right. \\
&\quad + \sigma_{re}\left(2\frac{R_p^2}{r^2} - \frac{R_p^4}{r^4}\right) \\
&\quad \left. + \tau_{r\theta e}\left(-2\frac{R_p^2}{r^2} + 2\frac{R_p^4}{r^4}\right)\right]\cos 2\theta \\
\sigma_{\theta p} &= \left[S_2\left(1 + 3\frac{R_p^4}{r^4}\right) + \sigma_{re}\frac{R_p^4}{r^4}\right. \\
&\quad \left. + \tau_{r\theta e}\left(-2\frac{R_p^4}{r^4}\right)\right]\cos 2\theta \\
\tau_{r\theta} &= \left[S_2\left(1 + 2\frac{R_p^2}{r^2} - 3\frac{R_p^4}{r^4}\right)\right. \\
&\quad + \sigma_{re}\left(\frac{R_p^2}{r^2} - \frac{R_p^4}{r^4}\right) \\
&\quad \left. + \tau_{r\theta}\left(-\frac{R_p^2}{r^2} + 2\frac{R_p^4}{r^4}\right)\right]\sin 2\theta \\
Ew_p &= \left[S_2\left(-\overline{1+\nu}r - 4\frac{R_p^2}{r} + \overline{1+\nu}\frac{R_p^4}{r^3}\right)\right. \\
&\quad + \sigma_{re}\left(-2\frac{R_p^2}{r} + \frac{1+\nu}{3}\frac{R_p^4}{r^3}\right) \\
&\quad \left. + \tau_{r\theta e}\left(2\frac{R_p^2}{r} - \frac{2}{3}\overline{1+\nu}\frac{R_p^4}{r^3}\right)\right]\cos 2\theta \\
Ev_p &= \left[S_2\left(\overline{1+\nu}r + 2\overline{1-\nu}\frac{R_p^2}{r} + \overline{1+\nu}\frac{R_p^4}{r^3}\right)\right. \\
&\quad + \sigma_{re}\left(\overline{1-\nu}\frac{R_p^2}{r} + \frac{1+\nu}{3}\frac{R_p^4}{r^3}\right) \\
&\quad \left. + \tau_{r\theta e}\left(-\overline{1-\nu}\frac{R_p^2}{r} - \frac{2}{3}\overline{1+\nu}\frac{R_p^4}{r^3}\right)\right]\sin 2\theta
\end{aligned}
\right\} \quad (12)
$$

The differential equation for bending of the plate $\nabla^2\nabla^2 u = 0$ is satisfied by the solution given below, and at the same time the bending moment $M_{rp} = M_{re}\cos 2\theta$, effective shear force $V_r = V_{re}\cos 2\theta$, and mean value of $u = 0$, when $r = R_p$:

$$
\left.
\begin{aligned}
u &= \left[M_{re}\left(-\frac{R_p^2}{2(3+\nu)} + \frac{(3-\nu)R_p^4}{6(3+\nu)(1-\nu)r^2} \right) \right. \\
&\left. + V_{re}\left(-\frac{R_p^3}{4(3+\nu)} - \frac{\nu R_p^5}{6(3+\nu)(1-\nu)r^2} \right) \right] \frac{\cos 2\theta}{D_p} \\
\frac{du}{dr} &= \left[M_{re}\left(-\frac{(3-\nu)R_p^4}{3(3+\nu)(1-\nu)r^3} \right) \right. \\
&\left. + V_{re}\left(\frac{\nu R_p^5}{3(3+\nu)(1-\nu)r^3} \right) \right] \frac{\cos 2\theta}{D_p} \\
M_{rp} &= D_p\left[\frac{\partial^2 u}{\partial r^2} + \nu\left(\frac{1}{r}\frac{\partial u}{\partial r} + \frac{1}{r^2}\frac{\partial^2 u}{\partial \theta^2} \right) \right] \\
&= \left[M_{re}\left(\frac{2\nu R_p^2}{(3+\nu)r^2} + \frac{(3-\nu)R_p^4}{(3+\nu)r^4} \right) \right. \\
&\left. + V_{re}\left(\frac{\nu R_p^3}{(3+\nu)r^2} - \frac{\nu R_p^5}{(3+\nu)r^4} \right) \right] \cos 2\theta \\
M_{\theta p} &= D_p\left[\nu\frac{\partial^2 u}{\partial r^2} + \frac{1}{r}\frac{\partial u}{\partial r} + \frac{1}{r^2}\frac{\partial^2 u}{\partial \theta^2} \right] \\
&= \left[M_{re}\left(\frac{2R_p^2}{(3+\nu)r^2} - \frac{(3-\nu)R_p^4}{(3+\nu)r^4} \right) \right. \\
&\left. + V_{re}\left(\frac{R_p^3}{(3+\nu)r^2} + \frac{\nu R_p^5}{(3+\nu)r^4} \right) \right] \cos 2\theta \\
M_{r\theta p} &= (1-\nu)D_p\left(\frac{1}{r}\frac{\partial^2 u}{\partial r \partial \theta} - \frac{1}{r^2}\frac{\partial u}{\partial \theta} \right) \\
&= \left[M_{re}\left(-\frac{(1-\nu)R_p^2}{(3+\nu)r^2} + \frac{(3-\nu)R_p^4}{(3+\nu)r^4} \right) \right. \\
&\left. + V_{re}\left(-\frac{(1-\nu)R_p^3}{2(3+\nu)r^2} - \frac{\nu R_p^5}{(3+\nu)r^4} \right) \right] \sin 2\theta \\
Q_r &= -D_p\frac{\partial}{\partial r}\nabla^2 u = \left[\frac{4M_{re}R_p^2}{(3+\nu)r^3} \right. \\
&\left. + \frac{2V_{re}R_p^3}{(3+\nu)r^3} \right] \cos 2\theta \\
V_r &= Q_r - \frac{1}{r}\frac{\partial M_{r\theta}}{\partial \theta} \\
&= \left[2M_{re}\left(\frac{3-\nu}{3+\nu} \right)\left(\frac{R_p^2}{r^3} - \frac{R_p^4}{r^5} \right) \right. \\
&\left. + V_{re}\left(\frac{(3-\nu)R_p^3}{(3+\nu)r^3} + \frac{2\nu R_p^5}{(3+\nu)r^5} \right) \right] \cos 2\theta
\end{aligned}
\right\} \quad (13)
$$

Second-Order Displacements in Cylinder. Three simultaneous differential equations of compatibility relate the three displacements u, v, w [2] and a solution for w, for a reasonably long cylinder, may be written as

$$
\left.
\begin{aligned}
w_c &= [e^{\lambda_1\xi}(w_1 \cos \lambda_2\xi + w_2 \sin \lambda_2\xi) \\
&\quad + e^{\lambda_3\xi}(w_3 \cos \lambda_4\xi + w_4 \sin \lambda_4\xi)] \cos 2\theta
\end{aligned}
\right\}
$$

Then u and v are determined by the equations

$$
\left.
\begin{aligned}
u_c &= \{e^{\lambda_1\xi}[(u_1w_1 + u_2w_2) \cos \lambda_2\xi \\
&- (u_2w_1 - u_1w_2) \sin \lambda_2\xi] + e^{\lambda_3\xi}[(u_3w_3 + u_4w_4) \cos \lambda_4\xi \\
&\quad - (u_4w_3 - u_3w_4) \sin \lambda_4\xi]\} \cos 2\theta \\
v_c &= \{e^{\lambda_1\xi}[(v_1w_1 + v_2w_2) \cos \lambda_2\xi \\
&- (v_2w_1 - v_1w_2) \sin \lambda_2\xi] + e^{\lambda_3\xi}[(v_3w_3 + v_4w_4) \cos \lambda_4\xi \\
&\quad - (v_4w_3 - v_3w_4) \sin \lambda_4\xi]\} \sin 2\theta
\end{aligned}
\right\} \quad (14)
$$

where $\xi = x/R_c$, and λ_1, λ_2, and so on, are roots of the related characteristic equation. Table 2 contains machine-computed values of λ for a range of t_c/R_c and Poisson's ratio = 0.3, and Table 3 gives values of the displacement coefficients u_1, u_2, v_1, v_2, etc.

Table 2 Second-order exponential coefficients

t_c/R_c	$-\lambda_1$	$-\lambda_2$	$-\lambda_3$	$-\lambda_4$
0.05	6.10750	5.41488	0.31399	0.28546
0.10	4.58247	3.61560	0.45639	0.37896
0.15	3.95831	2.79677	0.56735	0.43360
0.20	3.61230	2.30193	0.65839	0.46732
0.25	3.39025	1.96191	0.73443	0.48856
0.30	3.23409	1.70983	0.79870	0.50208
0.35	3.11699	1.51306	0.85359	0.51080
0.40	3.02479	1.35355	0.90093	0.51651
0.45	2.94949	1.22040	0.94213	0.52034
0.50	2.88604	1.10669	0.97831	0.52302
0.55	2.83125	1.00771	1.01033	0.52502
0.60	2.78296	0.92019	1.03887	0.52665

The five tractions in the cylinder that are of importance in establishing continuity at the faying surface are M_x, Q_x, $M_{x\theta}$, $Q_{x\theta}$, and N_x, and they are related to the foregoing displacements by these equations [3]:[3]

$$
\left.
\begin{aligned}
M_x &= -D_c\left[\ddot{w}_c + \frac{\nu}{R_c^2}(v_c' + w_c'') \right] \\
Q_x &= -D_c\left(\dddot{w}_c + \frac{1}{R_c^2}\ddot{w}_c'' + \frac{1}{R_c^2}\dot{v}_c' \right) \\
M_{x\theta} &= (1-\nu)\frac{D_c}{R_c}(\dot{w}_c' + \dot{v}_c) \\
Q_{x\theta} &= \frac{Et_c}{2(1+\nu)}\left(\frac{1}{R_c}u_c' + \dot{v}_c \right) \\
N_x &= \frac{Et_c}{1-\nu^2}\left[\dot{w}_c + \frac{\nu}{R_c}(v_c' - w_c) \right]
\end{aligned}
\right\} \quad (15)
$$

At the faying surface, $\xi = 0$ and the displacements and rotation reduce to

$$w_e = (w_1 + w_3)\cos 2\theta, \quad u_e = (u_1w_1 + u_2w_2 + u_3w_3 + u_4w_4)\cos 2\theta$$

$$v_e = (v_1w_1 + v_2w_2 + v_3w_3 + v_4w_4)\sin 2\theta$$

$$\dot{w}_e = (\lambda_1w_1 + \lambda_2w_2 + \lambda_3w_3 + \lambda_4w_4)(\cos 2\theta)/R_c$$

Also, the effective shear force at the faying surface is

$$Q_{Mce} = \left(Q_x - \frac{1}{r}\frac{\partial M_{x\theta}}{\partial \theta} \right)_e = -D_c\left[\dddot{w} + \frac{2-\nu}{R_c^2}(\ddot{w}'' + \ddot{v}') \right]_e$$

Consequently, four edge tractions, M_{xe}, Q_{Mce}, $Q_{x\theta e}$, and N_{xe} may be expressed in terms of four constants of integration w_1, w_2, w_3, w_4. By inverting the 4×4 matrix thus formed, we express the four constants of integration in terms of the edge tractions and thereby obtain the four edge coefficients; i.e., the values of w_e, u_e, v_e, and $R_c(\partial w/\partial x)_e$ caused by unit values of M_{xe}/R_c, Q_{Mce}, $Q_{x\theta e}$, and N_{xe}. Computed values of these edge coefficients, for a range of t_c/R_c from 0.05 to 0.60, are listed in Table 4.

Two additional force-displacement relations, useful in a detailed stress analysis, are

$$
\left.
\begin{aligned}
N_\theta &= \frac{Et_c}{1-\nu^2}\left(\frac{v_c' - w_c}{R_c} + \nu\dot{u}_c \right) \\
M_\theta &= -D_c\left(\frac{v_c' + w_c''}{R_c^2} + \nu w_c \right)
\end{aligned}
\right\} \quad (16)
$$

[3] Dots denote differentiation with respect to x; primes with respect to θ.

Table 3 Second-order displacement coefficients

t_e/R_e	u_1	u_2	u_3	u_4
0.05	−0.01959	0.03323	−0.07136	−0.07980
0.10	−0.01953	0.05770	−0.09620	−0.11964
0.15	−0.01518	0.08424	−0.11317	−0.15503
0.20	−0.00874	0.11319	−0.12624	−0.18888
0.25	−0.00118	0.14446	−0.13724	−0.22188
0.30	0.00700	0.17795	−0.14688	−0.25441
0.35	0.01550	0.21363	−0.15555	−0.28660
0.40	0.02411	0.25154	−0.16348	−0.31854
0.45	0.03272	0.29182	−0.17077	−0.35028
0.50	0.04112	0.33467	−0.17742	−0.38185
0.55	0.04916	0.38039	−0.18350	−0.41328
0.60	0.05664	0.42934	−0.18900	−0.44460
t_e/R_e	v_1	v_2	v_3	v_4
0.05	−0.000626	0.06950	0.50129	−0.006926
0.10	−0.002336	0.13848	0.50499	−0.01450
0.15	−0.004721	0.20660	0.51067	−0.02327
0.20	−0.007372	0.27387	0.51786	−0.03306
0.25	−0.009916	0.34042	0.52616	−0.04418
0.30	−0.01216	0.40655	0.53529	−0.05639
0.35	−0.01403	0.47262	0.54507	−0.06953
0.40	−0.01557	0.53896	0.55540	−0.08345
0.45	−0.01680	0.60606	0.56623	−0.09800
0.50	−0.01798	0.67424	0.57754	−0.11304
0.55	−0.01933	0.74404	0.58932	−0.12848
0.60	−0.02115	0.81597	0.60159	−0.14422

Table 4 Second-order edge coefficients (times E)

t_e/R_e	$\bar{W}_M$	$\bar{W}_Q$	$\bar{W}_{Q'}$	$\bar{W}_N$
0.05	−3045.905509	−5881.630192	−2844.321326	411.147021
0.10	−681.145860	−1015.845305	−484.505001	91.774397
0.15	−265.262151	−355.798039	−168.085369	36.502994
0.20	−131.268450	−165.517477	−78.623441	18.431618
0.30	−45.480419	−54.334939	−26.591203	6.784288
0.40	−20.439083	−23.733809	−12.166165	3.242635
0.50	−10.824862	−12.680137	−6.971540	1.937249
0.60	−6.336669	−7.477912	−4.439122	1.272391
t_e/R_e	$\bar{V}_M$	$\bar{V}_Q$	$\bar{V}_{Q'}$	$\bar{V}_N$
0.05	−904.308831	−2812.983289	−1414.369437	202.722893
0.10	−199.848053	−471.755638	−243.608247	45.725775
0.15	−76.619819	−162.253979	−86.806289	18.763264
0.20	−37.450596	−74.685879	−40.264325	9.935006
0.30	−12.519615	−24.436655	−15.858318	4.140942
0.40	−5.337335	−10.669008	−8.252263	2.296985
0.50	−2.650903	−5.753511	−5.321426	1.560218
0.60	−1.419095	−3.438866	−3.810414	1.161288
t_e/R_e	U_M	U_Q	$U_{Q'}$	U_N
0.05	234.372771	404.938093	201.898677	−64.457121
0.10	67.091772	90.304615	46.299950	−22.102699
0.15	29.151994	35.495483	18.991501	−11.906503
0.20	15.296357	17.578110	10.051118	−7.770131
0.30	5.607556	6.131950	4.161578	−4.404830
0.40	2.581699	2.749280	2.291239	−3.031543
0.50	1.383040	1.487311	1.529679	−2.323100
0.60	0.814356	0.882556	1.121936	−1.884197
t_e/R_e	$R_e\eta_M$	$R_e\eta_Q$	$R_e\eta_{Q'}$	$R_e\eta_N$
0.05	15907.168258	3701.069691	1245.071267	−284.999721
0.10	2826.710727	832.897010	283.261741	−83.042429
0.15	1001.377373	326.507812	113.075561	−37.424776
0.20	469.830710	161.989620	57.613730	−20.377795
0.30	155.322876	56.598700	21.528266	−8.240282
0.40	68.838394	25.389538	10.447759	−4.220100
0.50	36.204303	13.738339	6.324018	−2.652972
0.60	21.243909	8.151820	4.204521	−1.818587

CHARLES CONCORDIA

Manager-Engineering Practices, Analytical Engineering Section, General Electric Company, Schenectady, N. Y.
Fellow ASME

Effect of Steam-Turbine Reheat on Speed-Governor Performance

This paper shows the effect on the frequency stability and response of an electric power system of the use of steam-turbine reheat. It is shown that in general reheat tends to decrease the damping of the frequency variations of the system as a whole, to increase the damping of tie-line power oscillations, and to increase the maximum frequency deviation occasioned by an abrupt load change. The system responses were determined by means of an analog computer.

Introduction

THE subject of speed-governor performance on electric power systems has been studied for many years. An analytical study [1][1] reported in 1941 showed that for steam-turbine governing systems, with their relatively small time lags, the dynamic characteristics of the governing system were of minor importance, and that the principal significant parameters were the steady-state quantities, dead band, and incremental speed regulation. Since that time, power systems have increased greatly in size, speed governors have been designed in accordance with the performance standards [2] prepared in 1946 by a joint ASME-AIEE committee, and load disturbances have, in general, become smaller relative to system size. Because of these factors, one would naturally suppose that the governor dynamics has become even less important. Studies of tie-line power and frequency control [3–5] of steam-electric systems have tended to confirm this view.

However, one factor has arisen which may tend to increase the importance of governing-system dynamics. This is the widespread use of reheat turbines, which introduces into part of the system an additional time lag of several seconds. The purpose of this paper is to present the results of an analysis of the performance of steam-turbine speed-governing systems as affected by turbine reheat. The results may of course also be interpreted as showing the effect of a large time lag introduced into the speed-governing system by any other cause as well.

Conclusions

Based on the results of the present study, the use of turbine reheat: (*a*) Decreases the damping of the frequency variations of the power system as a whole, (*b*) greatly increases the maximum frequency deviation following an abrupt change of load, and (*c*) increases the damping of the relatively high-frequency power oscillations occurring on system tie lines.

Systems Studied

As shown in Fig. 1, three cases were studied.

Case I. The entire power system is represented as a single machine, so that oscillations among the machines are neglected, and only the oscillations of the system as a whole are studied.

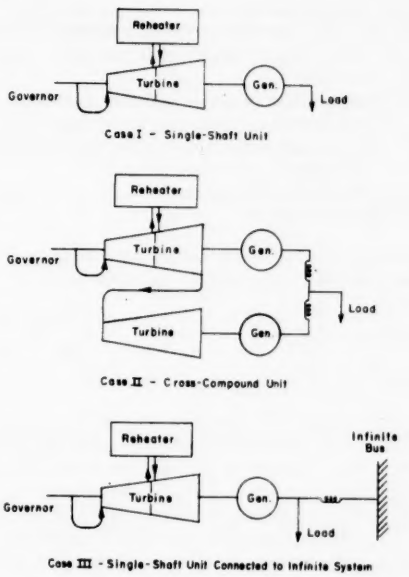

Fig. 1 Systems studied

Case II. The entire power system is represented as a cross-compound machine, so that oscillations between the high and low-pressure components are considered. Fig. 1 shows the reheat occurring in the h-p turbine, but actually the location of the reheater was varied over the whole range, from the h-p to the l-p end of the steam-flow path. In all cases the capacity was assumed to be equally divided between the two shafts, so the reheater was sometimes in the h-p, and sometimes in the l-p turbine.

Case III. The performance of a single-shaft machine, as shown by its oscillations relative to the rest of the (infinitely large) system, is represented by Case III. In this case oscillations of the system as a whole are neglected.

Analysis

Since it was desired to learn as much as possible about the dynamic performance of the system as affected by reheat, the system was studied by representing it in considerable detail on a differential analyzer and observing its response to sudden load changes. This gave a complete picture of the frequency variations as a function of time following the disturbance. In particular, the maximum frequency deviations and the rate of decay were noted. The slow correcting action of frequency and tie-line-

[1] Numbers in brackets designate References at end of paper.

Contributed by the Power Division and presented at the Annual Meeting, New York, N. Y., November 30–December 5, 1958, of THE AMERICAN SOCIETY OF MECHANICAL ENGINEERS.

NOTE: Statements and opinions advanced in papers are to be understood as individual expressions of their authors and not those of the Society. Manuscript received at ASME Headquarters, April 3, 1958. Paper No. 58—A-36.

power control was not considered, and constant pressure in the steam supply was assumed.

The system of Case 1 may be represented by two equations as follows:

The summation of the torques acting on the power system is

$$(Mp + T_d)\Delta\omega = \Delta P - \Delta L \tag{1}$$

where

M = the total effective rotary inertia of the system, measured in terms of the starting time in seconds
T_d = the over-all per-unit damping torque (or self-regulation) coefficient of the system, combining the variation of prime-mover torque with speed with fixed valve and the variation of load torque with frequency
$\Delta\omega$ = the speed (or frequency, which in this case is taken to be the same) deviation in per unit of normal frequency
ΔP = the variation of prime-mover input torque produced by control-valve motion, in per unit
ΔL = the per-unit step change of load used to initiate a disturbance
p = the derivative operator d/dt
t = time in seconds

The change of prime mover torque ΔP is produced by speed-governor action and is given by the equation

$$\Delta P = -\left[f + \frac{(1-f)}{T_R p + 1}\right] \frac{1}{T_6 p + 1} \frac{1}{T_1 p + 1} \frac{\Delta\omega}{R} \tag{2}$$

where

f = the fraction of total capacity upstream from the reheater and thus not subject to the reheater time lag
T_R = a time constant in seconds representing the time lag caused by steam storage in the reheater
T_6 = the time constant in seconds caused by steam storage between the control valve and the turbine
T_1 = a time constant in seconds representing all the time lags of the speed-governing system
R = the per-unit speed-governor steady-state incremental regulation

The only basic difference between equation (2) and the equations used in reference [1] is the addition of the factor in brackets, which expresses the effect of the reheater. Note that this factor can be put in the form:

$$\left[\frac{fT_R p + 1}{T_R p + 1}\right] \tag{3}$$

This is the same form as occurs in hydraulic-turbine speed governors [6], and shows that the reheater makes the governing system appear as one that has a per-unit transient speed regulation of (R/f) and a droop-reset (or washout) time constant of (fT_R) seconds.

For Case II the system torque-balance equations are:

for the high-pressure unit

$$\left[M_1 p + T_{d1} + \frac{T_s'}{p}\right] \Delta\omega_1 - \left[T_{d12} + \frac{T_s'}{p}\right] \Delta\omega_2 = \Delta P_1 - 0.5\Delta L \tag{4a}$$

for the low-pressure unit

$$\left[M_2 p + T_{d2} + \frac{T_s'}{p}\right] \Delta\omega_2 - \left[T_{d12} + \frac{T_s'}{p}\right] \Delta\omega_1 = \Delta P_2 - 0.5\Delta L \tag{4b}$$

where

$M_1(M_2)$ = rotary inertia of high (low) pressure unit in seconds
T_{d12} = per-unit damping-torque coefficient of oscillation between the two units
$T_{d1} - T_{d12}, (T_{d2} - T_{d12})$ = per-unit damping torque coefficient caused by inherent variation of prime mover and load torque with frequency for high (low) pressure unit
T_s' = 377 T_s for a 60-cps system
T_s = per-unit synchronizing-torque coefficient produced by the electrical tie between the two units
$\Delta\omega_1(\Delta\omega_2)$ = per-unit speed of high (low) pressure unit
$\Delta P_1(\Delta P_2)$ = variation in prime mover per-unit input torque of the high (low) pressure unit produced by the control-valve motion
ΔL = per-unit step change in load used to initiate a disturbance, assumed equally divided between the two units

The variations of prime-mover torques ΔP_1 and ΔP_2 are produced by the action of the speed governor on the h-p unit and, for the case where the reheat occurs in the h-p unit, the equations are

for the high-pressure unit

$$\Delta P_1 = -\left[f + \frac{F - f}{T_R p + 1}\right] \frac{\Delta\omega_1}{(T_6 p + 1)(T_1 p + 1)R} \tag{5a}$$

for the low-pressure unit

$$\Delta P_2 = -\left[\frac{1 - F}{T_R p + 1}\right] \frac{\Delta\omega_1}{(T_6 p + 1)(T_1 p + 1)R} \tag{5b}$$

where

F = the fraction of total capacity in the h-p unit, and f is smaller than F

For the case where the reheat occurs in the l-p unit, the equations are

for the high-pressure unit

$$\Delta P_1 = -\frac{F\Delta\omega_1}{(T_6 p + 1)(T_1 p + 1)R} \tag{6a}$$

for the low-pressure unit

$$\Delta P_2 = -\left[f - F + \frac{1 - f}{T_R p + 1}\right] \frac{\Delta\omega_1}{(T_6 p + 1)(T_1 p + 1)R} \tag{6b}$$

where now f is greater than F.

For Case III the torque equation for the machine considered is

$$\left(Mp + T_d + \frac{T_s'}{p}\right) \Delta\omega = \Delta P - \Delta L \tag{7}$$

This is the same as equation (1) except for the addition of the synchronizing torque between the machine and infinite system.

As for Case II,

$T_s' = 377\ T_s$

T_s = per-unit synchronizing-torque coefficient between the machine and the system

The variations of prime-mover torque ΔP for Case III are given by equation (2), just as for Case I.

Results

Some of the specific results obtained are shown in Figs. 2–8, which give per-cent frequency, or speed, deviation as a function of time, following an abrupt load change of 1 per cent of system capacity. Since the system is assumed to have a linear response, for any other abrupt load change the deviation will be directly proportional to the magnitude of the load change. In all cases the governor incremental-speed regulation = 0.05 per unit, the steam-storage time constant $T_6 = 0.25$ sec, and the governing-system time constant $T_1 = 0.375$ sec. For Cases I and III, $M = 10$ sec. For Case II, $M_1 = 2.6$ sec, $M_2 = 7.4$ sec, and $F = 0.5$.

Fig. 2 shows for Case I the effect of varying the amount of the total system subject to reheat, with $T_d = 1.0$ and $T_R = 10$ sec. The case $f = 0$, where all the capacity is downstream from the reheater, is not of direct interest in the present study, but is presented in order to show the detrimental effect of a large governing-system time lag. It is evident that reheat is detrimental to stability and response if the fraction $1 - f$ of system capacity subject to reheat is greater than about 75 per cent. This percentage roughly corresponds to having reheat on all machines, so it would appear that actual systems should still be stable even

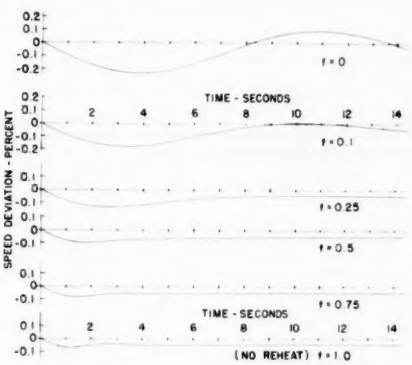

Fig. 2 Case I, effect on system response of amount of system capacity subject to reheat

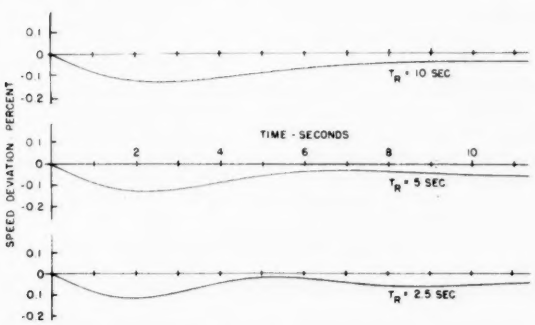

Fig. 3 Case I, effect on system response of reheater time constant—$f = 0.25$

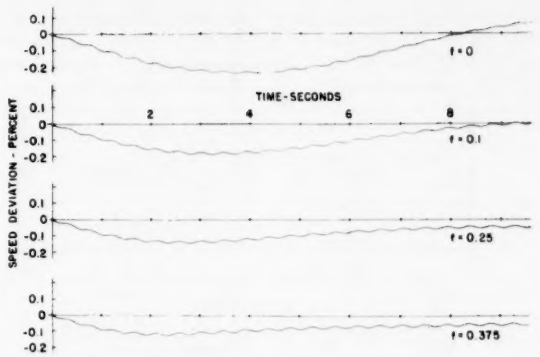

Fig. 4(a) Case II, high pressure—effect on system response of amount of capacity subject to reheat—$T_{d12} = 0.5$

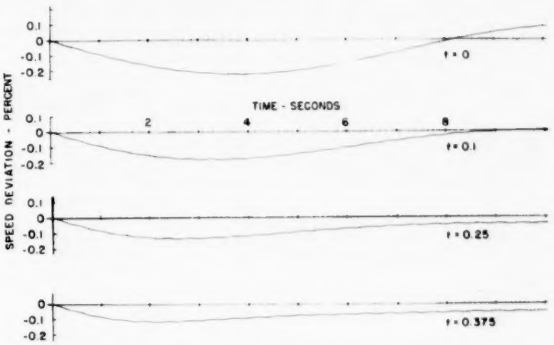

Fig. 4(b) Case II, low pressure—effect on system response of amount of capacity subject to reheat—$T_{d12} = 0.5$

with all reheat machines. Moreover, the effective over-all damping-torque coefficient T_d will usually be greater than 1.0 in actual power systems, which will increase the degree of stability.

Fig. 3 shows the effect of varying the reheater time constant T_R with $f = 0.25$. It is evident that decreasing T_R from 10 to 2.5 sec decreases the degree of stability only slightly.

Figs. 4 and 5 show for Case II the effect of varying the amount of reheat. The reheater time constant $T_R = 10$ sec. The case of Fig. 4 differs from that of Fig. 5 only in the amount of damping of the oscillations between the high and low-pressure units. Except for the high-frequency oscillations between the units, the results are almost the same as indicated by Fig. 2. The relatively much larger high-frequency oscillations of the h-p machine (ω_1), compared to those of the l-p machine (ω_2), are explained by the relative values of the rotary inertias M_1 and M_2.

Fig. 6 shows the effect of varying the magnitude of the synchronizing torque between the two units, both for no reheat ($f = 1.0$) and for 75 per cent reheat ($f = 0.25$). The reheater time lag $T_R = 10$ sec. The variation of two to one is seen to have little effect on stability.

Fig. 7 shows the same effects for the case of a much smaller reheater time constant $T_R = 2.5$ sec. It is evident that the system is made less stable with this rather small value of T_R.

It would appear that it is not usually necessary to represent the system in such detail as is included in Case II. However, the ease of representation afforded by the differential analyzer has enabled this case to be thoroughly explored with very little additional complexity.

Finally, Fig. 8 shows for Case III the effect of reheat on the frequency oscillations for two values of synchronizing-torque co-

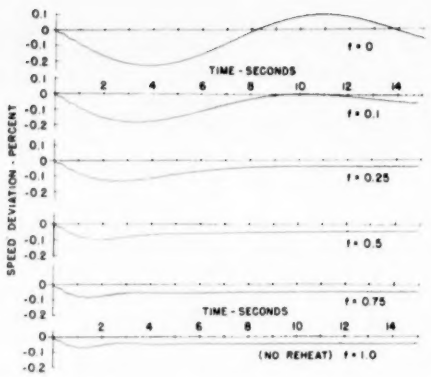

Fig. 5(a) Case II, high pressure—effect on system response of amount of capacity subject to reheat—$T_{d12} = 4.0$

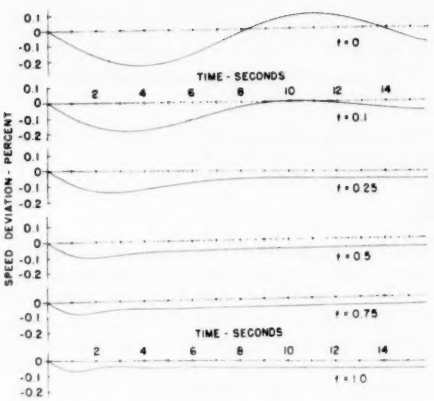

Fig. 5(b) Case II, low pressure—effect on system response of amount of capacity subject to reheat—$T_{d12} = 4.0$

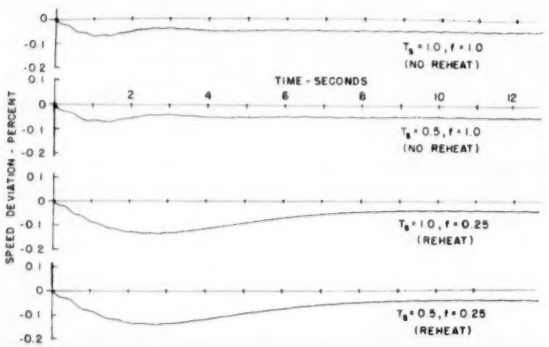

Fig. 6(a) Case II, high pressure—effect on system response of synchronizing torque and of reheat—$T_{d12} = 4.0$

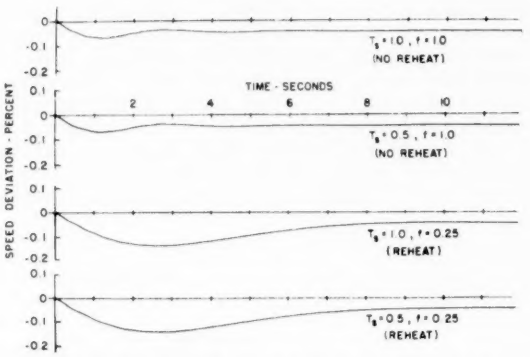

Fig. 6(b) Case II, low pressure—effect on system response of synchronizing torque and of reheat—$T_{d12} = 4.0$

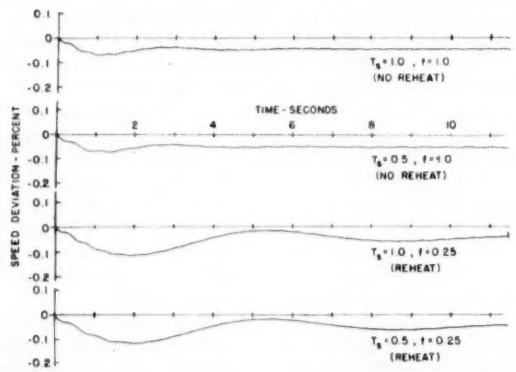

Fig. 7(a) Case II, high pressure—effect on system response of synchronizing torque and of reheat, with very small reheater time lag—$T_{d12} = 4.0$

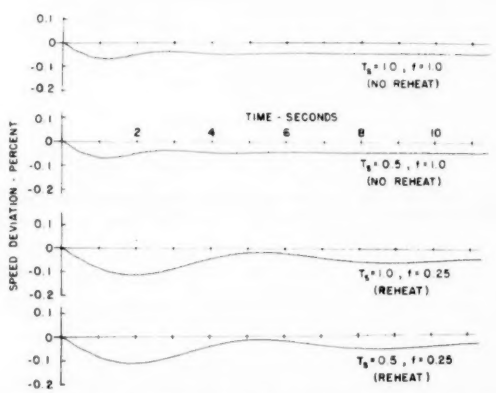

Fig. 7(b) Case II, low pressure—effect on system response of synhronizing torque and of reheat, with very small reheater time lag—$T_{d12} = 4.0$

efficient $T_s = 1.0$ and $T_s = 0.25$, with a reheater time constant of 5.0 sec. The presence of reheat is seen to improve the damping of the tie-line power oscillations, as evidenced by the frequency oscillations plotted, when the synchronizing torque is large (as might be the case for a tie between two machines in a power system), but to have practically no effect when the synchronizing torque is small (as might be the case for a tie between two power systems).

APPENDIX 1

Time Lag Caused by Reheater

Following is a derivation of the approximate expression for reheater time lag, in brackets in equation (2), valid for relatively small displacements.

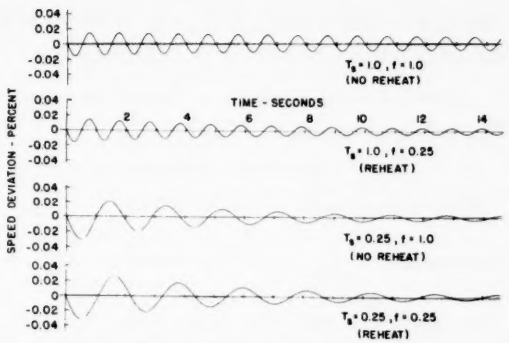

Fig. 8 Case III, effect on unit response of synchronizing torque and of reheat—T_d = 4.0, T_R = 5.0 sec

If q_1 is the steam flow upstream from the reheater and q_2 is the steam flow downstream from the reheater, the power P may be approximately expressed by

$$P = eq_1 + hq_2 \tag{8}$$

The steam flows are given approximately by

$$q_1 = ap_1 - bp_2 \tag{9a}$$

$$q_2 = cp_2 \tag{9b}$$

where

p_1 is the pressure at the control valves, and
p_2 is the pressure at the reheater.

Thus

$$P = eap_1 - ebp_2 + hcp_2 = eap_1 + (hc - eb)p_2 \tag{10}$$

For the reheater

$$g\frac{dp_2}{dt} = q_1 - q_2 = ap_1 - (b + c)p_2 \tag{11}$$

or

$$\left[\left(\frac{g}{b + c}\right)p + 1\right]p_2 = \frac{a}{b + c}p_1 \tag{12}$$

with $p = d/dt$.

Substituting equation (12) in equation (10)

$$P = \left[ea + \frac{(hc - eb)\dfrac{a}{b + c}}{\left(\dfrac{g}{b + c}\right)p + 1}\right]p_1 \tag{13}$$

which is of the same form as in equation (2).

Note that, because of the assumed dependence of q_1 on its back pressure p_2, the relative magnitudes of the two components of P are not exactly proportional to e and h, so f is only approximately the fraction of capacity upstream from the reheater.

APPENDIX II

Damping Torques for Case II

The damping torques acting on the h-p unit are: From the prime mover, depending on its own speed, $a\,\Delta\omega$; from the load, depending on the system frequency, and thus on the average speed $b(\Delta\omega_1 + \Delta\omega_2)$ (note that $2b$ is the coefficient of the average speed); from the generator amortisseurs, depending on the difference in speed between the two units, $c(\Delta\omega_1 - \Delta\omega_2)$. The total torque on the h-p unit is thus:

$$a\Delta\omega_1 + b(\Delta\omega_1 + \Delta\omega_2) + c(\Delta\omega_1 - \Delta\omega_2)$$
$$= (a + b + c)\Delta\omega_1 - (c - b)\Delta\omega_2 \tag{14}$$

Similar expressions can be written for the l-p unit.
Thus

$$T_{d1} = a + b + c$$

$$T_{d12} = c - b$$

$$T_{d1} - T_{d12} = a + 2b$$

With $\Delta\omega_2 = \Delta\omega_1$, the torque is $(a + 2b)\,\Delta\omega_1 = (T_{d1} - T_{d1})_2\Delta\omega_1$

With $\Delta\omega_2 = -\Delta\omega_1$, the torque is $(a + 2c)\Delta\omega_1 = (T_{d1} + T_{d12})\Delta\omega$

References

1 C. Concordia, S. B. Crary, and E. E. Parker, "Effect of Prime-Mover Speed Governor Characteristics on Power-System Frequency Variations and Tie-Line Power Swings," *Trans. AIEE*, vol. 60, 1941, pp. 559–567, 733–735.

2 Recommended Specification for "Speed-Governing of Steam Turbines Intended to Drive Electric Generators Rated 500 Kw and Up," prepared by Joint AIEE and ASME Committee, AIEE no. 600, May, 1949.

3 C. Concordia, H. S. Shott, and C. N. Weygandt, "Control of Tie-Line Power Swings," *Trans. AIEE*, vol. 61, 1942, pp. 306–313, 395.

4 C. Concordia and L. K. Kirchmayer, "Tie-Line Power and Frequency Control of Electric Power Systems," *Trans. AIEE*, vol. 72, part 3, June, 1953, pp. 562–572.

5 C. Concordia, L. K. Kirchmayer, and E. A. Szymanski, "Effect of Speed Governor Dead Band on Tie-Line Power and Frequency Control Performance," *Trans. AIEE*, vol. 76, part 3, no. 31, August, 1957, pp. 429–435.

6 C. Concordia and L. K. Kirchmayer, "Tie-Line Power and Frequency Control of Electric Power Systems—Part II," *Trans. AIEE*, vol. 73, part 3 A, April, 1954, pp. 133–146.

7 C. Concordia, "Inter-Relation of Speed Governing Systems and Loads," Proceedings of the 23rd Conference of the Oil and Gas Power Division, ASME, 1951.

8 C. Concordia and L. K. Kirchmayer, "Load-Swing Control by Turbine Regulator," *Electric Light and Power*, September, 1953, pp. 116–123.

9 François Cahen and André Chevallier, "Le Réglage Puissance-Phase, Nouvelle Méthode Pour le Réglage Automatique de la Fréquence d'un Réseau Comportant de Multiples Usines Génératrices," Bulletin SFE, October, 1953.

10 François Cahen, "Load-Phase Tie-Line Energy Control of Interconnected Power Systems," *Trans. AIEE*, Power Apparatus and Systems, April, 1955.

11 M. Cuenod, A. Jacques, and R. Renchon, "Experimental Study of Frequency Stability by the Impulse Method," CIGRE Paper no. 302, 1956.

12 D. Gaden, "Recherche d'une Condition de Stabilité," and "Commentaires sur la Condition de Stabilité," Ecole Polytechnique de L'Université de Lausanne, Publication no. 28, 1954.

13 R. Keller and W. Frey, "Contribution to the Control of the Frequency and Power of Large Networks," CIGRE, 1954, Report no. 318.

14 F. Cahen, A. Chevallier, R. Robert, B. Favez, and J. Carpentier, "Problems of Automatic Frequency and Tie-Line Power Control in Large Networks," CIGRE, 1956, Report no. 325.

15 S. B. Morehouse, "Recent Development and Trends in Automatic Control of Large Interconnected Power Systems," CIGRE Paper no. 313, 1956.

DISCUSSION

H. M. Paynter[2]

The author has once more enhanced the literature on power system regulation in this meritorious contribution. Without in any way decrying the superb use of analog art and craft displayed herein, the writer wishes to point to the possibility of substantial generalization of results through recognition that Equation (2) of the paper represents an example of what the writer has called a *monotone process* [16, 17].[3] All such processes may be conveniently represented in the form

$$F(p) = \exp\left(\delta - T_m p + \frac{1}{2} T_s^2 p^2 - \frac{1}{6} T_a^3 p^3 + \frac{1}{24} T_e^4 p^4 - \ldots\right)$$

with

δ = logarithmic gain

T_m = mean delay

T_s = dispersion time

T_a = skew time

T_e = excess time

. . . etc. . . .

For the operator of Equation (2), these constants become:

$$\delta = -\ln R$$

$$T_m = (1-f)T_R + T_1 + T_6$$

$$T_s^2 = (1-f^2)T_R^2 + T_1^2 + T_6^2$$

$$T_a^3 = 2[(1-f^3)T_R^3 + T_1^3 + T_6^3]$$

$$T_e^4 = 6[(1-f^4)T_R^4 + T_1^4 + T_6^4]$$

With values typical of those used in the paper, namely:

$$T_R = 10 \text{ sec}; \quad T_1 = 0.375 \text{ sec}$$

$$f = 0.25; \quad T_6 = 0.25 \text{ sec}$$

the monotone time constants become:

$$T_m = 8.125 \text{ sec}$$
$$T_s^2 = 94.75 \text{ sec}^2$$
$$T_a^3 \cong 2000 \text{ sec}^3$$
$$T_e^4 \cong 60{,}000 \text{ sec}^4$$

In such a case, the process will behave nearly identically to a single lead-lag model having comparable values of T_m and T_s, namely:

$$F(p) \cong \frac{1}{R}\left[\frac{2p+1}{10p+1}\right]$$

Generally, this means simply that the reheat operator

$$\left[\frac{fT_R p + 1}{T_R p + 1}\right]$$

is the *dominant* term and an analysis based *solely* on this term will yield significant results. For example, in Case I, this gives as a characteristic equation:

$$(RMT_R)p^2 + (RM + RT_d T_R + fT_R)p + (1 + RT_d) = 0$$

For values of $R = 0.05$, $T_d = 1.0$, $M = 10$ sec this gives:

$$(0.5T_R)p^2 + (0.5 + 0.05T_R + fT_R)p + 1.05 = 0$$

Then if T_R is held constant at 10 sec this gives:

$$5p^2 + (1 + 10f)p + 1.05 = 0$$

Undamped natural period $= 2\pi\sqrt{5} \cong 15$ sec

$$\text{Damping ratio} = \frac{1}{\sqrt{20}} + \sqrt{5}\, f \cong 0.2 + 2f$$

These results correspond to Fig. 2 of the paper. Thus the conclusion: f greater than 0.25 corresponds to a damping ratio greater than 0.7.

Similar results may be obtained for Fig. 3. Of course, only the dominant low frequency stability and response may be obtained in this way, but such approximations should not be overlooked, both for their value in verifying and validating analog studies and for suggestions as to sensitivity relations between system response and parameter changes.

In any event, the author should be encouraged by all to continue this useful task of exploration.

References

16 H. M. Paynter, "On an Analogy Between Stochastic Processes and Monotone Dynamic Systems," from Regelungstechnik: Moderne Theorien und ihre Verwendbarkeit, Oldenbourg Verlag, Munchen, Germany, pp. 243–250.

17 H. M. Paynter and Y. Takahashi, "A New Method of Evaluating Dynamic Response of Counterflow and Parallel-Flow Heat Exchangers," TRANS. ASME, vol. 78, 1956, pp. 749–758.

H. M. Stone[4]

Computer analysis of utility system generation components is providing information for better equipment design and indicating operational characteristics which may be expected from installed apparatus. The author is commended for recognizing and analyzing a subtle aspect of steam turbine reheat operation.

Another phase of the same work is field testing to determine if equipment installed in a complex power system functions as predicted, designed, and specified. Southern California Edison Company has designed and built a Mobile Dynamics Test Laboratory to field test generating unit speed governors and generation controls. Two recently installed steam turbine reheat units rated 156 megawatts were tested. Dead band, frequency response, transient response, and response as controlled from an automatic area load frequency control system were determined.

Time delays as great as 120 seconds were measured between speed changer motor signal input and first change of generator megawatts when rate of generation change was limited to 4 megawatts per minute. The major part of this time lag was caused by backlash between cam shaft rack and pinion which allowed the governor dead band to reach 0.12 per cent. This is double the allowable governor dead band of 0.06 per cent as specified by the ASME-AIEE governor standards. As a result of the large dead time to automatic control of steam turbine reheat units, older, less economic units are required to pick up and carry load. This action does not match the system automatic incremental cost loading schedule. Methods of correcting the abnormal dead time are being investigated.

Measured total governor delay time of reheat steam turbines was found to be several times the maximum computed magnitude of delay time caused by reheat as stated in the paper.

[2] Massachusetts Institute of Technology, Cambridge, Mass., and American Center for Analog Computing, Boston, Mass. Mem. ASME.

[3] Numbers in brackets designate References at end of this discussion.

[4] Assistant Apparatus Engineer, Southern California Edison Company, Los Angeles, Calif. Assoc. Mem. ASME.

Author's Closure

We wish to thank Professor Paynter for his very kind remarks. We are wholly in agreement with him that it is always desirable to abstract the pertinent parameters in order to make a useful simplified model of the actual system. He presents a very interesting analysis of the results of our paper. We have made somewhat similar simplified analyses but for the purposes of the paper thought it best to present a few specific and complete examples.

Mr. Stone brings out again the importance of governor dead band. This importance was pointed out in reference [1] of the paper, and limitations on dead band were included in the recommended governor specifications of reference [2] of the paper. As power systems have grown larger, frequency deviations have become smaller, and dead band is becoming even more important. With regard to the time delay of 120 seconds mentioned by Mr. Stone we have made the following check calculation. A dead band of 0.12 per cent speed corresponds, at 5 per cent regulation, to 2.4 per cent load change. This is very close to 4 megawatts, which is 2.6 per cent of 156 megawatts. With a rate of load change of 4 mw per minute, an equivalent time delay of 56 seconds would be produced. In order to produce 120 seconds' time delay the incremental regulation would have to be 2.3 per cent. Also, it may be possible that the power system frequency changed during the test interval in such a direction as partially to cancel the load control signal. It is evident that, regardless of the dead band, it is always possible to choose a rate of load change which will result in a very large apparent time delay. We should of course remember that the error in load itself, which is perhaps the most important, is in all cases no greater than, and very probably somewhat less than, the quotient of the speed dead band divided by the regulation. A dead band of 0.06 per cent and a regulation of 5 per cent will result in an equivalent load dead band of 1.2 per cent. It may be that the dead band allowed by the standard specifications should be reviewed in view of desired values of regulation and of desired precision of load allocation.

R. E. BRANDON

Engineer, Large Steam Turbine-Generator Department, General Electric Company, Schenectady, N. Y. Assoc. Mem. ASME

H. C. BAHR

Engineer, Large Steam Turbine-Generator Department, General Electric Company, Schenectady, N. Y. Mem. ASME

Load Capacity Tests on Tapered-Land and Pivoted-Shoe Thrust Bearings for Large Steam-Turbine Application

Results of full-scale maximum load capacity tests on large, 3600-rpm, pivoted-shoe and tapered-land thrust bearings are reported. The results show 700 psi capacity for the pivoted-shoe bearing and 1085 psi for the tapered-land type. Additional evidence of thermal distortion and its effect on thrust-bearing capacity are discussed. A brief description of a new thrust-bearing test installation also is included.

THE PAST DECADE has seen large increases in steam-turbine capacities and in initial steam conditions. These changes have increased both potential thrust and shaft diameters, which in turn require thrust bearings with greater area, and operating at larger diameters.

For years the authors' company has been the only major turbine manufacturer to utilize tapered-land thrust bearings. Development tests made approximately 25 years ago by Sheppard[1] established the characteristics and design of tapered-land thrust bearings for a broad range of application. In addition to the very broad experience with tapered-land thrust bearings, experience has been obtained with pivoted-shoe bearings on some 25 of the largest central station turbine-generators installed between 1954 and 1956.

In 1953 a testing program was initiated to determine the characteristics and load-carrying capacity of both types of thrust bearings. It was hoped the tests would reveal what effect, if any, the continued increases in bearing size and runner speed have had on load-carrying capacity. Also sought was a basis that could be established for the selection of either type of bearing.

Approximately 60 tests have now been made in a new test facility. All tests have been of short-term duration, on full-scale thrust bearings (150 to 350 sq in. active area), and at speeds of 1800 and 3600 rpm.

The results that follow compare metal temperatures, horsepower loss, and the ultimate capacity of similar, large, pivoted-shoe and tapered-land thrust bearings. Many of the tests carried the bearings to destruction.

Test Installation

The thrust-bearing test machine was installed in 1953. The assembly drawing, Fig. 1, illustrates how this device is hydraulically operated to simultaneously load two opposed thrust bearings, thus eliminating resultant thrust on the driving mechanism.

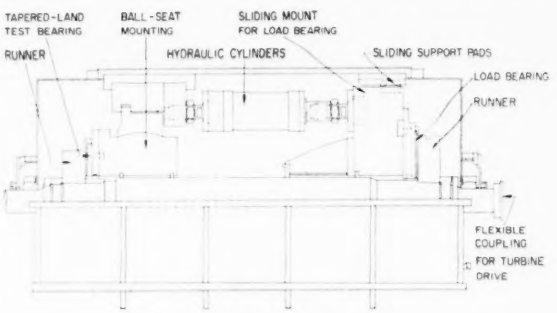

Fig. 1 Assembly arrangement of thrust-bearing test machine

This machine has a capacity of 450,000 lb, is driven by a 1500-hp steam turbine, and can operate from 1500 to 3600 rpm. Its operation to date has been very successful. Fig. 2 shows the test machine and its control panel in preparation for a typical test. The machine is shown partially disassembled, with the load bearing exposed.

Description of Bearings

The tapered-land bearing, Fig. 3, consists basically of a circular thrust plate, split in two halves, which is rigidly supported to carry the thrust load. The babbitt-bearing face is divided into lands by radial oil-feed grooves. The surface of each land is machined with a compound taper, Fig. 4, which slopes in the direction of rotation from the leading to the trailing edge and, to a lesser degree, from the inner to the outer radius at the leading edge of the land. The lubricating oil, which is admitted under pressure to the radial oil-feed grooves, thus forms a wedge-shaped oil film, due to the rotating thrust collar.

Since the surface of the lands is fixed, any compensation for misalignment must be accomplished by the supporting housing, and common practice is to mount this member on a ball seat. It is recognized that self-alignment with a ball-seat-type mounting inherently involves some degree of friction, which, if excessive, could prevent proper alignment of the bearing face, thus reducing the potential capacity of the thrust bearing. Factory tests, as well as actual operating experience, however, indicate that a properly fitted ball seat will permit the thrust bearing to align satisfactorily.

The pivoted-shoe bearing, Fig. 5, contains segmental shoes which are free to pivot in any direction on pivot points centrally located on the back of each shoe. Oil is fed into the bearing

[1] F. C. Linn and R. Sheppard, "Thrust Bearings," TRANS. ASME, vol. 60, 1938, pp. 245–252.

Contributed by the Power Division and presented at the Annual Meeting, New York, N. Y., November 30-December 5, 1958, of THE AMERICAN SOCIETY OF MECHANICAL ENGINEERS.

NOTE: Statements and opinions advanced in papers are to be understood as individual expressions of their authors and not those of the Society. Manuscript received at ASME Headquarters, September 4, 1958. Paper No. 58—A-172.

AUTHORS' NOTE: When this paper was written the authors included information and expressed opinions believed to be correct and reliable. Because of the constant advance of technical knowledge, the widely differing conditions of possible specific application, and the possibility of misapplication, any application of the contents of this paper must be at the sole discretion and responsibility of the user.

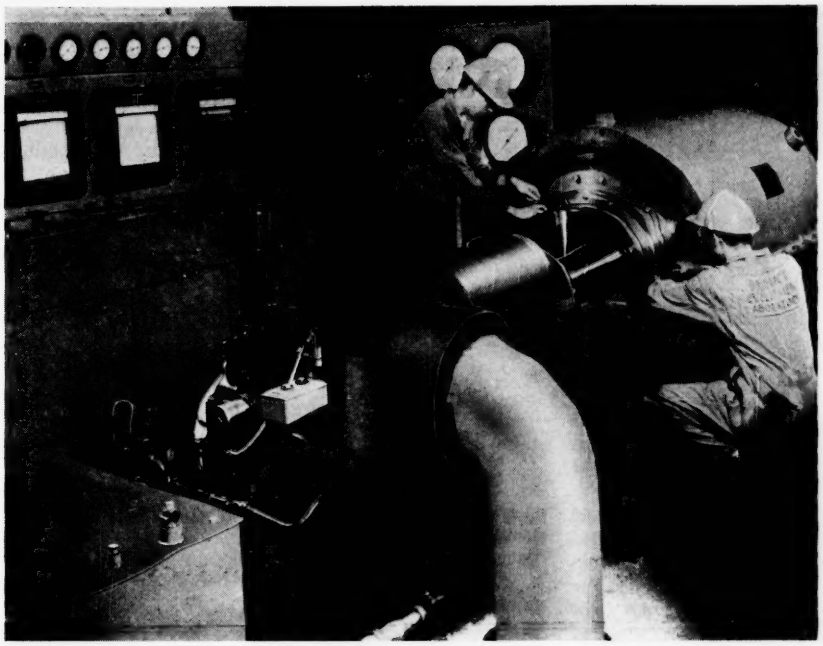

Fig. 2 Thrust-bearing test machine being prepared for operation (partially disassembled) and control panel

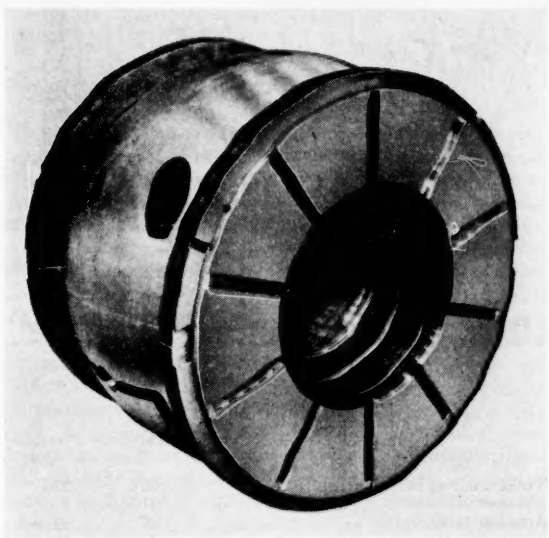

Fig. 3 270-sq-in. tapered-land thrust plate with typical ball-seat mounting, including journal bearing

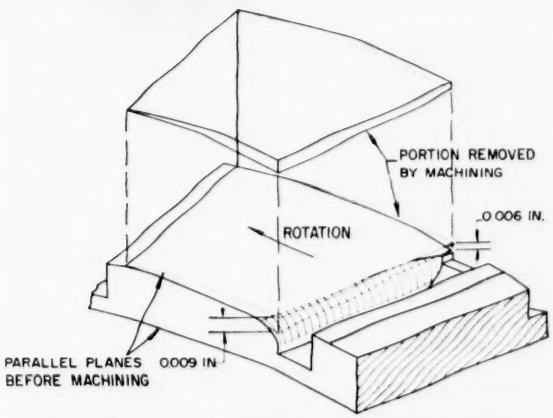

Fig. 4 Diagram, machined bearing surface of the tapered land

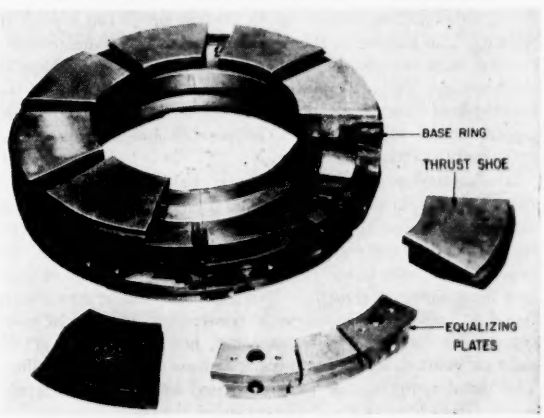

Fig. 5 254-sq-in. pivoted-shoe thrust bearing

around the inner radius of the shoes, and the hydrodynamic action of the lubricant tends to tilt the shoes to form the proper oil-film shape. Proper alignment is maintained through a system of equalizing plates which supports the shoes within a rigid-base ring assembly. This construction equalizes the load over the various shoes and also compensates for any dishing of the thrust collar resulting from load or temperature gradient.

Results

Two of the largest thrust bearings tested at 3600 rpm were a 270-sq-in. tapered-land bearing and a 254-sq-in. pivoted-shoe

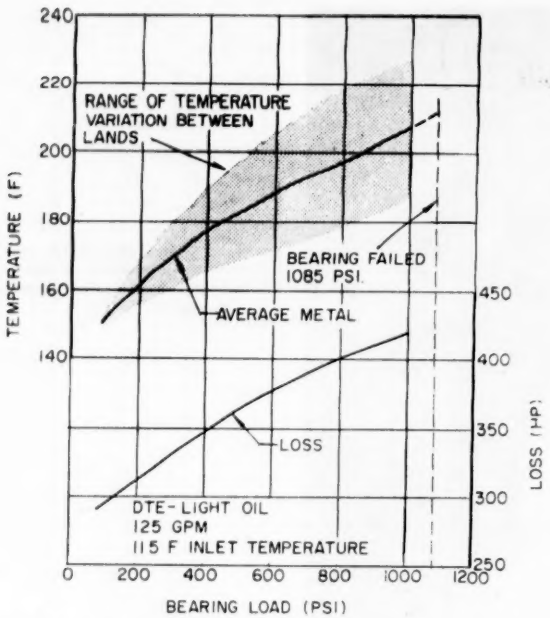

Fig. 6 Plot of metal temperatures and losses for 270-sq-in. tapered-land thrust bearing 3600 rpm

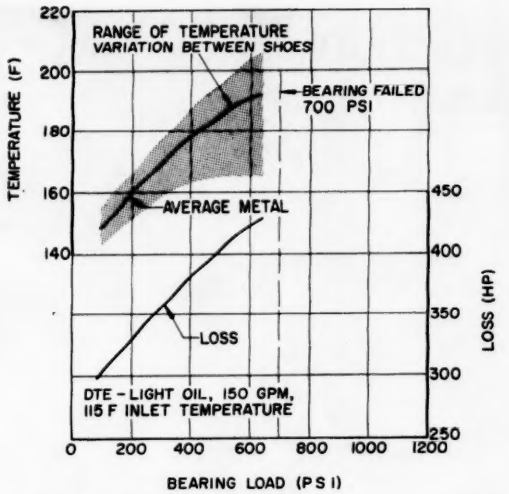

Fig. 7 Plot of metal temperatures and losses for 254-sq-in. pivoted-shoe thrust bearing 3600 rpm

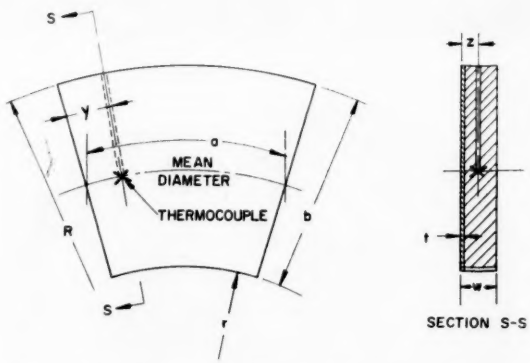

Fig. 8 Geometry of tapered-land and pivoted-shoe bearings

bearing. Both of these two types of bearings in this size already had been installed in several large steam turbines and were operating satisfactorily. For test purposes, each bearing was supported in the testing machine in a manner nearly identical with the actual turbine assembly. During actual testing the bearing was loaded gradually in uniform increments, and thermocouples recorded bearing-metal and oil-discharge temperatures.

Test results for one 270-sq-in. tapered-land bearing are shown in Fig. 6. This bearing was tested to the point of failure, which was indicated by a wiping of the babbitt surface at 1085 psi. The bearing-metal thermocouples were sensitive to load and showed a rather uniform rise as load was increased, reaching an average of 210 F at 1000 psi. Also shown in Fig. 6 is the horsepower loss as measured by a heat balance of the oil flow. The ball-seat mounting appeared to be aligning the bearing satisfactorily as indicated by the relatively uniform temperature distribution around the thrust plate.

Performance of the pivoted-shoe bearing, Fig. 7, shows relative metal temperatures ranging on an average up to 190 F prior to failure. The pattern of these shoe temperatures indicated that loading was reasonably distributed over the eight shoes of the bearing. The horsepower losses were similar to that of the tapered-land bearing, although they appeared about 10 per cent greater at the higher loads. The pivoted-shoe bearings failed completely at 700 psi.

The similarity of the bearings may be seen in Fig. 8. The mean velocity, in the range of 18,000 fpm, is practically the same in each case, and the dimensions of the land and shoe bearing surface are quite similar. It thus appears reasonable, for practical purposes, to compare the relative performances of these two large bearings directly. Bearing-metal temperatures were found to be a useful indicator of relative performance in these tests. The discharge oil temperature, however, was of practically no value in indicating bearing distress or impending failure. The metal temperatures were measured by means of thermocouples imbedded in the steel portion of the bearing from $^1/_2$ to $^3/_4$ in. back from the babbitt face, with one such thermocouple installed in each bearing land (or shoe) at a point on the mean circumference which would be near the high-temperature region. This procedure was in accordance with common practice in locating thermocouples for monitoring large turbine thrust bearings. The average of all these thermocouples at each load

Characteristics of Test Bearings

	Tapered-land	Pivoted-shoe
Total area, sq in.	270	254
Number of lands	10	8
Area per land, sq in.	27	31.8
Mean diameter, in.	19.12	19.37
Mean velocity, fpm	18000	18300
a = mean width of land, in.	5.01	6.08
b = radial height of land, in.	5.37	5.37
a/b = ratio	0.93	1.13
r = inner radius, in.	6.87	7.0
R = outer radius, in.	12.25	12.37
t = minimum babbitt thickness, in.	3/16	1/8
w = over-all thickness, in.	1	1 7/8
y = thermocouple location, in.	7/8	1
z = thermocouple location, in.	1/2	3/4

point constitutes the metal temperature curves plotted in Figs. 6 and 7.

Each bearing was furnished with an oil supply calculated to provide a 25–30 deg F temperature rise of the oil when operating at normal design limits, with an inlet-oil temperature of 115 F. For all tests, the oil used was light turbine oil (DTE-797) which had the following properties:

Viscosity, Saybolt seconds	154 SSU at 100 F
	89 SSU at 130 F
	43 SSU at 210 F
Specific gravity	0.857 at 100 F
	0.821 at 210 F
Acid number	0.06

Many variables, such as dimensional tolerances and oil cleanliness, affect slightly the performance and capacity of thrust bearings. It would not be surprising, for instance, to find variations of 10 per cent in the maximum capacity of two bearings made from the same drawings. It is important to note, therefore, that the foregoing results are not from isolated tests.

The results shown for the pivoted-shoe bearing are representative of some 12 tests on similar bearings of 254-sq-in. area, three of which were carried to destruction. None of these tests indicated the ultimate capacity to be in excess of approximately 700 psi.

The results shown for the tapered-land bearing are indicative not only of two duplicate bearings tested, but of some 25 additional tests on other sizes and geometrical arrangements, all showing the capacity of tapered-land bearings to be in excess of 1000 psi.

Temperature Measurements

Bearing-metal temperature measurements proved to be a very valuable source of information concerning operation of thrust bearings and are the only indication of impending trouble as the bearing approaches its maximum load. Similarly, they can indicate difficulties due to bearing misalignment or from any other source of unbalanced load. The temperature variation between the various lands plotted in Figs. 6 and 7 is typical of those found in most tests.

The metal temperature results plotted in Figs. 6 and 7 are taken from thermocouples located up to $^3/_4$ in. below the babbitt surface. If these thermocouples were located closer to the babbitt, they of course would read higher temperatures, reaching the maximum temperature level at the surface of the babbitt itself. Many such measurements have been taken with thermocouples located nearer the babbitt and even at the babbitt surface. While surface measurements appear slightly more sensitive to changes in load or film thickness, there appears to be some possibility that the techniques of installing these surface thermocouples may injure the load-carrying capacity of the bearing itself. For the type of tests reported here, thermocouples located well below the babbitt have been satisfactory, and readings compare accurately with installations in operating turbines.

Thermal Distortion

During these and many other similar or special tests, it became apparent to the authors that thermal distortion is an important factor in the determination of maximum load-carrying capacity. The following evidence and hypothesis are offered to support this conclusion:

Frequently, in the course of a test, it was possible to remove the load and inspect a bearing taken to the verge of failure. For example, the tapered-land bearing shown in Fig. 9 was unloaded from 1075 psi after temperature measurements had indicated it was in distress. The slight pattern of marking caused by runner contact indicates that the plate was humping or distorting, since the marks occur only in the central portion of what was originally a flat surface, as shown in Fig. 4. The probable mode of distortion is schematically shown in Fig. 10. This form of distortion is quite likely at high loads, where the babbitt surface may be 150 deg F hotter than the relatively cool side of its steel backing.

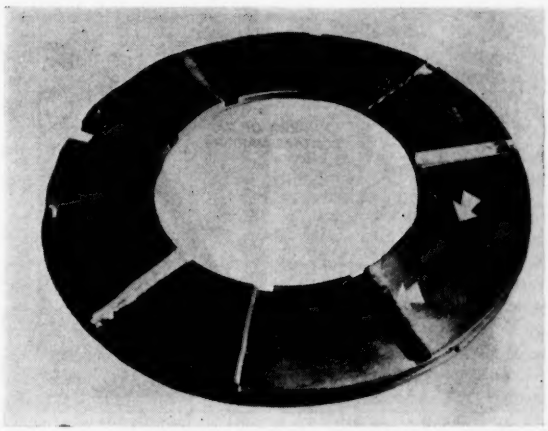

Fig. 9 Tapered-land thrust bearing after loading to 1075 psi. Note partial contact marking on trailing edges, indicating distortion.

This distortion can result in local areas carrying much more than their share of the total load, ultimately leading to babbitt failure in these overloaded areas. This local breakdown is the start of a progressive deterioration leading to total failure of the bearing. Further, any distortion of the runner, such as "dishing," undoubtedly will add to this localized loading.

A single effort to measure film thickness in an operating tapered-land thrust bearing provided further evidence of the occurrence of plate distortion. The film thickness-measuring device was located at the outer diameter of the thrust plate at the discharge edge of the land. The measurement indicated that the film thickness at this point was approximately four times the average minimum film thickness (based on theoretical calculations).

In similar fashion, indications of thermal distortion have been noticed on large pivoted-shoe bearings. Fig. 11, for example, shows slight markings on a pivoted-shoe bearing which occurred at 688 psi. The irregular pattern of marking indicated that the bearing was not flat at the time this wear took place. Similarly,

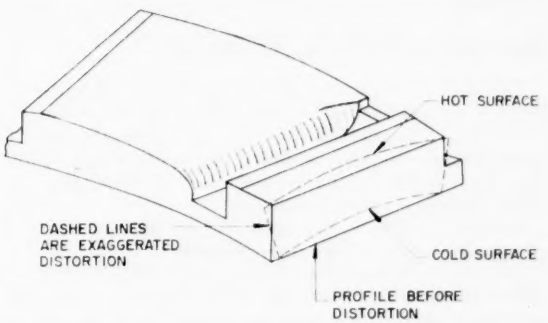

Fig. 10 Schematic diagram of radial distortion of plate, caused by temperature gradient

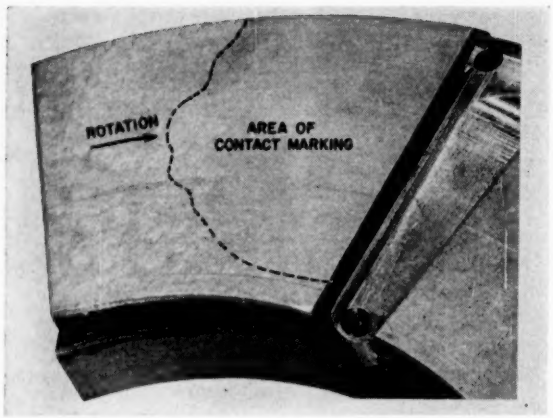

Fig. 11 Pivoted-shoe bearing after loading to 688 psi. Note irregular marking, indicating distortion.

after actual wiping of a pivoted-shoe bearing, measurements have indicated that at the time of wiping the bearing was "crowned" so that a hollow remained in the center of the babbitt surface after it cooled.

This "crowning" effect, in the circumferential direction, has often been discussed as desirable, and, to a degree, it probably is. In the radial direction, however, the effect of thermal distortion can be only to unload the edges of the shoes so that the central portion carries much more than the expected load. Thus it is concluded that both types of bearings are affected by thermal distortion.

It is important to note that in tapered-land bearings the pressure loading from the oil film acts in opposition to the distortion caused by thermal gradients. This reduces the sensitivity of tapered-land bearings to thermal distortion, as the pressure tends to flatten the bearing against its backing. Evidence of this characteristic is indicated from the modifications made to two tapered-land thrust bearings which initially failed to carry 1000 psi. The modification consisted of reducing the thickness of the bearing plate so that oil pressure more easily could keep the bearing flat against its backing despite the temperature gradients. After this change, each bearing carried loads in excess of 1000 psi.

Pivoted-shoe bearings, however, are constructed with a support near the center of the shoes, so that the pressure forces act in the same direction as the thermal-distortion forces. It appears to the authors that continued increases in pivoted-shoe bearing sizes at high runner speeds may decrease significantly the maximum load capability, unless some method is found to reduce the harmful effects of thermal distortion.

Other Tests on the Pivoted-Shoe Bearing

To make certain that the pivoted-shoe bearing was lubricated properly, several modifications were tried, as shown in Figs. 12, 13, and 14. These devices assured full oil flow to each shoe and to some degree actually pressurized the bearing casing. In no case was a significant improvement found, thus indicating that the original oil system was satisfactory.

Similarly, variations in quantities of oil flow and initial oil temperature did not provide any improvement.

One final test was conducted on the pivoted-shoe bearings, as shown schematically in Fig. 15. This modification was tried with the expectation that some improvement could be made by anticipating the distorted shape of the shoe. Thus a slight hollow was machined in the babbitt faces on the basis that the

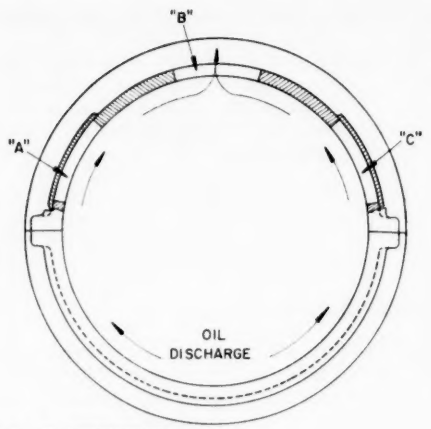

A, B, & C = OIL DISCHARGE SLOTS
(A & C BLANKED OFF DURING SPECIAL TEST)

Fig. 12 Diagram showing blocked oil-discharge holes for special test of pivoted-shoe thrust bearing

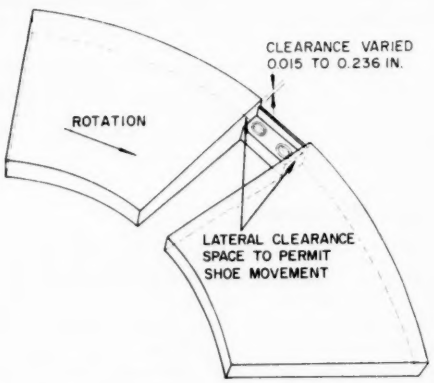

Fig. 13 Diagram showing simple dams between shoes for special test of pivoted-shoe thrust bearing

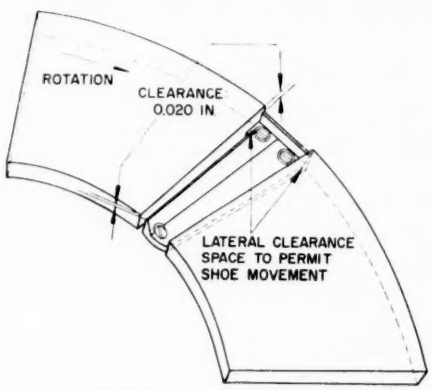

Fig. 14 Diagram showing compound dams between shoes for special test of pivoted-shoe thrust bearing

bearing surface might more nearly approach the ideal when it was distorted under load conditions. Slight wiping occurred at the edges, as shown in Fig. 16, at an average load of 668 psi, indicating that no significant improvement was realized. Nevertheless,

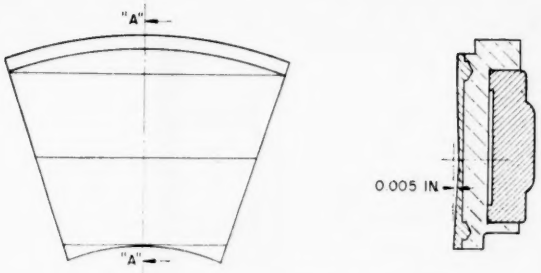

Fig. 15 Diagram of specially machined pivoted-shoe thrust bearing

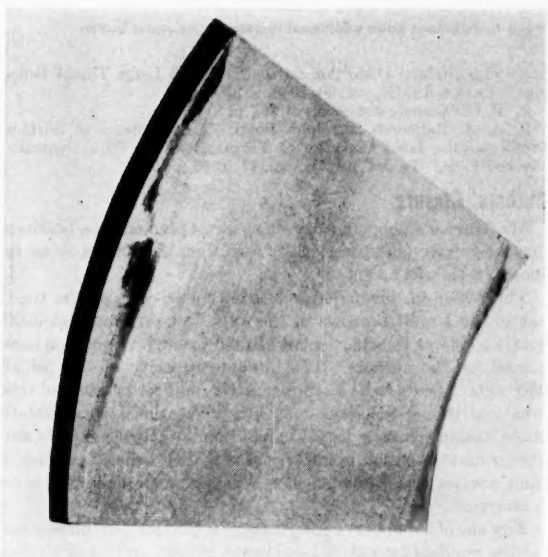

Fig. 16 Specially machined pivoted-shoe thrust bearing after carrying 668 psi. Note polished areas at inner and outer radii.

this approach might improve the maximum load-carrying capability of pivoted-shoe bearings, if further refinements to the initial contour were to be pursued.

Summary

1 The test results indicate that the maximum load-carrying capacity of the 270-sq-in. tapered-land thrust bearing at 3600 rpm is in excess of 1000 psi.

2 The test results for the 254-sq-in. pivoted-shoe bearing at 3600 rpm indicate maximum capacity to be not over 712 psi, and the effort thus far expended to improve this load capacity has had no appreciable effect.

3 The measured metal temperatures and horsepower loss are approximately equivalent for both types of bearings at the same unit load.

4 Both types of bearings suffer from the effects of thermal distortion, although the compensating aspects of the oil-film pressure tend to reduce this effect on tapered-land thrust bearings.

5 Increased bearing area and higher runner velocity have not affected significantly the high-load capacity of the tapered-land bearing.[1]

Acknowledgments

The authors wish to express their appreciation to their associates, particularly R. Sheppard, for their assistance in the preparation of this paper.

DISCUSSION

Paul C. Warner[2]

It appears to this discusser that most, if not all, of the careful investigators [1, 2, 3][3] into the performance of the conventional fluid film type of thrust bearing soon come to the conclusion that for good performance, the thrust bearing and its supporting structure must be carefully engineered to provide, and to maintain during use, bearing surfaces of the proper size, shape, and contour. Much of the difficulty in doing this is felt to be due to the fact that one of the most important features to be provided and maintained is the contour of the shoe face. Deviations from the desired contour of as little as + 0.00025 in. are of importance, and, as may be imagined, such deviations are not only hard to control, they are in many cases extremely difficult to measure. In addition to the sources of deformation of the thrust shoe and/or collar listed by the author, i.e., (1) temperature gradients in collar and shoe and (2) elastic deformation of collar and shoe due to the pressure distribution, there can be trouble from distortions due to (3) bimetallic effects from the shoe facing-backing combination and (4) the fact that the relatively soft babbitt facing operates in a range where it has low strength and is in fact subject to creep.

From this general viewpoint, the experience of the discusser's company both in field work, and in experimental work is in qualitative agreement with the experience and test results reported by the authors in that the same types of difficulties seem to limit thrust bearing capacity. The capability limit of 700 psi put forth by the authors for the tilting shoe type of thrust bearing is not in agreement with our experience or test results. We have too many field experiences and too many test points at loads appreciably above 700 psi to accept any such limit. In fact, the matter appears to be fairly complicated, and under very adverse conditions a much lower capability will be obtained, whereas under normal or good conditions higher limits are obtained. We feel, however, that prudent design and operation require that thrust loads be maintained at low levels. Perhaps it should be noted that the bearings which we apply to electric utility turbines, and those which have been tested by us are of a six-shoe variety and perhaps somewhat different in design detail from the eight-shoe bearing tested by the authors.

The discusser's company utilizes temperature measuring locations considerably different from those employed by the authors' company both for field monitoring of thrust bearings and for development testing (see Fig. 17). This, of course, means that temperature data and limits are not directly comparable since sharp temperature gradients occur in some parts of a thrust shoe [2]. Nevertheless, our temperature versus load curves do not look too dissimilar from the authors' Fig. 6. One advantage of the thermocouple locations indicated in Fig. 17 is that the temperature rise of the oil from the inlet of the bearing to the leading edge of the thrust shoe may be used as a criterion for selecting the proper oil flow for a given application, Fig. 18. This method appears to be more rational than selecting the flow to produce a certain temperature rise across the bearing, since, in the words of the authors, "discharge oil temperature was of practically no value in indicating bearing distress or impending failure," an opinion which is heartily shared by this discusser.

[2] Development Engineering, Steam Division, Westinghouse Electric Corporation, Philadelphia, Pa. Assoc. Mem. ASME.

[3] Numbers in brackets designate References at end of discussion.

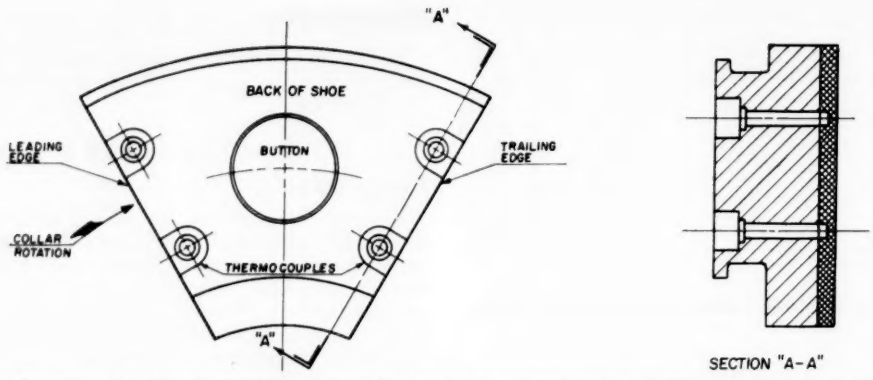

Fig. 17 Thermocouple location for development tests. Most production installations have additional thermocouple under button.

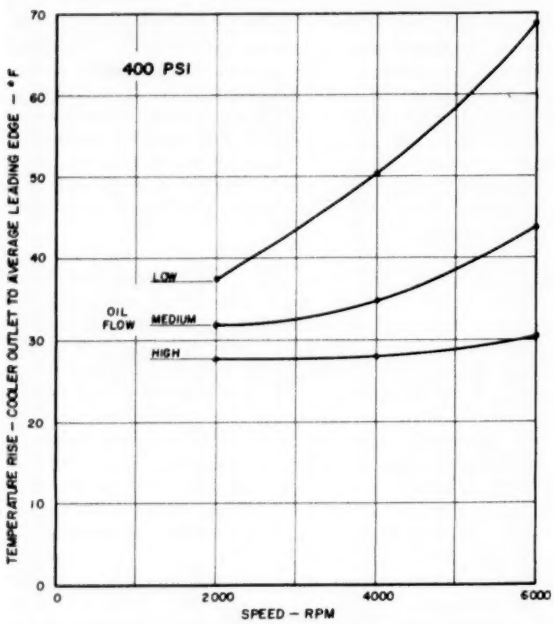

Fig. 18 Variation of inlet edge babbitt temperature with speed and oil flow

Incidentally, while babbitt temperatures are felt to be a much better index of bearing operation than discharge oil temperature, it is felt that such measurements will not accurately foretell impending failure. The reason for this opinion is partially illustrated by the scatter in temperatures seen in Fig. 6.

Temperature measurements and oil film thickness measurements in an extensive series of tests have permitted us to approximate the amount of shoe distortion occurring for various bearing operating conditions. Such estimates are not in good agreement with the 0.005 in. out of flat implied by the authors' Fig. 15, hence the lack of improvement in load carrying capability found by the authors for this alteration is not too surprising.

Initially a much more detailed and better documented discussion of the authors' valuable paper was planned. In view of the length involved, however, it is planned to submit the material as a paper in the near future.

References

1 R. A. Baudry, E. C. Kuhn, and W. W. Wise, "Influence of Load and Thermal Distortion on the Design of Large Thrust Bearings," TRANS. ASME, vol. 80, 1958, p. 807.

2 P. C. Warner, discussion of [1], p. 816.

3 A. A. Raimondi and John Boyd, "The Influence of Surface Profile on the Load Capacity of Thrust Bearings With Centrally Pivoted Pads," TRANS. ASME, vol. 77, 1955, p. 321.

Authors' Closure

Mr. Warner's point that the capacity of pivoted shoe bearings may be greater (and occasionally less) than the 700 psi found in these tests is well taken.

The 254-sq-in. pivoted-shoe bearing tested was, at the time, one of the largest bearings of this type to be operated at 3600 rpm, and it was thus particularly suited to the investigation conducted by the authors. The ultimate capacity of 700 psi at 3600 rpm appears to be a representative limit for bearings of this area and runner velocity, and with conventional steel-babbitt shoes having centrally located pivot points. However, it is not the authors' intention to imply, nor is it their belief, that such a limit applies to all pivoted-shoe bearings, regardless of size or geometry.

Any one of a number of criteria may be used for determining the oil flow required for a given bearing application, and we agree that the method suggested by the discusser may be perfectly valid. The selection of any such criterion, however, is a somewhat arbitrary matter, and its advantages will depend to a large degree on empirical information. It is not clear from his Fig. 18 just what the oil flow requirements are, but if "medium" is the desired flow, then either method appears to give about the same result. The real test of adequate oil flow is not the temperature of the inlet edge of a shoe, or the temperature of the drain, but the continuity of cool oil supplied to the thinnest part of the oil film at high load. Any system which satisfies this requirement without introducing excessive quantities of oil should be satisfactory.

The method used to determine the required oil flow, however, is not related necessarily to the method of monitoring the bearing to predict distress or impending failure. Temperature measurements taken near the discharge of a land (either in the babbitt or the steel) have been the most accurate method of anticipating trouble or failure. It is true that the variation shown in Figs. 6 and 7 handicap the accuracy of the prediction. Nevertheless, in the laboratory it is almost always possible to unload a test bearing just short of failure by careful attention to the temperature measurements. Similarly, in field turbines, temperature measurements prove valuable as a constant monitor of changes in rotor thrust or bearing conditions.

As thrust bearings are improved (by reduction of harmful thermal distortion, for example) it is expected that temperature scatter will be greatly reduced, and a specific temperature reading will thus become even more significant.